Physical, Morphological and Chemical Structure & Property Relationships for α-Keratins in Bleached Human Hair

A thesis submitted to The University of Manchester for the degree of Doctor of Philosophy (PhD) in the Faculty of Engineering and Physical Sciences

2013

Daijiazi Zhang

School of Materials

Table of Contents

Word Count: 54,024

List of Figures

List of Tables

Abstract

The University of Manchester
Daijiazi Zhang
Physical, Morphological and Chemical Structure & Property Relationships for α-Keratins in Bleached Human Hair
02/07/2013

The surface and structural change of human hair fibre have been analysed to determine the oxidation effects for bleached hairs. Three types of bleached hairs (6% H_2O_2 bleach, 9% H_2O_2 commercial bleach and commercial persulphate bleach (contains 9% H_2O_2)) as well as virgin hair were evaluated with the increasing treatment time using Scanning Electron Microscopy (SEM), Reflective Spectrophotometry, Differential Scanning Calorimetry (DSC) and Fourier Transform Infrared (FTIR) Spectroscopy. It is obvious that longer treatment times result in the greater surface and structural damage. However, commercial persulphate bleach causes less surface damage for the cuticle. 6% H_20_2 bleach has overall moderate damage effects on both cuticle and cortex over the treatment time. 9% H_2O_2 commercial bleach indicates two different damage stages. The first 1.5h bleached hairs show mild oxidation to the surface, whereas the damage becomes heavy after 2h. This phenomenon results in that 9% H_2O_2 commercial bleach has a more intensive oxidation damage in the cortex than the commercial persulphate bleach. This is in line with DSC investigation which shows that the intermediate filament of 9% H_2O_2 commercial bleach is heavily damaged after the extensive oxidation time (≥2h). Although commercial persulphate bleach contains the stronger oxidising agent, it has a less surface damage than 9% H_2O_2 commercial bleached hair in FTIR-ATR measurement, and a similar oxidation effect on the matrix as 6% H_20_2 bleached hair in FTIR transmission investigation. In addition, it has been verified by colour measurements that bleached hairs have an overall lighter, yellowish and reddish colour. Consequently, commercial persulphate bleached hair is much lighter and more yellow than 9% H_2O_2 commercial bleached hair and 6% H_20_2 bleached hair. DSC investigations reveal that the three bleaches have a homogenous oxidation effect on IFs and IFAPs. The deconvolution results using three Gaussian distributions confirm this observation. The stronger bleach results in a homogenous structural damage on both para- and ortho-cortex with increasing bleaching time. Commercial persulphate bleach and 9% H_2O_2 commercial bleach have a progressive damage effect on the *ortho*- and *para*- cortex than 6% H_20_2 bleach. Kinetics analysis is conducted for the virgin and bleached hairs by using various heating rates according to ASTM-E698. The activation energies of 260 kJ/mol for the virgin hair and 295 kJ/mol for the commercial persulphate bleached hair (2h) are determined from the slope of the regression line of peak temperature, T_D (as $1/T_D$) and heating rate, β (as lnβ) on the basis of the Arrhenius-equation. The predominant structural damage for various heating rates only occurs in the IF. It is shown that a linear increase in ΔH_D occurs for lower heating rates, while it is constant for higher heating rates. This can be ascribed to the hypothesis that a lower heating rate favours a crystal transformation change (α-β transformation), while a higher rate favours a crystalline-amorphous transformation. SEM examines the morphological changes of hair samples after DSC. The cortex has been dissolved at the lower heating rate. The commercial persulphate bleached hairs (2h) show an overall shrunk cuticle surface and fewer and smaller hydrolysed protein granules, due to the previous damage of the α-helix in the cortical cell.

Declaration

No portion of the work referred to in the thesis has been submitted in support of an application for another degree or qualification of this or any other university or other institute of learning.

Copyright Statement

Acknowledgement

I would like to take this opportunity to express my gratitude to Prof. Franz J. Wortmann and Dr. Gabriele Wortmann for their consistent encouragement and spiritual support throughout all years of my PhD study. They not only mentored me scientifically, but also stimulated me on “How to be a good researcher”.

I would like to give a big acknowledgment to Dr. Huw Owens for his kind assistance in using the reflective spectrophotometer for the colour measurements, and to Mrs Polly Crook for her technical advice for the thermal analysis by DSC. Moreover, I would like to give special thanks to Mr. David Kenyon and Mr. Phil Cohen for their help regarding the sample preparation in this work.

I am also grateful to the colleagues who worked in the same laboratory with me for their scientific discussions and help.

I gratefully acknowledge the financial support during this project from Henkel AG &Co KGaA, Hamburg, GER.

Last but not least, I would especially like to appreciate my family and friends. They have supported me during the whole PhD project and have encouraged me to overcome the difficulties in my life.

Abbreviations

AFM	Atomic Force Microscopy
ATR	Attenuated Reflectance
Cer	Ceramides
Ch	Cholesterol
ChE	Cholesterol Esters
ChS	Cholesterol Sulphate
CIE	Commission Internationale de L'Eclairage
CMC	Cell Membrane Complex
DMA	Dynamic Mechanical Analysis
DTGS	Deuterated Triglycine Sulphate
DSC	Differential Scanning Calorimetry
FFA	Free Fatty Acids
FTIR	Fourier Transform Infrared Spectroscopy
ΔH_D	Denaturation Enthalpy
ΔH_D^0	Denaturation Enthalpy of Virgin Hair
ΔH_D^R	Relative Denaturation Enthalpy
ICTA	International Committee for Thermal Analysis
IF	Intermediate Filament
IFAP	Intermediate Filament-associated Protein
IR	Infrared Spectroscopy
IRS	Internal Reflection Spectroscopy
HGT Protein	High Glycine/tyrosine-rich Protein
HS Protein	High-sulphur Protein

H_{gt}^{0}	Absolute Valley Depth of Cysteic Acid of Virgin Hair
H_{gt}^{R}	Relative Value of Absolute Valley Depth of Cysteic Acid
KAP	Keratin- associated Protein
LFM	Lateral Force Microscopy
MDSC	Modulated DSC
18- MEA	18-methyleicosanoic acid
MIR	Mid-infrared
RH	Relative Humidity
SAXS	Small Angle X-ray Scattering
SEM	Scanning Electron Microscopy
SNR	Single-to-noise Ratio
SPD	Spectral Power Distribution
T_D	Denaturation Temperature
T_D^0	Denaturation Temperature of Virgin Hair
T_D^R	Relative Denaturation Temperature
TEM	Transmission Electron Microscopy
UHS Protein	Ultra-high-sulphur Protein
XPS	X- ray Photoelectron Spectroscopy

Chapter 1 Introduction

1.1 Morphology and Chemical Structure of Human Hair

Keratins are a group of specialised proteins containing a high content of cystine, which has the capacity to cross-link the polypeptide chains by intermolecular disulphide linkages. Structurally, keratins have been classified by two principal types of pattern, namely the α-helical conformation for hard keratins of mammals, and the β-sheet structure for those of birds and reptiles, respectively. Depending on how much cystine they contain, the α-keratins are further subdivided into two groups, "hard" and "soft". The tougher material like horn, hoof and hair, which contains more than 3% sulphur, is defined as hard keratin and flexible keratin such as stratum corneum in skin, which has a lower sulphur content (less than 3%), is defined as soft keratin (Asquith, 1977).

Human hair is a keratin-containing appendage that grows from cavities in the skin, called follicles. Hair follicles extend from the surface of the skin through the stratum corneum and the epidermis into the dermis (Robbins, 2002). They are composed mainly of fibrous proteins, which characteristically contain cystine residues, forming intra- and intermolecular cross-links. The disulphide bond is one of the strongest bonds in the natural world. The disulphide cross-links in hair keratin thus lead to high mechanical strength and distinguish hair fibre from other fibrous proteins, such as silk and collagen.

Human hair is a very complex fibre. Morphologically, a fully formed hair fibre (about 50-100 μm in diameter) is primarily composed of three different structural units. From the outside these are the cuticle, cortex and medulla, respectively. A schematic representation of a human hair with its various layers of cellular structure is presented in Figure 1.1.

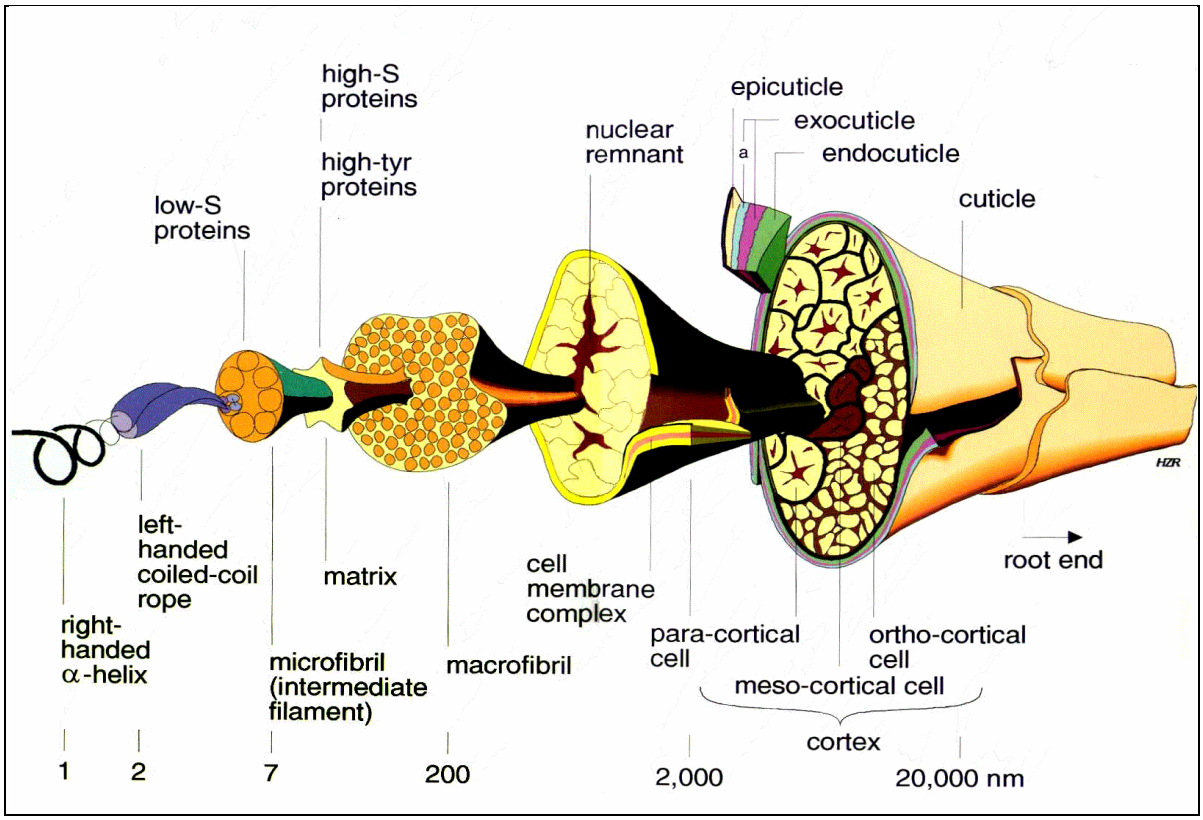

Figure 1.1: Schematic diagram of a human hair with its various layers of cellular structure (Feughelman, 1997)

1.1.1 Cuticle

The cuticle is the outermost protective layer, which is composed of flat, overlapping scales that surround the central fibre core, or cortex. Each cuticle cell is approximately 0.5μm thick, with about 5 μm exposed surface, and approximately 45-60 μm long. In human hair, the cuticle is generally 5-10 scales thick, so that the thickness of cuticle layer is in the range of 2.5 to 5 μm.

The cuticle is a barrier to the sorption of large molecules such as dyes, and protects the cortex from physical damage (Feughelman, 1997). The cuticle has a scale-like structure, in which the cuticle cells are attached at the root end and point towards the tip of the hair fibre, like shingles on a roof. Each cuticle cell consists of a number of sublamellar layers, namely, epicuticle, A-layer, exocuticle, and endocuticle. Individual cells are separated by the cell membrane complex (Figure 1.2).

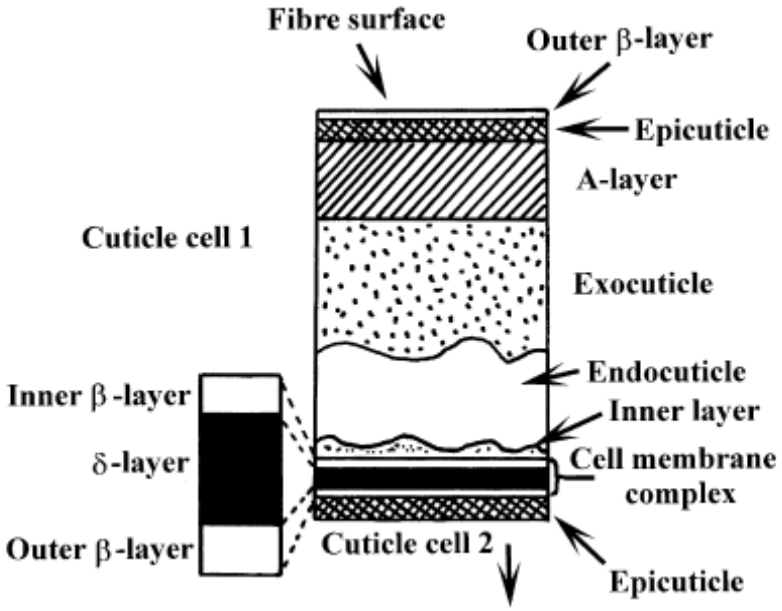

Figure 1.2: The fine structure of a human hair cuticle cell, which is separated from the adjacent cell by the cell membrane complex (Swift, 2001b)

Table 1.1 describes the various layers of the cuticle cell and their respective cystine level (Robbins, 2002). The epicuticle layer (about 3 nm thick) envelops the entire cuticle cell and is a semipermeable, partly proteinaceous membrane, which allows the diffusion of only small molecules into the cell (Ruetsch, 2001). It is covered with a thin layer of 18-methyleicosanoic acid (18-MEA), which is covalently attached to epicuticle proteins through thioester linkages involving cystine residues. This 18-MEA layer makes up the outer β-layer of the cuticular cell membrane complex and is thus responsible for low friction and provides a hydrophobic surface (Bhushan, 2010).

Underneath the outermost portion of the epicuticle is the A-layer of the cuticle cell membrane, which has a very high cystine content (~30%). The A-layer is highly crosslinked and acts as a biochemically stable layer, giving the cuticle surface considerable mechanical toughness and chemical resilience.

The exocuticle (also known as the B-layer), which is immediately adjacent to the A-layer, is also a cystine-rich component (~15%) forming about two-thirds of the scale structure (Feughelman, 1997). On the inwardly facing side of each cuticle cell is a thin layer of material which is referred to as the inner layer. Between the exocuticle and the inner layer is the endocuticle which is deficient in cystine (~3%), and is mechanically

the weakest component of the cuticle structure. The endocuticle swells considerably more in water than the exocuticle, due to their different cystine contents and thus the corresponding cross-linking of the protein structure (Feughelman, 1997).

Table 1.1: The various layers of the cuticle, their cystine content and details about their properties (Robbins, 2002)

Cuticle Layer	Cystine Content (%)	Details
Epicuticle	~12	18-MEA lipid layer attached to outer epicuticle contributes to lubricity of the hair
A-layer	~30	Highly crosslinked
Exoxuticle	~15	Mechanically tough
Endocuticle	~3	Chemically resilient
Inner Layer		
Cell Membrane Complex (CMC)	~2	Lamellar structure consists of inner β-layer, δ-layer, and outer β-layer

1.1.2 Cell Membrane Complex (CMC)

The cell membrane complex (CMC), also known as intercellular matter or non-keratinous region, is an adhesive material holding all the components of the hair together, such as overlapping cuticle cells, cuticle and cortex cells, and neighbouring cortex cells. It consists of a cell membrane and adhesive proteinaceous material. The fraction of the CMC has been estimated to be about 3% (Bradbury, 1973). It is believed that the cell membrane complex is the primary pathway for diffusion of chemical agents (Robbins, 2002). The CMC itself has a lamellar structure, which is made up of a central, polysaccharidic δ-layer, known as "intercellular cement", enclosed by two lipid-rich β-layers. The outer β-layer separates the cuticle cells from each other, however, it is weakly bound to the δ-layer (Bhushan, 2010). The CMC is primarily nonkeratinous protein, and is low in cystine content (< 2%), but high in polar sulphur-containing amino acids (cysteine, thiocysteine). An important lipid component of the CMC is 18-methyleicosanoic acid (18-MEA), which also appears on the outer surface of each cuticle (upper layer) and is covalently connected to epicuticle protein

structures. Additionally, the CMC is also present in the cortex but with a variable thickness of the δ-layer.

1.1.3 Cortex

The central hair fibre core, or cortex, which is surrounded by the protective layer of the cuticle, makes up 90% of the hair mass. The cortex is largely responsible for the physical and mechanical properties of the fibre and is composed of the cortical cells and the cell membrane complex. The elongated, spindle-shaped cortical cells, are generally 1 to 6 μm thick, approximately 100 μm long and run longitudinally in parallel to the axis of the fibre.

The major structure within cortical cells are the closely packed macrofibrils, which represent up to 60% of the cortex material by mass. The macrofibrils, approximately 0.1 to 0.4 μm in diameter, consists of two main structures, microfibril and matrix, which are distinguished by their structures and amino acid compositions. The microfibril, or intermediate filament (IF), is a partly crystalline fibrous protein, which is mainly composed of α-helical proteins with low content of cystine (~6%). However a gel-like matrix with a high cystine content (~21%), acts as an embedding medium for the intermediate filaments. The matrix varies in quantity and composition for different keratins, whereas the microfibrils appear consistently from one keratin to another (Feughelman, 1997). The matrix/intermediate filament ratio has been reported to be unity in human hair (Robbins, 2002, Wolfram, 2003).

The matrix forms the largest structural portion of the cortex, is structurally less organised and often classified as the amorphous region, although some evidence suggests that it contains some structural organisation. Proteins of the matrix are sometimes referred to as keratin-associated proteins (KAP) or intermediate filament-associated proteins (IFAP). They are classified into three groups: high-sulphur (HS), ultra-high-sulphur (UHS) and high glycine/tyrosine-rich (HGT) proteins.

The macrofibrils exhibit different variations in packing arrangement within the cortex. Two or even three types of cortical cells are identified with different cystine (sulphur) contents. These are the *ortho*-cortical cells, containing less matrix between the intermediate filaments and a lower proportion of sulphur content (~3%), *para*-cortical cells with a higher concentration of disulphide linkages (~5%), and mesocortical cells, which show an intermediate cystine content between *ortho*- and *para*-cortical cells. The cell groups may form two distinctive domains, e.g. in Merino wool called, respectively, *ortho*-cortex (60-40%), which is more hydrophilic and heavily stained by some dyes, and the *para*-cortex (40-10%), which is more readily stained by silver's salts (Maclaren, 1981).

The composition of α-helical and coiled-coil segments in the intermediate filament is summarised in Figure 1.3. Within the central rod domain, there are four main coiled-coil segments 1A, 1B, 2A and 2B (Parry, 1985, Robbins, 2002). Each of these segments is a left-handed two-stranded coiled-coil rope, which shows a hepta-peptide sequence (heptade) repeat unit. The coiled coils are interrupted at three positions by non-helical fragments (*L1* links 1A to 1B, *L2* links 2A to 2B and finally *L12* links 1B to 2A. The link *L12* is about twice the size of *L1* or *L2*) and are terminated by non-helical N- and C- domains. A break in the heptade pattern, which involves some distortion in the rope structure, is indicated in the centre of segment 2B. It was suggested that the N- and C-terminal domains are likely to play a crucial role in directing molecular and filament aggregation (Parry, 1985).

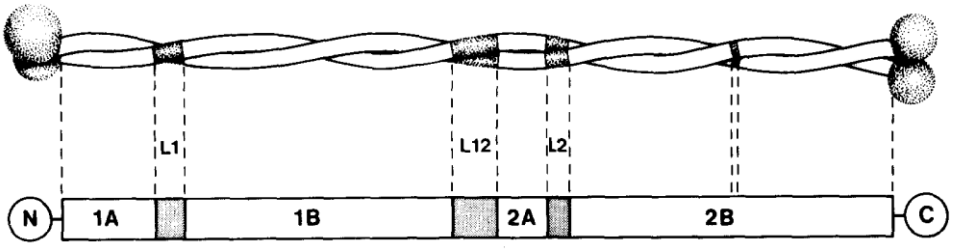

Figure 1.3: Schematic diagram of the rod domain of an intermediate filament dimer (Parry, 1985)

Formation of the macrofibrils related to an aggregation process of intermediate filaments is shown in Figure 1.4. The N- and C- terminal domains of each polypeptide facilitate the assembly of coiled-coils (dimers) into protofilaments (tetramers), two of

which constitute a protofibril. Four protofibrils are packed to be a microfibril (7 to 8 protofilaments), which associates with other microfibrils to form a macrofibril.

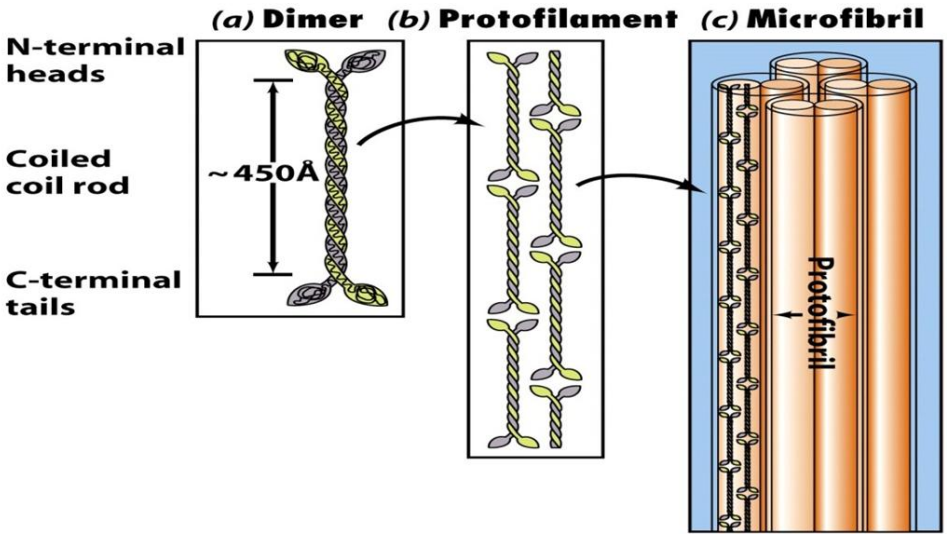

Figure 1.4: Higher order α-Keratin structure (Voet, 2008). (a) Two keratin polypeptides form a dimeric coiled coil. (b) Two staggered coiled coils associated head-to-tail to constitute protofilaments. (c) Two of the protofilaments assembled to create a protofibril, four of which form a microfibril.

1.1.4 Medulla

Fine animal hairs (e.g., merino wool) have little or no medulla, but with increasing fibre diameter, the medulla, which is the innermost layer of the hair fibre, can sometimes be found. In human hair the medulla may be absent or, if present, may be either continuous along the fibre axis, or discontinuous, and in some instances the presence of a double medulla is observed.

Morphologically, the medulla is a 5 to 10 μm diameter channel of loosely packed and largely empty cells forming an amorphous structure more centrally located in the cortex. It has a porous structure formed by sponge-like keratin (Marhle, 1971, Nagase, 2002), which affects both colour and shine in white, brown and blond hair by influencing the reflection of light.

The medulla has a high lipid and a cystine content. It is, however, rich in citrulline (Kreplak, 2001a). A layer of CMC separates the medulla from the cortex (Swift, 1997a).

1.2 The Chemical Composition of Human Hair Fibres

It is important that human hair is an "integrated" system, with the chemical components acting together. Depending on its moisture content, human hair consists approximately 65–95% of keratin proteins, and the other constituents are water, lipids (structural and free), pigments, and trace elements.

1.2.1 Proteins

Proteins are made up of long chains of various mixtures of some 20 to 50 amino acids (Bhushan, 2010). Human hair is predominantly proteinaceous and has a group of fibrous proteins known as α-keratin (Feughelman, 1997, Zviak, 1986). Like all proteins, human hair proteins contain both cationic and anionic groups, and are therefore amphoteric. The cationic character is due to the protonated side chains of arginine, lysine, histidine, and the small portion of free amino groups at the ends of the peptide chains. The characteristic of anionic groups is due to the side chains of aspartic, glutamic acid and carboxyl end groups.

Figure 1.5 represents the condensation process of amino acids in proteins. The amino acid residues are joined together by peptide bonds. After a number of these condensation reactions it ultimately produces a high molecular weight protein, such as keratin.

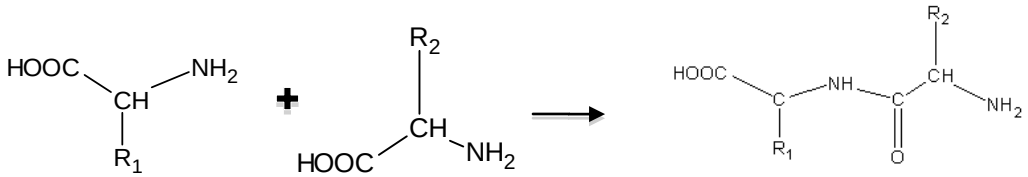

Figure 1.5: The condensation reaction of amino acids (Creighton, 1993)

Chemically, all ethnic hairs are found to have similar protein structure and composition, (Menkart, 1984, Dekio, 1988a, Nappe, 1989, Dekio, 1990b). Although the quantities and types of amino acids differ slightly between individuals, their ratios are very

similar. Table 1.2 gives an example of the amino acids present in hair and their relative quantities.

Table 1.2: Typical amino acid composition of human hair. The analysis varies slightly between individuals (Nishikawa, 1998)

Amino Acid	% of Total Residues	Amino Acid	% of Total Residues
Lysine	2.7	Proline	8.4
Histidine	0.9	Glycine	6.4
Arginine	5.8	Alanine	4.6
Aspartate + Asparagine	4.9	Half-cystine	17.8
Threonine	6.8	Valine	5.8
Serine	11.7	Methionine	0.6
Glutamate + Glutamine	11.4	Isolucine	2.6
Leucine	5.8	Tyrosine	2.0
Phenylalanine	1.6		
Total	99.8		

It is obvious that the majority composition of amino acids in human hair is glutamic acid, serine and cystine (shown as half-cystine), they make up 11.4%, 11.7% and 17.8% of hair protein, respectively. Cystine is a dimeric amino acid formed by the oxidation of two cysteine residues that covalently linked by two sulphur atoms, generating a very strong bond, known as a disulphide linkage. Cystine residues provide the stability to hair except during chemical processes, such as reduction, oxidisation, hydrolysis and weathering. The differences in cystine content between various structures in human hair result in the significant differences in their physical properties.

The primary chemical difference between bleached hair and virgin hair is a lower cystine content, a higher cysteic acid content, and lower amounts of tyrosine and methionine in the bleached hair (Robbins, 2002). This result is in good agreement with Zahn's original conclusion that the bleaching agents react with human hair protein primarily at the disulphide bonds (Zahn, 1966).

It is interesting to observe that morphological components in hair can be classified as a series of hierarchical two-phase composites (microfibril and intermicrofibrillar matrix;

macrofibril and intermacrofibrillar matrix; exocuticle and endocuticle; cortex and cuticle). Different types of protein in the hair are found in these various phases (Swift, 1997b).

The cuticle of human hair contains a large percentage of cystine, cysteic acid, proline, serine, threonine, isoleucine, methionine, leucine, tyrosine, phenylalanine, and arginine, but only little tryptophan and histidine compared to the other layers of the hair shaft (Bradbury, 1966). Also the cuticle includes a low but important amount of the fatty acids, 18-methyleicosanoic acid (18-MEA), which is responsible for the water repellent behaviour of the surface. And the protein portion of the cell membrane complex (CMC) was found to be rich in the dicarboxylic amino acids, namely, aspartic acid, and glutamic acid.

There is less cystine in the cortex than in the cuticle, but the cortex is richer in diacidic amino acids, lysine, and histidine. In the cortex, the intermediate filaments and the matrix are discriminated by their chemical compositions. The intermediate filaments have a high content in leucine, glutamic acid, and those amino acids which are generally present in α-helical proteins, but small amounts of cystine (~6%), lysine, and tyrosine (Fraser, 1972). Comparatively the matrix is rich in cystine (about 21%, calculated from the sulphur content of γ-keratose of human hair), proline, and those amino acids that are adverse to the helix formation such as in KAP proteins (Robbins, 2002).

The medulla has a poor solubility, and is thus difficult to isolate. Blackburn showed, in a good agreement with Rogers's results, that the medulla has a low cystine content and relatively large amounts of acidic and basic amino acids (Blackburn, 1948, Roger, 1964). These observations suggest that the medulla will be more susceptible to reactions with acids and alkalis and to ion exchange reactions such as reactions with anionic and cationic surfactants, ionic dyes and metals. But the medulla will be less sensitive to reaction with reducing agents (Robbins, 2002).

1.2.2 Water

Water is an important component of keratin fibres. Its content plays a critical role in determining the physical and cosmetic properties of human hair (Robbins, 2002). The

moisture content in a keratin fibre depends on the relative humidity (RH) (Downes, 1961). A virgin hair can absorb more than 30% of its own weight of water, but it can reach 45% when it is damaged. Hair length can increase by 2% and its diameter by 15% to 20% through the absorption of water. It should be noted that the process of absorption is very rapid, 75% of the maximum possible amount of water is absorbed within 4 minutes.

Water is a highly polar molecule, it interacts with the hydrogen bonds and other polar groups in the α-keratin chains. Two types of water are associated with the α-keratin protein, absorbed or "bound" water and adsorbed or "free" water. At low humidities, below 25%, water molecules are principally bonded to hydrophilic side chains (guanidine, amino, carboxyl, phenolic, etc) and peptide bonds through hydrogen bonds and Columbic interactions. With increasing humidity, additional water is absorbed, water enters as "solution water", resulting in a decrease in the energy of binding of water already associated with the protein. At very high % RH (>80%), multi-molecular sorption (water-on-water) occurs, and this refers to the "free" water interacting and condensing onto the first "bound" layer (Robbins, 2002).

1.2.3 Lipids

Lipids from human hair mainly include cholesterol esters (ChE), free fatty acids (FFA), cholesterol (Ch), ceramides (Cer) and cholesterol sulphate (ChS). Some of them (ChE and FFA) result from sebum attributable to the sebaceous glands, whereas others (Ch, Cer, ChS and additional FFA) are ascribed to the intrinsic constitutive lipids biosynthesised in hair matrix cells (CMC). They are known as surface (external) lipids and internal lipids, respectively. In addition, a part of the internal lipids is free lipid, and another part is structural lipid of the cell membrane complex (Robbins, 2002).

Internal lipids are the principal constituent of cell membrane lipids (Hilterhaus-Bong, 1989, Körner, 1995), which contribute to the formation of a stable and strong CMC. The CMC has a barrier function (Swartzendruber, 1989, Grubauer, 1989), and acts as a protective layer, preventing external materials from penetrating the hair fibre.

Some researcher have confirmed that hair lipids have an influence on physicochemical phenomena such as diffusion, cell cohesion and mechanical strength (Nishimura, 1989, Sideris, 1990, Braida, 1994, Philippe, 1995), despite their low content (1–9% dry weight) compared to proteins (>90%).

1.2.4 Pigments

Hair pigments, which give the colour to hair, are mainly concentrated in the cortex as melanins. Melanin is produced by a group of specialised cells called melanocytes. These cells exist near the hair bulb and are present in the form of discrete granules, referred to as pigment granules. Pheomelanin and eumelanin are the two types of basic pigments. Their chemical structures are presented in Figure 1.6.

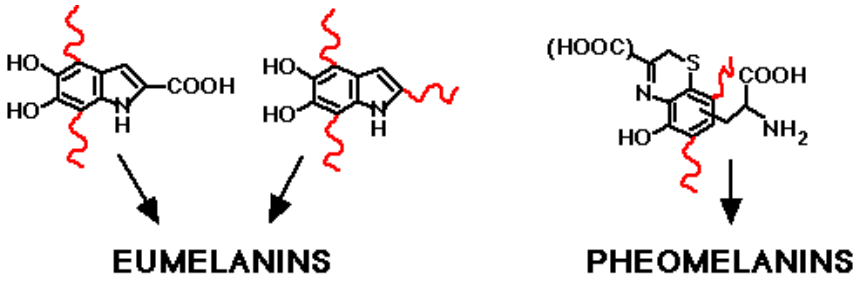

Figure 1.6: Chemical structures of eumelanins and pheomelanins (Colbert, 2004). Curly red lines indicate sites of attachment to the extended polymer or proteins.

Pheomelanin is the most common melanin in the Caucasian hair, which is responsible for the lighter colours such as red and fair. It is soluble in aqueous alkali, trifluoroacetic acid, formic acid, and several highly polar organic solvents. Eumelanin, which produces the dark shades such as brown and black, contains nitrogen (6-9%) but insignificant amounts of sulphur (0-1%) and is insoluble in solvents and chemically resistant to all but powerful oxidizing agents, such as hydrogen peroxide. The ratio between two pigments determines the hair colour (Robbins, 2002). Vincensi et al. (1998) studied red hair, observing that the amounts of pheomelanin and eumelanin vary with sex, age and colour shade. However, the absence of either type of melanin results in white hair.

1.2.5 Chemical Elements

In terms of the chemical elements, hair is composed of 50.7% carbon, 20.9% oxygen, 17.1% nitrogen, 6.4% hydrogen and 5.0% sulphur. Trace elements contained in the hair are magnesium, arsenic, iron, chromium and other metals and minerals. Most of them are incorporated in the hair from extraneous sources and probably integrated into the fibre structure by salt linkages or as coordination complexes with side chains of pigments and/or proteins.

1.3 Bonding Mechanisms in Keratin

In the α-keratin structure, stability is determined by a variety of bonding mechanisms, which is shown in Figure 1.7. Except the strong covalent disulphide bonds, other weaker interactions such as coulombic interactions between side chain groups, hydrogen bonds between neighbouring groups, van der Waal's interactions, isodipeptide bridges between segments of two hypothetical peptide chains and, in the presence of water, hydrophobic bonds also contribute to its stability (Zviak, 1986, Feughelman, 1997, Johnson, 1997).

The covalent disulphide (-S-S) linkages are formed by an oxidation reaction between adjacent thiol (-S-H) groups of opposing cysteine molecules in the polypeptide chain, thereby resulting in the formation of cystine (Johnson, 1997, Williams, 1994), which contributes significantly to the physical and chemical properties of hair keratin (Feughelman, 1997).

Coulombic interactions, also refer as salt links, are electrostatic forces, acting between ionised acidic and basic side chain residues, i.e. the negatively charged carboxylic acid groups ($-COO^-$) and positively charged amino groups ($-NH3^+$) (Zviak, 1986, Johnson, 1997, Feughelman, 1997). These charged groups exist under neutral pH conditions. At high pHs with an excess of OH^- present $-NH_3^+$ converts to $-NH_2$ while at low pHs with an excess of hydrogen ions present $-COO^-$ forms $-COOH$. The coulombic interactions thus disappear at both above conditions.

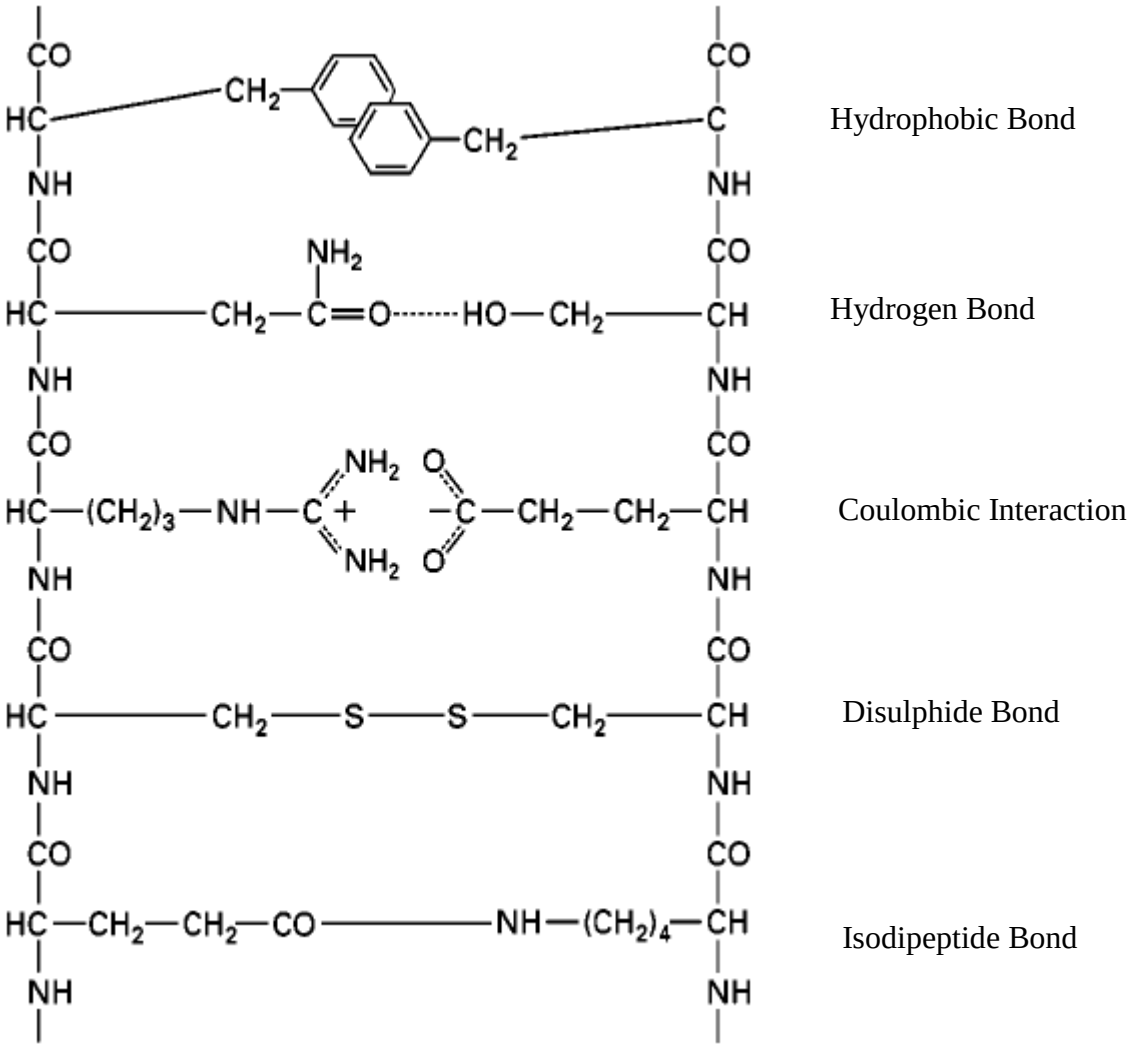

Figure 1.7: Structural formula of a fictive peptide chain to illustrate five important interactions between amino acid side-chains in keratins (Zahn, 2003).

There are two types of hydrogen bonding which exist in the α-keratin structure. One type (─O…H─O─) corresponds to the bonding between water molecules and hydroxyl groups and another type (─O…H─N─) is present between the amide ─NH and the carbonyl group as well as the amide C=O of side chains (see Figure 1.8). Hydrogen bonds play a central role for the stabilisation of the α-helical structure in keratin.

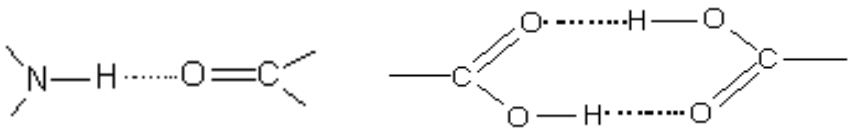

Figure 1.8: Typical hydrogen bonds involving the atoms of oxygen and nitrogen (Feughelman, 1997)

Van der Waal's forces (or van der Waal's interaction), are involved in the cohesive bonding of the chains and side chains of α-keratin fibres, which provide molecular stability. Finally, hydrophobic bonds (only in the presence of water) have the specialised capacity of binding the single α-helices into double α-helical ropes, which ultimately form intermediate filaments (Feughelman, 1997). Both van der Waal's forces and hydrophobic bonds have a non-directional action. Since they are long-range weak forces, these bonds are susceptible to breakdown and reformation.

An isodipeptide bridge is formed by the reaction between glutamic acid and lysine. A second covalent bridge, though relatively rare, is caused by the isodipeptide Nε-(γ-glutamyl) lysine residue which provides an additional stabilising effect in the resistant cell membranes and the cuticle (Zahn, 2005).

1.4 The Keratin-Water System

Feughelman (1959) suggested a 2-phase model for the keratin fibre, in which water-impermeable microfibrils (phase C) are embedded in a water-penetrable matrix (phase M), as shown in Figure 1.9. This two-phase model plays an important role in explaining the chemical and physical properties of α-keratin fibres and their changes with moisture content.

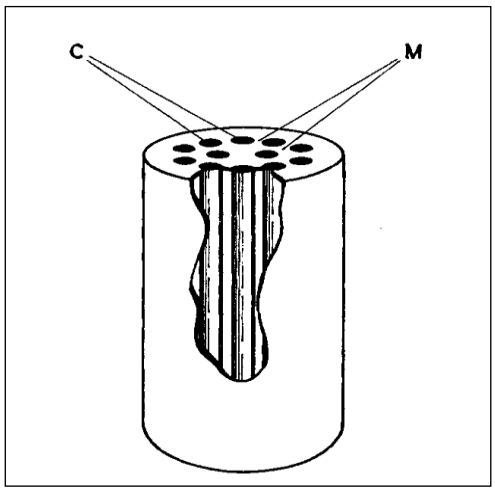

Figure 1.9: Cylindrical two-phase model of an α-keratin fiber consisting of rigid water-impenetrable phase C set parallel to the fiber axis, embedded in the matrix phase M, which is water-penetrable (Feughelman, 1959).

Due to the two-phase model, a dried hair, which is absorbing water from the liquid state, must continuously adjust its swollen outer annular layer to adapt to the swelling which happens inside the cylindrical fibre. The water penetrable phase M swells in the presence of water, whereas the water impenetrable phase C stays unchanged.

Phase C has been identified as the crystalline α-helical structure present in the microfibrils or filaments. Since phase C is arranged parallel to the fibre axis for the fibre, swelling in water mainly occurs in the diametral direction.

1.5 Chemical Treatments

Common hair chemical treatments include reducing hair, such as permanent waving, and oxidizing hair, such as bleaching and dying. A permanent wave treatment reduces the cystine disulphide bond, and then reforms the bonds with the oxidising agent. Bleaching and dying treatments oxidise cystine and other amino acids with alkaline hydrogen peroxide. Hair damage caused by these chemical treatments, altering the chemical and physical properties of the α-keratin fibre, can be discriminated from untreated fibre. Currently, bleaching damage effects on hair samples in terms of physical and chemical properties are of particular interest.

1.5.1 Bleaching Principle

The objective of bleaching is to oxidise the hair pigments in the cortex and thereby to lighten the natural hair shade by an irreversible chemical reaction. Bleaching relies upon oxidative destruction of the highly conjugated system of the indole residues of the melanins. The melanin still exists in the bleached hair, but appears colourless. The bleaching agent reacts more readily with the dark eumelanin pigment than with the pheomelanin, so some gold or red residual colour may remain. Additionally, bleached hair displays a pale yellow tint due to the natural yellow colour of keratin (Robbins, 2002).

Bleaching is applied through a mixture of several components, where the primary chemical is hydrogen peroxide. Hydrogen peroxide, as the most common oxidising agent, is adopted because it oxidises the melanin faster than proteins so colour lightening can be achieved faster to prevent further protein damage (Robbins, 2002). Generally, the higher the hydrogen peroxide concentration, the greater the changes in hair colour. A bleaching formula usually contains 6 - 12% of hydrogen peroxide combined with a booster such as ammonium and potassium persulphates. Ammonia is employed to open the outer layer of the hair cuticle, which allows the peroxide to oxidise the melanin. The pH is around 10 and stabilisers (e.g. sequestrants) are often used to reduce the rate of decomposition of the peroxide to provide satisfactory shelf life. During bleaching some keratin dissolves, however the weight losses are very small (Wolfram, 1970b).

Wolfram et al. (1975) confirmed that the melanin pigments encapsulated within the granules are not accessible to oxidising agents, unless the granules are degraded or solubilised. The bleaching process follows two steps, first, a fast dissolution step occurs in which the pigment granules are dispersed and dissolved by hydrogen peroxide. Hydrogen peroxide is not as strong an oxidising agent as permanganate or peracetic acid, but it is actually more effective for dissolving the granules (Robbins, 2002). It is worth pointing out that the disintegration of the pigment granules and their solubilisation are not likely to affect the colour of hair significantly (Wolfram, 1970b). After the granules are dissolved, this is then followed by a much slower decolouration step, which determines the overall bleaching rate. The pigment granules are distributed within the cortex. As a consequence of the decolouration of the melanin, an oxidation effect also takes place in the keratin, and this is often referred to as “oxidative or bleaching” damage (Wolfram, 1970b). After the progressive treatment time, the melanin granules were dissolved by the peroxide, leaving most of the granular cavities empty. This makes hairs more porous which will hence absorb larger amounts of water (Johnson, 1997). Besides, although persulphate is not as strong an oxidant as hydrogen peroxide, persulphate mixed with peroxide is more effective than peroxide alone (Robbins, 2002). Thus, persulphate and peroxide complement each other in terms of their ability to bleach melanin pigment in human hair.

As described previously (Section 1.2.1), hair is primarily a proteinaceous fibre. Strongly oxidising alkaline solutions thus not only act on the melanin itself, but also attack the accessible reaction sites of the protein. This results in weakening of the cell membrane complex, oxidation of the cystine residues of the matrix in the cortex and of other hair components, which are rich in cystine, such as A-layer and exocuticle. As a result, the bleached fibre becomes more brittle, drier, rougher and weaker, and is more susceptible to breakage. In addition, bleaching leads to a lower cross-link density and thus increases any hydrophilic property, due to anionic site formation e.g. cysteic acid residue (Jachowicz, 1987, Johnson, 1997).

1.5.1.1 The Disulphide (S-S) Cleavage Mechanism

The bleaching reaction between keratin and H_20_2 is defined mainly by the cystine residues. The decrease in cystine is almost quantitatively matched by a corresponding increase in cysteic acid. Figure 1.10 presents the oxidation cleavage of the disulphide bond during the chemical bleaching. Complete oxidation of cystine residues yields cysteic acid residues or sulphonic acid residues ($-SO_3H$), but other oxidative intermediates are also formed under controlled conditions of oxidation, such as the cystine monoxide (-SO-S-) and cystine dioxide ($-SO_2$-S-).

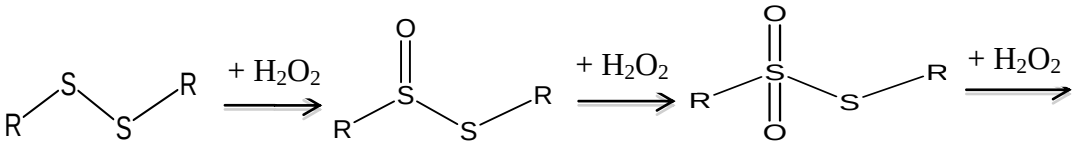

Cystine Residues Cystine Monoxide Cystine Dioxide

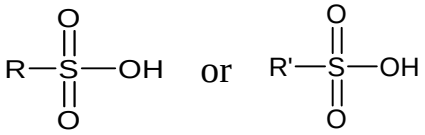

R/R': side-chain of different structure

Cysteic Acid Residues/Sulphonic Acid Residues

Figure 1.10: Scheme of the S-S cleavage mechanism for the bleaching process (Robbins, 1971)

1.6 Objectives

The aim of this PhD study is to examine keratin surface and structural change caused by various bleaching treatments (oxidation) and to interpret the interrelations between the properties by numerous methods. In this work, untreated and three types of bleached human hairs (6% H_20_2 bleach, 9% H_20_2 commercial bleach and commercial persulphate bleach (contains 9% H_2O_2)) were characterised by a multidisciplinary approach using Differential Scanning Calorimetry (DSC), Fourier Transform Infra-Red Spectroscopy (FTIR) with Attenuated Total Reflectance technique (ATR) and Transmission, Scanning Electron Microscopy (SEM) and Reflective spectrophotometry.

Reflective spectrophotometry is employed to determine the colour changes of bleached hair.

Thermal analysis by DSC will be used to measure the denaturation and decomposition behaviour of both untreated hair and treated hair over a range of temperatures compared to a reference. A kinetic study of the denaturation process is also performed.

Attenuated reflectance (ATR) and transmission modes of FTIR spectroscopy are introduced to characterise and quantify oxidation of treated hair of cysteic acid with respect to the formation.

The morphological changes of the cuticle surface topography as a consequence of damage processes are assessed by means of SEM.

The data obtained from each method will be compared to illustrate how different oxidation treatments affected the hair samples. There are various treatment factors which affect the oxidation results, such as temperature, pH, peroxide volume, humidity etc, but the effect of bleaching time was the most obvious factor when compared with other bleaching parameters (Yuen, 2009), thus the investigation of oxidative duration is of special interest.

1.7 Reference

ASQUITH, R. S. 1977. *Chemistry of Natural Protein Fibers,* New York, Plenum Press.

BHUSHAN, B. 2010. *Biophysics of Human Hair: Structural, Nanomechanical, and Nanotribological Studies,* Springer.

BLACKBURN, S. 1948. The composition and reactivity of medullated keratin. *Biochemistry Journal,* 43**,** 114-117.

BRADBURY, J. H. 1973. The Structure and Chemistry of Keratin Fibers. *Advances in Protein Chemistry,* 27**,** 111-211.

BRADBURY, J. H., CHAPMAN, G.V., HAMBLY, A.N., KING, N.L.R., 1966. Separation of Chemically Unmodified Histological Components of Keratin Fibres and Analyses of Cuticles. *Nature,* 210**,** 1333-1334.

BRAIDA, D., DUBIEF, C., LANG, G., HALLEGOT, P., 1994. Ceramide: a new approach to hair protection and conditioning. *Cosmetics and toiletries,* 109**,** 49-57.

COLBERT, A., SCHOLAR, M., 2004. Towards Probing Skin Cancer using Endogenous Melanin Fluorescence. *The Penn State Manair Journal* 11**,** 8-15.

CREIGHTON, T. E. 1993. *Proteins: Structures and Molecular Properties,* New York, W.H.Freeman and Company.

DEKIO, S., JIDOI, J., 1988. Hair low-sulfur protein composition does not differ electrophoretically among different races. *The Journal of Dermatology,* 15**,** 393-396.

DEKIO, S., JIDOI, J., 1990. Amount of fibrous and matrix substances from hair of different races. *The Journal of Dermatology,* 19**,** 62-64.

DOWNES, J. G. 1961. The Attainment of a Defined State of Dryness in Accurate Determinations of the Regain of Wool Samples. *Textile Reseach Journal,* 31**,** 66.

FEUGHELMAN, M. 1959. A Two-Phase Structure for Keratin Fibers. *Textile Reseach Journal,* 29**,** 223.

FEUGHELMAN, M. 1997. *Mechanical Proeprties and Structure of Alpha-Keratin Fibres: Wool, human hair and related fibres,* University of New South Wales Press.

FRASER, R. D. B., MACRAE, T.P., ROGERS, G.E., 1972. *Keratins : their composition, structure and biosynthesis,* USA, Charles C Thomas.

GRUBAUER, G., FEINGOLD, K.R., HARRIS, R.M., ELIAS, P.M., 1989. Lipid content and lipid type as determinants of the epidermal permeability barrier. *Journal of Lipid Research,* 30**,** 89-96.

HALL, K., WOLFRAM, L.J., 1975. Isolation and identification of the hair protein component of hair melanin. *Journal Cosmetic Chemists,* 26**,** 247.

HILTERHAUS-BONG, S., ZAHN, H., 1989. Contributions to the chemistry of human hair. II. Lipid chemical aspects of permanently waved hair. *International Journal of Cosmetic Science,* 11**,** 167-174.

JACHOWICZ, J. 1987. Hair damage and attempts to its repair. *Journal of the Society of Cosmetic Chemists,* 38**,** 263-286.

JOHNSON, D. H. 1997. *Hair and Hair Care,* New York, Marcel Dekker, Inc,.

KÖRNER, A., PETROVIC, S., HOCKER, H., 1995. Cell Membrane Lipids of Wool and Human Hair Form Liposomes. *Textile Research Journal* 65**,** 56-58.

KREPLAK, L., BRIKI, F., DUVAULT, Y., DOUCET, J., MERIGOUX, C., LEROY, F., LÉVÊQUE, J. L., MILLER, L., CARR,G. L., WILLIAMS, G. P., DUMAS, P., 2001. Profiling lipids across Caucasian and Afro-American hair transverse cuts, using synchrotron infrared microspectrometry. *International Journal of Cosmetic Science,* 23**,** 369-374.

MACLAREN, J. A., MILLIGAN, B., 1981. *Wool Science: The chemical reactivity of the wool fibre,* Merrickville, Science Press.

MARHLE, G., ORFANOS, G.E., 1971. The spongious keratin and the medulla of human hair. *Archives of Dermatological Research,* 241**,** 305-316.

MENKART, J., WOLFRAM, L.J., MAO, I., 1984. Caucasian hair, Negro hair, and wool: similarities and differences. *Journal Society Cosmetic Chemists,* 35**,** 21-43.

NAGASE, S., SHIBUICHI, S., ANDO, K., KARIYA, E., SATOH, N., 2002. Influence of internal structures of hair fiber on hair appearance. I. Light scattering from the porous structure of the medulla of human hair. *Journal of Cosmetic Science,* 53**,** 89-100.

NAPPE, C., KERMICI, M., 1989. Electrophoretic analysis of alkylated proteins of human hair from various ethnic groups. *Journal Society Cosmetic Chemists,* 40**,** 91-99.

NISHIKAWA, N., TANIZAWA, Y., TANAKA, S., HORIGUCHI, Y., MATSUNO, H., ASAKURA,T., 1998. PH Dependence of the Coiled-coil Structure of Keratin Intermediate Filament in Human Hair by 13C NMR Spectroscopy and the Mechanism of Its Disruption. *Polymer Journal* 30**,** 125-132.

NISHIMURA, K., NISHINO, M., INAOKA, Y., KITADA, Y., FUKUSHIMA, M., 1989. Interrelationship between the hair lipids and the hair moisture. *Nippon Koshohin Kagakkaishi,* 13**,** 134-139.

PARRY, D. A. D., FRASER, R.D.B., 1985. Intermediate filament structure: 1. Analysis of IF protein sequence data. *International Journal of Biological Macromolecules,* 7**,** 203-213.

PHILIPPE, M., GARSON, J.C., GILARD, P., HOCQUAUX, M., HUSSLER, G., LEROY, F., MAHIEU, C., SEMERIA, D., VANLERBERGHE, G., 1995. Synthesis of 2-N-oleoylamino-octadecane-l,3- diol: a new ceramide highly effective for the treatment of skin and hair. *International Journal of Cosmetic Science* 17**,** 133-146.

ROBBINS, C. R. 1971. Chemical Aspects of Bleaching Human Hair. *Journal of the Society of Cosmetic Chemists, ,* 22**,** 339-348.

ROBBINS, C. R. 2002. *Chemical and Physical Behavior of Human Hair,* New York,, Springer-Verlag.

ROGER, G. E. 1964. Structural and Biochemical features of the Hair Follicle. *In:* MONTAGNA, W., LOBITZ, W. C., (ed.) *The epidermis.* New York: Academic Press.

RUETSCH, S. B., KAMATH, Y., WEIGMANN, H.D., 2001. Photodegradation of Human Hair: A Microscopy Study. *In:* GIACOMONI, P. U. (ed.) *Sun Protection in Man.* Amsterdam: Elsevier Science.

SIDERIS, V., HOLT, L. A., LEAVER, I. H., 1990. A microscopical study of the pathway for diffusion of rhodamine B and octadecylrhodamine B into wool fibres. *Journal of the Society of Dyers and Colourists,,* 106**,** 131-135.

SWARTZENDRUBER, D. C., WERTZ, P. W., KITKO, D. J., MADISON, K. C., DOWNING, D. T., 1989. Molecular models of the Intercellular Lipid Lamellae in Mammalian Stratum Corneum. *Journal of Investigative Dermatology,* 92**,** 251–257.

SWIFT, J. A. 1997a. *Fundamentals of Human Hair Science,* Weymouth Dorset, Micelle Press.

SWIFT, J. A. 1997b. Morphology and histochemistry of human hair. *In:* JOLLES, P., ZAHN, H., HOCKER, H., (ed.) *Formation and Structure of Human Hair.* Berlin: Birkhauser Verlag.

SWIFT, J. A., SMITH, J. R., 2001. Microscopical investigations on the epicuticle of mammalian keratin fibres. *Journal of Microscopy,* 204**,** 203-211.

VINCENSI, M. R., D'LSCHIA, M., NAPOLITANO, A., PROCACCINI, E. M., RICCIO, G., MONFRECOLA, G., SANTOIANNI, P., PROTA, G., 1998. Phaeomelanin versus eumelanin as a chemical indicator of ultraviolet

sensitivity in fair-skinned subjects at high risk for melanoma: a pilot study. *Melanoma Research,*, 8.

VOET, D., VOET, J.G., PRATT, C. W., 2008. *Fundamentals of Biochemistry: Life at the molecular level,* New York, John Wiley & Sons.

WILLIAMS, A. C., EDWARDS, H. G. M., BARRY, B. W., 1994. Raman spectra of human keratotic biopolymers: Skin, callus, hair and nail. *Journal of Raman Spectroscopy,* 25**,** 95-98.

WOLFRAM, L. J. 2003. Human Hair: A unique physicochemical composite. *Joural American Academy of Dermatology,* 48**,** 106-114.

WOLFRAM, L. J., HALL, K., HUI, I., 1970. The Mechanism of Hair Bleaching. *J. Soc. Cosmet. Chem,* 21**,** 875-900.

YUEN, C. W. M., KAN, C.W., LAU, K.W., CHOW, Y. L., 2009. Effect of Different Human Hair Bleaching Conditions on the Hair coloration with Hair Boosting Shampoo as Colorant. *Fibers and Polymers,* 10**,** 709-715.

ZAHN, H., WORTMANN, F. J., WORTMANN, G., SCHAEFER, K., HOFFMANN, R., FINCH, R., 2003. Wool. *Ullmann's Encyclopedia of Industrial Chemistry.* Weinheim, Germany: Wiley-VCH Verlag.

ZAHN, H., WORTMANN, F. J., HÖCKER, H., 2005. Considerations on the occurrence of loricrin and involucrin in the cell envelope of wool cuticle cells. *International journal of sheep and wool science,* 53**,** 2.

ZAHN, H. J. 1966. Chemical Vorgiinge in the bleaching of wool and human hair with hydrogen peroxide and peroxysiiuren. *Society of Cosmetic Chemists,* 17**,** 687-701.

ZVIAK, C. 1986. *The Science of Hair Care,* New York, Marcel Dekker.

Chapter 2 Sample Preparation

2.1 Sample Material

Two batches of virgin Caucasian commercial hairs were used for the studies (Kerling, Germany) to perform the oxidation reaction, namely hair batch I (13cm long) and hair batch II (18cm long). Three treatments of the hair samples were studied and are referred as: 6% H_2O_2 bleached hair, 9% H_2O_2 commercial bleached hair, and commercial persulphate (contains 9% H_2O_2) bleached hair. Particularly, hair batch I was used for the oxidative treatment of 6% H_2O_2 and 9% H_2O_2 commercial bleach, and hair batch II was introduced for the use of commercial persulphate bleach (contains 9% H_2O_2). Hairs are oxidised for bleaching times of 1/2h, 1h, 1½h, 2h, 2½h, 3h, 3½h and 4h, respectively, with fresh bleaching solution every half an hour.

2.2 Bleaching Products & Procedures

2.2.1 Bleaching Products

2.2.1.1 6% H_2O_2 Bleaching

6% laboratory-grade H_2O_2 was prepared; pH was adjusted with NH_4OH to around 10.2 in this experiment. All bleaching treatments were done at room temperature with a liquid: fibre ratio of 400:1 (hair tress ~ 250mg, bleaching solution ~ 100ml)

2.2.1.2 9% H_2O_2 Commercial Bleaching

9% H_2O_2 commercial bleaching developer was prepared (Henkel, Germany); pH was adjusted with NH_4OH to around 10.2 in this experiment. The commercial developer recipe is described as below:

Developer (IGORA Royal 20 vol 9% H_20_2 bleaching lotion, Schwarzkopf)

Aqua (Water), Hydrogen Peroxide (9%), Cetearyl Alcohol, Propylene Glycol, Ceteareth-20, Steartrimonium Chloride, Paraffinum Liquidum (Mineral oil), Etidronic Acid, 2,6-Dicarboxypyridine, Disodium Pyrophosphate, Pottassium Hydroxide, Parfum (Fragrance), Sodium Benzoate

2.2.1.3 Commercial Persulphate Bleaching

The bleaching powder and 9% H_2O_2 commercial bleaching developer (Henkel, Hamburg, Germany) were mixed with a ratio of 1:2. The bleach powder recipe is described as below:

Dust-free bleach powder for controlled lightening (IGORA Vario Blond Plus bleaching powder, Schwarzkopf)

Potassium Persulphate, Magnesium Carbonate Hydroxide, Sodium Metasilicate, Paraffinum Liquidum, Ammonium Persulphate, Cellulose Gum, Silica, Acrylates Copolymer, Triticum Vulgare Starch, Disodium EDTA, Calcium Stearate, Hydrolysed Keratin, Sodium Starch Octenylsuccinate, Sodium Hexametaphosphate, Parfum, CI 77007

2.2.2 Bleaching Procedure

2.2.2.1 6% H_2O_2 Bleaching

The hair samples were bleached in the prepared solution. Once the oxidative treatment was accomplished, bleached samples were rinsed immediately under running tap water for 3-5 minutes, subsequently 500ml tap water were prepared and the rinsing water was changed every 30 mins. The water pH was recorded before and after this change. This process aimed to remove unfixed bleach from the hair. When the value of pH was stable, the hair samples were dried under ambient room conditions overnight before further investigations.

2.2.2.2 9% H_2O_2 Commercial Bleaching

The freshly prepared bleaching solution was applied to the dry hair sample evenly from root to tip using a brush. Each hair sample was covered by aluminium foil to avoid evaporation and the chemical reaction with air. The bleaching solution was changed every 30 mins to achieve optimum bleaching effect.

Samples were rinsed with warm water for 5 mins between each change of the bleaching solution until the required treatment time had been achieved. After the whole procedure, the hair tresses were rinsed with warm water to remove all the remaining bleaching mixture for 5 mins, and then were dried under ambient room conditions overnight before further investigations.

In addition, hair samples, which were bleached for 3½h and 4h, were rinsed with water overnight.

2.2.2.3 Commercial Persulphate Bleaching

The required amount of bleaching powder and bleaching developer were put into a bowl and mixed together before use. The bleaching mixture was applied to hair evenly from root to tip using a brush. Each hair sample was covered by aluminium foil to avoid evaporation and the chemical reaction with air. The bleaching paste was changed every 30 mins to achieve optimum bleaching effects. The hair tresses were turned over every 6 mins to assist the even application of the cream.

Samples were rinsed with warm water for 5 mins between each change of bleaching cream until the required treatment time had been achieved. After the whole procedure, the hair tresses were rinsed with warm tap water to remove all the remaining bleaching mixture for 5 mins and were dried at ambient room temperature overnight before further investigations.

In addition, hair samples, which were bleached for 3½h and 4h, were rinsed with water overnight.

Chapter 3 SEM Investigation of the Surface Properties of Human Hair

3.1 Introduction

Although the cuticle accounts for only 10% by weight of the hair fibre, it plays a protective role for the cortex against mechanical, chemical and thermal damage (Swift, 1999) and is responsible for the surface properties of the fibre. Thus the effect of cosmetic treatments on the cuticle has been of great interest for the cosmetics industry (Robbins, 1994).

3.1.1 Evaluation Method for Surface Properties

Numerous techniques have been used to study the properties of the hair cuticle, including scanning electron microscopy (SEM) (Poletti, 2003), transmission electron microscopy (TEM) (Swift, 2001a), X-ray photoelectron spectroscopy (XPS) (Dalton, 2000), atomic force microscopy (AFM) (Smith, 1998, Poletti, 2003, Gurden, 2004), confocal microscopy (Corcuff, 1993), microdiffraction (Kreplak, 2001b), secondary ion mass spectrometry (Gillen, 1999), goniometry (Feughelman, 2001) and lateral force microscopy (LFM) (McMullen, 2001).

3.1.1.1 Scanning Electron Microscopy (SEM)

SEM is the standard method for examining the surface topography of human hair. SEM images, using the electrons reflected from a specimen, provide topographical (surface features of an object), morphological (shape and size of the particles making up the object) and compositional (the elements and compounds that the object is composed of and the relative amounts of them) information regarding the hair sample.

Because the SEM generally utilises vacuum conditions and uses electrons to form an image, sample preparation is necessarily required for SEM measurements. Since hair fibres are a non-metal material, it must be covered with a very thin layer of a conductive material to prevent charging by the electrons. This coating process is called "sputter coating". Both metallisation and measurement needs to be operated under vacuum, but surface metallisation and vacuum exposure could potentially cause modifications to the surface details (Poletti, 2003).

3.1.1.1.1 Advantages and Disadvantages of SEM

The SEM was chosen for this study because its micrographs contain much more topographical information than other microscopic techniques (Dibianca, 1973). The produced images reveal surface structural details over a wide range of magnifications. Even at a relatively low magnification, the SEM still has advantages for hair characterisation compared to light microscopy, such as a clear view of cuticle uplift or surface breakage (Dibianca, 1973).

Most SEMs are comparatively easy to operate. In addition, its relatively short data acquisition time (less than 5 minutes/image), highly portable digital data format, much enhanced resolution, a large depth of focus and the greater magnification, result in the SEM having substantial advantage over other microscopic techniques. SEM is, however, not able to reproduce colour and can only provide limited quantitative data regarding the surface.

Light microscopy has an advantage over electron microscopy that it can be used for observing internal structures, i.e. medulla and pigmentation, which are also very individual features for hair fibres (Kadikis, 1987, Palenik, 1983, Sich, 1990). As a result, Sich (1990) concluded that electron microscopy and light microscopy could be employed in a complementary manner for the study of topographical features and internal structures of hair fibres, respectively.

3.1.2 The SEM Investigation of Human Hair

The surface characteristics of the cuticle cells, such as scale shape, height, and distribution, are considered to be unique to each hair fibre, thus, SEM is employed to identify, distinguish and classify the different keratin fibres by measuring the step height (the height of one cuticle relative to the adjacent one) of the cuticle scale edge. (Kadikis, 1987, Langley, 1981, Wortmann, 1986).

However, one of the main problems of the analysis of human hair is the difficulty of representative sampling, because the variability of the surface architecture, distribution and appearance of the scales for hairs from one head are already indefinite, due to the natural and cosmetic history (Dibianca, 1973). Additionally, variation is caused by differences in the region of the head, from which they originate, and differences along the length of the fibre from root to tip, as a result of the natural weathering process (e.g. exposure to sunlight) (Brown, 1974) and the personal grooming habits (e.g. brushing), to which hairs are subjected (Gurden, 2004). Consequently, the use of imaging to determine the change of the surface on the hair should consider two factors: (a) compare hair samples from the same regions and (b) measure as many images as necessary to achieve a representative description (Gurden, 2004).

3.2 Objectives

The investigation of the surface topography of both untreated and chemically treated human hairs at a microscopic level has provided a basis for the understanding of damaged keratin fibre on a structural level. The prime objective of the SEM investigation is to explore a method for establishing the extent of damage from oxidative treatments. For the surface property investigation, the feasibility of the "Knot Test" method is investigated to assess numerically the effects of the various bleaching treatments on the conditions of the hairs. The morphological changes of hair fibres were determined by the "Knot Test" methodology as a function of the severity of the treatment of the hair.

For this study, three types of hair fibre were analysed:

(1) Untreated fibres with little damage to the cuticle

(2) Mildly bleached fibres, which show moderate chipping and jaggedness of the cuticle edges

(3) Heavily bleached fibres, which display the largest extent of damage to the cuticle

3.3 Experimental

Swift and Smith (2000) verified that different features of the hair fibre surface gradually change along its length from root to the tip of the fibre. Although hair length and diameter varied in all hair samples, the characteristic morphology showed little variation for any individuals. Virgin and three types of bleached hairs were examined in this study in order to investigate the differences between complete and weakened cuticle cells. The untreated hairs are considered as standard and are defined as having an intact cuticle and absence of chemical damage. The bleaching conditions are described in the Chapter 2.

Most human hairs are assumed to have a similar damage stage in the middle part of the hair length, thus the SEM experiments were conducted on the middle parts of the hair samples. Ten fibres per tress were randomly selected and knotted, making sure to achieve tight knots without exerting excessive force. Since there are three hair tresses in each treatment time, 30 hair fibres per treatment time were knotted. Hair fibres then were securely mounted on metal stubs using double sided adhesive tape. 30 virgin hairs also were chosen and knotted as a reference.

Due to the instrumental limitations and the nonconductive nature of hair, the work is undertaken after applying a metallic conductive gold coating. The samples were vacuum sputter coated with a thin layer of gold (30nm) and kept in high vacuum (-10^{-4} Torr) for 1 minute. This process was repeated 3 times using the Sputter Coater 91000 (Edwards, UK). SEM images were obtained with the scanning electron microscopy SM 300 (Topcon, UK) at 5 kV accelerating voltage and 8x spot size. 300x as a standard magnification was chosen for all the knot test investigations.

3.4 Results and Discussions

3.4.1 Morphological Structures of Bleached Hairs

Oxidation causes structural damage to hair fibres. The SEM technique was used to examine the surface of hair fibres after they had been subjected to various specified oxidation treatments. Dibianca (1973), after viewing many hairs under the SEM, found that the damage areas of cuticles, could generally be classified into four categories, i.e., fly away fibres, exposed cortex, split end, and general shaft damage.

With the "Knot Test" method, the knotted hair has a tendency of lifting on the cuticle surface under high-stress bend; the higher the stress on the knot, the severer the hair damage is, thus, the bigger extent of cuticle lifting. Figures 3.1-3.5 indicate features of interest relevant to changes by the oxidation treatment on the single hair fibre's surface subjected to knot formation.

Untreated hairs in Figure 3.1A were examined in order to provide a standard visual comparison. Bleaching treatments lead to degrading effects as shown in Figures 3.1B and 3.2A. One of the obvious appearances in the bleached hairs is the increased tendency of cuticle 'lifting' and this is possibly due to reduced adhesion of scales to each other resulting from the solubilisation of CMC.

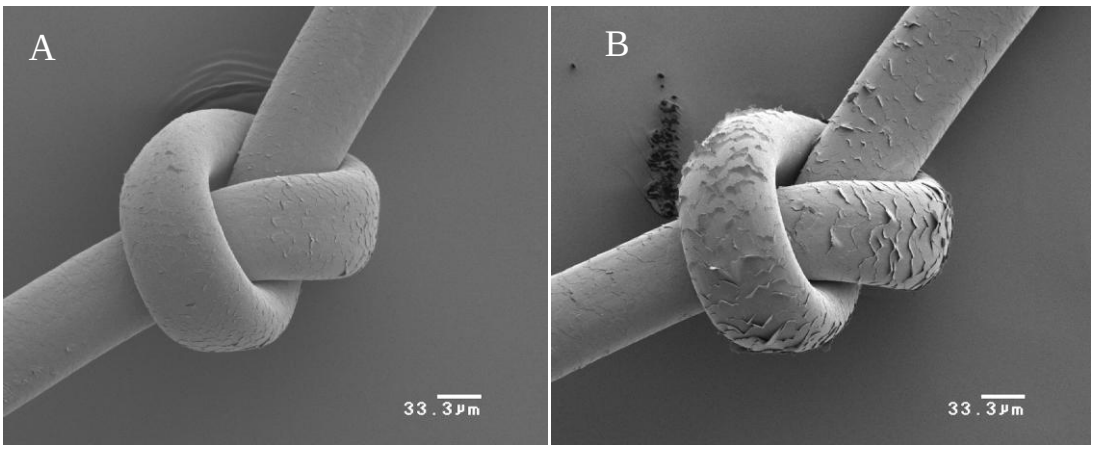

Figure 3.1: (A) Micrograph of an untreated hair fibre with somewhat broken edges; **(B)** Micrograph of a bleached hair fibre. The appearance is somewhat similar to untreated hair, though slightly greater uplift of scales is observed.

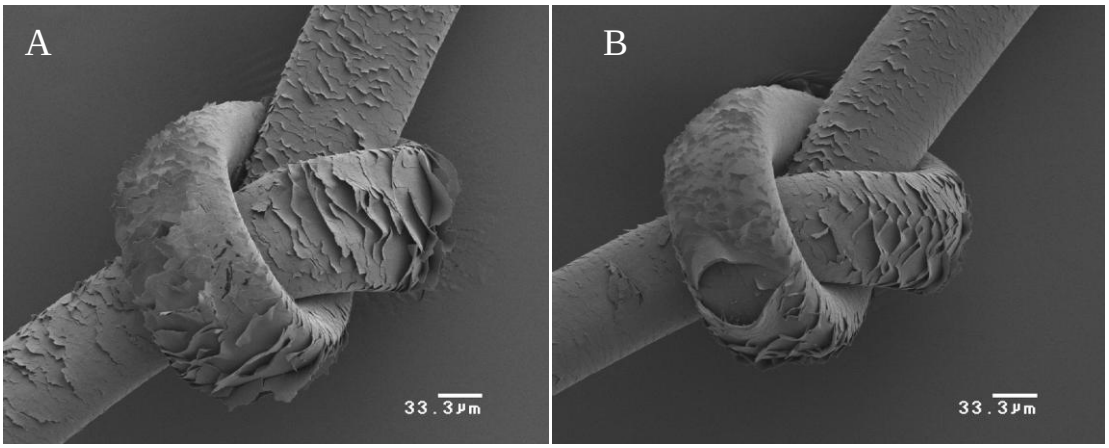

Figure 3.2: (A) Micrograph of a bleached hair fibre, showing severe cuticle uplift; **(B)** Micrograph of a bleached hair fibre, the greater lift up of scales is shown, and the hole in the cuticle is observed.

Hair surfaces in Figure 3.2B and 3.3A show much more damage. A hole or rip is apparent in the cuticle in Figure 3.2B with the greater lift up of scales. Parts of the cuticle outer sublamellar layers were chipped away in Figure 3.3A and up-lifting of the cuticle cells occurred. The sub-layers (A-layer, endocuticle, inner layer) are exposed. The cortex is visible through the fracture.

The SEM image in Figure 3.3B demonstrates an almost complete lack of cuticle scales on the fibre, where only some remnants of scales remain. Arrow indicates these remnant cuticle scales. Probably, the cuticle of this fibre is more susceptible to removal.

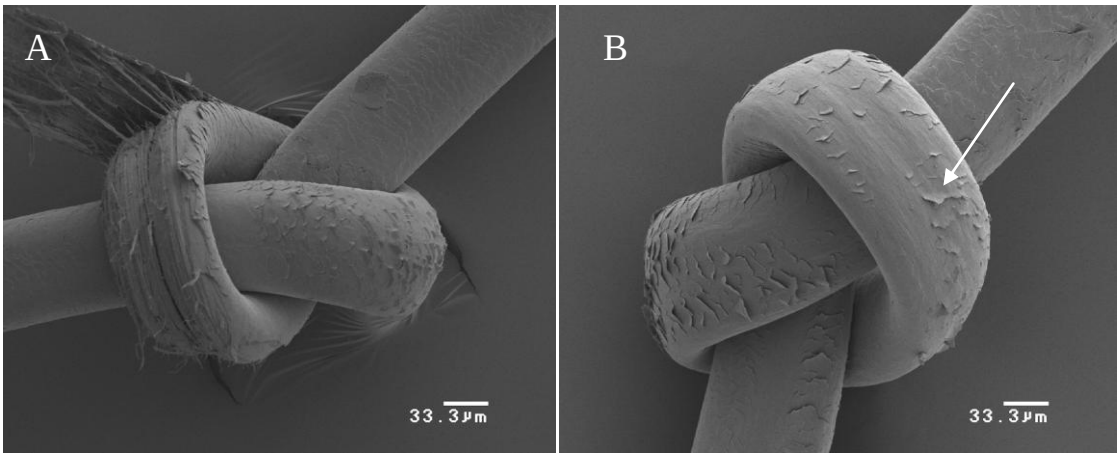

Figure 3.3: (A) Micrograph of bleached hair fibre showing exposed cortex; **(B)** Micrograph of bleached hair fibre, indicating a major lack of cuticle scales on the fibre, with cuticle scales remnants remain.

The phenomena of cuticle loss or fragmentation can be observed in the Figure 3.4. The surface of the hair has prominent transversal cracks in Figure 3.4A. The cuticle scales are susceptible to separate from the hair, leading to exposed cortex by the extensive cuticular detachment. Macrofibrils of the cortex are observed in Figure 3.4B through the opening of the cuticle. Cortical macro- and micro-fibrils are clearly visible in the fracture zone in Figure 3.5. Both step fracture and fragmentation are characteristic patterns when the cuticle is in poor condition.

Swift (1972) showed that the cleavage of the cuticle cells generally occurs within the endocuticle layer, so the fragments are observed. In this manner, the damaged fibre is more susceptible to the oxidative degradation, thus accelerating the process of cuticle degradation and scale removal.

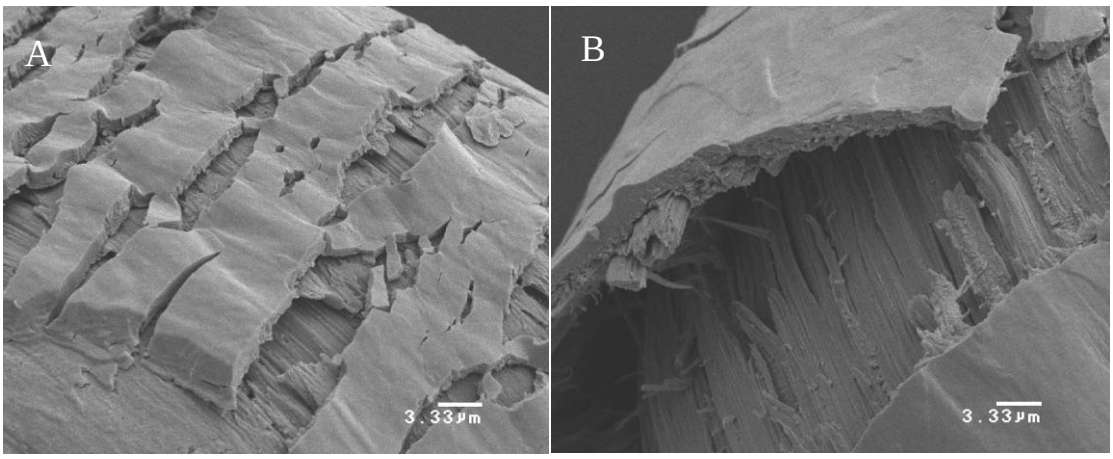

Figure 3.4: (A) The fracture has exposed the underlying cortex; **(B)** Macrofibrils of the cortex are observed through the opening of the cuticle.

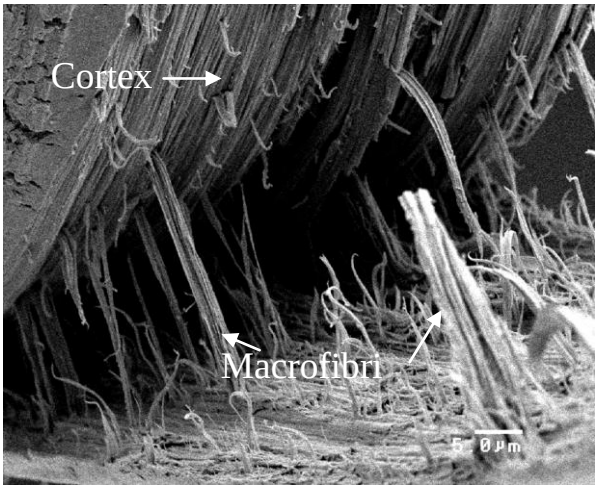

Figure 3.5: Cortical macro-fibrils are clearly visible in the fracture zone of a bleached hair fiber

3.4.2 Knot Test

Cysteic acid derives from cystine by oxidative cleavage in hair fibre (Robbins, 1969). Therefore, the destruction of the cross-link probably decreased the strength of the cuticle and this decrease would cause scale lift and exfoliation of the cuticles during the hair damage. For this reason, the "knot test" as a novel numerical description is applied to evaluate the cuticle damage systematically. The damage of a hair knot is assessed and classified based on two established standard damage class groups, as shown in Figures 3.6 and 3.7. The acquired data for 30 fibres per hair tress and per treatment is processed using statistic analysis in Excel software.

When the hair fibres are subject to bleaching damage, the cuticle is initially destroyed, resulting in the cuticle edge being gradually degraded (Garcia, 1978). Figure 3.6 shows a scheme which illustrates the progress of hair damage on mildly damaged fibres, ranging from Damage Class A1 to A6. Generally, the lower the damage class, the less is the extent of damage, thus less cuticle lifting occurs. For example, the individual keratin scales in Class A1 have fairly smooth edges, and overlap, forming a flat, tight sheath around the hair shaft (often called "virgin hair"), whereas Class A6 demonstrates complete cuticle lifting. In this way, observations on scale lifting provide an effective method for distinguishing between the extents of damage.

Severe bleaching would cause the jagged-like edges of the cuticle scales to lift-up and to become completely removed from the surface, exposing the underlying cortical layers (Barton, 2011). As a consequence, a new damage classification for heavily damaged fibres (Figure 3.7) is introduced to complement the damage classification scheme.

According to the damage degree, there is a second group with six additional damage classes, referred to Damage Classes B1 ─ B6, respectively. The total lack of surface structure is seen in the most extreme case in Figure 3.7, where no cuticle scale or only one layer of cuticle is left. Cracks start to appear on the last layer of cuticle in Class B2, and pronounced transversal cracks are observed until this layer of cuticle chipped away, thereby leaving the cortex exposed (Damage Class B6).

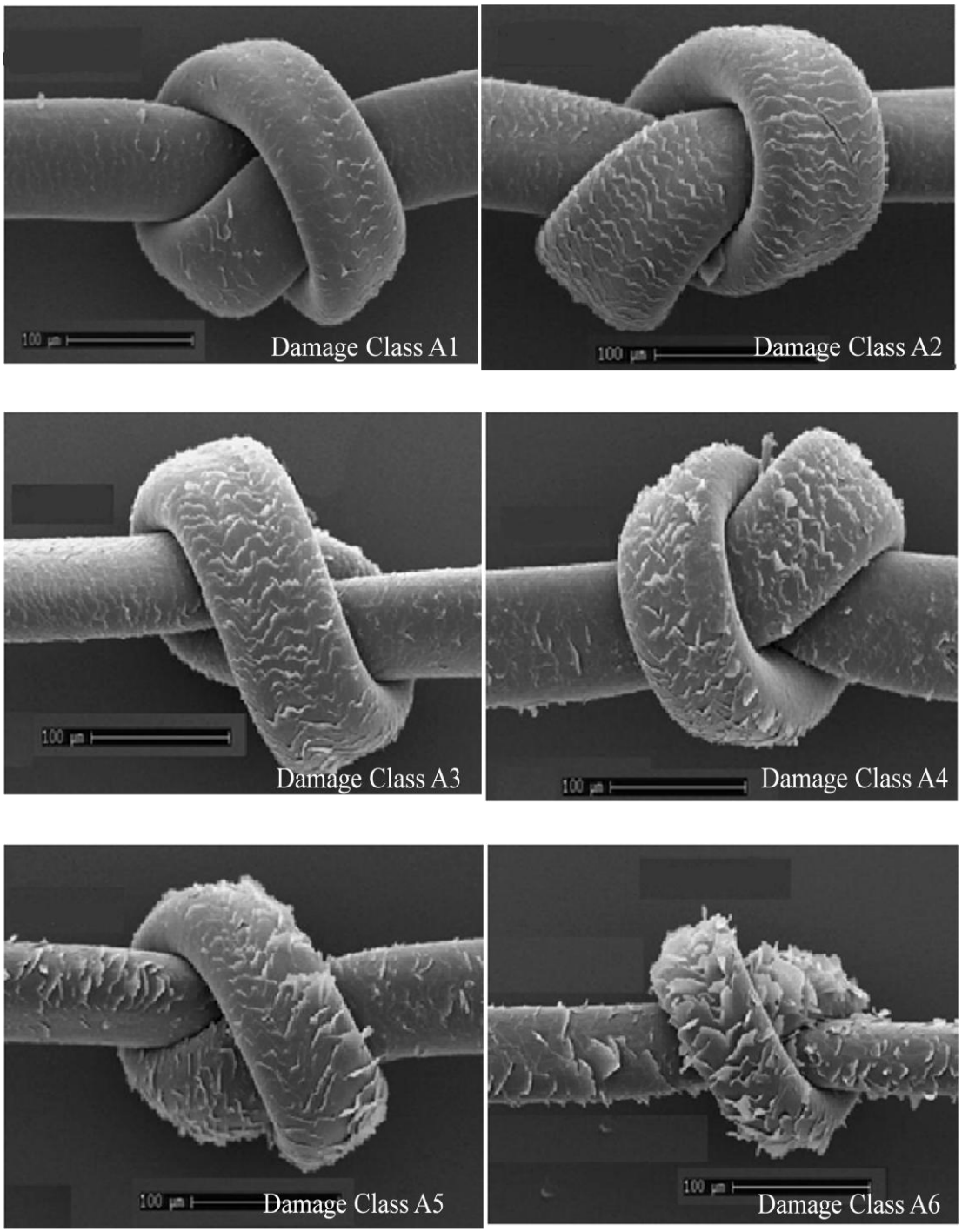

Figure 3.6: Standard damage classification for mildly damaged fibres

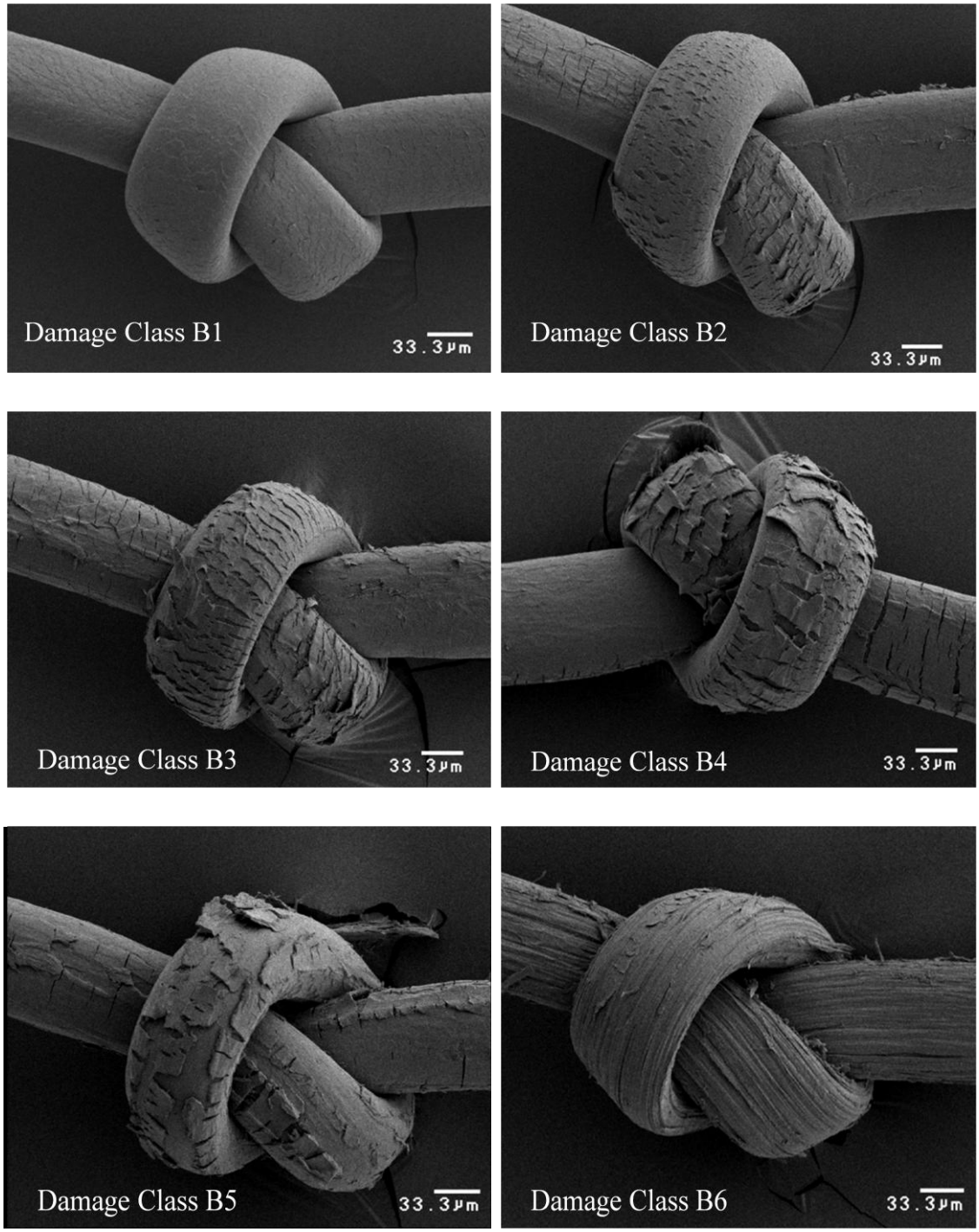

Figure 3.7: Damage classification for heavily damaged fibres

3.4.2.1 Results of the Knot-Test

The two groups of damage classifications, mildly damaged classification A and heavily damaged classification B, were employed as a reference to be compared with the target hair samples to achieve the corresponding numerical counts for each hair

sample. Hairs were classified three times into the various classes in order to achieve reproducible results.

As described in the Chapter 2, there are two batches of virgin hair utilised in the oxidative treatment, batch I and batch II. In Table 3.1 batch II virgin hair (N=30) has a smaller fibre count in mildly damage group A2 (18.9%), A3 (28.9%) and A5 (7.8%) than batch I virgin hair, which has 25.6%, 36.7% and 14.4%, respectively. However, 12.2% of batch II virgin hair (classified as heavily damage group B1) shows batch II virgin hair has a slightly more sever damage extent than batch I virgin hair.

Table 3.1: Fibre count of virgin hair samples (N=30) in each classification based on the mean of three measurements, as a percentage %. Standard error is given in the Figure 3.8.

Damage Class / Hair Batch	A1	A2	A3	A4	A5	A6	B1	B2	B3	B4	B5	B6
Batch I	5	25.6	36.7	20	14.4							
Batch II	7.8	18.9	28.9	21.1	7.8	3.3	12.2					

Figure 3.8 summarises the damage phenomena of each type of virgin hair in detail, the main damage classifications of both virgin hairs belong to Damage A2, A3 and A4, revealing that the virgin hairs are subjected to less damage attack. In addition, the virgin hair batch II shows a relatively higher damage classification than the batch I, this has been displayed in Table 3.1.

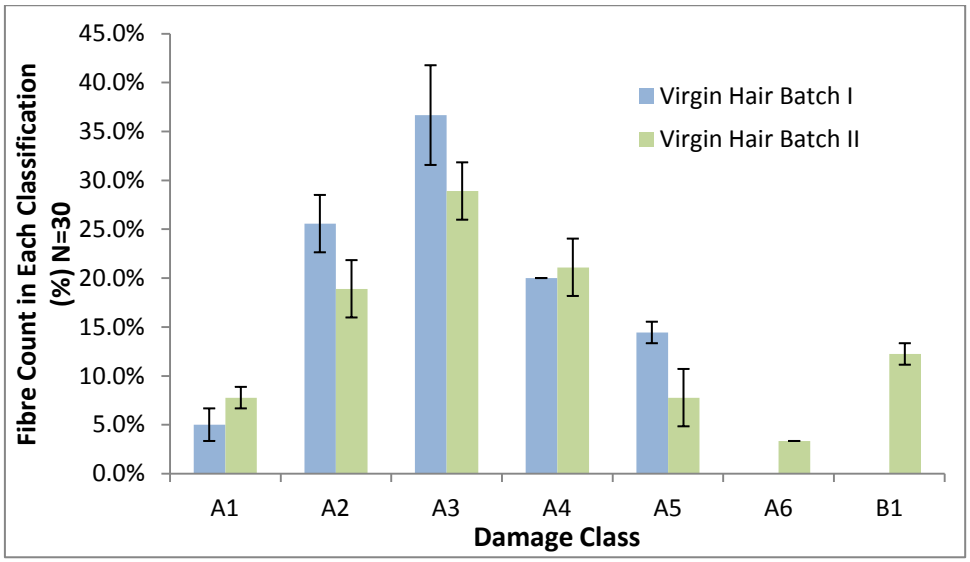

Figure 3.8: Fibre count of virgin hair samples (N=30) in each classification based on the mean of three measurements, with standard error, as a percentage %

It is clear in Table 3.2 that during the various treatment times, most knot test results for 6% H_20_2 bleached hairs are in mildly damage group A, except 3.3% of 1h 6% H_20_2 bleached hairs are in heavily damage group B1. This indicates that 6% H_20_2 bleach has an overall moderate damage effect on the hair surface.

Table 3.2: Fibre count of 6% H_20_2 bleached hair samples (N=30) in each classification, at different bleaching times, based on the mean of three measurements, as a percentage %. Standard error is given in the Figure 3.9.

Damage Class / Treatment Time	A1	A2	A3	A4	A5	A6	B1	B2	B3	B4	B5	B6
0.5 h	6.7	34.4	27.8	24.4	3.3	3.3						
1h	13.3	22.2	37.8	16.7	3.3	3.3	3.3					
1.5h	3.3	26.7	48.9	12.2	6.7	3.3						
2h	14.4	35.6	40.0	10.0								
2.5h	20.0	22.2	40.0	13.3	4.4							
3h	20.0	25.6	26.7	17.7	6.7	3.3						
3.5h	3.3	25.6	32.2	31.1	4.4	3.3						
4h	4.4	21.1	37.8	21.1	8.9	6.7						

A similar damage result is found in Figure 3.9 for the 6% H_20_2 bleached hair. Most damage classifications are found in damage classes A2, A3, and A4. In addition, there are some other damage classifications in the mildly damage classification scheme A, revealing that the 6% H_20_2 bleached hairs have an overall moderate oxidative damage effect.

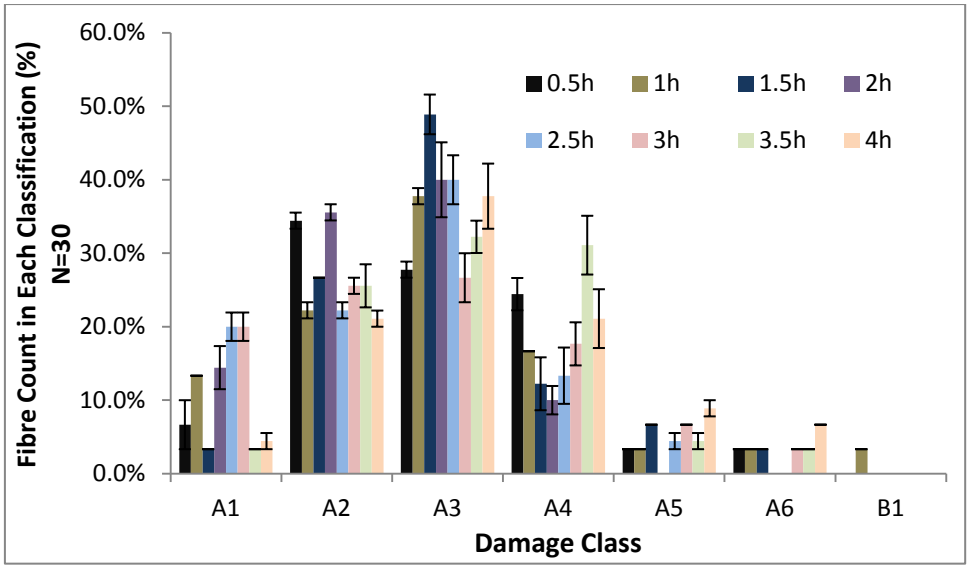

Figure 3.9: Fibre count of 6% H_20_2 bleached hair samples (N=30) in each classification, at different bleaching times, based on the mean of three measurements, with standard errors, as a percentage %

A distinctive result is observed for the 9% H_20_2 commercially bleached hair in Table 3.3. 1.5h bleached hairs show milder damage effects, which are reflected in mild damage classification A, whereas 9% H_20_2 commercial bleached hairs after 2h shows severer oxidised damage, which occurs in heavy damage classification B.

Table 3.3: Fibre count of 9% H_20_2 commercial bleached hair samples (N=30) in each classification, at different bleaching times, based on the mean of three measurements, as a percentage %. Standard error is given in the Figure 3.10.

Damage Class / Treatment Time	A1	A2	A3	A4	A5	A6	B1	B2	B3	B4	B5	B6
0.5h	17.8	24.4	31.1	13.3	3.3	3.3	6.7					
1h	5.6	28.9	23.3	32.2	6.7	3.3						
1.5h	17.8	17.8	23.3	21.1	4.4		15.6					
2h							37.8	32.2	13.3	10.0		6.7
2.5h							17.8	46.7	22.2	10.0	3.3	
3h							22.2	31.1	26.7	14.4	5.6	
3.5h							30.0	32.2	8.9		3.3	27.8
4h							52.2	12.2	11.1	3.3	5.6	16.7

The damage classifications for 9% commercially bleached hairs are observed in both mild damage group A and heavy damage group B, as shown in Figure 3.10. As described earlier, the results up to 1.5h fall into category A. The remaining bleached samples show intensive damage and are classified in group B. The number of fibres in classes B1 and B2 are largest, followed by A2, A3, and A4. Thus, 9% commercially bleached hair is subjected to more sever oxidation effect on the cuticle than 6% H_20_2 bleached hair.

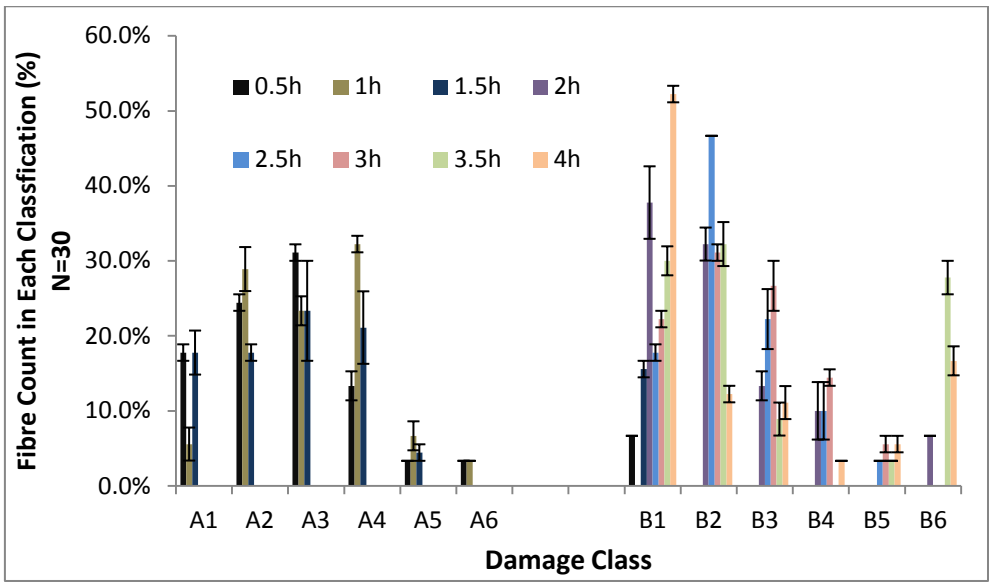

Figure 3.10: Fibre count of 9% H_20_2 commercial bleached hair samples (N=30) in each classification, at different bleaching times, based on the mean of three measurements, with standard errors, as a percentage %

The commercial persulphate bleached hairs display an unexpected phenomenon in Table 3.3, their damages are mainly classified in Damage Class A and B1. 4h commercial persulphate bleached hairs display 3.3% of fibres in damage classification A1 and 90% of fibres in damage classification B1, indicates that the extended treatment time results in the least topographical damage to the hair surface by the commercial persulphate bleach.

Table 3.4: Fibre count of commercial persulphate bleached hair samples (N=30) in each classification, at different bleaching times, based on the mean of three measurements, as a percentage %. Standard error is given in the Figure 3.11.

Treatment Time (h)	A1	A2	A3	A4	A5	A6	B1	B2	B3	B4	B5	B6
0.5	16.7	21.1	17.8	21.1	15.6		7.8					
1	11.1	17.8	35.6	12.2	10.0	3.3	10.0					
1.5	21.1	25.6	15.6	3.3	10.0	3.3	17.8					3.3
2	34.4	15.6	15.6	6.7			26.7	3.3				
2.5	25.6	17.8	11.1				42.2	3.3				
3	14.4	3.3					75.6	6.7				
3.5	4.4						88.9	6.7				
4	3.3						90.0	3.3				3.3

Commercial persulphate bleached hairs show a uniform damage effect in Figure 3.11. Most of the bleached hairs are in Damage B1 with increasing treatment time. This demonstrates that the extended commercial persulphate bleach reduced the damage effect on the cuticle surface of the hair. However, further work will need to further investigate this phenomenon.

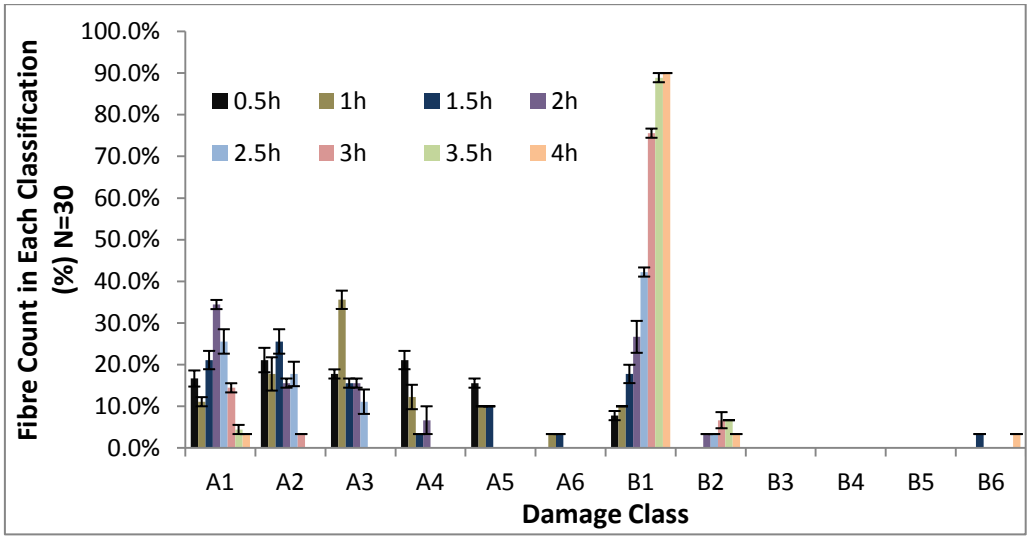

Figure 3.11: Fibre count of commercial persulphate bleached hair samples (N=30) in each classification, at different bleaching times, based on the mean of three measurements, with standard errors, as a percentage %

Due to the complexity of fibre count in each classification among the three bleaches, an individual numerical damage classification is needed. The Equation 3.1 provides a numerical specification of overall damage classification in each type of bleached hairs (N=30) and the corresponding results are summarised in Table 3.5 - 3.9.

$$\text{Overall Damage Classification} = \frac{(1\cdot A1+2\cdot A2+3\cdot A3+4\cdot A4+5\cdot A5+6\cdot A6)}{Nn} + \frac{(1\cdot B1+2\cdot B2+3\cdot B3+4\cdot B4+5\cdot B5+6\cdot B6)}{30-Nn} \quad \ldots\ldots\ldots (3.1)$$

Where, N_n is the number of hair fibres in each group

According to the Equation 3.1, the fibre count of virgin hair samples (N=30) in each classification is calculated in Table 3.5. It is apparent that both batch I and II virgin hair have a similar damage group A value (~3.2), and the virgin hair type II has an additional value in damage group B (0.9).

Table 3.5: Overall damage classification of two groups of damage classes for virgin hair samples (N=30 fibres)

Hair Batches	Damage Group A	Damage Group B
Batch I	3.2	
Batch II	3.2	0.9

The overall damage classification for the 6% H_20_2 bleached hair is summarised in Table 3.6. Comparatively, the uniform damage effect in damage group A appears, (as reflected in damage class values of 2.5 ~ 3.3, except the 1h bleached hair, which has a value of 1 in damage group B) to further prove that 6% H_20_2 bleached hairs are subjected to a moderate damage effect.

Table 3.6: Overall damage classification of two groups of damage classes for 6% H_20_2 bleached hair samples (N=30 fibres) at the different bleaching times

Treatment time (h)	Damage Group A	Damage Group B
0.5	2.9	
1	2.8	1
1.5	3.1	
2	2.5	
2.5	2.6	
3	2.8	
3.5	3.2	
4	3.3	

The overall damage classification of the 9% H_20_2 commercial bleached hair in Table 3.7 reveals that 1.5h of treatment has a slightly higher degree of damage, which is around 2.7 ~ 3.2 for damage group A. However, longer bleaching times affect the structural damage of the bleached hair after 2h, as observed in damage group B values (approximately 2.3 ~ 3.0).

Table 3.7: Overall damage classification of two damage types for 9% H_20_2 commercial bleached hair samples (N=30 fibres) at the different bleaching times

Treatment time (h)	Damage Group A	Damage Group B
0.5	2.7	1
1	3.2	
1.5	2.8	1.0
2		2.2
2.5		2.3
3		2.5
3.5		3.0
4		2.5

There is a gradual decrease from 3.0 to 1.0 in damage group A with the increasing treatment time in Table 3.8, whereas the overall damage classification for the commercial persulphate bleached hairs appears in damage group B as the value of 1.0 ~ 1.9. The results show that the prolonged treatment time produces the least topographical damage to the hair surface, thus, commercial persulphate bleach treatment has an optimised oxidation effect on the hair cuticle with the extended treatment time.

Table 3.8: Overall damage classification of two damage types for commercial persulphate bleached hair samples (N=30 fibres) at the different bleaching times

Treatment time (h)	Damage Group A	Damage Group B
0.5	2.9	1.0
1	3.0	1.0
1.5	2.5	1.9
2	2.0	1.1
2.5	1.8	1.1
3	1.3	1.1
3.5	1.3	1.1
4	1.0	1.3

3.5 Conclusion

SEM analysis of the surface morphology of hair knots showed that moderate to severe damage was caused to the cuticle layer as a result of the various bleaching processes. Such damage is more apparent in hair that had been bleached in 9% commercial H_20_2 for 2hrs.

A systematic numerical approach to the “Knot Test” is applied to evaluate hair damage situation based on two types of damage classifications: Mild Damage Classification A and Heavy Damage Classification B. The results show that commercial persulphate bleach treatment produced the least topographical damage with the prolonged treatment time. 6% H_20_2 bleach has an overall moderate damage effect over the

treatment time. 9% H_20_2 commercial bleach displays an extensive damage result. The first 1.5h bleached hairs are subject to the mildly oxidative treatment, and the damage becomes more sever after 2 hours.

3.6 Reference

BARTON, P. M. J. 2011. *A Forensic Investigation of Single Human Hair Fibres using FTIR-ATR Spectroscopy and Chemometrics.* Doctor of Philosphy (PhD), Queensland University of Technology.

BROWN, A. C., SWIFT, J.A., 1974. Low voltage SEM of keratin fibre surfaces,. *Scanning Electron Microscopy,* 241**,** 67-74.

CORCUFF, P., GREMILLET, P., JOURLIN, M., DUVAULT, Y., LEROY, F., LEVEQUE, J.L. 1993. 3D reconstruction of human hair by confocal microscopy. *J. Soc. Cosmet. Chem,* 44**,** 1-12.

DALTON, J. S., ALLEN, G.C., HEARD, P.J., HALLAM, K.R., ELTON, N.J., WALKER, M.J., MATZ, G., 2000. Advancements in spectroscopic and microscopic techniques for investigating the adsorption of conditioning polymers onto human hair. *Journal of Cosmetic Science,* 51**,** 275-287.

DIBIANCA, S. P. 1973. Innovative Scanning Electron Microscopic Techniques for Evaluating Hair Care Products. *J. Soc. Cosmet. Chem,* 24**,** 609-622.

FEUGHELMAN, M., WILLIS, B.K., 2001. Mechanical extension of human hair and the movement of the cuticle. *J Cosmet Sci.,* 52**,** 185-93.

GARCIA, M. L., EPPS, J. A., YARE, R. S., 1978. Normal cuticle-wear patterns in human hair. *J. Soc. Cosmet. Chem,* 29**,** 155-175.

GILLEN, G., ROBERSON, S., NG, C., STRANICK, M., 1999. Elemental and molecular imaging of human hair using secondary ion mass spectrometry. *Scanning. ,* 21**,** 173-81.

GURDEN, S. P., MONTEIRO, V.F., LONGO, E., FERREIRA, M.M.C., 2004. Quantitative analysis and classification of AFM images of human hair. *Journal of Microscopy,* 215**,** 13-23.

KADIKIS, A. 1987. Comments on "Quantitative Fiber Mixture Analysis by Scanning Electron Microscopy". *Textile Research Journal,* 57**,** 676.

KREPLAK, L., MÉRIGOUX, C., BRIKI, F., FLOT, D., DOUCET, J., 2001. Investigation of human hair structure by microdiffraction: direct observation of cell membrane complex swelling. *Biochim Biophys Acta.,* 1547**,** 268-74.

LANGLEY, K. D., KENNEDY, T. A., 1981. The Identification of Specialty Fibers. *Textile Research Journal,* 51**,** 703.

MCMULLEN, R. L., KELTY, S. P., 2001. Investigation of Human Hair Fibers Using Lateral Force Microscopy. *Scanning.,* 23**,** 337-345.

PALENIK, S. 1983. Light microscopy of medullary micro-structure in hair identification. *Microscope,* 31**,** 137.

POLETTI, G., ORSINI, F., LENARDI, C., BARBORINI, E., 2003. A comparative study between AFM and SEM imaging on human scalp hair. *Journal of Microscopy,* 211**,** 249-255.

ROBBINS, C. R. 1994. *Chemical and Physical Behavior of Human Hair,* Berlin, Springer.

ROBBINS, C. R., KELLY, C., 1969. Amino acid analysis of cosmetically-altered hair. *J. Soc. Cosmet. Chem,* 20**,** 555.

SICH, J. 1990. "Which is best for identifying animal fibers - Scanning electron microscopy or light microscopy?" *Textile chemist and colorist* 22**,** 23-25.

SMITH, J. R. 1998. A quantitative method for analysing AFM images of the outer surfaces of human hair. *J. Microsc.,* 191**,** 223-228.

SWIFT, J. A. 1999. Human hair cuticle: biologically conspired to the owner's advantage. *Journal of the Society of Cosmetic Chemists,* 50**,** 23-47.

SWIFT, J. A., BROWN, A. C., 1972. The critical determination of fine changes in the surface architecture of human hair due to cosmetic treatment *Journal of the Society of Cosmetic Chemists,* 23**,** 695-702.

SWIFT, J. A., SMITH, J. R., 2000. Atomic force microscopy of human hair. *Scanning.,* 22**,** 310-318.

SWIFT, J. A., SMITH, J. R., 2001. Microscopical investigations on the epicuticle of mammalian keratin fibres. *Journal of Microscopy,* 3**,** 203-211.

WORTMANN, F. J., ARNS, W., 1986. Quantitative fiber mixture analysis by scanning electron microscopy: Part 1: Blends of mohair and cashmere with sheep's wool. *Textile Research Journal,* 56**,** 442-446.

Chapter 4 Colour Measurement of Human Hair

4.1 Introduction

Colour cannot exist without light, coloured light is perceived when the spectral composition of the observed radiation varies over the visible range of wavelengths (Hunt, 1995).

The electromagnetic radiation with wavelengths between 380 nm and 760 nm (790-400 terahertz) is detected by the human eye and perceived as visible light. When a beam of visible white light passed through a glass prism a series of coloured bands are produced, resulting in seven colours ranging from violet to red and their wavelengths are shown in Figure 4.1.

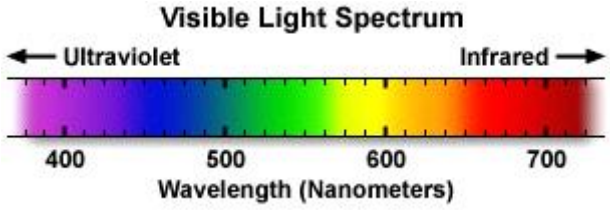

Figure 4.1: The visible portion of the spectrum is expanded to show the hues associated with different wavelengths of light

When light strikes an object, the colour of a surface depends on how much light is absorbed by the material and how much is scattered, transmitted and reflected at each of the wavelengths in the visible spectrum (Berns, 2000). The specular reflection, which is directly reflected at the surface of the fibre like a mirror, is not "coloured light".

4.1.1 Human Colour Vision & CIE Colour Space

The human eye is particularly sensitive to colour. It has been estimated that humans can distinguish around 10 million colours (Wyszecki, 2006), thus, human colour vision is introduced to consider the basic principles of colour perception.

4.1.1.1 Human Colour Vision

Different people may have different colour vision. Without the observers, who perceive the light, there would be no colour (Hunt, 1998). So the eye plays a role of a transducer in converting the electromagnetic energy, which is in the form of light, into the nerve impulses (Hill, 1997).

Light entering our eyes is imaged onto the retina at the back of the eye. The eye contains two types of light-sensitive cells, called rods and cones. They both are located in the retina in the last layer of nerve cells furthest from the cornea. Rods are not colour-sensitive cells, they work with the weak illumination (scotopic or night vision), but cones detect light with high illumination (photopic vision). There are three types of cone receptors with a maximum sensitivity for wavelengths in the red, green and blue regions of the visible spectrum, called short-wavelength-sensitive (S) cones, middle-wavelength-sensitive (M) cones, and long-wavelength-sensitive (L) cones, respectively. Thus, in principle, three primaries (R, G, B) describe a colour sensation. If either of the cones is missing or defective, it causes the defective colour vision.

As illustrated in the Figure 4.2, the spectral sensitivity as a function of wavelength, varies depending on the type of cone. S- cones are sensitive to the short wavelength region, M- and L- cones are sensitive to the middle and long wavelength regions, respectively. Particularly the L-cone and the M-cone spectral sensitivities are close together compared to the S-cone sensitivity, thus improving colour discrimination (Berns, 2000).

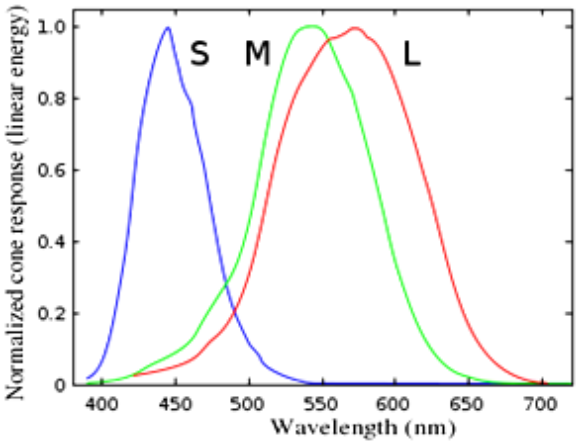

Figure 4.2: Normalized response spectra of human eye cones, S, M, and L types, to monochromatic spectral stimuli with wavelength in nanometres (Stockmam, 1993).

The human observer perceives colour as a ratio of the intensities from the S, M and L cones. Colour perception starts with the spectral characteristics of the light source, which are then modified by the reflectance of the object (Battle, 1997). The resulting light then stimulates the eye to generate a signal, which is eventually interpreted by the brain.

4.1.1.2 CIE system

Colour perception always depends on three elements: the light, the object and the observer. Colour is a complex perception, it changes under different sets of conditions, such as source (e.g., spectral properties and the amount of light), object (e.g., size and texture) and observer (e.g., spectral sensitivities, lens properties, macular pigment, light and chromatic adaptation) (Berns, 2000). To measure the colour of an object objectively, the international committee (Commision Internationale de L'Eclairage, CIE) set up a standardised colour specification system in 1931, refer as 1931 CIE system. Although additional systems have been added, the basic principles and systems are the same. And almost all modern colour measurements are based on the CIE system.

4.1.1.2.1 The 1931 CIE system

In 1931 the CIE developed a system for specifying colour stimuli using tristimulus values for three imaginary primaries, the amounts of the three primaries are called tristimulus values and are referred as X, Y, and Z in the 1931 CIE system. Tristimulus values can be calculated by the reflectance spectrum of a sample, and the reflectance spectrum can be measured using a reflectance spectrophotometer.

Tristimulus values provide a numerical specification of the colour. A different colour has different tristimulus values and hence the specification is different (Rigg, 2007). In order to eliminate the variations of colour specification, the CIE had defined standard light sources and a standard observer, together with standard observing and viewing conditions.

Standard illuminants and Standard sources

The most important light source is daylight. A light source can be quantified by measuring its *spectral power distribution* (SPD), which is a function of wavelength across the visible spectrum. CIE makes a distinction between sources and illuminants. A light source is a physical emitter of light, such as the sun or a lamp, an illuminant which refers to a specified spectral energy distribution, is the specification for a potential light source. All light sources can be specified as an illuminant, but not all illuminants can be physically realised as a light source.

In 1931, the CIE recommended three standard illuminants, known as A, B and C, respectively. llluminant A represents incandescent light of a tungsten filament lamp, which has the same SPD as a Planckian or black body radiator at a colour temperature of 2856 K. A black body is an ideal thermal radiator. The SPD of the emitted light from a black body depends only on the temperature of the surface, but not its nature. The higher the temperature of the emitting surface, the greater the total power of the emitted radiation, and the lower the wavelength of maximum emission (Broadbent, 2001). The temperature of a black body is measured from its colour temperature, usually expressed in Kelvins (K).

The CIE also defined illuminant B: tungsten with a yellow filter, which simulates sunlight at the correlated colour temperature of 4874K, and illuminant C: tungsten with a blue filter, which simulates daylight at the correlated colour temperature of 6774K, however, both illuminants are not suggested.

In 1963, the CIE recommended a series of D illuminants based on natural daylight across the UV, visible and near–IR region (300-830 nm) (Sinclair, 1997). It enables daylight spectral power distributions to be calculated for a wide range of correlated colour temperatures. CIE illuminant D65, with an approximate correlated colour temperature of 6500K, is now accepted as a standard illuminant (CIE 1986) for surface colour industries, and D50 is used in the graphic arts and computer industries (Berns, 2000).

Standard Observers

The original 1931 CIE standard observer was based on colour-matching function using a 2^o field of view, whose visual field size is between 1^o and 4^o. Thus the CIE 1931 standard observer is also known as the CIE 1931 2° standard observer. But a 2^o field of view is much narrower than that normally used for the critical colour appraisal (Rigg, 2007), and cannot remain a match for large-field visual colour judgements. In 1964 the CIE adapted a new standard observer to describe the vision of a human more accurately, which is called 10^o observer or 1964 CIE supplementary standard observer. Although neither is likely to correspond closely to the individual observer, either may well correspond reasonably closely to a real observer (Rigg, 2007).

The standard observer is characterised by colour-matching functions. Colour-matching functions define how human eyes match a colour stimulus with an additive mixture of three primaries: monochromatic red, green and blue lights. According to the trichromatic theory of colour vision, any colour stimulus can be specified by the amounts of the primaries to match a particular colour.

Viewing condition

The CIE has recommended four types of illumination and viewing geometries for reflectance measurement: 45º/normal (45/0), normal/45º (0/45), normal/diffuse (0/d) and diffuse/normal (d/0), as presented in the Figure 4.3.

In the 45/0 geometry, the sample is illuminated with one or more beams of light at the incident angle of 45º to the surface and the light is normally viewed. In the opposite mode (0/45 geometry), the sample is illuminated normally to its surface and measures at about 45º angle, while the incident light is polarised. The 45/0 and 0/45 geometries both ensure all components of gloss to be excluded from measurements.

In the 0/d geometry, the sample is illuminated from an angle near the normal and the reflected energy is collected from all angles using an integrating sphere (a hollow sphere which is painted white inside). In the d/0 geometry, the sample is illuminated

from all angles using an integrating sphere and viewed at an angle near the normal to the surface. These two geometries are optically reverse to each other and therefore result in the same measurement results.

But most D/0 instruments are actually using D/8 rather than true D/0 geometry, a small amount of specular component may be excluded by a dark spot or light trap on the sphere, thus sphere instruments may allow specular reflection to be included or excluded (Figure 4.4). In the specular-included mode, the total reflectance (diffuse + specular) can be measured.

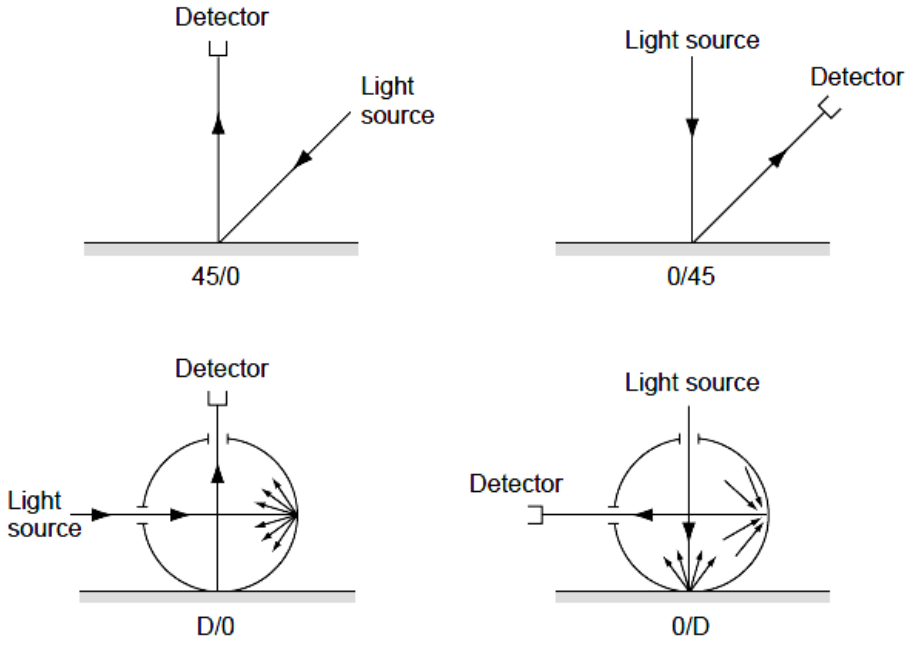

Figure 4.3: CIE-recommended illuminating and viewing geometries (Battle, 1997)

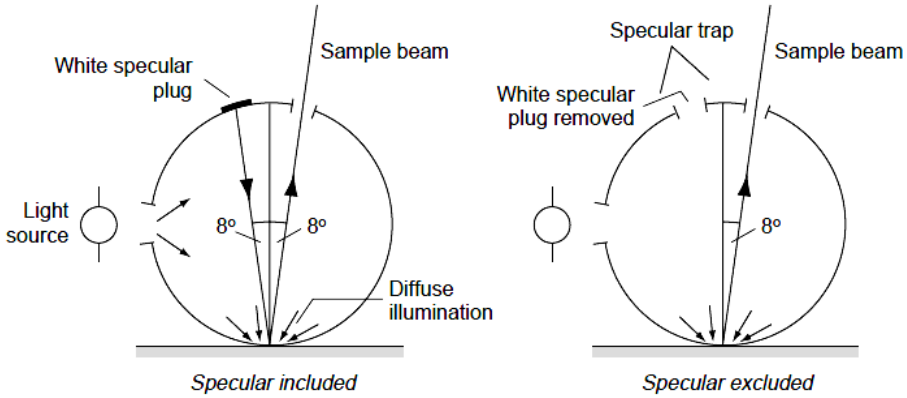

Figure 4.4: Comparison between D/8 specular-included and specular-excluded modes (Battle, 1997)

4.1.1.2.2 CIE 1976 Colour system

As mentioned previously for the colour-matching function, it is difficult to relate the tristimulus values of an object to its appearance because the XYZ values have very little real meaning to most observers (Rigg, 2007). Consequently, a two-dimensional plane with the lightness (Y) of a sample was introduced by projecting the tristimulus values onto the unit plane (x+y+z=1), this plane is known as the chromaticity diagram (CIE xyY), and its chromaticity coordinates are recorded as x and y (Klaman, 2002).

However the CIE xyY colour space is not perceptually uniform and the colour differences in the colour space are not uniform, which means equal distances in the diagram do not correspond to equal visual differences (Hunt, 1971, Ohno, 2000). Therefore, after a number of non-linear transformations of the CIE 1931 XYZ space, a uniform colour space, namely CIE 1976 LAB (or CIE L*a*b*) colour space as one of these transformations was finally introduced. A three-dimensional plot of the tristimulus values XYZ determines a colour space.

CIE L*a*b*, or CIELAB system is a very popular colour scale for colour and colour difference specification. It measures colour on three axes that are nearly linear with human perception (Ford, 1998). This model has the benefit of corresponding to the human perception of colour and provides a grid point for each specific colour (TASI, 2004).

In the CIE L*a*b* colour system, the lightness (or intensity) of a colour is measured on the vertical *L** axis. The maximum for L* is 100, which represents a perfect reflecting diffuser. The minimum for L* is zero, which represents black. The a* and b* axes have no specific numerical limits. Positive a* is red. Negative a* is green. Positive b* is yellow. Negative b* is blue. Below a diagram representing the CIELAB colour space is shown in Figure 4.5. One unit on the *L**, *a**, or *b** axes is considered to be the limit of human discrimination between colour (TASI, 2004). This colour grid allows the mathematical comparison of colours and also allows colours to be corrected for different conditions. Our research has used the cut-off point of ±100 because there are the practical limits of the software and instrument used in the colour measurement (Napier, 2007).

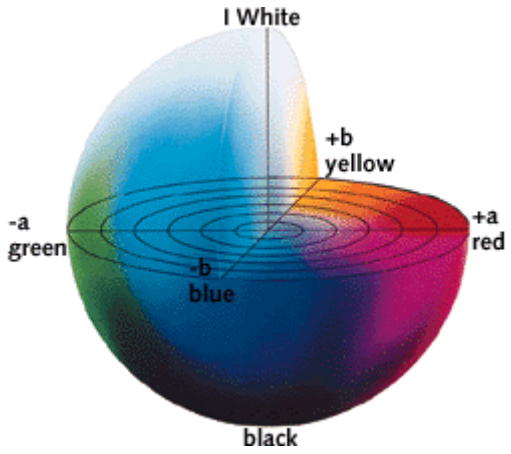

Figure 4.5: CIE L*a*b* colour system (Qian, 2012)

Colour Difference

Two non-matched colours always have different sets of the tristimulus values X, Y and Z. Since the CIE XYZ colour space is not a uniform colour space, it is not particularly useful for colour difference evaluation (Broadbent, 2001). Consequently, the CIE LAB colour difference equation is used for the colour specification.

A colour-difference space is a three-dimensional space, the total colour difference between two non-matching colours is the Euclidean distance between the points for their respective coordinates in the CIELAB colour space (Broadbent, 2001), given by:

$$\Delta E^* = [(\Delta L^*)^2 + (\Delta a^*)^2 + (\Delta b^*)^2]^{1/2} \quad (4.1)$$

Where ΔL* refers to the lightness difference (lighter if positive, darker if negative), Δa* refers to the red-green difference (redder if positive, greener if negative) and Δb* refers to the yellow-blue difference (yellowish if positive, bluer if negative).

The value, ΔE*, defines the extent of the total colour difference, but it does not provide information about how the colours differ.

4.1.2 Colour Measurement

There are two types of instrument to measure the colour of opaque samples: reflectance spectrophotometers and colorimeters.

4.1.2.1 Reflectance Spectrophotometry

Reflectance spectrophotometry is an established method for measuring hair colour at the macroscopic level, and it has been more consistent than digital image analysis (Vaughn, 2008, 2009).

Spectrophotometric measurements provide the numerical description of the reflection or transmission of light by an object. The resulting reflection or transmission spectrum gives the fraction of the incident light that an object reflects or transmits as a function of wavelength (Broadbent, 2001). The reflectance measures the ratio of reflected to incident light from a sample at many points across the visible spectrum (see in Eqn 4.2). The reflectance of a sample is generally expressed as percentage, and the perfect reflecting diffuser has a reflectance of 100%. But the obtained reflectance values are the relative values. The light used to illuminate the sample does not affect reflectance and transmittance. Thus, XYZ, or L*a*b* coordinates can be calculated with the illuminant (Battle, 1997).

$$\text{Reflectance} = \frac{\text{Intensity of Reflected Light}}{\text{Intensity of Incident Light}} \tag{4.2}$$

It has to be noted that there is no light transmission through the material and only reflection from the opaque sample surface. Figure 4.6 illustrates a schematic of a reflection spectrophotometer. A light source is used to illuminate the sample using a specific illumination and viewing geometry. Reflected or transmitted light is then passed to the spectral analyser, where the light is resolved into its spectral components. This allows the light detector and control electronics to be measured across the visible spectrum. And a highly diffusive, reflecting, white coating covers the interior wall of the sphere to achieve accurate diffuse measurements.

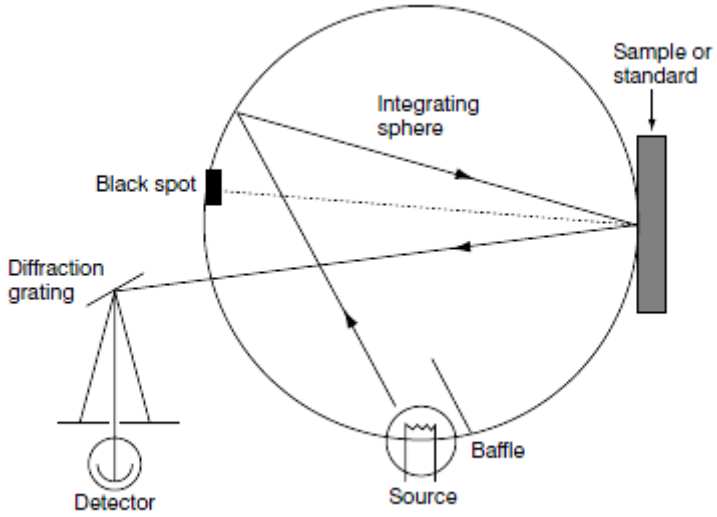

Figure 4.6: Schematic of a reflection spectrophotometer with an integrating sphere (Broadbent, 2001). The incoming light beam is diffusely reflected inside an integrating sphere, when using the D/8 geometry, some of the light, which comes from specular reflection from sample, then passing to the detector.

4.1.2.2 Colorimeters

A tristimulus colorimeter is a very cost-effective and portable colour-measuring instrument and has the benefit of being able to measure colour difference in a quality-control situation (Battle, 1997). As the human eye, it has red, green and blue photo detectors, which measure tristimulus values of the light (Figure 4.7). When the light source, such as a quartz halogen bulb, illuminates the sample at 45^{o} to the normal, the reflected light is collected and then passed to a detector, which consists of three filters in front of its own light-sensitive diode. Thus, the response of the filter/diode combination corresponds to the differential spectral response of the eye (Battle, 1997).

But its absolute accuracy is restricted, since the practical manipulation of the light source responses to the filter/diode detector always just satisfies the CIE definitions. The illuminant and observer data are fixed as D65 and 10^{o}, and the instrument is restricted to determine the relative differences (Malacara, 2002). As a result, a colorimeter cannot measure the metamerism. Metamerism occurs when two samples with different spectral reflectance data may look the same with a given light source, but are very different under another.

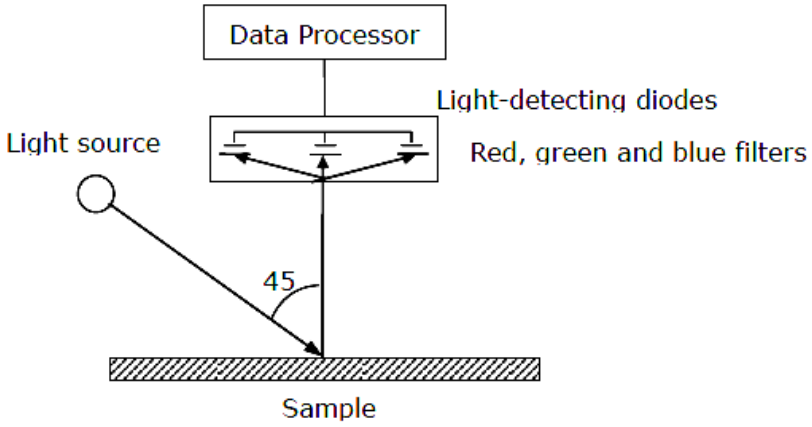

Figure 4.7: The basic features of a colorimeter with 45/0 geometry (McDonald, 1997)

4.2 Objectives

It has been verified that instrumental assessment determines colour differences more accurate than average human observers. The purpose of this colour investigation was to see whether a colour-measuring unit could provide a reproducible, objective method in determining the colour changes of bleached human hairs utilizing the CIE *L*a*b** colour space. Three types of bleached hairs were used, namely, 6% H_20_2 bleach, 9% H_20_2 commercial bleach and commercial persulphate bleach.

4.3 Experimental

Hair colour was measured using a reflectance spectrophotometer (Spectraflash 600, Datacolor, Switzerland) with D/8 viewing geometry, 10^o CIE standard observer and D65 light source, which represents daylight without spectral highlights.

Before each measurement the instrument was calibrated using a standard white tile (supplied with the machine), whose reflectance at each wavelength is known compared to a perfect diffuse reflecting surface.

In the colour measurement, the samples of virgin and bleached hairs were examined. Due to the non-uniformity of the hair, it is important to examine the variation along the length on each hair tress. Hair samples were twisted tightly and placed vertically with a special holder against the measuring aperture of the instrument. They were measured at four randomly chosen points on each hair tress in the direction of tip to root. Three more measurements were performed on the same hair tress from left, right and back to assess the reproducibility of the readings. Three tresses per treatment were tested to obtain a representative average value. Although the differences arising from variations of hair samples exist, they were found to be negligible compared with those arising from the treatment given to the hair.

Reflectance spectrophotometer measures the reflected wavelengths of the incident light and their intensity of the hair samples. Measured data were imported into the Microsoft Excel 2007 for calculating the values of the colour parameters. Irrelevant details refer to Chapter 8: Appendix.

4.4 Results and Discussion

The pigments contained in hair consume hydrogen peroxide at a measurably faster rate than hair without pigment (Wolfram, 1970a, Hall, 1975). Thus peroxide reacts faster with hair pigment than with hair protein (Robbins, 2002), so that the initial response of oxidative change to hair fibre is colour change.

The raw data of L^* (lightness), a^* (red - green colour axis), b^* (yellow - blue colour axis) of the three types of bleached hair are shown in Tables 4.1, 4.2 and 4.3, respectively. Since there are no negative L^*, a^* and b^* values in the tables, none of the bleached hair has a blue or green or darker hue. All bleached hair samples have an overall brighter colour change, as was expected.

In Table 4.1, 6% H_20_2 bleached hairs display an increase in L^* value from 27.6 to 50.1 and b^* value from 9.8 to 26.4, while the a^* value shows only a relatively minor change from 5.7 to 9.0. However the a^* value behave differently in Tables 4.2 and 4.3, where L^* and b^* values have a considerably increase over the treatment time. L^* values

increase from 27.6 to 62.5 for 9% H_20_2 commercial bleach and 28.7 to 75.3 in commercial persulphate bleach. Similarly *b** values increase from 9.8 and 10.8 to 20.3 and 23.9 for 9% H_20_2 commercial bleach and commercial persulphate bleach, respectively.

Table 4.1: The CIELAB results for 6% H_2O_2 bleached hair samples at different bleaching times, in the form of the arithmetic means with standard error

Bleaching Time (h)	*a**	*b**	*L**
0	5.7±0.0	9.8±0.1	27.6±0.2
½	8.5±0.2	17.2±0.2	34.1±0.3
1	9.5±0.0	21.5±0.1	39.7±0.0
1½	9.6±0.1	22.8±0.1	41.7±0.3
2	9.7±0.1	24.7±0.1	44.8±0.2
2½	9.6±0.0	24.3±0.2	44.8±0.1
3	9.4±0.1	24.9±0.2	45.9±0.3
3½	9.0±0.0	24.9±0.0	47.4±0.2
4	9.0±0.1	26.4±0.1	50.1±0.2

Table 4.2: The CIELAB results for 9% H_2O_2 commercial bleached hair samples at different bleaching times, in the form of the arithmetic means with standard error

Bleaching Time (h)	*a**	*b**	*L**
0	5.7±0.0	9.8±0.1	27.6±0.2
½	9.7±0.1	22.5±0.3	40.8±0.4
1	9.3±0.1	24.3±0.4	45.3±0.9
1½	8.9±0.1	25.6±0.2	49.8±0.3
2	7.7±0.3	24.7±0.3	54.1±0.9
2½	6.3±0.1	23.1±0.3	57.5±0.7
3	6.8±0.2	23.6±0.2	56.1±0.7
3½	5.3±0.2	21.3±0.2	62.3±0.6
4	5.0±0.1	20.3±0.1	62.5±0.8

Table 4.3: The CIELAB results for commercial persulphate bleached hair samples at different bleaching times, in the form of the arithmetic means with standard error

Bleaching Time (h)	a^*	b^*	L^*
0	6.4±0.1	10.8±0.2	28.7±0.4
½	10.2±0.1	27.4±0.1	49.9±0.3
1	9.5±0.1	29.0±0.1	55.1±0.2
1½	8.6±0.1	30.0±0.2	60.1±0.2
2	7.2±0.1	29.3±0.2	65.2±0.3
2½	6.6±0.1	28.9±0.1	67.2±0.2
3	5.1±0.1	27.1±0.2	70.8±0.2
3½	3.4±0.1	25.4±0.3	73.4±0.2
4	2.8±0.1	23.9±0.2	75.3±0.3

The colour difference parameters: ΔL^*, Δa^*, Δb^* and ΔE^* were calculated according to the Equation 4.1, and the corresponding results are given in Tables 4.4, 4.5 and 4.6. The values of ΔL^*, Δb^* and ΔE^* for the bleached hairs have positive values, which means that bleached hair has a tendency of being lighter and more yellow in comparison to the reference virgin hair. Although some Δa^* values are negative, bleached hair still has a redness hue, but the value is smaller than for virgin hair.

Table 4.4: The colour changes of ΔL^*, Δa^*, Δb^* and ΔE^* for 6% H_2O_2 bleached hair samples at different bleaching times

Bleaching Time (h)	Δa^*	Δb^*	ΔL^*	ΔE^*
0	----	----	----	----
½	2.8	7.4	6.4	10.2
1	3.8	11.7	12.1	17.2
1½	3.9	12.9	14.1	19.5
2	3.9	14.8	17.2	23.1
2½	3.9	14.4	17.2	22.8
3	3.7	15.0	18.2	23.9
3½	3.3	15.0	19.8	25.1
4	3.3	16.5	22.5	28.1

Table 4.5: The colour changes of ΔL^*, Δa^*, Δb^* and ΔE^* for 9% H_2O_2 commercial bleached hair samples at different bleaching times

Bleaching Time (h)	Δa^*	Δb^*	ΔL^*	ΔE^*
0	----	----	----	----
½	3.9	12.7	13.2	18.7
1	3.6	14.4	17.7	23.1
1½	3.1	15.8	22.2	27.5
2	1.9	14.9	26.5	30.5
2½	0.6	13.3	29.9	32.7
3	1.1	13.8	28.5	31.7
3½	-0.4	11.5	34.7	36.5
4	-0.7	10.9	34.9	36.5

Table 4.6: The colour changes of ΔL^*, Δa^*, Δb^* and ΔE^* for commercial persulphate bleached hair samples at different bleaching times

Bleaching Time (h)	Δa^*	Δb^*	ΔL^*	ΔE^*
0	----	----	----	----
½	3.8	16.5	21.2	27.1
1	3.1	18.2	26.5	32.3
1½	2.2	19.1	31.5	36.9
2	0.7	18.5	36.5	41.0
2½	0.2	18.1	38.5	42.6
3	-1.4	16.3	42.2	45.2
3½	-3.0	14.5	44.7	47.1
4	-3.6	13.0	46.6	48.5

Bleached hair fibres are subjected to an oxidative degradation effect, which impacts on the melanin granules, leading to colour loss. The quantity and the distribution of eumelanin and pheomelanin in hair varies in their ratio (Wolfram, 1987), so that a*- and b*- values were used to examine the decomposition of the pigments in bleached hair. The graphs of 9% H_2O_2 commercial bleach and commercial persulphate bleach

exhibit a similar trend in Figures 4.8 and 4.9. They both increase at the beginning and then decrease towards the end of the bleaching time.

As mentioned in Chapter 1, bleaching is a diffusion-controlled process (Robbins, 2002). a*-and b*- values indicate a significant colour change at the beginning of the reaction time. Even at the early stage, the peroxide has made its way into the cortex to oxidise the melanins. The time for *a** to reach its maximum value (0.5h) is shorter than for *b** (1.5h). This is due to the fact that red pheomelanin is more resistant to oxidative degradation than the black-brown eumelanins, hence, eumelanins are oxidised earlier than pheomelanins. A sudden drop of both a*- and b*- values suggests that the oxidation of pheomelanin starts after 0.5h and the degradation of protein occurs once the eumelanins were dissolved (1.5h), which leads to the reduced b*- values. The black-brown eumelanins are the main colour contributors for virgin Caucasian hair. The final yellow colour for bleached hair is ascribed to the natural colour of hair keratin (Wolfram, 1970a).

As a result, hair samples show a progressive damage effect after attacked by 9% H_2O_2 commercial bleach, and especially by the commercial persulphate bleach, where the bleaching effect is enhanced in the presence of the persulphate with the peroxide (Robbins, 2002).

On the contrary, the values of *a** and *b** for 6% H_2O_2 bleached hairs show a stable trendline relationship in Figures 4.8 and 4.9. The values keep increasing to achieve their equilibrium level during the whole treatment, revealing that 6% H_2O_2 bleach has a mild degradation effect on the melanin of the hair. It is still decolorising the eumelanin at this stage, while the other two bleaches start oxidising the keratin. This conclusion confirms the observations from the SEM "Knot Test" investigations that 6% H_20_2 has an overall moderate damage effect over the oxidation time.

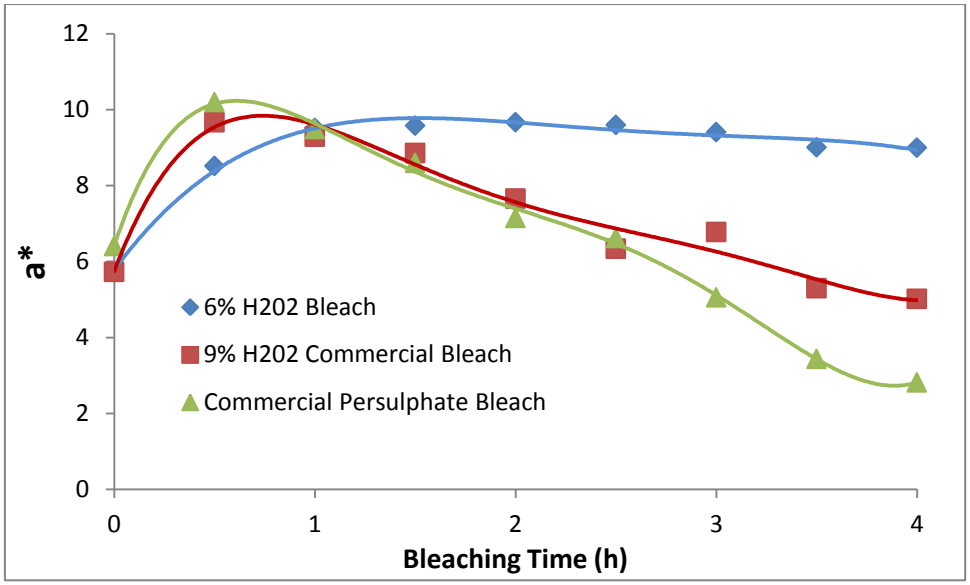

Figure 4.8: Values of *a** for 3 bleaches: (6% H_2O_2 bleach, 9% H_2O_2 commercial bleach, commercial persulphate bleach) for up to 4 hours bleaching time. The trendline curves are empirical and based on polynomial relationships.

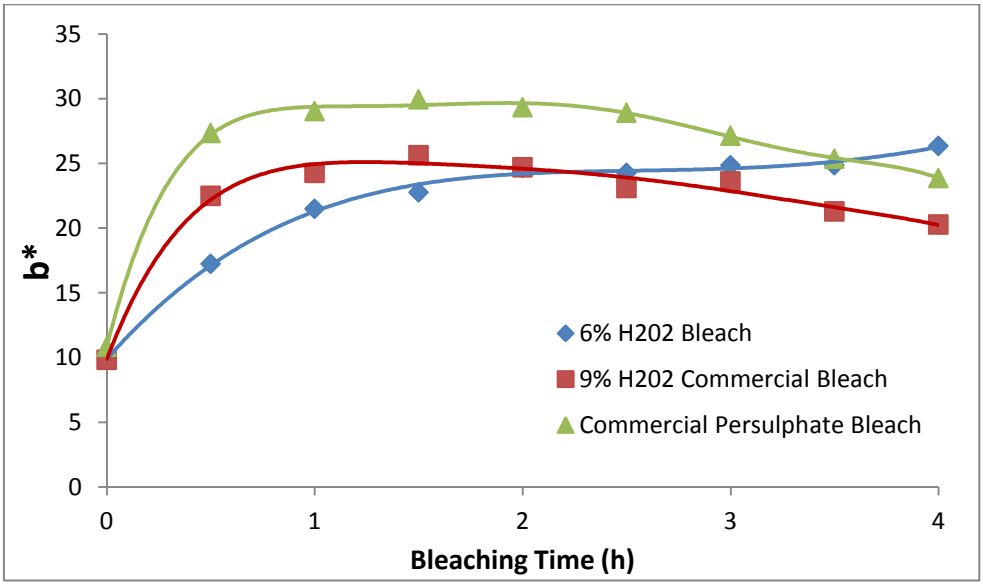

Figure 4.9: Values of *b** for 3 bleaches: (6% H_2O_2 bleach, 9% H_2O_2 commercial bleach, commercial persulphate bleach) for up to 4 hours bleaching time. The trendline curves are empirical and based on polynomial relationships.

Three treatments have a consistent upwards tendency in *L**, as shown in Figure 4.10. Melanin pigments are oxidised by peroxide bleach, so the hair samples become lighter. Commercial persulphate bleach exhibits a larger lightness value than 9% H_2O_2 commercial bleach and 6% H_2O_2 bleach, which shows that the stronger oxidising agent (persulphate) in the commercial persulphate bleach gives rise to a stronger degradation

of the pigment and thus to a large increase in the lightness value. However, the three types of bleach haven't reached their equilbrium level during the whole treatment time up to 4 hours.

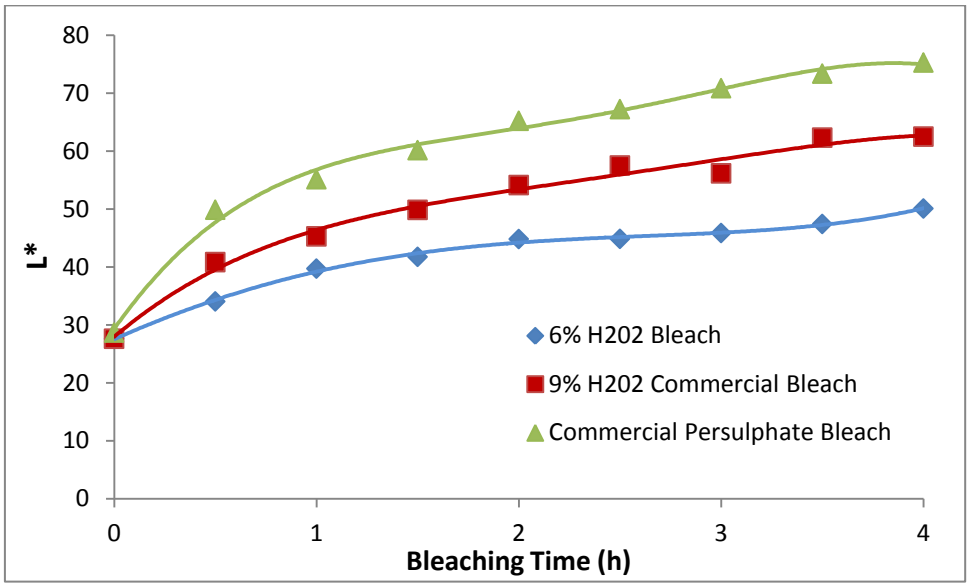

Figure 4.10: Values of L^* for 3 bleaches: (6% H_2O_2 bleach, 9% H_2O_2 commercial bleach, commercial persulphate bleach) for up to 4 hours bleaching time. The trendline curves are empirical and based on polynomial relationships.

The total colour difference ΔE^* of three bleaches are calculated by Eqn.4.1 in Tables 4.1, 4.2 and 4.3, and are presented in Figure 4.11. ΔE^* is a single value which takes into account the differences between L^*, a^* and b^* of the bleached hair and standard virgin hair. It may potentially be misleading in some cases where ΔL^*, Δa^* and Δb^* provide negative values, when ΔE^* is still within the tolerance.

In Figure 4.11 it shows that the progressive change of hair colour occurs with increasing bleaching time. An obvious colour change is observed for the strongest bleach and the longest bleaching time. The higher the concentration of peroxide, the longer the treatment time, the larger is the ΔE^*-value, thereby the greater is the hair colour difference. Commercial persulphate bleach thus leads to an overall larger colour change than 9% H_20_2 commercial bleach and 6% H_20_2 bleach. However, there is no equilibrium for ΔE^*- value seems to be reached for three types of bleach.

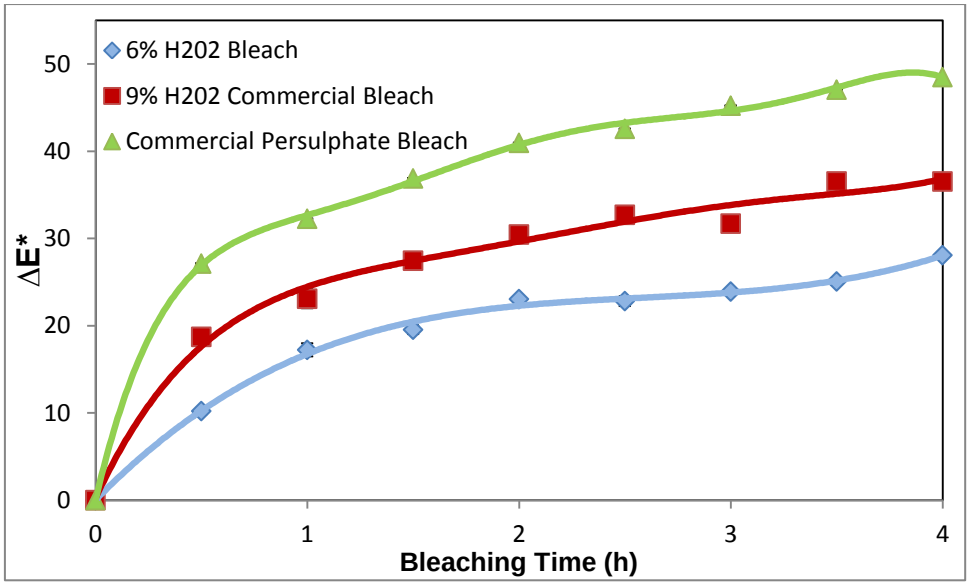

Figure 4.11: Values of ΔE^* for 3 bleaches: (6% H_2O_2 bleach, 9% H_2O_2 commercial bleach, commercial persulphate bleach) for up to 4 hours bleaching time. The trendline curves are empirical and based on polynomial relationships.

The redness hue is caused by the breakdown and the solubilisation of the pigment particles in the cortex (Wolfram, 1987) , but it has been suggested that the a^* of hair plays very little role in determining the colour change. Thus b^* and L^* are the main components in the CIE L*a*b* colour evaluation.

The changes of L^* and b* occur with the melanin oxidation process. A consistent increase in L^* as well as in b* over the reaction time is observed on 6% H_20_2 bleach in Figure 4.12, giving evidence that they both have a homogenous damage effect on the melanin. An up-turn of the curves seem to appear in the last half hour, which may be attributed to the considerable solubilisation of the black-brown melanin granules in this mild oxidation treatment.

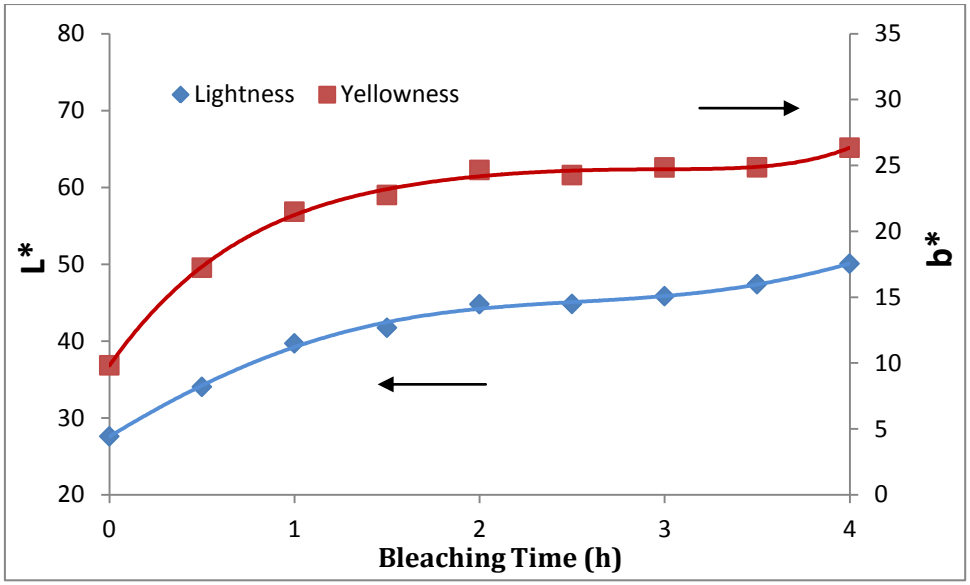

Figure 4.12: The relationship of L*- and b*- values for 6% H_20_2 bleach over the 4h bleaching time. The trendline curves are empirical and based on polynomial relationships.

It is worth pointing out that the plots of *L** vs. *b** in Figures 4.13 and 4.14 for 9% H_20_2 commercial bleach and commercial persulphate bleach follow a similar trend. b*-values increases initially and then decrease to interact with the L*- curve, which keeps the upwards tendency all the time. This shows that the solubilisation of eumelanins is the primary prerequisite in determining the change of *b**. The reduced b*- values result from the oxidation of keratin. *L** would have a dramatic change when the melanin has been oxidised.

The two curves meet at 3h and 2.5h for 9% H_20_2 commercial bleach and commercial persulphate bleach, respectively. The reason for the earlier meeting point for commercial persulphate bleach is because this type of oxidised hair has a relatively higher *L** and *b** values, caused by an aggressive oxidising agent, such as persulphate.

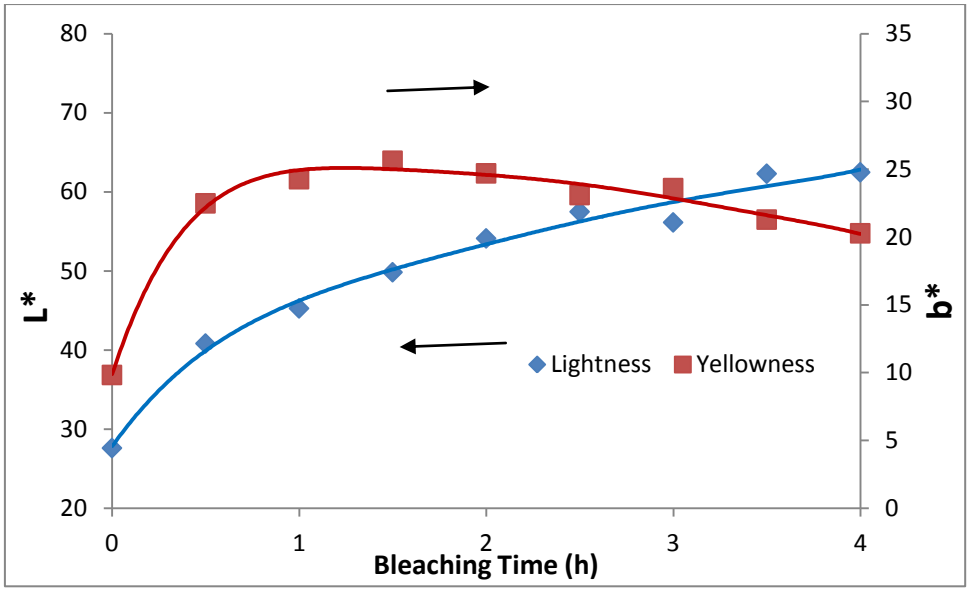

Figure 4.13: The relationship of L*- and b*- values for 9% H_20_2 commercial bleach over the 4h bleaching time. The trendline curves are empirical and based on polynomial relationships.

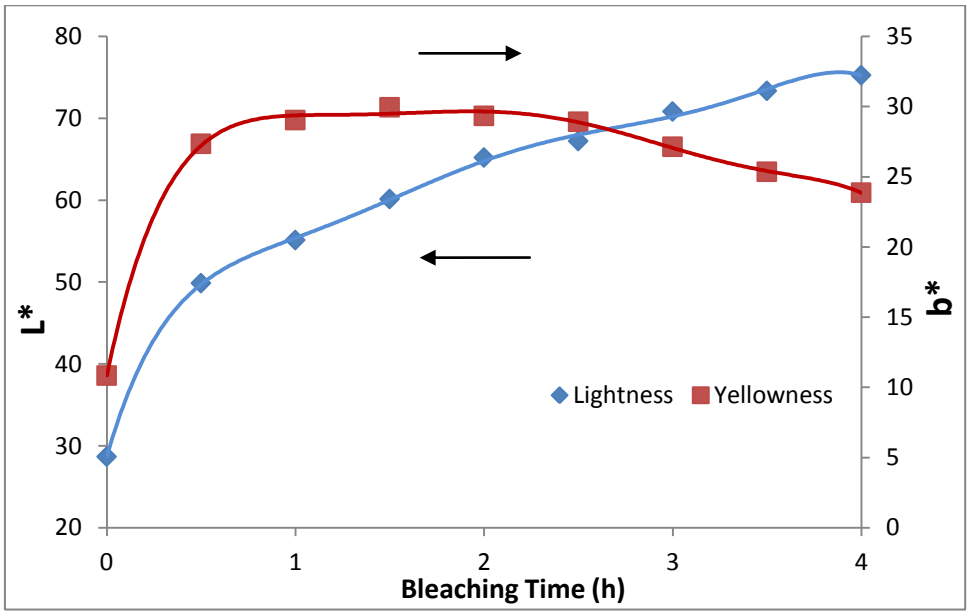

Figure 4.14: The relationship of L*- and b*- values for commercial persulphate bleach over the 4h bleaching time. The trendline curves are empirical and based on polynomial relationships.

Oxidised melanin, causing the changes in L^* and b^* for 9% H_20_2 commercial bleach and commercial persulphate bleach, display a similar semi- circular shape of the graph in Figure 4.15. They both increase in a regular pattern until reaching their maximum values, where the curves start decreasing, and these maximum values appear when

black-brown melanin had been completely degraded and dissolved, as described in the Figures 4.8 and 4.9.

6% H_20_2 bleach curve shows a uniform increase for both b*- and L*- values. *b** and *L** increase simultaneously, which demonstrates that 6% H_20_2 bleached hair has a homogenous damage effect on the yellowness and lightness. But it overlaps with some of the 9% H_20_2 commercial bleach values. This provides an indication that 6% H_20_2 bleach would decrease with further bleaching time once it reaches the maximum value, and this further proves that the 6% H_20_2 bleach has a mild damage effect on the melanin granules. In comparison, commercial persulphate bleach has larger values of *L** and *b**, because it is the stronger oxidising agent.

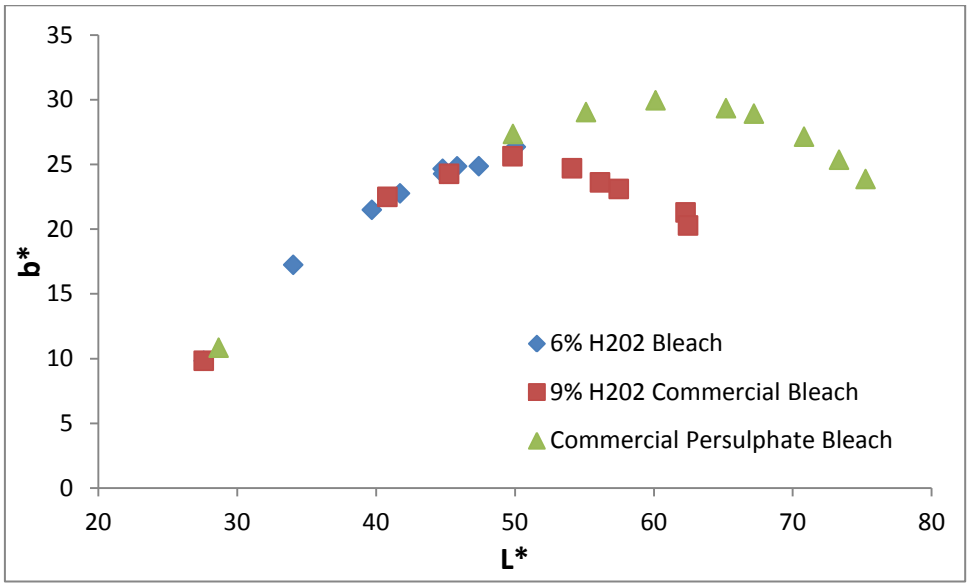

Figure 4.15: The plot of *L** vs. *b** for hairs subjected to three types of bleaches

The spectral reflectance character of the three types of bleach is used as a guide to the effects of bleaching on the colour characteristics of the hair in the visible region in the Figures 4.16, 4.17, and 4.18, respectively.

Overall, there is a dominant increase in the wavelength on the three bleaches with the prolonged treatment times, shown in Figures 4.16, 4.17, and 4.18. The longer bleaching times lead to a higher reflectance of light. On the other hand, different bleaches result in different reflectance curves. Commercial persulphate bleach shows the largest reflectance, followed by 9% H_20_2 commercial bleach and 6% H_20_2 bleach.

It is well known that when light strikes the hair, most of the light is absorbed in dark coloured hair, thus leaving less light reflected. This phenomena provides the evidence that commercial persulphate bleached hair has a relatively lighter appearance than 9% H_20_2 commercial bleach and 6% H_20_2 bleach.

The overall reflectance values for 6% H_20_2 bleach are presented in Figure 4.16. The curve increases significantly in the first 1h reaction time, and then gradually approaches its maximum value. The significant change can be understood in that bleaching is a diffusion-controlled process and the steady increase occurs after overcoming the initial slow rate of diffusion (Hessefort, 2008).

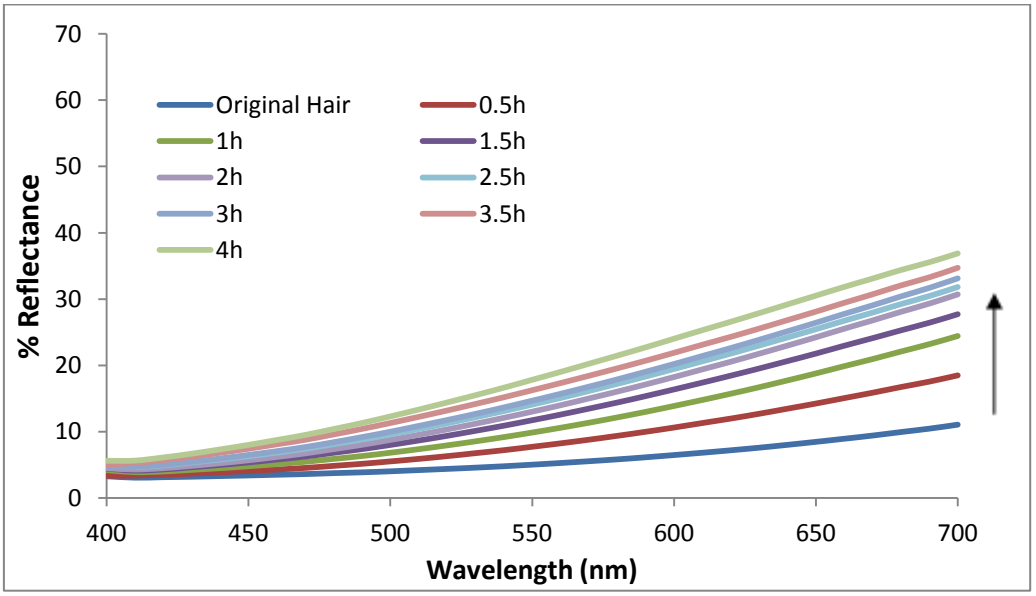

Figure 4.16: Reflectance of 6% H_20_2 bleached hair samples in the visible spectrum. The raw data is given in Chapter 8, Table 8.1.

Relatively, commercial persulphate bleached hair behaves oppositely. The curves in Figure 4.17 observe a major change for 0.5h. Each curve shows a uniform increase for the whole region, with even spacing. This phenomenon indicates that this type of bleaching leads to an overall larger colour change and the bleached hair becomes much lighter over time. This conclusion is also reflected in Table 4.3.

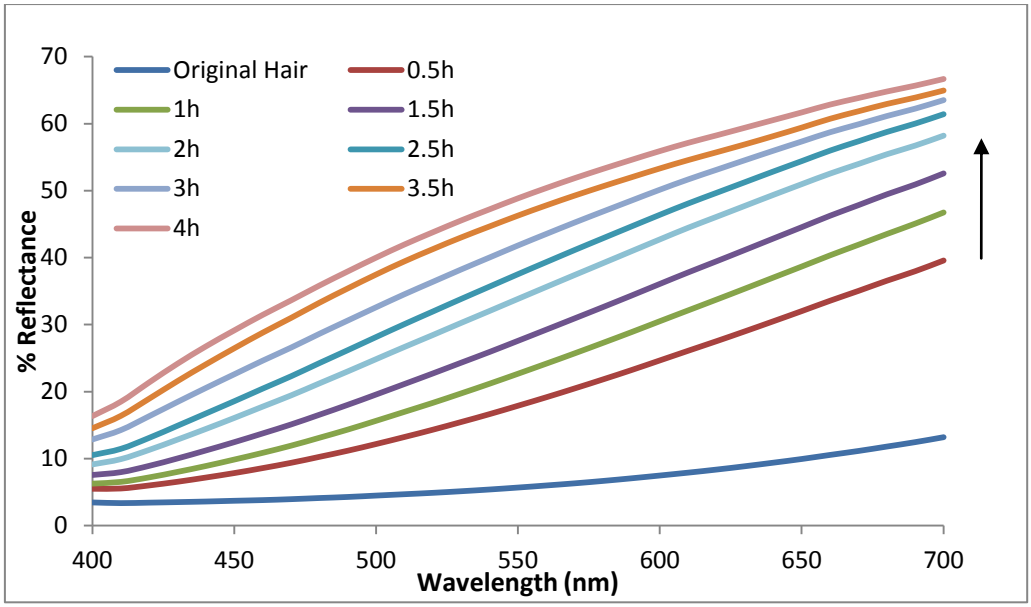

Figure 4.17: Reflectance of commercial persulphate bleached hair samples in the visible spectrum. The raw data is given in Chapter 8, Table 8.2.

9% H_20_2 commercial bleach demonstrates some similarities to both 6% H_20_2 bleach and commercial persulphate bleach in Figure 4.18. The curves show a large difference for 0.5h, and equal spacing of the curves for the rest of the reaction time. In addition, the curves for 2.5h and 3h, and the curves for 3.5h and 4h overlap. This is attributed to the similar reflectance of the bleached hair surfaces.

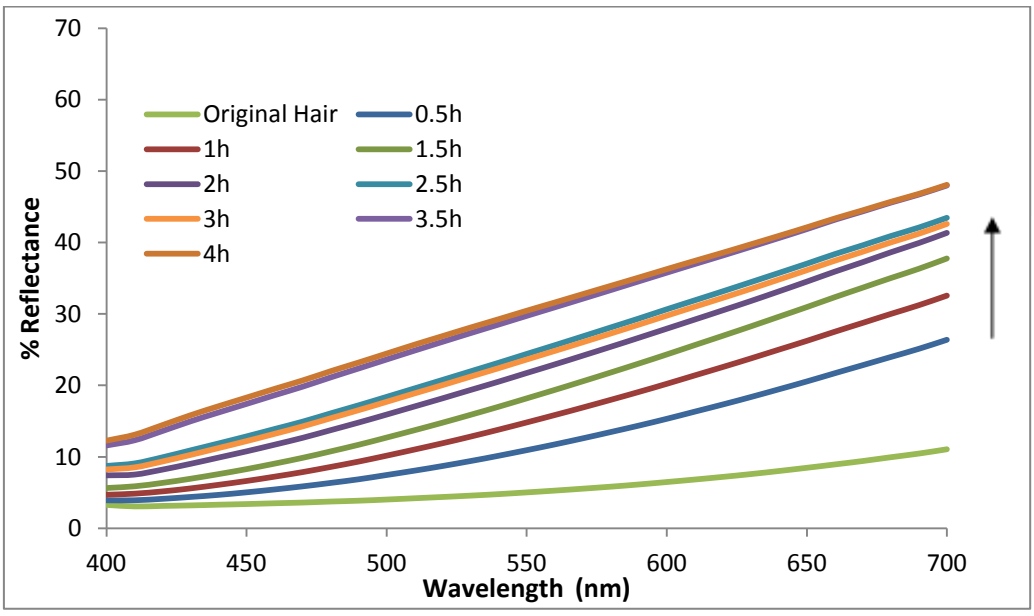

Figure 4.18: Reflectance of 9% H_20_2 commercial bleached hair samples in the visible spectrum. The raw data is given in Chapter 8, Table 8.3.

4.5 Conclusion

It is known that the initial response of oxidative damage of a hair fibre is the colour change. The CIE LAB colour space as an effective tool for the study of colour specification was employed to evaluate the damage effects caused by the three bleaches.

In general, the bleached hairs have an overall lighter, yellowish and reddish colour. It is obvious that the lightness of the bleached hair is associated with pigment oxidation, whereas the yellowness value is determined by two steps. The maximum value appears when the solubilisation of black-brown melanin has been accomplished and is followed by a reduced value as a result of protein (keratin) degradation.

Since the a*- value of hair plays very little role in determining the colour change, the b*- and L*- values are the main contributors in the CIE L*a*b* colour evaluation. The higher the concentration of peroxide, the longer treatment time, the larger is the ΔE*-value, thereby the greater is the hair colour difference. 9% H_20_2 commercial bleach and especially the commercial persulphate bleach demonstrate a higher overall increase in colour change than the 6% H_20_2 bleach, which only has a mild oxidation effect. Consequently, the commercial persulphate bleached hair is much lighter and more yellow than 9% commercial bleached hair and 6% bleached hair.

4.6 References

BATTLE, D. R. 1997. The measurement of colour. *In:* MCDONALD, R. (ed.) *Colour Physics for Industry.* Second Edition ed. Bradford, England: Society of Dyers and Colourists.

BERNS, R. S. 2000. *Billmeyer and Saltzman's principles of color technology,* New York, A Wiley-Interscience Publication.

BROADBENT, A. D. 2001. *Basic Principles of Textile Coloration*, Society of Dyers and Colourists.

FORD, A., ROBERTS, A., 1998. Colour Space Conversions. London: Westminster University, .

HALL, K., WOLFRAM, L.J., 1975. Isolation and identification of the hair protein component of hair melanin. *Journal Cosmetic Chemists,* 26**,** 247.

HESSEFORT, Y., HOLLAND, B.T., CLOUD, R.W., 2008. True porosity measurement of hair: a new way to study hair damage mechanisms. *J Cosmet Sci,,* 59**,** 303-315.

HILL, A. R. 1997. How we see colour. *In:* MCDONALD, R. (ed.) *Colour Physicas for Industry.* Second Edition ed. Bradford, England: Society of Dyers and Colorists.

HUNT, R. W. G. 1971. Colour Measurement *Review of Progress in Coloration* 2**,** 11-19.

HUNT, R. W. G. 1995. *The reproduction of colour in Photography, Printing & Televison,* Kingston-upon-Thames, Fountain press.

HUNT, R. W. G. 1998. *Measuring Colour* Kingston-upon-Thames, Fountain Press.

KLAMAN, M. 2002. *Aspects on Colour Rendering, Colour Prediction and Colour Control in Printed Media.* Royal Institutes of Technology.

MALACARA, D. 2002. *Colour Vision and Colorimetry: Theory and Application,* Washington, SPIE-The international Society for Optical Engnieering.

MCDONALD, R. 1997. *Colour Physics for Industry*, Bradford, England, Society of Dyers and Colorists.

NAPIER, S. 2007. *Personal communication,* Australia, Biolab Group.

OHNO, Y. 2000. CIE Fundamentals for Color Measurements. *IS&T NIP 16 International Conference on Digital Printing Technologies***,** 540-545.

QIAN, X. Y., WANG, Y. J., WANG, B., F., 2012. Fast color contrast enhancement method for color night vision. *Infrared Physics & Technology,* 55**,** 122-129.

RIGG, B. 2007. Colorimetry and the CIE system. *In:* MCDONALD, R. (ed.) *Colour Physical for Industry.* Bradford, England: Society of Dyers and Colorists.

ROBBINS, C. R. 2002. *Chemical and Physical Behavior of Human Hair,* New York,, Springer-Verlag.

SINCLAIR, R. S. 1997. Light, light sources and light interactions. *In:* MCDONALD, R. (ed.) *Colour Physics for Industry.* Second Edition ed. Bradford, England: Society of Dyers and Colourists.

STOCKMAM, A., MACLEOD, D. I. A., JOHNSON, N. E., 1993. Spectral sensitivities of the human cones. *Journal of the Optical Society of America A,* 10**,** 2491-2521.

TASI. 2004. *Colour theory: understanding and modelling colour* [Online]. Bristol: University of Bristol. Available: http://www.tasi.ac.uk/advice/creating/pdf/colour.pdf [Accessed December 5,2007.

VAUGHN, M., VAN OORSCHOT, R., BAINDUR-HUDSON, S., 2008. Hair Color Measurement and Variation. *American Journal of Physical Anthropology* 137**,** 91-96.

VAUGHN, M., VAN OORSCHOT, R., BAINDUR-HUDSON, S., 2009. A comparasion of hair colour measurement by digital image analysis with reflective spectrophotometry. *Forensic Science International,* 183**,** 97-101.

WOLFRAM, L. J., ALBRECHT, L., 1987. Chemical- and photo-bleaching of brown and red hair *Journal of the Society of Cosmetic Chemists,* 38**,** 179-192.

WOLFRAM, L. J., HALL, K., HUI, I., 1970. The Mechanism of Hair Bleaching. *Journal Cosmetic Chemists,* 21**,** 875-900.

WYSZECKI, G. 2006. *Color,* Chicago, World Book Inc.

Chapter 5 Thermal Analysis of Human Hair

5.1 Thermal Analysis

Keratin fibres undergo physical and structural changes when they are heated or drawn. These changes are sometimes accompanied by endothermic or exothermic changes in the thermal measurement of keratins obtained by differential scanning calorimeter (DSC) (Konda, 1973).

5.1.1 Differential Scanning Calorimetry (DSC)

Differential scanning calorimetry, according to the ICTA (International Committee for Thermal Analysis) nomenclature committee, is a technique in which the difference in heat flux (power) to the sample (pan) and to a reference (pan) is monitored against time or temperature while the temperature of the sample in a specified atmosphere is programmed (Groenewoud, 2001). The instrument used is a differential scanning calorimeter (DSC). The DSC cell is composed of two heating compartments, one is for the sample and the other for the reference. The reference is usually a sample pan, which is left empty. There are two principal types of instruments used for DSC investigations: *power-compensation differential scanning calorimetry* (power-compensation DSC) and *heat-flux differential scanning calorimetry* (heat-flux DSC). Their schematic experimental setups are shown in the Figure 5.1.

In power-compensation DSC two nearly identical (in terms of heat losses) measuring holders (microfurnaces) are supplied with individual heaters and their temperatures are measured with separate sensors. The temperature of both holders can be linearly varied as a function of time, being controlled by an average-temperature control loop (Groenewoud, 2001). The detection of any temperature difference between the furnaces leads to an immediate adjustment of the heating power in such a way that the temperature is (almost) identical in both furnaces. The additional (or reduced) heating power is directly correlated with the heat flow into or out of the sample.

One single heater is used in the heat-flux DSC to increase the temperature of both sample cell and reference cell. Small temperature differences, which occur due to exothermic/endothermic effects in the sample, are recorded as a function of the programmed temperature (Groenewoud, 2001). This temperature difference is measured and converted into a heat flow signal through a calibration procedure.

By convention, endothermic events are displayed as upwards signals in *power-compensation* DSC curves and as downwards signals in *heat-flux* DSC curves.

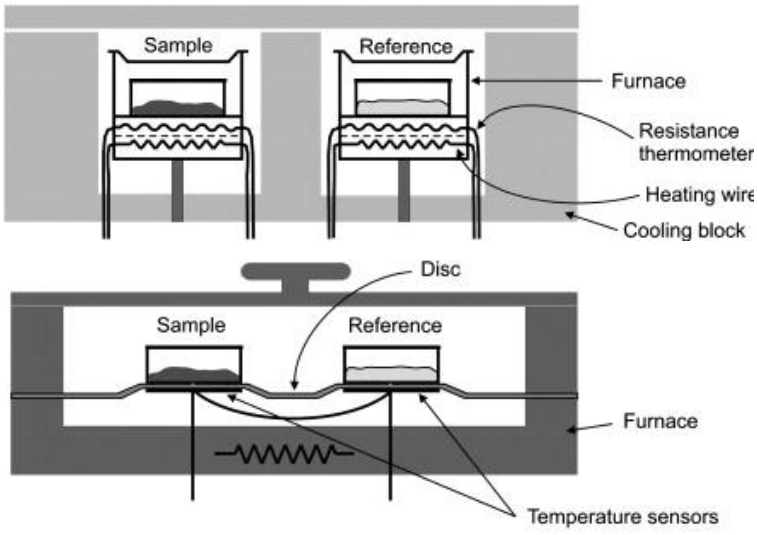

Figure 5.1: Schematic representation of the experimental setup in power compensation DSC (top) and heat flux DSC (bottom, disk-type system) (Bunjes, 2007).

5.1.2 Thermal Stability of Polymers

Differential Scanning Calorimetry (DSC) is one of the most effective analytical techniques to characterize the physical properties of polymers. DSC allows determining heat capacities in both solid and liquid states, phase transition temperatures and the corresponding enthalpy and entropy changes, as well as heat capacity changes (Schick, 2002).

5.1.2.1 Thermal Stability of Proteins

Proteins as common biopolymers, have complex structures, which include the numerous levels such as, primary, secondary, tertiary and quaternary structures (Alberts, 1998). When this structure is destroyed, it may involve partial or entire unfolding of the protein through breaking the hydrogen bonds, which stabilises the higher-order native structures of proteins (Figure 5.2). This process is called denaturation. Denaturation is the process by which a protein is transformed from an ordered ("native") state to a less-ordered state due to the rearrangement of hydrogen bonding without any change to covalent bonds in the polypeptide backbone of the protein molecule (Bischof, 2002). Since a protein can be either partial or total denaturated, this process can be reversible or irreversible. In the case of heat denaturation of proteins at temperature > 45°C, the process is generally considered as irreversible (Bischof, 2005).

The hydrophobic interaction has a predominant role in determining the stability of the folded or native state of the protein rather than other interactions, such as hydrogen bonds, Van der Waals forces and electrostatic interactions. The hydrophobic interaction between exposed non-polar amino acid residues on the surfaces of the protein molecule is short-range and orientation dependent (Chiew, 1995). The maximum stabilities can occur at different temperatures, however, the stability of the folded state decreases at both higher and lower temperatures, and the denatured proteins often show irreversible behaviour at high temperature.

In the case of hair proteins, the helical domains of the IFs in the protein try to unfold at elevated temperatures. The ideal, unfolded protein is the random coil, in which the rotation angle about each bond of the backbone and side-chains is independent of bonds distant in the amino acid sequence. In the context of thermodynamics, when sufficient energy is transferred to a relatively compact ordered protein structure, a change in the molecular conformation occurs, which results in a more flexible, disorganized, opened polypeptide chain structure. This is viewed as protein denaturation. The involved energy usually contains two parts: one is an activation energy barrier (kinetic), and the other is enthalpic (total heat absorption or release).

The kinetic (activation energy) barrier determines the temperature and time dependence of the denaturation process. As the temperature rises, it becomes thermodynamically favourable (i.e., sufficient energy to exceed the free-energy barrier of activation) for the protein to denature (Bischof, 2005). The final denatured state can be at a higher or lower total energy than the original state. When the final state is at a lower energy, this involves a strongly exothermic process, such as coagulation, aggregation, and/or gelation of denatured proteins (Bischof, 2005) (Figure 5.2).

Kinetic models assume that protein denaturation is a rate process. There are many models for describing the protein thermal denaturation. The simplest, but most widely used kinetic model to express the ‘‘2-state’’ behaviour is the first order irreversible rate reaction model. In this case, the process of protein denaturation may be represented by a transition between two distinguishable states:

$$N \rightarrow U \tag{5.1}$$

Where N represents the native or folded state and U represents the unfolded state, although the compact intermediate state could represent a subset of U, which is continuously alternating between various energetically unfavourable states (Creighton, 1990).

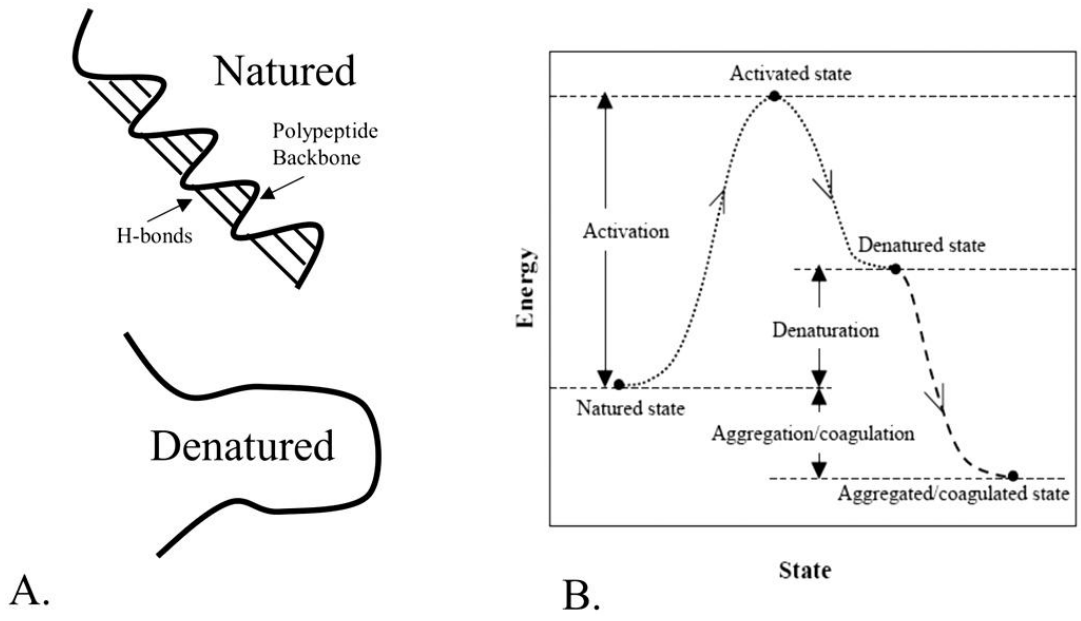

Figure 5.2: (A) describes the hydrogen bonds of a simple α-helix secondary structure within one protein. (B) describes the energy states of protein denaturation (not to scale). There is a state of activation (energy input to the system) followed by denaturation to an energy state above or below that of the initial natured state (Bischof, 2005).

Higher-order kinetic models, which assume that one or more intermediate states exist between the native and denatured states, were also adopted in several studies (Lyubarev, 2000, Cravalho, 1992, Sanchez-Ruiz, 1992), which found that higher-order models could fit experimental results better than the first-order model.

The simple first-order model (Equation.5.1) assumes that each denatured protein molecule transforms irreversibly in a first order reaction into a species from which the native form cannot be recovered. A more complex approach is described by the Lumry-Eyring model (Lumry, 1954). In this model, the irreversible protein denaturation process involves two steps, (i) a reversible unfolding of the native protein (N) followed by (ii) a first order, irreversible step, which involves the secondary structure unfolding to a final state (F), which is unable to fold back to the native one, as:

$$\mathrm{N} \underset{k_2}{\overset{k_1}{\rightleftharpoons}} \mathrm{U} \xrightarrow{k} \mathrm{F}, \tag{5.2}$$

Where *N*, *U* and *F* represents native, partially unfolded and final (irreversibly denatured) protein form; k_1, k_2 and k are the rate constant for the corresponding reactions. Comparison shows that the one-step model in Equation 5.1 is a particular case of the Lumry and Eyring model (Equation.5.2).

There are two main situations when the Lumry and Eyring model (Equation.5.2) is reduced to a one-step irreversible model (Equation.5.1). In the first case the value of k_2 is much higher than the values of k_1 and k, so that the direct reaction of the first step is rate-limiting and the reverse reaction is practically absent. If this step is fast enough, the DSC transition is entirely determined by the kinetics of formation of the final state and equilibrium thermodynamics analysis is not permissible. Another situation happens when the rates of the direct and reverse reactions of the first step (k_1 and k_2) are much higher than the rate of the second step (k), but equilibrium for the first step is shifted toward the form N (Sanchez-Ruiz, 1992).

5.1.2.1.1 Thermal Stability of Keratin Fibres

DSC studies on a wide variety of keratin materials have been conducted by investigating the thermal properties of the main morphological components, namely of IFs and matrix (IFAP), in wool and other keratinous fibres. Schwenker et al (1960) verified that, when a keratin fibre is heated it goes through a number of changes/phases before it eventual degrades to charred residue.

The thermal analysis by DSC allows investigation of the structural changes and the degree of degradation of hair keratin based on the enthalpy data and denaturation temperature of keratin. Assuming the validity of Feughelman's (1959) two-phase model (intermediate filament and matrix) and a 2-state transition model (native and denatured) for the denaturation transition in the keratin fibres, the denaturation enthalpy reflects the progress of the helix-coil transition in the crystalline sections of the intermediate filaments (Wortmann, 1993). In the IFs the concentration of cystine is low and the location and distribution of the sulphur crosslinks are known to be material invariant (Sparrow, 1988). On the other hand, the cystine crosslinks are mainly present outside the helical regions in the matrix material. A significant positive and largely linear correlation was found between denaturation temperature and cystine content for various keratins (Spei, 1989, Crighton, 1985), so that the denaturation temperatures for the various keratins can largely be attributed to the matrix material and mainly to its cystine and thus crosslink concentration. In this way, the denaturation enthalpy depends on the stability of the intermediate filaments, which are composed of α−helical proteins, while denaturation temperature is kinetically controlled by the crosslink density of the matrix, in which the intermediate filaments are embedded (Wortmann, 2002). The limiting step of the thermal denaturation process is considered to be the fission of S–S bonds between the IF and matrix (IFAP) (Istrate, 2009).

The theory that the denaturation enthalpy is related to the amount and structural integrity of α-helical material in the IFs while the denaturation temperature reflects the thermal stability of the matrix has been applied to interpret the effects of cosmetic treatments. Leroy et al. (1992) observed a decrease in denaturation peak area through bleaching. This can be attributed to a loss of crystalline material, as observed by SAXS (small angle X-ray scattering) (Franbourg, 1996) or to a general decrease in native α-

helical material, which can be denatured (Schmidt, 1994). Wortmann et al. (2002) realized that after excessive bleaching and permanent wave treatments, the denaturation temperature and enthalpies were reduced for both types of samples. It was also concluded by Popescu et al. that bleaching affects the amorphous matrix and α−helix faster than the permanent wave treatment (Popescu, 2003).

However extensive damage to the α-helical material is not necessarily accompanied by a loss of X-ray crystallinity (Kanetaka, 1993). Kuzuhara (2006, 2007) used raman spectroscopy on human hair to measure the protein denaturation from α- to random form by oxidation and reduction, to prove the "native helix" hypothesis, which was originally proposed by Wortmann (2002, 2006). They believed that the denaturation enthalpy relates in fact only to the amount of "native" α-helical material, which still shows a denaturation transition, regardless of the total amount of α-helical material in hair, which may already be chemically degraded to some extent.

5.1.3 DSC Investigation of Keratins

Different techniques of thermal analysis of keratin reveal different endothermic transitions. Some environmental effects, which affect the endotherms of keratin fibres in the DSC measurement, should be taken into account, such as DSC cell types, sample preparation, heating rates, the use of open or sealed vessels, and thermal media.

Water and oxygen are two of the factors that influence the degradation of keratin by heat, thus the thermal behaviour of keratin fibres were studied by two DSC methods, "dry DSC" and "wet DSC". The effect of damage is evaluated while the keratin fibre is heated with the use of an open or closed system.

5.1.3.1 DSC Investigations of Keratin in the Dry State

The "dry DSC" method allows the moisture content of the keratin sample to evaporate with increasing temperature. Endothermal effects sometimes appear as a doublet above 200^{o}C (Haly, 1967, Spei, 1989). Spei and Holzem (1987) have shown that the

denaturation peak can usually be detected adequately and evaluated for dry fibres, but that the effect is always secondary in size compared to a large background peak due to general keratin pyrolysis (Wortmann, 2002). Leroy et al (1992) investigated virgin, bleached and perm-waved hair by DSC in the dry state. They observed that with bleaching the DSC peak for dry fibres shifts to higher temperature and the denaturation peak area decreases. Cao (1999) developed a method, using silicone oil as the thermal medium for human hair in DSC analysis, to avoid the water evaporation.

5.1.3.2 DSC Investigation of Keratin in the Wet State

Keratin is known to become softer with water uptake (decrease in modulus) (Milczarek, 1992). Most thermal transitions analysis have been conducted on samples placed under vacuum, immersed in water, or enclosed in a container with a known amount of H_2O. In this closed system the lack of oxygen may avoid the oxidative reaction, although the interaction with water and other pyrolysis products may accelerate the decomposition.

The properties of hair, which has been completely dried on vacuum or highly plasticized by immersion in water under pressure, are drastically different compared to ambient conditions. At ambient conditions keratin contains considerable amounts of water, which form an integral part of its structure. It has been indicated that thermal transitions in keratin are strongly affected by water and depend on the amount present (Milczarek, 1992).

It is generally assumed that water absorbed in keratin exists in three forms: a) water adsorbed on strongly binding sites; b) water adsorbed on weakly binding sites and/or hydrogen bound to strongly adsorbed water; c) loosely bound or free water (Sakabe, 1987, Watt, 1980). At temperatures around 100^{o}C a broad endothermic DSC maximum signal is often observed (Schwenker, 1960, Humphries, 1972), which is related to the removal of free and weakly bound water. The liberation of strongly bound water happens at temperatures above 140 ^{o}C (Watt, 1959). Horio et al. (1965) found that the loss of cystine caused by heating at 140 ^{o}C was greatly increased by an increase in the amount of water sealed with the sample.

In soluble proteins the helix thermally denatures predominantly at temperatures below 80^{o}C, but the insoluble keratin proteins denature above 100 ^{o}C. This is ascribed to the rigidity of the matrix, whose viscosity impedes the segmental mobility of the α-helix and the unfolding process (denaturation) (Istrate, 2009). Previous studies demonstrated that the endothermic peak was observed at 230-250°C when the keratin fibre was dry but appeared at 120-150°C, when the fibres were wet (Haly, 1967, Crighton, 1990). This stabilization of the helix at high temperatures is attributed to the cross-link density of the matrix, into which the IFs are embedded, thus significantly enhancing its temperature tolerance. Since water acts an effective plasticizer in the matrix (Wortmann, 1985, Feughelman, 1997), the denaturation temperature decreases accordingly with increasing water content (Haly, 1967), while the denaturation enthalpy remains constant (Cao, 2005).

Milczareck et al. (1992) verified that water stabilizes the crystalline structure of keratin, while the partial removal of water disorganizes the crystalline phase. Hair samples kept in increasing relative humidities exhibited an increase in the enthalpy of water evaporation.

5.1.3.3 Two Hypothesis in the Peak Separation

Since Haly and Snaith (1967) first reported the observation of a bimodal endotherm in DSC studies of wool, this endothermic doublet has been observed in the range of the degradation temperature of the α-helix in cortical cells, and interpreted using two principally different theories.

Spei and his coworkers conducted DSC studies in the dry state on the various keratins (1990), as well as on isolated low-sulfur and high-sulfur proteins from Lincoln wool (1983, 1989). They verified that in case of endothermic doublets, the low-temperature peak around 230-240 ^{o}C is attributed to helix denaturation, while the high temperature peak (≈250-260^{o}C) corresponds to the matrix degradation from cystine pyrolysis (1987). Cao et al (1997a, 1997b) examined Merino wool in an intermediate state between dry and wet in silicon oil, which is used to preserve a certain amount of water in the fibres. They found that there is a shift of the endotherms to lower temperatures

compared to the dry state. They considered the lower temperature peak of the doublet at ≈ 170^{o}C (dT/dt = 5 ^{o}C/min) as originating from melting or rather denaturation of the α-helical, crystalline material of wool keratin. The broad, higher temperature endotherm beyond around 185^{o}C they considered as the thermal degradation of other histological components, which is in a good agreement with Spei's finding. This endotherm doublet interpretation is referred to as the "helix/matrix" hypothesis.

The helix/matrix hypothesis attributes a second peak or a shoulder to the matrix degradation. However, this might due to the denaturation of the para-cortex, introduced by the ortho/para-cortical hypothesis. Taking Cao's (1997a) finding as an example, the shape of a bimodal curve is explained by three peaks; ortho-cortex, para-cortex and their overlap, with a relatively small cortex denaturation peak.

Wortmann and Deutz (1998) confirmed the ortho/para-cortical hypothesis, which was proposed initially by Haly and Snaith (1967), Crighton and Hole (1985) and Crighton (1990). They suggested that the appearance of double denaturation endotherms for wool is due to the differences of the cystine content and disulfide linkages in the matrix of ortho- and para-cortical cell, which are pronounced enough to allow the separation of the peaks. Isolated ortho-cortical cells in water show a denaturation temperature at about 138°C, whereas the para-cortical cells have a T_D at about 144°C. The higher temperature at which the para-cells denature was attributed to a higher concentration of disulfide linkages (or cystine) (Wortmann, 1998). These values were in good agreement with the results obtained from the whole wool structure. The formation of two separate peaks has also been observed in the dry state, where the denaturation peaks yielded 230°C and 240°C. This again relates to the ortho- and para-cortical cells, respectively (Wortmann, 1998).

Tonin et al. (2004) confirmed the existence of the endotherm double peak for wool keratin and verified the decrease of denaturation in the first peak referring to the ortho cells without changes in the second endotherm peak for treated wool. However, other studies show that the bimodal endotherm of wool in water excess depends on the environment and the heating rate of DSC measurements (Cao, 1997a).

5.1.4 Nonisothermal Kinetics of Keratin Thermal Denaturation

Every chemical reaction is associated with a certain heat of reaction, consequently the heat flow rate is proportional to the rate of reaction. The assignment of the time dependence heat flow rates to defined reactions leads to kinetic data. The advantage of DSC in solving the kinetic problems is its simple, fast sample preparation and the wide range of experimental conditions, which can produce the information in a short time. It will immediately give a series of "reaction rates" as a function of the extent of reaction, depending on time and temperature. The aim of kinetic investigations is then to find quantitatively this functional relationship.

DSCs are generally operated by a controlled program which changes the temperature with time. There are two distinguished modes of operation, one is the constant heating rate (i.e., the classical DSC operation mode) and one is the variable heating rate (periodical or non-periodical change).

5.1.4.1 Constant Heating Rate

In this mode of operation the controlled program follows the time law:

$$T = T_0 + \beta t \tag{5.3}$$

Where, T = temperature

T_0 = starting temperature

β = the heating rate, dT/dt,

t = time

The temperature thus changes linearly in time. Because heat capacity can be defined as the amount of energy required to increase the temperature of a material by 1 Kelvin or degree Celsius, thus:

$$C\mathrm{p} = Q/\Delta T \tag{5.4}$$

Where, Cp = the heat capacity

ΔT = the change in temperature

Q = amount of heat required to achieve ΔT

When temperature is changing, the rate of heat flow is given by

$$dQ/dt = C_p \, dT/dt \tag{5.5}$$

With the heating rate $\beta = dT/dt$, Equation 5.5 leads to

$$dQ/dt = \beta \, Cp \tag{5.6}$$

or

$$Cp = (dQ/dt)/\beta$$

This provides one way of measuring heat capacity in a linear rising temperature experiment: one simply divides the heat flow by the heating rate. If the temperature programme is replaced by one comprising a linear temperature ramp modulated by a sine wave, this can be expressed as:

$$T = T_0 + \beta t + B \sin \omega t \tag{5.7}$$

Where, B = the amplitude of the modulation

ω = the angular frequency of the modulation

And this is the simplest and most used modulation type, namely, a periodic (harmonic, i.e., sinusoidal) temperature programme. In addition, B and ω together with β as the "underlying" heating rate, can be chosen freely within certain limits. The derivative of Equation.5.7 with respect to time is

$$dT/dt = \beta + \omega \, B\cos \omega t \tag{5.8}$$

Thus, it follows with Equation.5.5:

$$dQ/dt = Cp(\beta + \omega \, B\cos \omega t) \tag{5.9}$$

5. 1.4.2 Variable Heating Rate (Modulated Temperature)

In a conventional DSC, a constant heating rate is applied. Although there are many different forms of temperature programme, a sinusoidal temperature modulation is the most popular way, as illustrated in Figure 5.3. Modulated DSC, which uses a sinusoidally modulated temperature profile, superimposed a sine wave onto a conventional constant heating rate experiment.

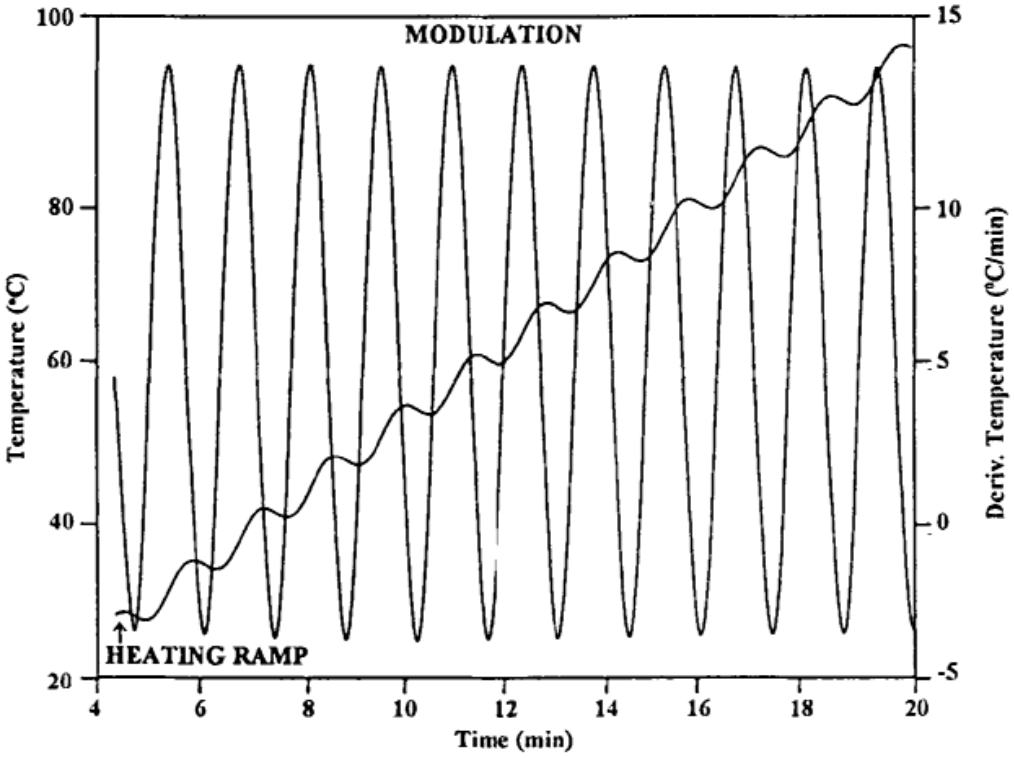

Figure 5.3: Temperature-modulated DSC heating profile (Gill, 1993)

The raw data are averaged over the period of one oscillation to remove the effect of modulation and provide the output *dQ/dt*, which is referred as the average or total heat flow. This output is equivalent to that of conventional DSC and yields the total heat capacity C_p^T as a function of temperature through:

$$C_p^T = 1/(\beta\, m)\, dQ/dt \qquad (5.10)$$

Where, $\beta = dT/dt$ is the heating rate

t = time

T = absolute temperature

m = sample mass

This curve for total heat flow is subtracted from the raw data and the modulation is then subjected to Fourier Transform Analysis to obtain the amplitude and phase difference of the heat flow response with respect to the temperature modulation. Through consideration of the cyclic heat capacity or modulus of complex heat capacity, it finally yields the so-called reversing heat capacity of the sample C_p^R (Gill, 1993, Schawe, 1996).

If the results are expressed as heat capacities, then the average total heat flow is divided by the underlying heating rate β. Thus,

$$(\Delta \mathrm{d}Q/\mathrm{d}t)/\beta = C_p^T = \text{the average or total heat capacity}$$

Furthermore, C_p^T is simplified (Schawe, 1996) by two components as:

$$C_p^T = C_p^R + C_p^{NR} \tag{5.11}$$

where C_p^{NR} is called as non-reversing (NR) or less commonly the kinetic heat capacity.

Although all of the parameters in Equation. 5.11 are expressed as heat capacities, they can equally well be expressed as heat flows.

$$\mathrm{d}Q/\mathrm{d}t = \text{average or total heat flow}$$

$$C_p^R \beta = \text{reversing heat flow}$$

$$C_p^{NR} \beta = \text{non-reversing heat flow}$$

If the underlying heat flow is changing slowly and smoothly under the modulation, averaging the modulated signal over the period of the modulation will approximately provides the same information as an un-modulated experiment. And the ”averaging” means the modulated experiment looks ‘smoothed’ to some extent.

5.1.4.3 Kinetic Investigation

While the sample is subjected to a controlled temperature ramp, it is reasonable to assume that it reflects a transformation which can be represented for the simplest case as:

$$B_0 \xrightarrow{k} B_1 \tag{5.12}$$

Where B_0 is the material before transformation and B_1 is the material after transformation. Any conversion is accompanied by an absorption or release of heat. In a quantitative way it is expressed by means of the enthalpy of the process (Wortmann, 2006):

$$\Delta H = \int_{T1}^{T2} C_p \, dT = \int_{t1}^{t2} C_p \, \beta \, dt \tag{5.13}$$

Where, ΔH = enthalpy

t = time

T = temperature

C_p = heat capacity

β is the heating rate (Equation.5.3), thus, the degree of conversion, α, is calculated from the DSC curve assuming that the area under the peak up to a given time is proportional to the degree of conversion:

$$\alpha = \frac{PA_t}{PA_{total}} \tag{5.14}$$

Where PA_t is the integral of the peak up to time t and PA_{total} is the overall peak area.

With this definition of conversion, the reaction rate is given by the following equation (Istrate, 2009):

$$\frac{d\alpha}{dt} = M(\alpha(T)) = k(T) f(\alpha) \tag{5.15}$$

Where $\frac{d\alpha}{dt}$ is the reaction rate, α is the degree of conversion, $k(T)$ is the rate constant as a function of the absolute temperature T, and $f(\alpha)$ is an unknown function of conversion.

The temperature dependence of the rate constant $k(T)$ is usually described by the empirical Arrhenius equation or less frequently by the Eyring equation, which follows from the theory of the activated complex:

$$\text{Arrhenius: } k(T) = A \cdot \exp\left(-\frac{E_A}{RT}\right) \tag{5.16}$$

Where, A = preexponential factor

E_A = activation energy

R = universal gas constant

$$\text{Eyring: } k(T) = \left(\frac{K_B \cdot T}{h}\right) \exp\left(\frac{\Delta S}{R}\right) \cdot \exp\left(-\frac{\Delta H}{RT}\right) \tag{5.17}$$

Where, K_B = Boltzmann constant

h = Planck constant

ΔS = activation entropy

ΔH = activation enthalpy

Here, $\Delta H = E_A - R \cdot T$

$$\Delta S = R \cdot \ln\left(\frac{A \cdot h}{e \cdot K_B \cdot T}\right)$$

The inseparable combination of rate law $f(\alpha)$, activation energy E_A, and preexponential factor A is sometimes referred to as the "kinetic triplet" (Maciejewski, 2000).

There are several methods for calculating the kinetic triplet, $f(a)$, E_A and A. A certain reaction model implies a specific analytical form of the kinetic function $f(a)$. There are also the model-free methods which allow calculating the value of the activation energy, E_A, without any knowledge of the reaction pathway. The advantage of analysing kinetic data using model-free methods is their independence of any model or mechanism, and they are thus able to describe the most complicated reaction behaviour

at different temperatures (Fernandez d'Arlas, 2007, Vyazovkin, 2006), as long as the reaction mechanism does not change with temperature and heating rate (Fernandez d'Arlas, 2007).

5.1.4.4 Kinetic Analysis Methods

It is necessary to discuss the kinetic analysis methods in relation to the temperature control modes. From the early 1970's, ASTM International has developed a series of kinetic methods to meet a variety of needs, these include E2041 which makes use of a single scan using the Borchardt and Daniels approach (1957), E2070 using the isothermal Šestak-Berggren approach (1971), and E698 using the multiple heating rates Ozawa (1970) and Flynn and Wall (1966b) approach.

The isoconversional method of Flynn, Wall and Ozawa (Flynn, 1966a, Ozawa, 1970) is a 'model-free' method, which involves measuring the temperatures corresponding to fixed values of α from experiments at different heating rates β and plotting $\ln(\alpha)$ against $1/T$. The slopes of such plots give $-E_A/R$. If E_A varies with α, the results should be interpreted in terms of multi-step reaction mechanisms (Burnham, 1999, Ozawa, 1970).

ASTM E698, as reviewed by Popescu and Segal (1998), is based on the Arrhenius-equation, which is used to investigate the dependence of the denaturation temperature T_D on the heating rate. The Arrhenius-equation for this interrelation of these two parameters can be expressed as followed:

$$\beta = A \exp\left[-E_A/(RT_D)\right] \qquad (5.18)$$

Where A is the pre-exponential factor, E_A is the activation energy of the process (J/mol), and R is the molar gas constant (8.314J/Kmol). E_A is determined from the slope of the line through the data in a so-called Arrhenius-plot, which is represented as $\ln \beta$ *vs.* $1/T_D$.

5.2 Objectives

DSC is the technique of choice to investigate the calorimetric effects associated with protein structural changes (Bischof, 2005). In this chapter thermal analysis was performed on bleached hair in water to determine the structural changes and the degree of degradation based on the enthalpy and denaturation temperature data and to discuss them in terms of the thermal properties of filaments and matrix. A kinetic approach based on ASTM E698 for the description of the oxidation influences is applied.

5.3 Experimental

There are generally two ways of measuring DSC of keratins, namely in water and in a dry environment (allowing the moisture to evaporate during heating). The DSC under dry condition was shown to give misleading information due to the interference of pyrolysis (Wortmann, 2002). Consequently, the present work deals exclusively with DSC of keratins in water.

There are two types of experiments performed. In the standard Modulated DSC mode (MDSC), the samples (6% H_2O_2 bleached hair, 9% H_2O_2 commercial bleached hair and commercial persulphate bleached hair) were heated with the temperature increasing linearly at a rate of 3^oC/min, and the corresponding heat flow was recorded. In the kinetic investigation, the samples (virgin human hair, mohair and 2h commercial persulphate bleached human hair) were heated with various heating rates between 0.1^oC and 7^oC, applying modulation parameters suitable for a given heating rate, as shown in the Table 5.1.

Table 5.1: The parameters for the heating rate and modulation

Heating Rate(^{o}C/min)	0.15	0.2	0.3	0.5	1	1.5
Modulation (^{o}C/min)	0.05	0.1	0.1	0.1	0.5	0.5
Heating Rate(^{o}C/min)	2	2.5	3	4	5	7
Modulation (^{o}C/min)	1	1	1	1	1	3

All analyses were conducted on a power-compensated DSC instrument (DSC Q10, TA-Instruments), using pressure-resistant (25bar), stainless-steel, large-volume capsules (TA Instruments) in the temperature range of 80-180^{o}C in excess water (high pressure DSC). Because the initial evaporation of water quickly builds up high pressure inside the pan, it suppresses further evaporation.

Randomly selected hairs taken from the midsection of a hair tress were used to produce hair snippets (~ 2mm in length). Prior to measurement the samples were stored under standard room condition (20^{o}C, 65%RH) to ensure invariant water content. Hair snippet samples between 3 and 10 mg were weighted into the sample container. The weight basis for all calculations was the conditioned weight of hair, containing 12% water (Wortmann, 2007). 40 µl water were added, the container was sealed with a lid using the sample encapsulating press, and the samples were stored overnight to achieve equilibrium water content and distribution. As a reference, an empty container was used. At least two samples for each experiment were measured.

Two assumptions have to be considered in determining the kinetics by DSC: (1) the heat flow relative to the instrument baseline is proportional to reaction rate and (2) the temperature gradients through the sample and the sample-reference temperature difference is small. By using small sample sizes (<10mg) and slow heating rates (or isothermal experiments) these assumptions are reasonable.

The collected DSC raw data were analysed using the TA Instruments Universal Analysis 2000 Program. The curves were processed using suitable, nonlinear baselines provided by software PeakFit V4.12, which led to improved estimates for the characteristic parameters. Processing the modulated DSC-data by the instrument's

software yielded curves for total heat capacity, (C_p^T), reversing heat capacity, (C_p^R) and non-reversing heat capacity, (C_p^{NR}). From the C_p^R curve the heat capacity change ΔC_p, which is underlying the phase transition, is provided. The curve of C_p^{NR} yields the peak temperature T_D and the peak area with the determined baseline, which is referred to as the denaturation enthalpy ΔH_D. Further data analyses were conducted using Excel software (Microsoft).

5.4 Results and Discussion

5.4.1 DSC of Virgin Hair in Water

By applying DSC to human hair in water, the thermal stabilities of the major morphological components in the cortex can be determined. All DSC curves recorded at 3°C/min heating rate for the hair samples exhibit the endothermic process. An example of untreated hair, for which the endothermal effect is observed at around 144°C, is illustrated in Figure 5.4.

The α-keratin denaturation peak of human hair is not reversible. When an endothermic peak becomes apparent in the curve of the non-reversing heat capacity C_p^{NR}, the denaturation enthalpy ΔH_D is determined by applying a linear baseline between the start (T_1) and end temperature (T_2) of the peak. The initial data obtained from the DSC-curves are hence the peak- or denaturation temperature T_D and the denaturation enthalpy ΔH_D. The start and end temperature of the baseline, defining the peak, are marked in Figure 5.4.

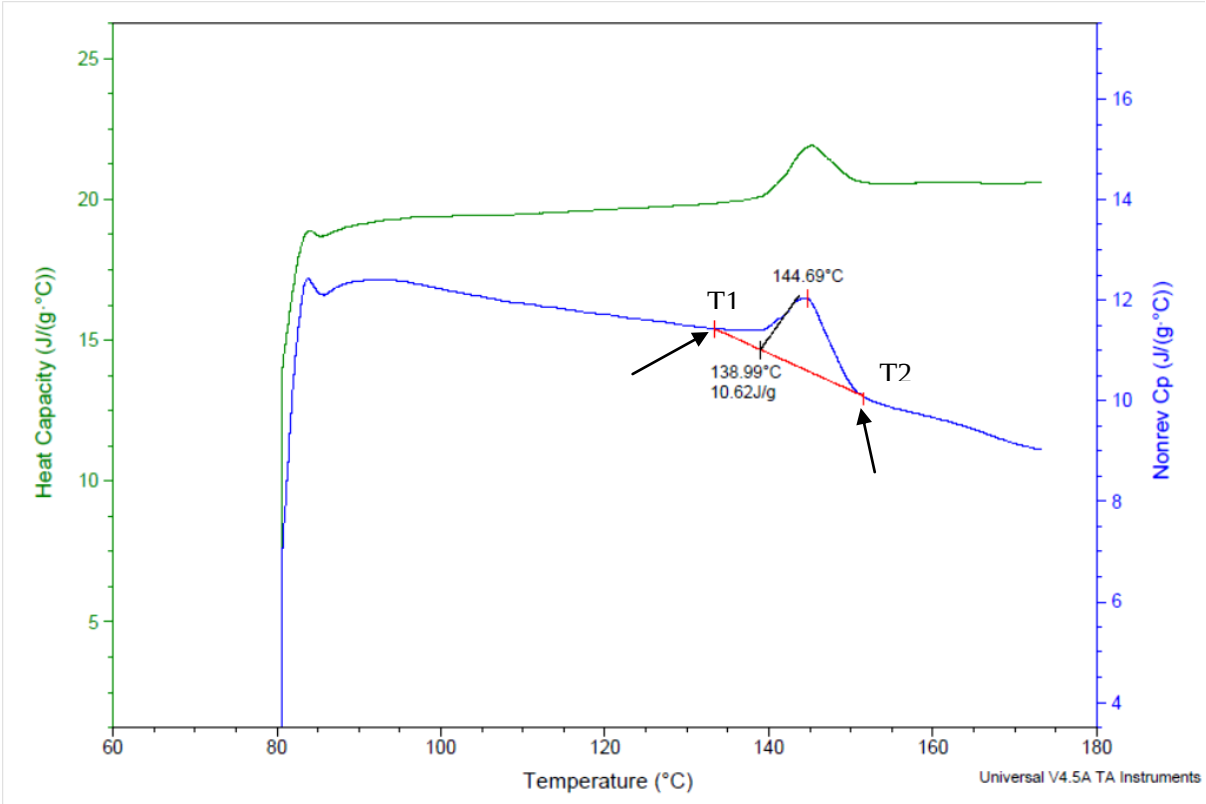

Figure 5.4: Typical non-reversing C_p^{NR} DSC curve for untreated human hair in water. The green curve represents the overall heat capacity of the human hair whereas the blue curve is the non-reversible heat capacity of the human hair.

The denaturation temperature and the peak area reflect different aspects of the thermal stability of the matrix and the filaments in the cortex of hair, respectively. The peak temperature, T_D, which is the denaturation temperature of the helical material, is influenced by the heating rate (Rüegg, 1977) as well as the surrounding environment (especially pH) (Bischof, 2005, Eyring, 1974, Joly, 1965). The denaturation enthalpy ΔH_D, which is the energy required for the helix denaturation, is independent of any denaturation model assumption (Cooper, 1999). It was shown by Spei et al (1987) that the area of the peak related to the keratin denaturation is a good measurement of the α-helix content. The recorded endotherm reflects the progress of the helix-coil transition in the crystalline sections of the intermediate filaments. However the endotherm varies in terms of shape and size from measurement to measurement (Cao, 1999).

There are several methods of determining the area of a DSC peak, depending on the selected shape of the baseline. The standard method is to use a straight baseline, while

in some cases a parabolic or hyperbolic baseline is applied. Milczarek et al (1992) found that the use of a hyperbolic shape of the baseline causes only a ~5% differences in the obtained peak area, compared with the linear baseline. Thus, the standard linear baseline is adapted in our thermal analysis study, which is provided by the TA Instruments Universal Analysis 2000 Program.

The reversible heat capacity of virgin hair is given by the MDSC-curve in the wet state (Figure 5.5). This C_p^R curve shows that there is a stepwise change in the range of the heat capacity of 1.14 J/(g·K). The ΔC_p^R is decided by measuring the distance between the upper and lower baselines, where the horizontal lines (- - -) define the anticipated maximum point and lowest point in the transition change. The non-reversible heat capacity ΔC_p^{NR} also is shown in the Figure 5.5. It is obvious that the two points which define the peak area on the non-reversible heat capacity curve correspond to similar temperatures with the maximum and lowest point in the phase transition change on the curve of reversible heat capacity in human hair.

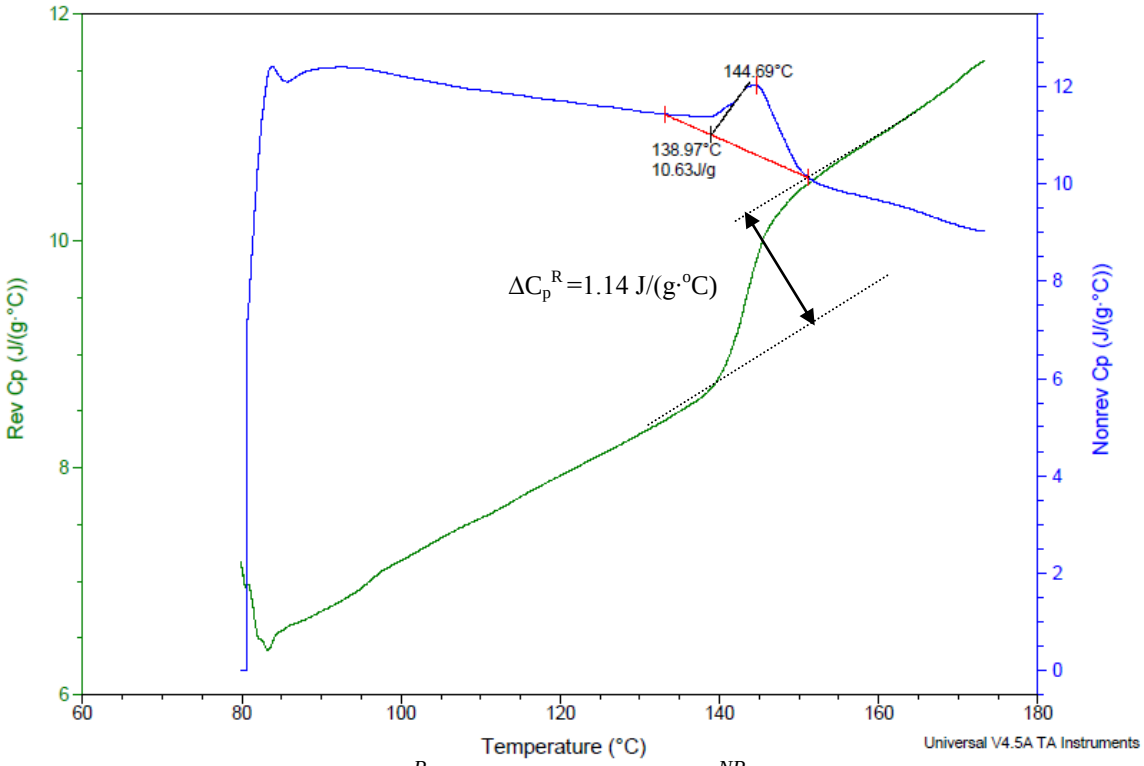

Figure 5.5: Typical reversing C_p^R and non-reversing C_p^{NR} DSC curves for untreated human hair in water. The green curve represents the curve of reversible heat capacity for human hair, whereas the blue curve shows the non-reversible heat capacity. The upper and lower baselines for the step-wise change are indicated and the value of ΔC_p^R is given.

In the further discussion, we will only concentrate on analyzing the thermal reaction in the DSC peak occurring in the 100-180^{o}C temperature range (α-keratin or crystalline peak).

5.4.2 Water Absorption Effect on the Keratin

In the process of sample preparation (Chapter 2), 9% H_2O_2 commercial bleached sample (3.5h, 4h) and commercial persulphate bleached sample (3.5h, 4h) were left in water overnight to investigate the influence of thermal analysis of soaking keratin in water for prolonged times.

The commercial persulphate bleached hairs were chosen as an example. The samples which had been bleached previously for 2.5h, 3h, 3.5h, and 4h were stored in water for an additional 48 hours at room temperature. The denaturation temperatures T_D and denaturation enthalpies ΔH_D of keratin were correspondingly compared, and the results are presented in the Table 5.2.

Table 5.2: The comparison between denaturation temperatures T_D and enthalpies ΔH_D for commercial persulphate bleached hairs before and after soaking in water for 48 hours

Bleaching Time (h)	T_D (^{o}C)		ΔH_D (J/g)	
	After Bleaching	Soak in Water (48h)	After Bleaching	Soak in Water (48h)
2.5	125.1±0.1	127.6±2.0	9.8±0.3	10.4±0.0
3	124.7±0.1	129.3±1.2	10.9±0.0	10.9±0.4
3.5	127.3±1.7	130.9±4.1	9.2±0.4	9.8±0.3
4	129.9±0.7	130.3±0.5	11.2±0.7	10.3±0.4

Although part of the α-helical phase is not accessible to water at room temperature (Feughelman, 1989), the individual microfibrils still show some degree of swelling (Spei, 1984), thus water may still access the α-helical regions of the microfibrils. This swelling is considerably less than that of the matrix, in which they are embedded. As

described in the previous literature discussion, the denaturation temperature of the helices is controlled by the viscosity of the surrounding matrix. The denaturation temperature drops accordingly with the water content, when water acts as a plasticiser in the matrix. This finding was confirmed by Haly and Snaith (1967) by DTA experiments on wool. Similar experiments also were conducted by Cao and Leroy (2005) on human hair by DSC. They believe that the denaturation enthalpy is not affected by a change of water content. This conclusion is reflected in the results in Table 5.3, which were obtained before and after soaking keratin in water.

In Table 5.3, all of the bleached samples follow the same trend, that there is a consistent increase in T_D after soaking in water. Little effect on ΔH_D is observed, giving the evidence that water plays a very important role for the denaturation temperature, which is kinetically controlled by crosslink density of the matrix (Wortmann, 2002).

Due to the above reason, the results of denaturation temperature and denaturation enthalpy at 3.5h and 4h were excluded from further thermal transition investigation, to avoid the unexpected results, since the storage time in water strongly affects the thermal transitions of keratin (Milczarek, 1992).

5.4.3 DSC on Various Bleaches Effects

DSC measures the effects of bleaching on the DSC curves of hair fibres in water. The effects, as reflected in changes of denaturation temperatures T_D and enthalpies ΔH_D, are discussed in terms of the thermal properties of filaments and matrix.

There are two hair sources involved in the bleaching procedure (see Chapter 2). Because of the differences between hair batches, the relative denaturation temperature (T_D^R) and the relative denaturation enthalpy (ΔH_D^R) were employed in this investigation, given by

$$T_D^R = (T_D / T_D^0) \tag{5.20}$$

Where, T_D^0 is the denaturation temperature of virgin hair

T_D is the denaturation temperature of target hair

And,

$$\Delta H_D{}^R = (\Delta H_D/\Delta H_D{}^0) \quad (5.21)$$

Where, $\Delta H_D{}^0$ is the denaturation enthalpy of virgin hair

ΔH_D is the denaturation enthalpy of target hair

In addition, the results for bleached hair samples which had been treated for 3.5h and 4h were taken off, because of the water storage effect (see section 5.4.2).

Tables 5.3-5.5 summarize the DSC results of denaturation temperature and denaturation enthalpy for the bleached samples for the various bleaching treatments. The values of $T_D{}^R$ and $\Delta H_D{}^R$ show a consistent decrease for all bleached hair samples. For a given bleaching time, commercial persulphate bleached hair shows a more pronounced damage effect than 9% H_2O_2 commercial bleach and 6% H_2O_2 bleached hair. The aggressive chemical treatment thus results in a lower enthalpy and a lower peak temperature, which implies less crystalline material in the IFs and less cross-link density in the matrix (IFAPs). In parallel, the longer the treatment time, the greater is the structural damage in the hair keratin. Commercial persulphate bleached hair (3h) has the lowest denaturation temperatures T_D value (123.9^{o}C) compared to all other bleached hairs.

Table 5.3: The results for T_D and ΔH_D for the 6% H_2O_2 bleached samples, in the form of the arithmetic means, as a representative of $T_D{}^R$ and $\Delta H_D{}^R$

Bleaching Time (h)	T_D (^{o}C)	$T_D{}^R$	ΔH_D (J/g)	$\Delta H_D{}^R$
0	145.4±0.4	1	11.5±0.1	1
0.5	142.1±0.7	0.98	10.9±0.3	0.95
1	140.8±0.3	0.97	11.1±0.5	0.97
1.5	141.9±0.7	0.98	10.6±0.1	0.92
2	140.3±0.2	0.97	11.2±0.1	0.98
2.5	140.5±0.5	0.97	11.0±0.7	0.96
3	140.0±0.3	0.96	11.1±0.6	0.96

Table 5.4: The results for T_D and ΔH_D for the 9% commercial bleached samples, in the form of the arithmetic means, as a representative of $T_D{}^R$ and $\Delta H_D{}^R$

Bleaching Time (h)	T_D (°C)	$T_D{}^R$	ΔH_D (J/g)	$\Delta H_D{}^R$
0	145.4±0.4	1	11.5±0.1	1
0.5	141.2±0.4	0.97	10.7±0.1	0.94
1	139.2±0.4	0.96	10.4±0.3	0.91
1.5	137.6±0.0	0.95	11.4±0.2	0.99
2	134.3±0.2	0.92	9.8±0.2	0.85
2.5	132.1±0.1	0.91	4.4±1.2	0.39
3	132.7±0.6	0.91	5.8±0.5	0.5

Table 5.5: The results for T_D and ΔH_D for the commercial persulphate bleached samples, in the form of the arithmetic means, as a representative of $T_D{}^R$ and $\Delta H_D{}^R$

Bleaching Time (h)	T_D (°C)	$T_D{}^R$	ΔH_D (J/g)	$\Delta H_D{}^R$
0	144.2±0.3	1	15.4±0.5	1
0.5	136.7±0.2	0.95	13.8±0.6	0.9
1	128.8±0.5	0.89	11.9±0.2	0.77
1.5	126.6±0.1	0.88	12.0±0.9	0.78
2	125.0±0.4	0.87	9.6±0.2	0.62
2.5	125.1±0.1	0.87	9.8±0.3	0.64
3	124.7±0.1	0.86	10.9±0.0	0.71

While comparing the three bleaching treatments (6% H_2O_2, 9% H_2O_2 commercial bleach and commercial persulphate bleach), a consistent decrease in $T_D{}^R$ as well as $\Delta H_D{}^R$ with prolonged bleaching time is observed in Figures 5.6 and 5.7, respectively. Commercial persulphate bleach decreases fastest in both $T_D{}^R$ and $\Delta H_D{}^R$ than 9% H_2O_2 commercial bleach and 6% H_2O_2 bleach, although $\Delta H_D{}^R$ of 9% H_2O_2 commercial bleach (Figure 5.7) drops faster after 2h than commercial persulphate bleach, indicating that the IF of 9% H_2O_2 commercial bleached hair is heavily damaged after the extensive oxidation time (2h). Commercial persulphate bleach and 6% H_2O_2 arrived their saturation within the 3 hours treatment, however 9% H_2O_2 commercial decrease linearly with the increasing time.

The curve of 6% H_20_2 bleach illustrates a quite stable value for $T_D{}^R$ and $\Delta H_D{}^R$ in Figures 5.6 and 5.7, implying that it has little damage effect on the keratin, or in another way that it plays little role for affecting both $T_D{}^R$ and $\Delta H_D{}^R$.

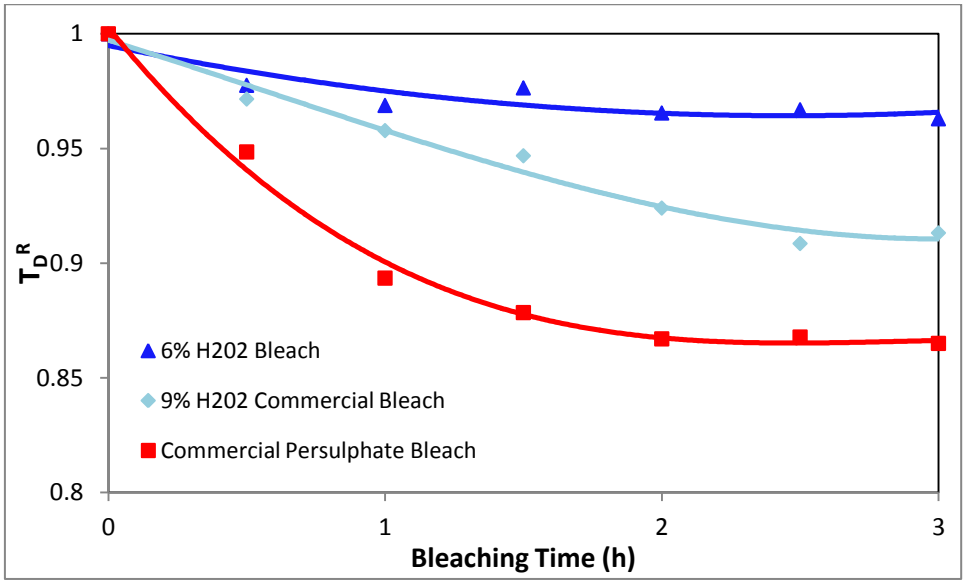

Figure 5.6: Relative denaturation temperature $T_D{}^R$ for 3 bleaches: (6% H_2O_2 bleach, 9% H_2O_2 commercial bleach, commercial persulphate bleach) for 3 hours bleaching time. The trendline curves are empirical and based on polynomial relationships.

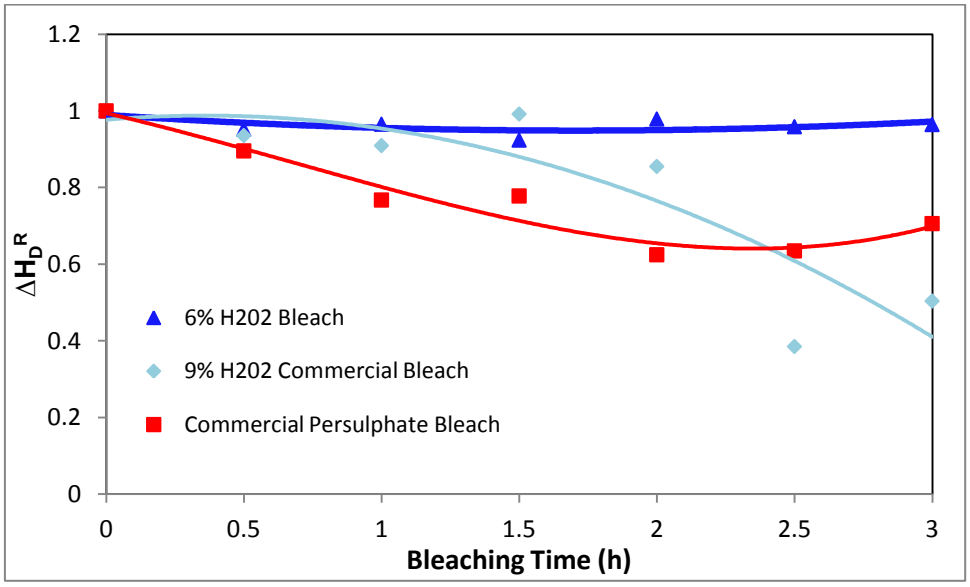

Figure 5.7: Relative denaturation enthalpy $\Delta H_D{}^R$ for 3 bleaches: (6% H_2O_2 bleach, 9% H_2O_2 commercial bleach, commercial persulphate bleach) for 3 hours bleaching time. The trendline curves are empirical and based on polynomial relationships.

DSC analyses confirm the damage of bleaching to hair keratin. The results show a lower keratin denaturation enthalpy, which is due to the increase in the disorganization of IF in the keratin structure, and a lower denaturation temperature, which is related to the reorganization of matrix crosslinks after the denaturation (Monteiro, 2005). The lower ΔH_D value, the less amounts of the α-form crystallites remain in the IFs. Likewise, the lower T_D value, the lower cross-link density in the matrix (IFAPs) (Wortmann, 2002). This phenomena is well explained by that bleaching leads to the increased concentrations of cysteic acid and thus to more ionic interactions, but this interaction will be broken in the wet state, the increase in the content of anionic groups induces an increase in water content, leading to a continuous decrease of matrix viscosity and thus of T_D (Wortmann, 2002).

The correlation between ΔH_D^R and T_D^R for the three bleaching treatments is explored in Figure 5.8 by plotting ΔH_D^R against T_D^R. A strong linear relationship is observed for 6% H_2O_2 bleach, commercial persulphate bleach and part of 9% H_2O_2 commercial bleach, suggesting that the three bleaches have a homogeneous oxidation effect on IFs and IFAPs. However the results for 9% H_2O_2 commercial bleach after 2h bleaching time are unexpected and it is considered that IFs are subjected to progressive damage after excessive bleaching treatment. Thus, there is a bigger decrease in denaturation enthalpy compare with the denaturation temperature. Consequently, the gradient of the denaturation enthalpy vs. denaturation temperature is prone to be lower.

The results of 6% H_20_2 bleach cluster in a narrow range of the ΔH_D^R and T_D^R in Figure 5.8, while both 9% H_2O_2 commercial bleach and commercial persulphate bleach distribute their denaturation values along both axes, except for the deviative results for 9% H_2O_2 commercial bleach. This conclusion further confirms that 6% H_20_2 bleach only has a moderate damage effect on the keratin, whereas there is a prominent structural change on both IF and matrix by commercial persulphate bleach and 9% H_2O_2 commercial bleach.

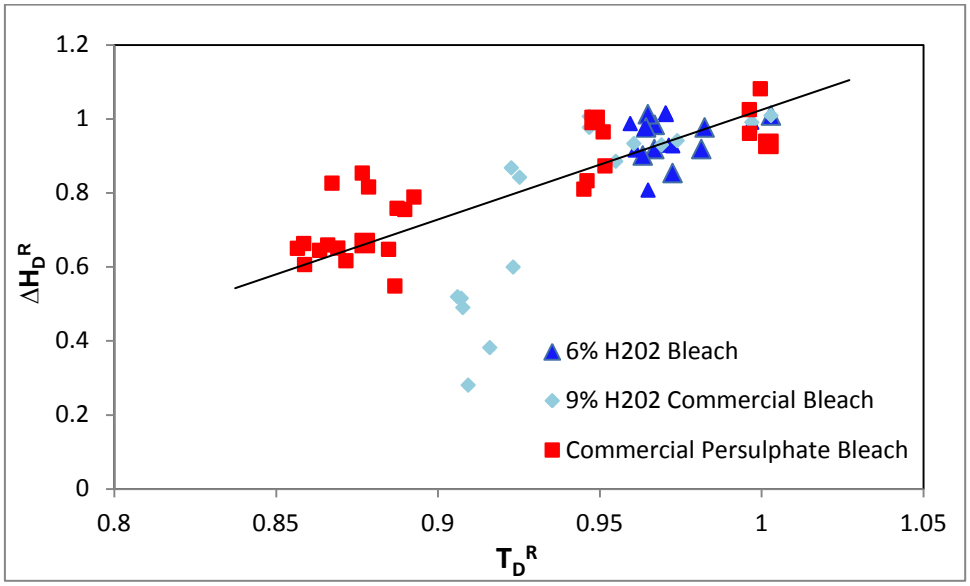

Figure 5.8: Plot of $\Delta H_D{}^R$ against $T_D{}^R$ for the 3 bleaches: (6% H_2O_2 bleach, 9% H_20_2 commercial bleach, commercial persulphate bleach) for up to 3 hours bleaching time.

5.4.4 Nonisothermal Kinetics of α-keratin Thermal Denaturation

5.4.4.1 Nonisothermal Kinetics on the Bleaching Effect in Human Hair

The course of the denaturation was investigated by a kinetic analysis of the DSC-curves for untreated and oxidised hair. There is a consensus that single-heating rate scans have severe limitations for a kinetic analysis (Opfermann, 2000, Burnham, 2000). The kinetic analysis of the endothermic process in the DSC measurements is thus carried out for different heating rates. Ten heating rates were utilized and the results for virgin hair and commercially persulphate bleached (2h) hair are presented in Tables 5.6 and 5.7.

Table 5.6: Results for virgin hair at various heating rates

Heating Rate(^{o}C/min)	0.15	0.5	1	1.5	2	2.5	3	4	5	7
Modulation (^{o}C/min)	0.05	0.1	0.5	0.5	1	1	1	1	1	3
ΔT (K)	128.4 128.3	133.1 133.8	138.1 140.6 137.8	138.4 138.4	140.4 139.8	141.0 141.0	143.6 146.4 144.2 142.9	145.4 145.6	147.0 148.5	147.8
ΔH(J/mol)	5.0 6.1	9.3 8.6	11.3 12.2 11.0	15.8 14.2	15.5 15.6	15.4 13.4	13.4 11.7 12.7 11.8	12.4 10.5	11.5 11.9	14.4

Table 5.7: Results for commercial bleached human hair (2h) at various heating rates

Heating Rate (^{o}C/min)	0.15	0.2	0.3	0.5	1	1.5	2	3	4	5	7
Modulation (^{o}C/min)	0.05	0.1	0.1	0.1	0.5	0.5	1	1	1	1	3
ΔT (K)	113.5 113.4 113.3	114.1 114.4 113.7	116.1 115.6 116.2	117.5 117.4 117.7	120.8 120.5 120.5	122.6 122.7 122.4	124.1 123.7 123.8	126.2 126.4 126.6	127.5 126.7 127.4	129.0 127.6 128.7	129.9 129.3 129.9
ΔH(J/mol)	1.9 2.2 2.2	4.0 3.1 3.7	3.7 4.3 4.1	5.8 6.7 6.6	6.9 7.8 6.8	7.4 7.0 6.3	6.5 6.3 7.2	7.9 7.9 7.8	7.7 8.5 8.5	7.8 7.6 8.9	9.7 9.9 7.5

The DSC curves used to create Tables 5.6 and 5.7 were analysed on the basis of ASTM-E698. The DSC curves recorded at various heating rates for the hair samples exhibit the endothermal processes shown in Figures 5.9-5.10. Different heating rates cause the endotherm peak to shift (Cao, 1997b). In agreement with Haly (1967), we found that a substantial shift to higher temperature is observed in term of the denaturation peak size in Figures 5.9 and 5.10 for both virgin hair and commercial persulphate bleached (2h) hair with increasing heating rate.

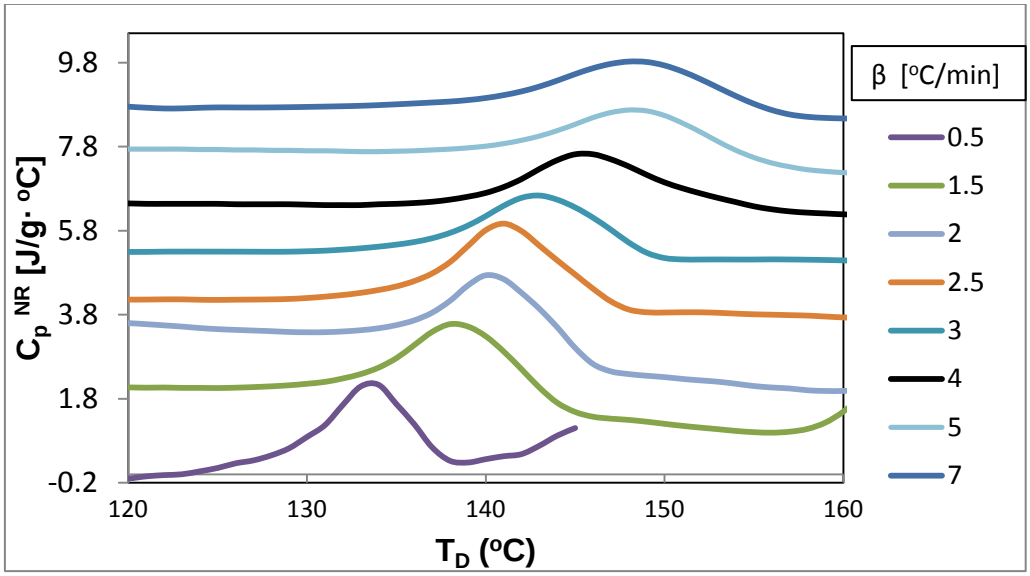

Figure 5.9: Denaturation non-reversing C_p^{NR} DSC curves for virgin hair at various heating rates. The raw data is given in the Chapter 8, Table 8.4.

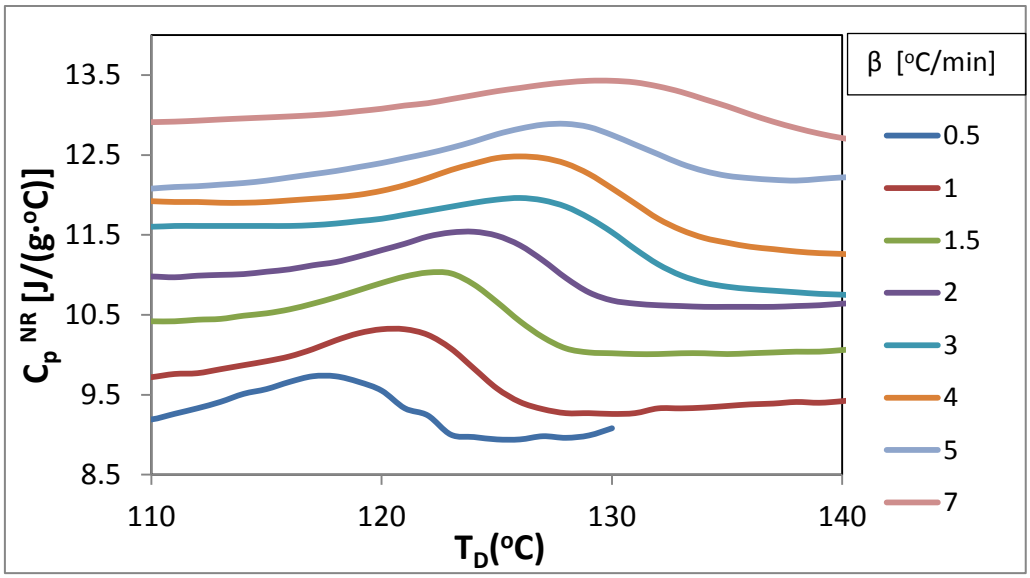

Figure 5.10: Denaturation non-reversing C_p^{NR} DSC curves for 2h commercially bleached hair at various heating rates. The raw data is given in the Chapter 8, Table 8.5.

Against the theoretical background given above, by measuring peak temperatures as a function of the heating rate, the relationship between heating rate, β (as lnβ) and $1/T_D$ of denaturated hair fiber for various heating rates are investigated in a so-called Arrhenius-plot. The advantages of the Arrhenius- plot method are simplicity of measurement, applicability to many types of reactions and relative insensitivity to secondary (side) reactions (Duswalt, 1974).

There are strong linear relationships between heating rate and $1/T_D$ as well as ΔH_D of denaturated hair fibre in Figures 5.11 and 5.12. Activation energies are determined from the slope of the linear regression between the non-reversing denaturation peak temperature (as $1/T_D$) and heating rate, β (as lnβ), corresponding to 260 kJ/mol for the virgin hair and 295 kJ/mol for the commercial persulphate bleached hair (2h). Both values are in a good agreement with the range of activation energies which are generally associates with protein denaturation (approx. 100-800 kJ/mol) (Bischof, 2005). In addition, Istrate et al. (2009) have verified that the kinetics are an autocatalytic mechanism and the value of the activation energy is close to disulphide bond scission rather than to protein denaturation.

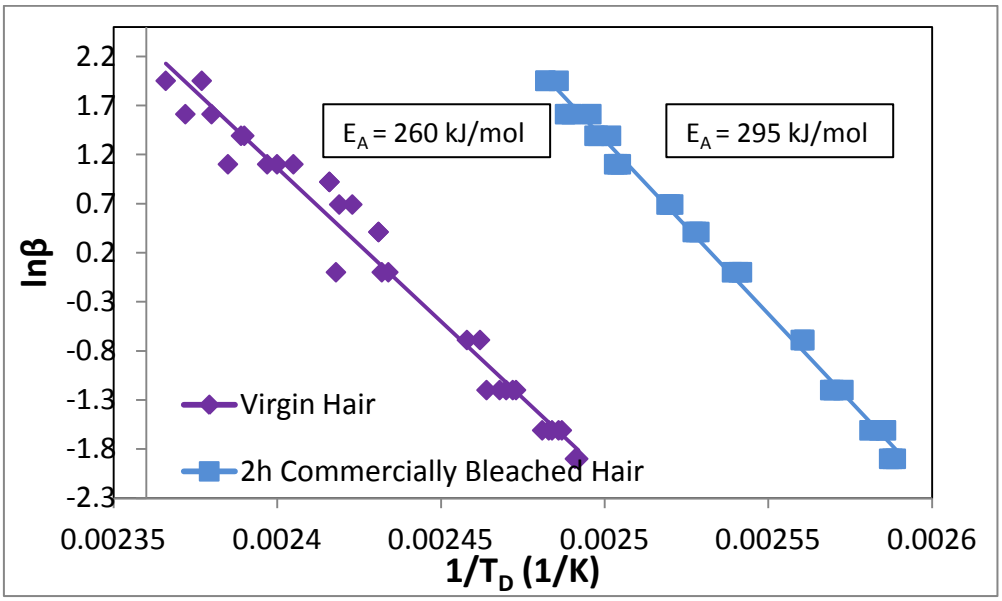

Figure 5.11: The relationship between heating rate, β (as lnβ) and $1/T_D$ for virgin and commercial persulphate bleached hair (2h). Linear regression lines were determined by the data from non-reversing heat capacity peaks only, yielding the values for the activation energy E_A, as given by Equation.5.19.

The high value of 295 kJ/mol of the commercially bleached hair in the wet state (see Figure. 5.11) reflects the high activation energy for chemical processes during keratin denaturation, but the difference of activation energy between virgin hair and commercial bleached hair is around 35KJ/mol, which is considered to be very small. This conclusion indicates that there is no obvious difference for matrix properties between virgin hair and commercially treated hair. This shows that the major structural change produced by the treatment only occurs in the α-helical component in IF, which is embedded into the matrix. The relationship of denaturation enthalpy ΔH_D and heating rate (Figure 5.12) provides a better explanation for this finding.

Linear regressions of ΔH_D vs. $ln\beta$ (Figure 5.12) on both virgin hair and commercial persulphate bleached hair (2h) show that there is a linear increase in ΔH_D for lower heating rates, while it is constant for higher heating rates. Again, this observation suggests that higher heating rates favour the formation of a random coil structure, while lower heating rates favour the formation of more organized, randomly oriented small β-domains (Haly, 1970). If the heating rate is sufficiently small, the phase change at the molecular level is from the α-helical structure to the β structure. On the other hand, if the rate of heating is sufficiently high and cooling is rapid, little or no β material is formed; in fact, there may be 'recrystalization' of material (Haly, 1970). So it is taken as an indication that a lower heating rate favours a crystal transformation change (α-β transformation), while a higher rate favours a crystalline-amorphous transformation.

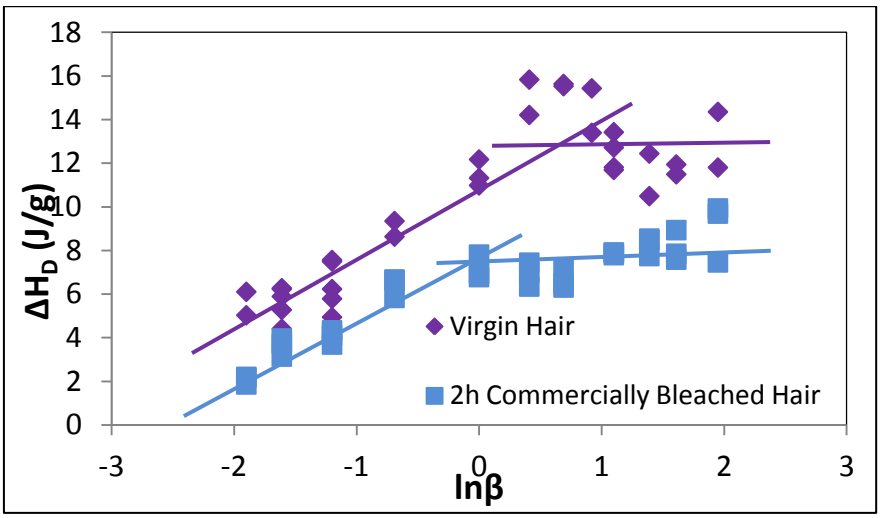

Figure 5.12: Relationship of denaturation enthalpy ΔH_D and lnβ for virgin and bleached hair

5.4.4.2 Nonisothermal Kinetics for the Denaturation of Mohair Fibres

Mohair is a very resilient hair fibre obtained from the Angora goat. In many respects, mohair resembles wool in structure, including the characteristic scale structure of the fibre. In term of its similar morphology and high keratin content, mohair is the closest hair fibre to the human hair with regard to its general properties and structure with respect to its thermal behaviour, which is reported by Tonin *et al.* (2004). In this section, mohair is thus employed as a reference sample to provide specific information about the nature and the course of the denaturation transition as well as the denaturation mechanisms through kinetic thermal analysis.

Figures 5.13 and 5.14 show a typical DSC curves for mohair in water, after heating the keratin at heating rates of 1^{o}C/min and 3^{o}C/min, respectively. Though double peaks were frequently observed for wool (Haly, 1967, Spei, 1989), the mohair sample shows a single-peak structure for the denaturation. But there is a shoulder near the denaturation temperature which appears at the lower heating rate towards higher temperature in the Figure 5.14. This is a common feature for α-keratins (Wortmann, 1993) and is related to specific cell inhomogeneity of helix denaturation in wool (Wortmann, 1998) and in human hair (Bryson, 2009), but the phenomena in mohair is of special interest, because mohair is generally assumed to be homogenous with regard to its cell structure.

It is not surprising that the virgin mohair sample demonstrates a similar DSC curve shape as human hair, but the denaturation temperatures of the α-helical component in mohair sample, shown at 133^{o}C and 138^{o}C in Figures 5.13 and 5.14, respectively, are slightly lower when compare to virgin human hair (138^{o}C, 144^{o}C) at 1^{o}C/min and 3^{o}C/min, respectively. This finding indicates that mohair has an overall similar α-helix content as well as cross-link density in the matrix as the human hair.

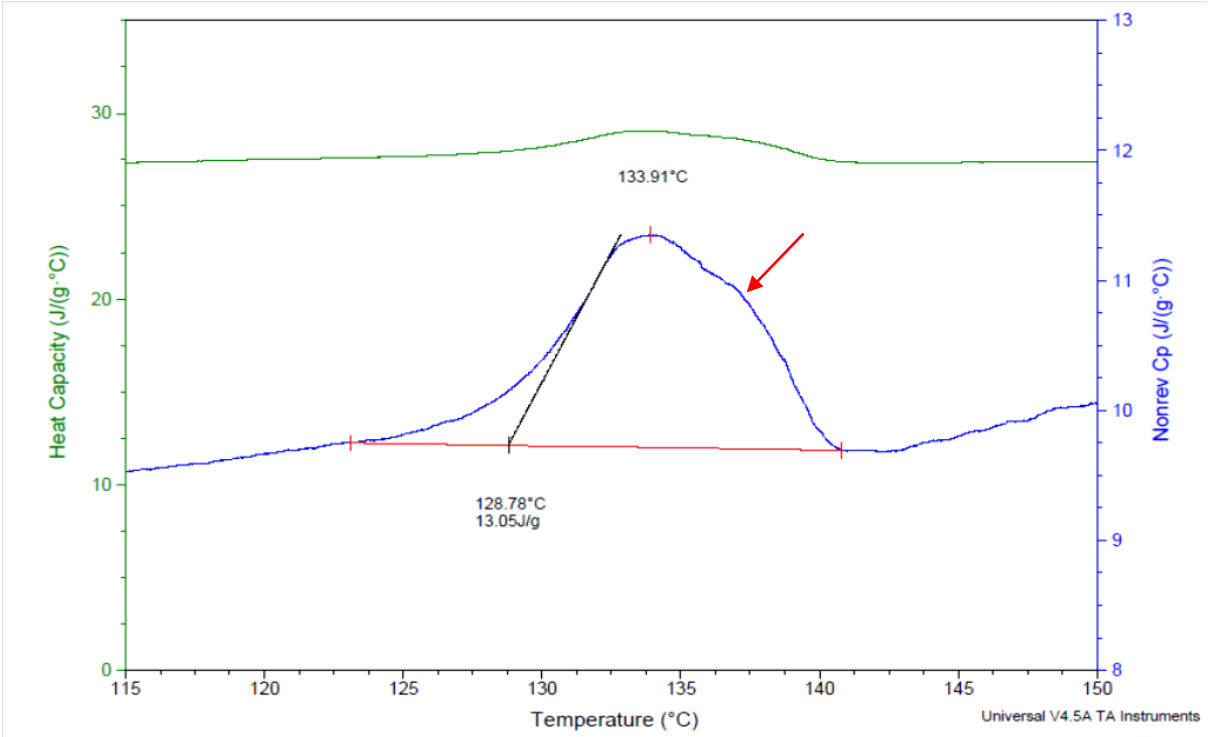

Figure 5.13: Typical non-reversing C_p^{NR} DSC curve for untreated mohair hair in water, when the heating rate is 1°C/min. The arrow shows the inhomogeneous cells component on the DSC curve.

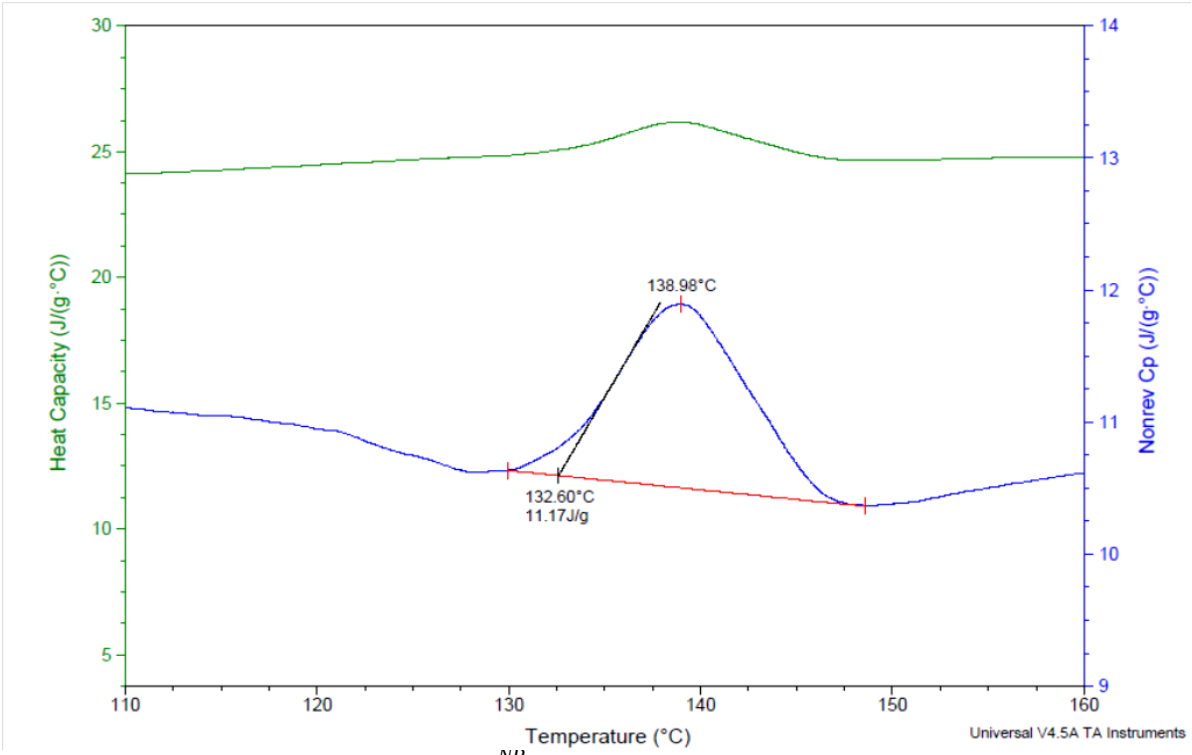

Figure 5.14: Typical non-reversing C_p^{NR} DSC curve for untreated mohair hair in water, when the heating rate is 3°C/min

Table 5.8 provides the corresponding kinetics results for the mohair sample for the ASTM E-698 kinetics approach by applying multiple heating rates.

Table 5.8: Results of mohair at various heating rates

Heating Rate (°C/min)	0.1	0.2	0.3	0.5	1	2	3	4	5	7
Modulation (°C/min)	0.05	0.1	0.1	0.1	0.5	1	1	1	1	3
ΔT(K)	120.1	126.8	128.3	132.0	133.9	136.4	139.0	141.3	141.2	143.8
	122.2	126.9	128.9	131.7	133.8	138.1	139.1	140.7	141.4	144.5
	122.5	126.9		132.1	134.8	137.8	138.6	140.5	141.3	144.8
ΔH(J/mol)	7.1	9.1	9.9	11.0	12.9	12.6	11.6	12.2	11.8	12.9
	7.6	10.4	11.0	12.2	11.9	13.7	12.0	13.3	11.1	12.4
	7.4	9.7		11.2	12.1	13.2	12.1	13.0	12.6	13.6

Figure 5.15 demonstrates the activation energy of 296 KJ/mol for the mohair sample, which is determined from the slope of the regression lines of $ln\beta$ vs. $1/T_D$ by the Arrhenius-equation.

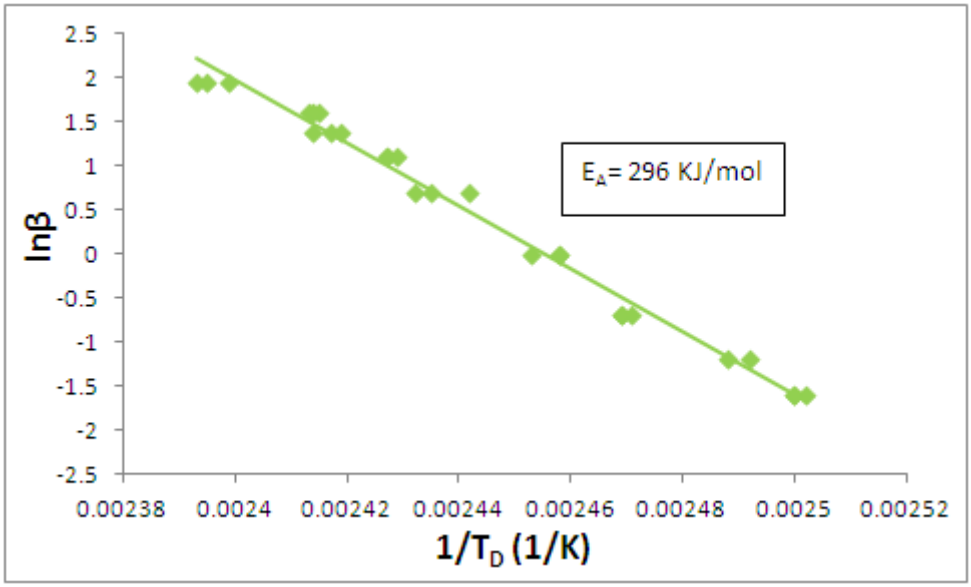

Figure 5.15: The relationship between heating rate, β (as lnβ) and $1/T_D$ for mohair. Linear regression lines were determined for data from non-reversing heat capacity peaks only, yielding the values for the activation energy E_A, as given by Equation. 5.19.

The heating rate effect on the mohair is reflected in the change of denaturation enthalpy. As the heating rate increases, there is a linear increase in ΔH_D for lower heating rates, while it is effectively constant for higher rates in Figure 5.16, further proved that the low heating rate has an extensive structural change in IF in the kinetic analysis. The reason of this phenomenon has been explained in section 5.4.4.1.

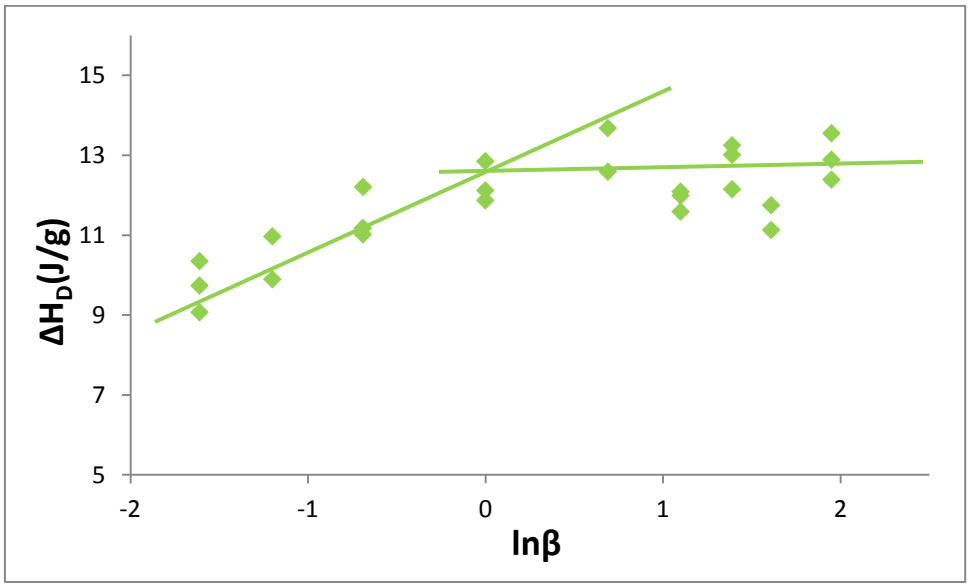

Figure 5.16: Relationship of denaturation enthalpy ΔH_D and lnβ for mohair

Furthermore, the linear regression of the mohair and virgin human hair are analysed and compared in Figure 5.17. It is apparent that the two samples follow similar trends. At the lower heating rates there is a linear increase in ΔH_D, whereas at the higher heating rate, the ΔH_D remains constant. The slope of linear regression for the lower heating rates increases from the mohair to virgin human hair, indicating that the amount of β- structure, which convert from α-helical material is abundant in the virgin mohair than in the virgin human hair. The values of denaturation enthalpies of mohair and human hair overlap at the higher heating rate. From this it can be concluded that both virgin keratin fibres have similar amounts of "native" α-helical material. (Wortmann, 2002, 2006).

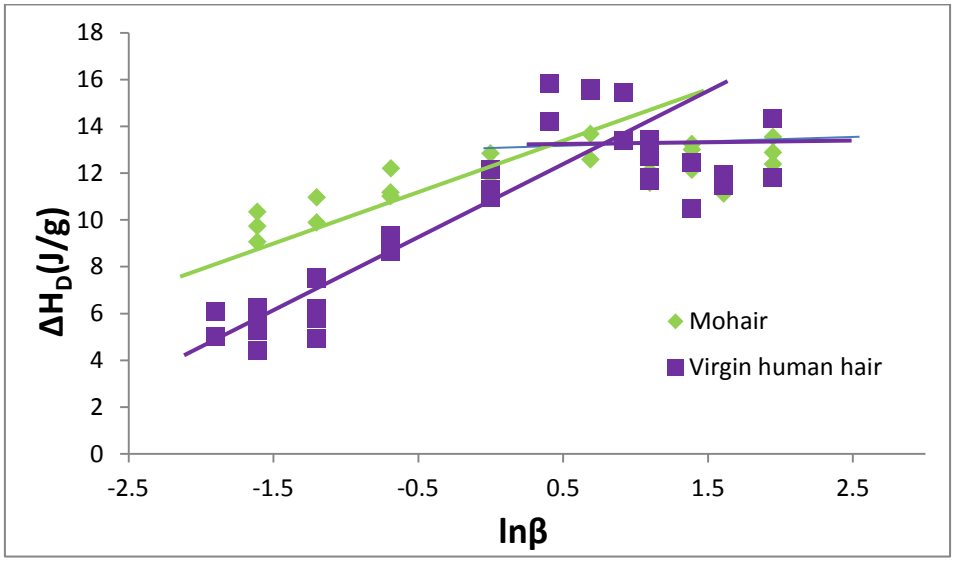

Figure 5.17: Relationship of denaturation enthalpy ΔH_D and lnβ for mohair and virgin human hair

5.4.4.3 Morphological Investigation of Denaturated Human Samples by SEM after DSC

- ***Morphological Investigation of Denaturated Virgin Hair by SEM***

SEM was employed to investigate the change of fibre appearance after the denaturation process in DSC (Figure 5.18). The hair samples were collected from the sample pans after DSC and dried at room temperature for the SEM investigation. All of the experimental settings are the same as described in the Chapter 3.

Five different heating rates were utilized to illustrate the morphological changes of the virgin hair by heating. Virgin hair has a smooth and intact cuticle edge (Fig.5.18 A), after heating at a high heating rate (7^{o}C/min) protein granules are observed on the hair cuticle surface, which are assumed to be hydrolyzed proteins crystallized in the dry state (Fig.5.18 B). The cuticle has the tendency to shrink at medium heating rates (5^{o}C/min) after denaturation of the α-helix in the IF structure (Fig.5.18 C). This is explained by the fact that helix denaturation leads to supercontraction of the cuticle appearance.

The phenomenon of cuticle distortion appears at a heating rate of 2^{o}C/min, when additional granules are found on the surface (Fig.5.18 D). As the process of denaturation proceeds, the protein molecule unfolds and the internally directed

hydrophobic regions in the molecule become exposed, so protein molecules aggregate by non-polar, hydrophobic groups into a large insoluble mass (Istrate, 2009). At very low heating rates (0.15^{o}C/min), the cortex has been total dissolved and only the cuticle remains (Fig.5.18 E), which confirms that hair fibre damage is stronger at lower heating rates.

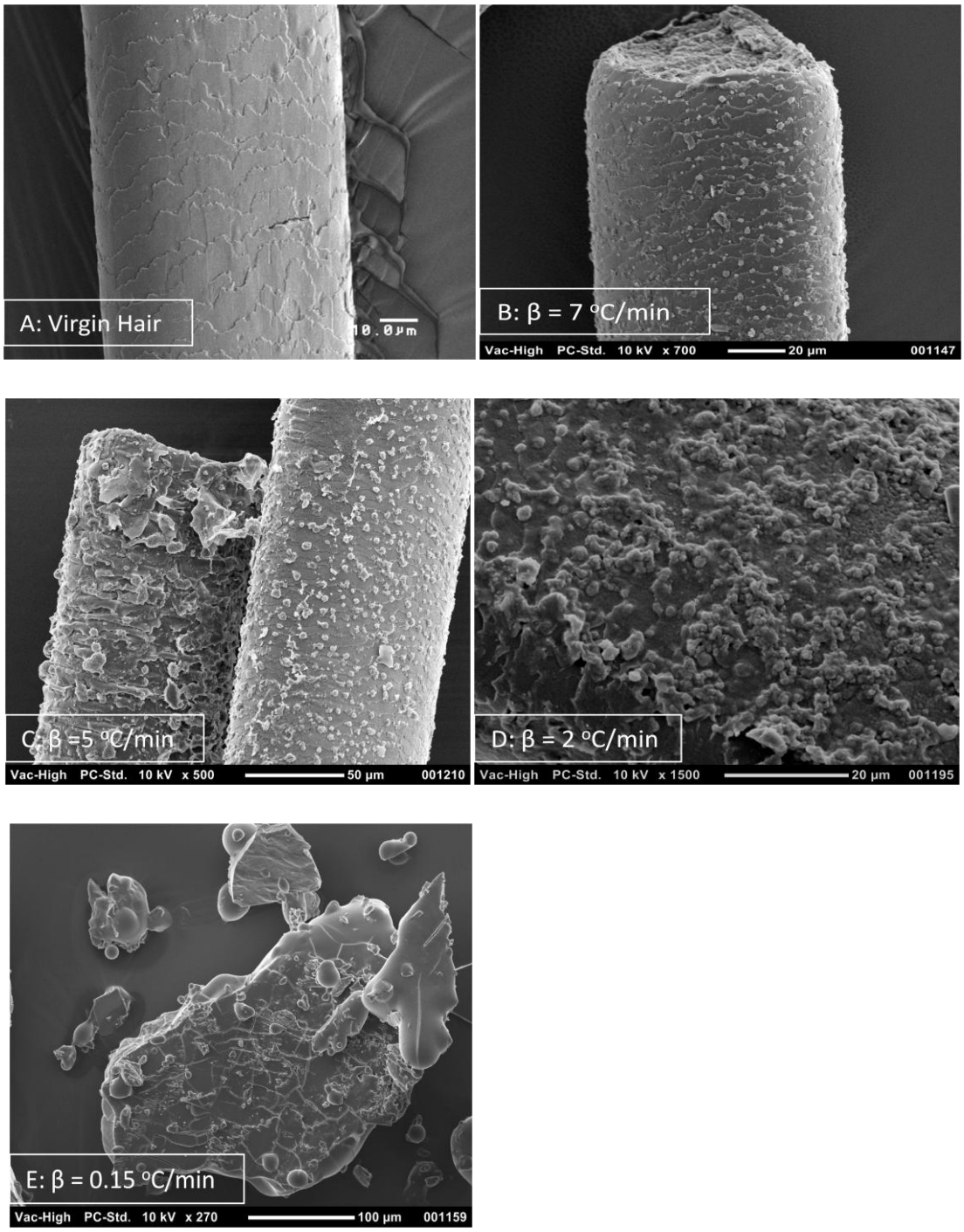

Figure 5.18: Cuticle fragment of virgin human hair fiber snippets by SEM after being heated in the DSC at various heating rates up to 7^{o}c/min.

- ***Morphological Investigation of Denaturated Bleached Hair (2h) by SEM***

The appearances of 2h commercially bleached hair fibres were also examined after the DSC-experiments at different heating rates by SEM (Figure 5.19). 2h commercially bleached hair has a smoother edge than virgin hair (Fig.19 A), at high heating rates (7^{o}C/min) only few protein granules are observed on the hair cuticle as hydrolyzed proteins crystallize (Fig.19 B). The phenomenon of cuticle disintegration appears only at medium rates (2^{o}C/min) (Fig.19 D). At very low rates (0.15^{o}C/min) the cortex is completely dissolved. Only cuticle remains (Fig.19 E).

In general, 2 h commercially bleached hair shows an overall shrunk cuticle appearance and less protein granules than the virgin hair at the various heating rates. This shrinkage phenomenon is primarily ascribed to that the denatured hair has a previously partly destroyed α-helix in the cortical cell. These crystalline components appear to exist the whole length of the cortical cell, thus the denaturation of the α-helices causes a length change of the fibre.

In addition, the previously damaged commercial bleached hair contains the fewer peptide and cystine bonds, thereby fewer and shorter protein granules appear on the cuticle surface.

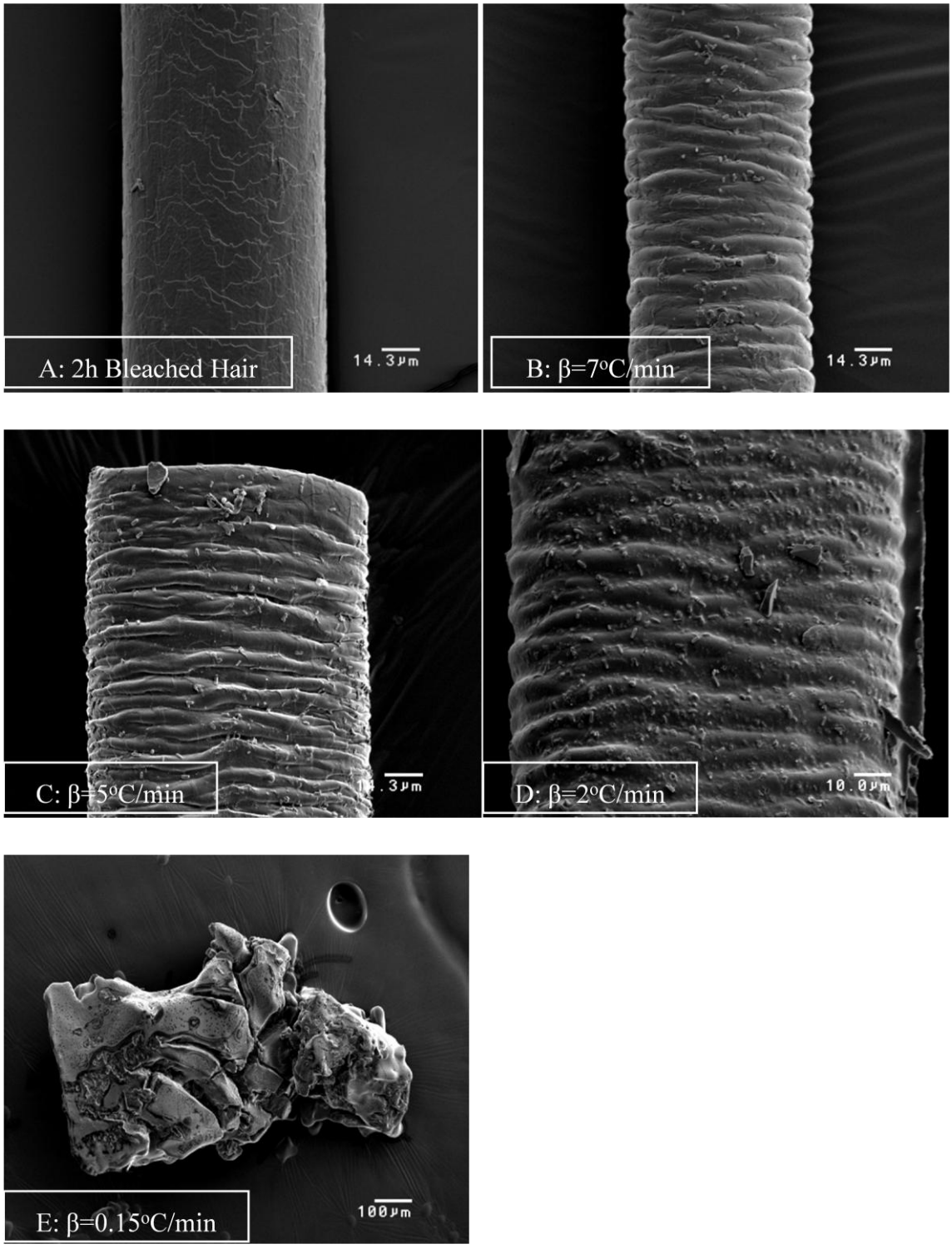

Figure 5.19: Cuticle fragment of commercial persulphate bleached human hair fiber snippets (2h) after SEM after being heated in the DSC at various heating rates up to 7^{o}c/min.

5.4.5 DSC Deconvolution

5.4.5.1 Background

As mentioned in section 5.1.3.3, the overlap of the denaturation peaks for the various types of cortical cells in the human hair and mohair, results in the formation of a shoulder in the denaturation peak on the high temperature side. The ortho- and para-cortical cells have a different morphological structures, which, e.g. in Merino wool, are arranged bilaterally in the crossed section. The orthocortex contains a lower concentration of disulfide linkages than the para-cortex, thus showing a lower denaturation temperature. In an aqueous medium, the denaturation temperature at 138°C is attributed to the ortho-cortical cells and that at 144°C is attributed to the para-cortical cells. The phenomena of a bimodal peak is also observed at 230 and 240°C in a dry environment, which it is again ascribes to the ortho- and para-cortical cells, respectively (Wortmann, 1998). In this section, peak deconvolution is now employed in order to resolve the shoulder denaturation peak of the keratin of human hair and mohair, for the purpose of accurate thermal analysis.

5.4.5.2 Analytical Approach

Although the deconvolution process enables the overlapping peak to be resolved, the results still have the possibility for bias. Wortmann and Deutz (1993, 1998) stated that the assignment of peak temperatures became more accurate as peak analysis software has improved. In order to explore the possibility that human hair and mohair may have two peaks similar to those observed in wool fibres, a deconvolution was conducted using an Excel spreadsheet and the “solver” function.

Our working hypothesis of the deconvolution of the peak overlapping was on the basis of an observation of Freire (1978) that the heat flow–temperature curves can be decomposed into the sum of Gaussian functions. The Gaussian function is a function of the form:

$$f(x) = ae^{-\frac{(x-b)^2}{2c^2}} \tag{5.22}$$

The graph of a Gaussian is a characteristic symmetric "bell curve" shape that quickly falls off towards plus/minus infinity. The parameter α is the height of the curve's peak, b is the position of the centre of the peak, and c controls the width of the "bell".

The initial DSC scans of human hair and mohair were produced by the TA software. They then were transferred into an established Excel program sheet to achieve a DSC curve. The first step of the deconvolution is to correct the shifted baseline of DSC curve prior to the decomposition into the Gaussian curves. In principal, the slope of the chosen points on the original DSC curve is identical to the slope which the straight line is determined by the TA software. Figure 5.20 demonstrates the process of baseline correction. A new baseline with its own slope is applied between two chosen points on the original curve and the data on the previous baseline accordingly are converted with the new baseline, therefore creating a DSC curve with a new perfectly horizontal baseline.

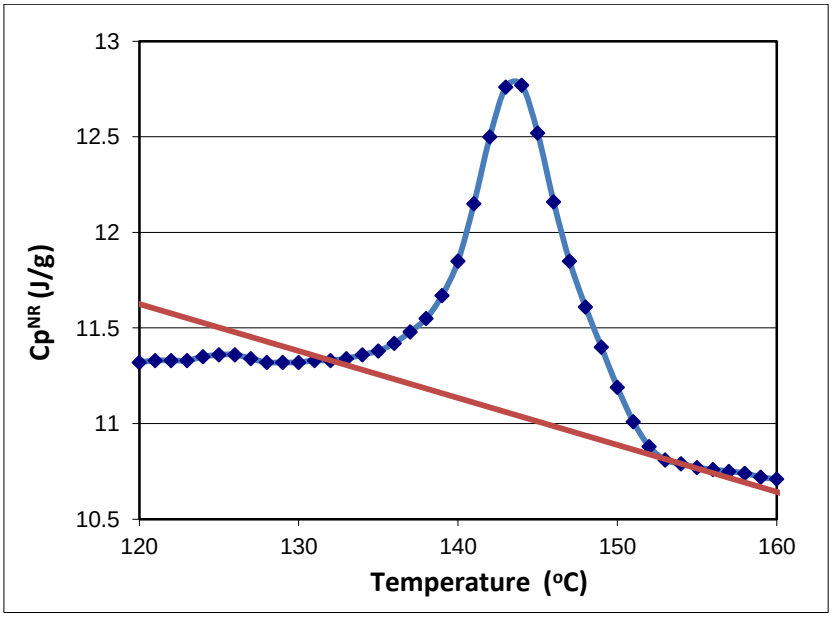

Figure 5.20: The DSC baseline of virgin human hair between the two chosen points, at a heating rate of 3°C/min.

Figure 5.21 represents the corrected DSC peak, which is achieved by subtracting the Cp^{NR} with its new linear baseline slope. Then this peak is deconvoluted using a set of three peaks according to Equation.5.22 in the Excel program (Figure 5.22). The parameter for three peaks were determined by this procedure and attributed to para-, ortho-, and background- cortical cells (see Figure 5.22).

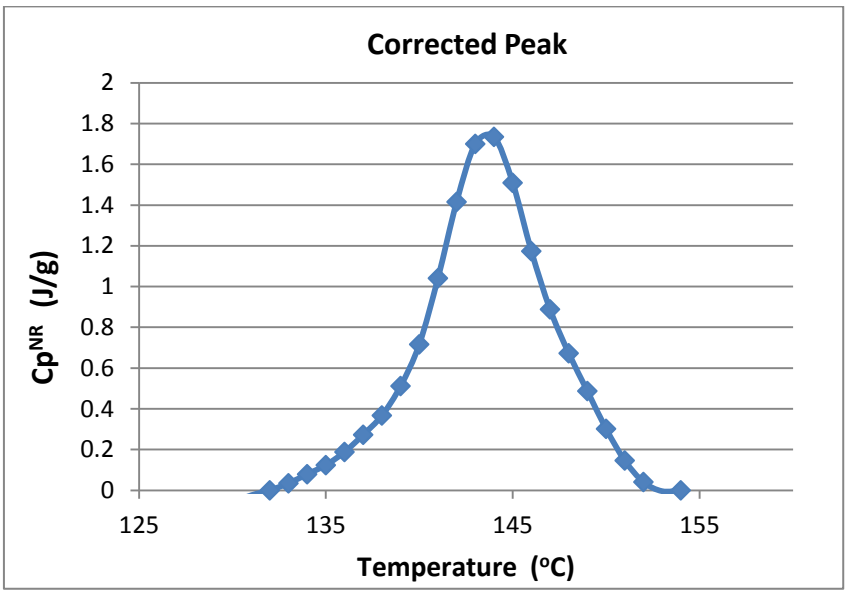

Figure 5.21: The corrected DSC peak of virgin human hair, at a heating rate of 3°C/min

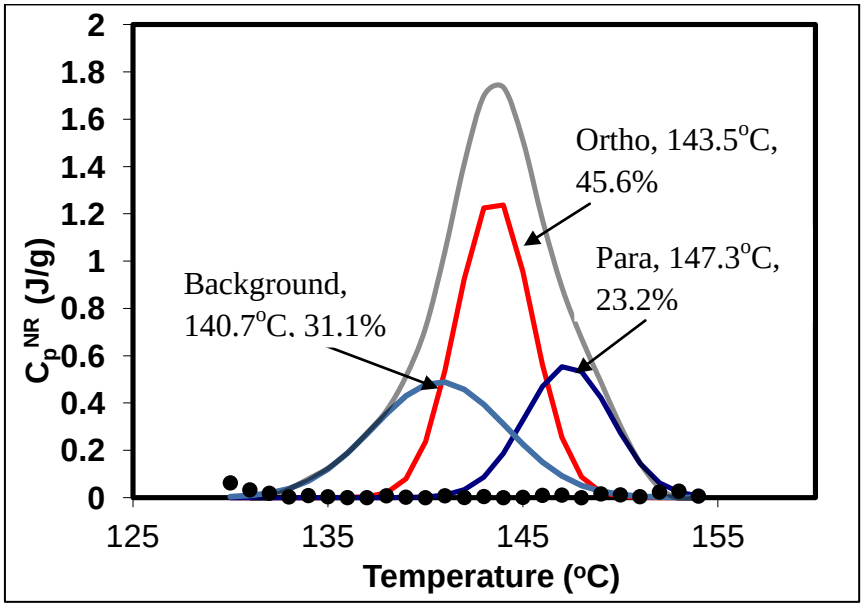

Figure 5.22: Deconvolution of the MDSC-curve for virgin human hair into three Gaussian distributions. The peaks are assigned to the three types of cell types as para-, ortho- and background cells. The dots (●) indicate the absolute differences between fit and experimental data. The heating rate is 3°C/min.

In Figure 5.22, a deconvolution of the DSC-peak for virgin human hair is shown for three Gaussian distributions, attributed to para-, ortho- and background- cells. Their peak temperatures and fractional enthalpies are given on the graph. According to the ortho/para hypothesis, the first peak at 143.5°C corresponds to an orthocortex and the second peak at 147.3°C is designated as paracortex because of its high cystine content. Its fractional enthalpy (%) corresponds to ortho- (45%) and para- cortical (23%) cells, respectively. It has been suggested that the DSC bimodal endotherm peaks are 4-7 ^{o}C apart in the presence of ortho- and para-cortical cells for wool and other keratins in water (Wortmann, 1998), the difference between the peak temperature (3.8^{o}C) is in satisfactory agreement with expectations for ortho- and para-cells.

The broad background peak (31%) summarizes the enthalpy fraction, which represents the sizeable fraction of cells, but it is not clearly associated with the two distinct cell types. The peak is assumed to comprise the small fractions of strongly staining (high sulfur) as well as weakly staining cells (low sulfur) in Bryson et al.'s (2009) microscopic observations. Since the background peak temperature (140 ^{o}C) is lower than *ortho* and *para*, it is unlikely that it refers to meso-cortical cells (Whiteley, 1977), but in our investigation the background peak is attributed to meso-cell peak to avoid the confusion.

The various set of raw data obtained from Section 5.4.3, which investigates the damage to the cortex for various bleaches and the raw data obtained from Section 5.4.4 on the kinetic analysis using various heating rates for virgin human hair and mohair, were all transferred into the Excel program sheet, by using a deconvolution program with a three peak assumption. The results are present and summarized in Tables 5.9-5.14.

5.4.5.3 Results and Discussion

- *Deconvolution Investigation of Human Hair on the Various Bleaches Effects*

In the case of keratin fibres, allocating the lower peak to the ortho- and the higher one to the para-cortex, the peak temperatures were determined and are summarized, together with the denaturation enthalpy as percentage fraction of the peak area. Tables

5.10—5.12 summarize the deconvolution results for the peak temperatures T_D and fractional enthalpies (%) for the cell types for 6% H_20_2 bleached hair, 9% H_20_2 commercial bleached hair and commercial persulphate bleached hair, respectively, at a heating rate of 3 ^oC/min.

For the comparison purpose among the three bleaches, the 6% H_20_2 bleached sample (2h) is taken as an example. With regard to the denaturation enthalpy of ortho- and para-cortical cells, it is obvious that the higher value of the para- cortex (56%) compared to the ortho-cortex (32%) in the 6% bleached hair is well meets the expectation, which is based on the investigations by Dobb (1970), that the ortho-cortex should contain about double the amount of α-helical material than the para-cortex. But the 9% H_20_2 commercial bleached hair (2h) and commercial persulphate bleached hair (2h) behaves irregularly. In both cases the enthalpy fraction attributed to the para-cortical cells is reduced, while the ortho-cortex appears largely unchanged. This needs further investigation.

Table 5.9: Peak temperatures and fractional enthalpies for para-, ortho- and meso-cortical cells for 6% H_20_2 bleached hairs at various bleaching times, in the form of the arithmetic means, standard error is given in the Figure 5.23.

Bleaching Time / Peak Temperature	0	0.5h	1h	1.5h	2h	2.5h	3h
Para	***147.1***	142.8	141.2	142.5	140.9	140.8	140.4
Ortho	***143.9***	139.3	138.0	138.6	138.6	138.1	138.2
Meso	***140.7***	133.4	131.3	132.4	133.2	133.1	133.1
Bleaching Time / Fractional Enthalpy (%)	0	0.5h	1h	1.5h	2h	2.5h	3h
Para	31.0	62.3	57.6	66.3	***56.7***	61.8	53.9
Ortho	44.4	29.8	38.8	29.8	***32.2***	26.7	37.7
Meso	24.6	8.0	3.6	4.0	11.2	11.5	8.5

Table 5.10: Peak temperatures and fractional enthalpies for para-, ortho- and meso-cortical cells for 9% H_20_2 commercial bleached hairs at various bleaching times, in the form of the arithmetic means, standard error is given in the Figure 5.24.

Bleaching Time / Peak Temperature	0	0.5h	1h	1.5h	2h	2.5h	3h
Para	147.1	141.8	140.7	139.1	137.1	133.1	136.1
Ortho	143.9	140.1	138.3	135.6	133.1	127.3	130.6
Meso	140.7	133.5	133.9	130.5	125.8	122.5	124.6
Bleaching Time / Fractional Enthalpy (%)	0	0.5h	1h	1.5h	2h	2.5h	3h
Para	31.0	33.8	26.9	27.0	***14.0***	49.6	26.7
Ortho	44.4	47.9	35.6	35.4	***34.4***	32.7	39.6
Meso	24.6	37.5	37.6	51.7	17.8	33.4	8.5

Table 5.11: Peak temperatures and fractional enthalpies for para-, ortho- and meso-cortical cells for commercial persulphate bleached hairs at various bleaching times, in the form of the arithmetic means, standard error is given in the Figure 5.25.

Bleaching Time / Peak Temperature	0	0.5h	1h	1.5h	2h	2.5h	3h
Para	147.1	138.1	130.6	128.2	126.4	127.3	126.1
Ortho	143.9	135.6	127.6	124.9	122.7	124.2	123.0
Meso	140.7	129.9	123.2	120.5	117.8	120.0	118.4
Bleaching Time / Fractional Enthalpy (%)	0	0.5h	1h	1.5h	2h	2.5h	3h
Para	31.0	30.5	32.0	39.3	***38.3***	33.1	28.8
Ortho	44.4	54.6	39.1	34.8	***34.7***	35.8	38.1
Meso	24.6	14.9	28.8	25.9	27.0	31.1	33.0

It was speculated previously that the 9% H_20_2 commercial bleach shows an irregular damage profile compared to 6% H_20_2 bleach and commercial persulphate bleach after 2h bleaching time. Therefore, the denaturation temperatures of the resolved cortical compositions of 6% H_20_2 and commercial persulphate bleached hairs are compared. The results are presented in Figure 5.23. It is obvious that commercial persulphate bleached hair has an overall more progressive damage influence on ortho- and para-cortical cell compositions than 6% H_20_2 bleached hair. The denaturation temperatures decrease faster for the first 2h bleaching time until reaching an equilibrium level. On the other hand, 6% H_20_2 bleach has a relatively gentle oxidation impact, although it

shows a big drop for denaturation temperature for the initial 1h treatment time. Its denaturation temperature still has a higher value than for the commercial persulphate bleached hair. This observation indicates that the para- and ortho- cortex of 6% H_20_2 bleached hair are subject to little structural change compared to commercial persulphate bleached hair, thus leading to higher denaturation temperatures.

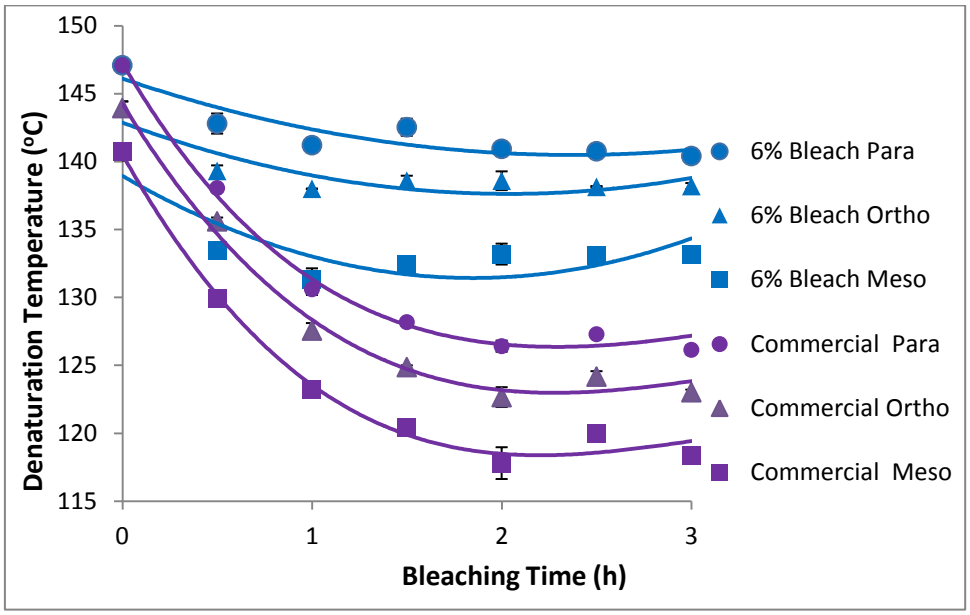

Figure 5.23: Denaturation temperatures of para-, ortho- and meso- cortical cell types on the basis of three Gaussian distributions for 6% H_20_2 and commercial persulphate bleached hairs up to 3hr bleaching time.

The three denaturation temperatures for 9% H_20_2 commercial bleach are analyzed in Figure 5.24. T_D decreases linearly over the whole reaction time for all of the three cell groups.

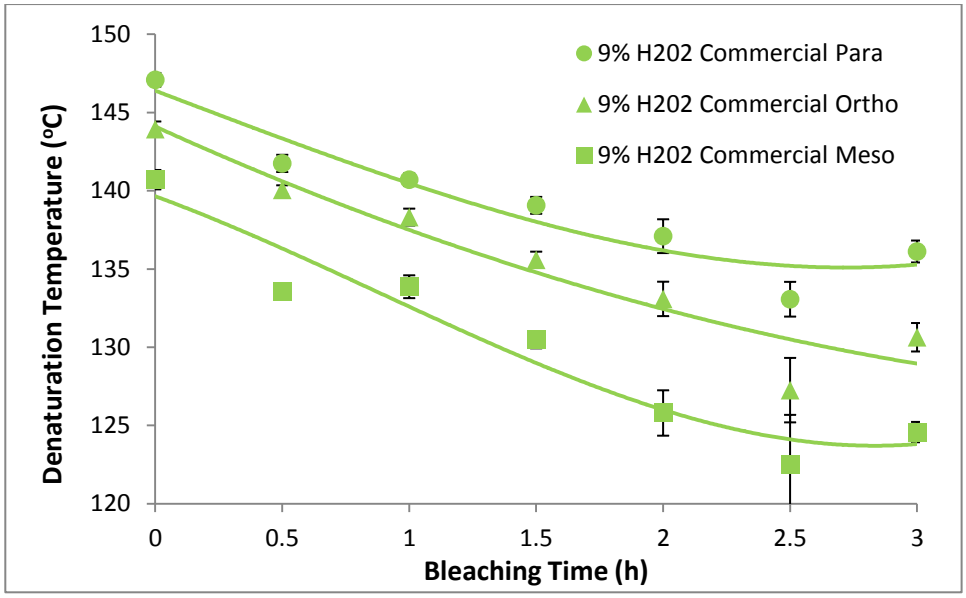

Figure 5.24: Denaturation temperatures of para-, ortho- and meso- cortical cell types on the basis of three Gaussian distributions for 9% H_20_2 commercial bleached hairs up to 3hr bleaching time.

Consequently, it can be seen from the Figures 5.23 and 5.24 that the commercial persulphate bleach has a strong damage effect on both para- and ortho- cortex. And 6% H_20_2 bleach has an overall mild structural impact on both two main cell types. This phenomenon confirms our previous finding in Section 5.4.3 that commercial persulphate bleach and 6% H_20_2 bleach approached their equilibrium within the 3hr treatment time, while 9% H_20_2 commercial bleach shows a linear decrease on the structure change with the increasing time.

The denaturation enthalpies are also compared. The comparison of the three cortical cell types in the form of their fractional percentages for 6% H_20_2 bleached hair is shown in Figure 5.25. The phenomenon reflects that the 6% H_20_2 bleach has a bigger damage effect on the ortho-cortex rather than the para-cortex. However, the values of the resolved cortical cells are uniformly distributed along the treatment time, further confirms that 6% H_20_2 bleach rather is the mild oxidising bleaching chemical among the three bleaches.

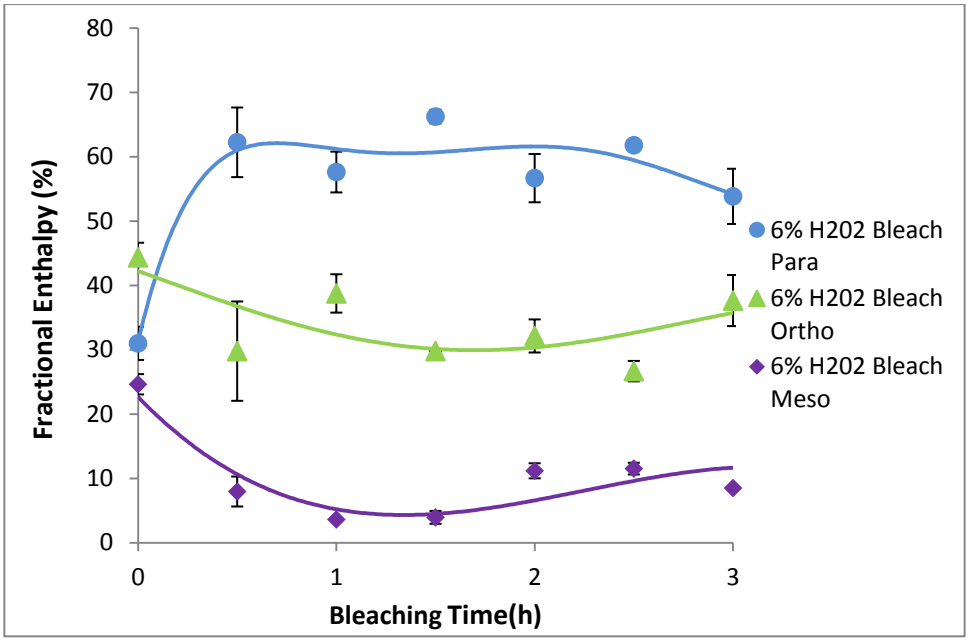

Figure 5.25: Fractional enthalpies of para-, ortho- and meso- cortical cell types on the basis of three Gaussian distributions for 6% H_20_2 bleached hairs up to 3hr bleaching time.

The data of 9% H_20_2 commercial bleached hair show an irregular pattern in Figure 5.26, both para- and ortho-cortical cells have a downward trend, and they seem to approach similar values of fractional enthalpy with the longer oxidation time, reflecting that 9% H_20_2 commercial bleach has a homogenous damage effect on the para-cortex and ortho-cortex.

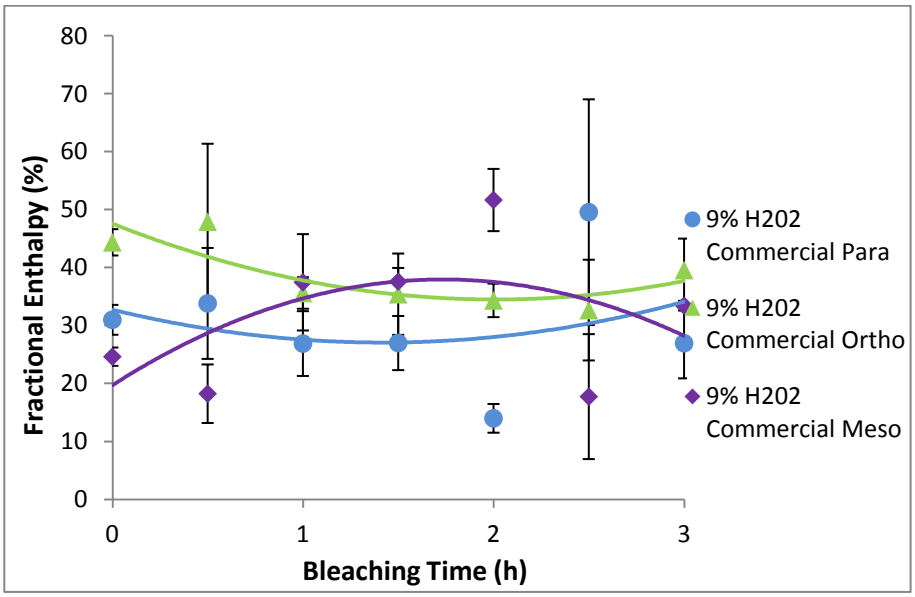

Figure 5.26: Fractional enthalpies of para-, ortho- and meso- cortical cell types on the basis of three Gaussian distributions for 9% H_20_2 commercial bleached hairs up to 3hr bleaching time.

In Figure 5.27, the value for the ortho-cortex in the commercial persulphate bleached hair keeps decreasing while both para- and meso- cell compositions increase until the values for all cortex components overlap at around 1.5hr bleaching time, which is in the range of around 30% fractional enthalpy. This observation is also found for 9% H_20_2 commercial bleached hair, consequently leading to the conclusion that the stronger bleaches result in a homogenous structural damage on both para-cortex and ortho-cortex.

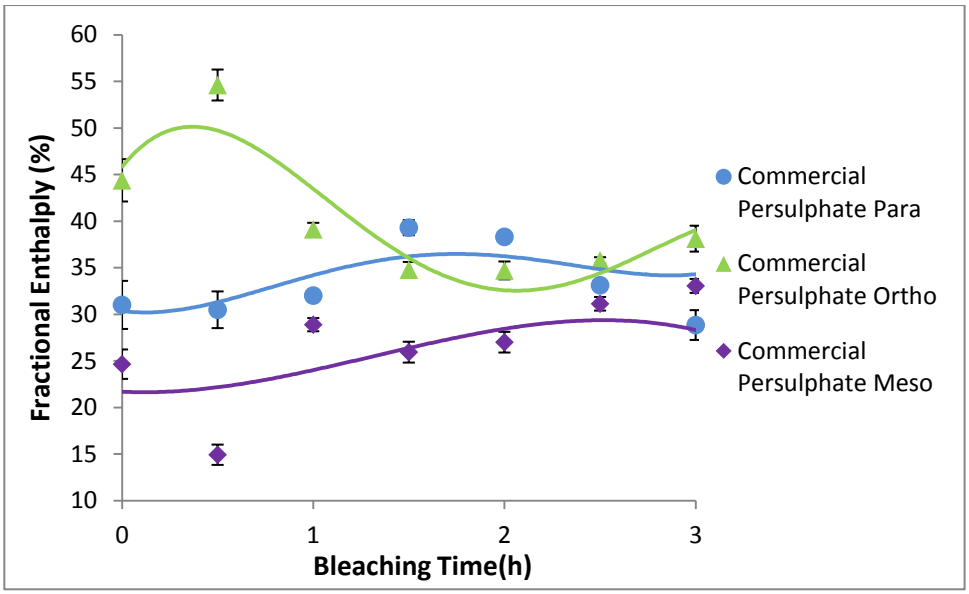

Figure 5.27: Fractional enthalpies of para-, ortho- and meso- cortical cell types on the basis of three Gaussian distributions for commercial persulphate bleached hairs up to 3hr bleaching time.

- *Deconvolution Investigation of Human Hair for Different Heating Rates*

The overall damage effects on intermediate filament and matrix through the commercial persulphate bleached hair (2h) at various heating rates were discussed in Section 5.4.4.4. In this investigation the deconvolution is utilized to further evaluate the oxidation effect on the different cortical cells (mainly the orthocortex and paracortex).

Since the paracortex has a higher sulphur content, the higher peak temperature is attributed to the para- rather than the orthocortex. In the Table 5.12, the value for virgin human hair of 147^{o}C corresponds to the paracortex, and 143^{o}C is attributed to the orthocortex component, for the heating rate of 3^{o}C/min.

Table 5.12: Peak temperatures and fractional enthalpies of three cell types in virgin hair at various heating rates, in the form of the arithmetic means, standard error is given in the Figure 5.28.

Heating rate(°C/min) / Peak Temperature	1.5	2	2.5	3	4	5	7
Para	140.4	142.4	142.8	**147.1**	148.9	150.4	150.8
Ortho	137.6	139.5	140.3	**143.9**	145.4	147.2	147.1
Meso	134.1	136.6	135.6	140.7	141.6	143.8	143.2
Heating rate(°C/min) / Fractional Enthalpy(%)	1.5	2	2.5	3	4	5	7
Para	33.0	34.0	43.0	31.0	38.0	45.3	37.9
Ortho	37.0	32.9	41.4	44.4	39.1	29.7	37.1
Meso	30.0	33.1	15.6	24.6	22.9	25.0	25.0

The enthalpy is also investigated in the form of the fractional enthalpies in Tables 5.12 and 5.13 for virgin and persulphate bleached hairs. It can be seen that virgin hair and commercial persulphate bleached hair (2h) have shown three distinctive cell compositions after the heating effects, and commercial persulphate bleached hair (2h) have an overall lower denaturation temperature for three cell compositions than the virgin hair.

Table 5.13: Peak temperatures and fractional enthalpies of three cell types in commercial persulphate bleached hair (2h) at various heating rates, in the form of the arithmetic means, standard error is given in the Figure 5.29.

Heating rate(°C/min) / Peak Temperature	1	1.5	2	3	4	5	7
Para	121.7	123.4	124.8	127.6	128.6	130.0	132.7
Ortho	117.8	119.9	120.6	123.8	124.5	125.7	127.9
Meso	112.6	115.8	115.7	119.4	120.0	121.0	122.4
Heating rate(°C/min) / Fractional Enthalpy(%)	1	1.5	2	3	4	5	7
Para	43.5	47.8	54.5	47.9	49.1	49.3	46.1
Ortho	37.0	39.2	39.5	38.3	35.6	35.7	35.9
Meso	19.6	13.1	6.0	13.8	15.2	15.0	18.1

A continuous increase in the denaturation temperature with the increasing heating rates is observed for all three cell types in virgin hair as well as commercial persulphate bleached hair (2h), as shown in Figure 5.28. The result reflects well the finding for the whole human hair in the Section 5.4.4.1. Although commercial persulphate bleached hair (2h) has an overall lower denaturation temperature for each cortical component for each heating rate, the distance between the values for para- and ortho- cortex for virgin hair is similar to that of commercial persulphate bleached hair (2h). This shows that there is a parallel change in the denaturation temperature for virgin hair and commercial persulphate bleached hair (2h). It further leads to the conclusion that heating rate affects the cystine linkages of the para- and ortho-cortex homogenously, regardless of the previous damage.

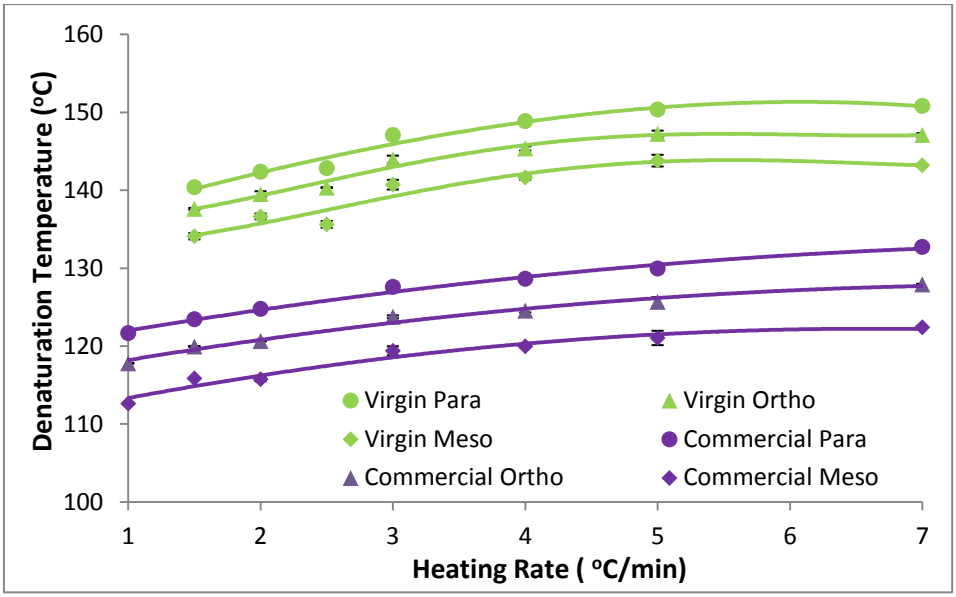

Figure 5.28: Denaturation temperatures of para-, ortho- and meso- cortical cell types on the basis of three Gaussian distributions for virgin and commercial persulphate bleached hairs (2h) at various heating rates.

However, there is no strong relationship between the fractional enthalpies for virgin hair and heating rate as shown in Figure 5.29, this is ascribes to the disulfide cross-link protection of the crystalline component. Commercial persulphate bleached hairs show a uniform performance for the three types of cells, indicating that a homogenous damage effect on the cortical components occurs for bleached hair.

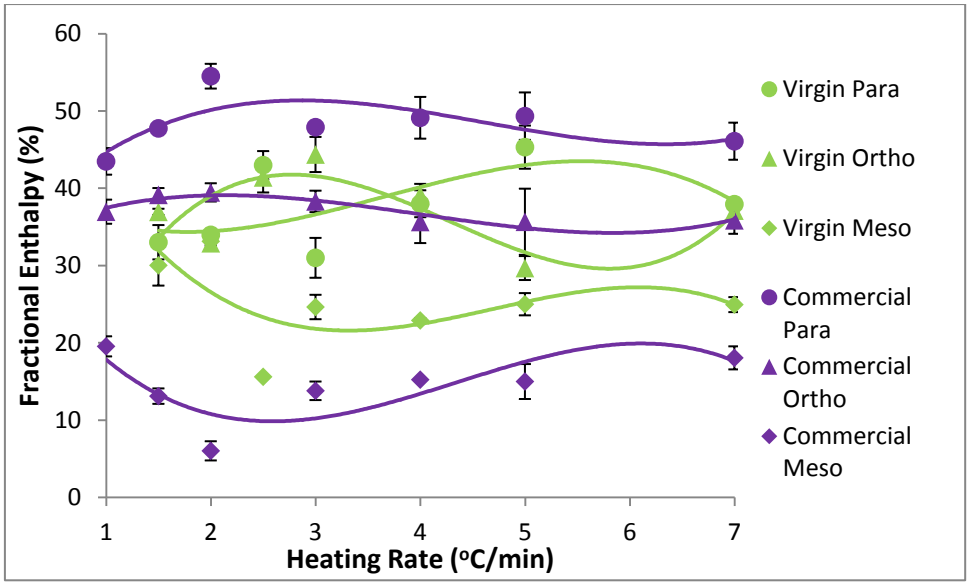

Figure 5.29: Fractional enthalpies of para-, ortho- and meso- cortical cell types on the basis of three Gaussian distributions for virgin and commercial persulphate bleached hairs (2h) at various heating rates.

- *Deconvolution investigation of Mohair on the kinetic analysis*

Mohair, which has the highest α-helix content among the animal fibres contains predominantly ortho-cortex, or meso- and orthocortex (Jones, 2006). But kid mohair also contains some para-cortex (Hunter, 2001). In the section 5.4.4.2, it had been found that there is a shoulder in the DSC-curve on the high temperature side at the heating rate of 1 ^{o}C/min in water. In this section 5.4.4.3, deconvolution is employed to investigate whether cell composition of mohair can be resolved into the three Gaussian distributions.

Separate denaturation temperatures have been found for the three different cell types: para-, ortho and meso-cortex (see Table 5.14). When the heating rate is 3^{o}C/min, according to the ortho/para hypothesis, the first peak at 136.3°C corresponds to orthocortex and the highest peak at 140.5°C is designated to paracortex, because of its high cystine content. The middle peak (138.2°C), which is intermediate between para- and ortho-cortex, is assigned to meso-cortex. Their fractional enthalpies (%) have been found to correspond to ortho- (34.3%), para- (50.4%) and meso-cortical (15.3%) cells, respectively.

Table 5.14: Peak temperatures and fractional enthalpies of para-, ortho- and meso-cortical cells in virgin mohair for various heating rates, in the form of the arithmetic means, standard error is given in the Figure 5.30.

Heating rate (°C/min) / Peak Temperature	1	2	3	4	5	7
Para	136.2	139.1	***140.5***	142.0	142.1	144.9
Ortho	131.0	135.4	***136.3***	137.6	139.2	138.6
Meso	133.4	136.7	***138.2***	139.5	139.6	140.7
Heating rate(°C/min) / Fractional Enthalpy(%)	1	2	3	4	5	7
Para	41.1	48.8	***50.4***	60.1	73.6	75.0
Ortho	28.5	38.9	***34.3***	25.7	16.0	14.8
Meso	30.4	12.3	***15.3***	14.1	10.5	10.2

The denaturation temperatures of three cell types in mohair increase continuously with the heating rate (Figure 5.30), but para-cortex shows a more dominant increase. This is in contrast to the fact that mohair has predominately ortho-cortex content than para-cortex. The reason for this abnormal result may be ascribed to (i) the randomly collected sample source, or (ii) the deconvolution with a "Excel sheet" program is not an appropriate analysis approach for this keratin fibre, which has only one or two types of cell cortex.

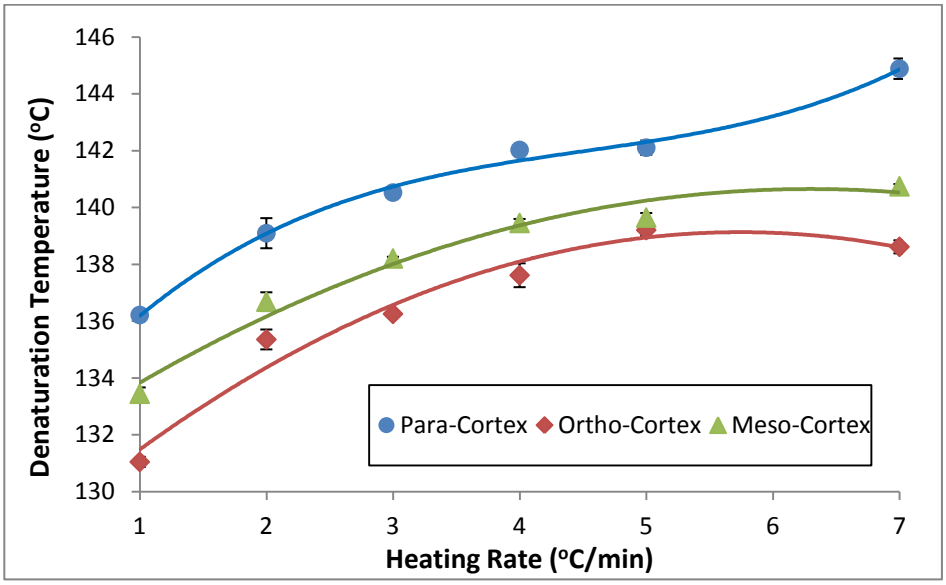

Figure 5.30: Denaturation temperature for para-, ortho- and meso- cortical cell fraction on the basis of three Gaussian distributions for virgin mohair at various heating rates.

The fractional denaturation enthalpies of the three cell types are given in Figure 5.31. For both ortho- and meso- cortex the values decrease apparently with the higher heating rate while the para-cortex shows a steady upward tendency over the heating range. However, this observation is unexpected.

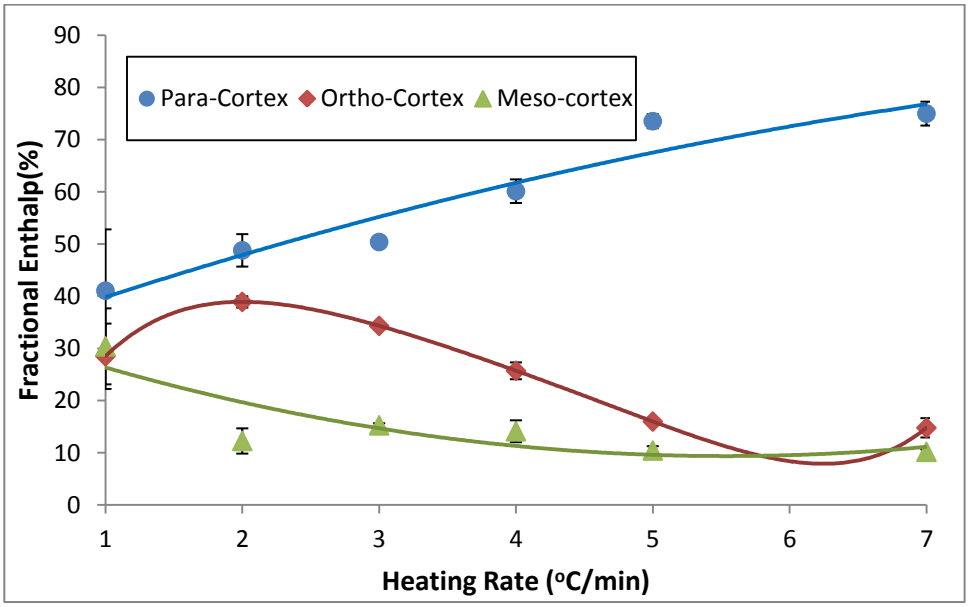

Figure 5.31: Fractional enthalpies for para-, ortho- and meso-cortical cell fraction on the basis of three Gaussian distributions for virgin mohair at various heating rates.

5.5 Morphological Changes on Three Ethnics Hair Types after DSC investigations

5.5.1 Theory and Background

Ethnicity is an important factor in determining the formulation of cosmetic products in the industry. Human hair is categorised into 3 major distinct groups according to ethnic origin: Asian, Caucasian and African. Different ethnic hair types are significantly different in their structure and properties. The distinction between these hair types is particularly related to diameter, geometry, crimp and colour.

Asian hair is found to be the strongest and thickest followed by Caucasian hair. African hair is generally more liable to damage and breakage, and has a lower moisture content than Asian or Caucasian hair. Asian hair is generally very straight, Caucasian

hair varies from straight to wavy to moderately curly, in contrast with the African hair which exhibits a characteristic tightly curled structure (Wei, 2005). These variations in the shape of hair from different ethnic origins depend on several factors, including the shape of the hair follicle and its opening; these vary from one person to another and also between races (Gray, 2001, Thibaut, 2005b). But all hair, irrespective of ethnic origin, have the same protein structure and composition (Menkart, 1984, Dekio, 1988b, Dekio, 1990a).

In this study, the morphology changes on three ethnic hair types are compared using SEM, which have been heated at different isothermal heating times by DSC measurement.

5.5.2 Experimental

5.5.2.1 Hair Samples

Caucasian, Asian and African hair samples were used in this study. The hair samples were collected from volunteers. Although the exact location from the root is unknown, it is estimated that hair samples used for testing were taken at 10-20 cm from the scalp. In most cases, the experiments were conducted on the middle parts of the hair samples (about 10 mm).

5.5.2.2 DSC Experimental Work

All the experimental settings are the same as described in Section 5.4.3. The standard modulated DSC mode (MDSC) was applied, and hairs from three different ethnic origins were heated with the temperature increasing linearly at a rate of 5^{o}C/min in the range of 80-180^{o}C. Thus denaturation temperature and denaturation enthalpy can be determined, as illustrated in Figure 5.32. Because there is no distinct difference between three types of hair, their denaturation temperature is observed at a similar location (~147^{o}C).

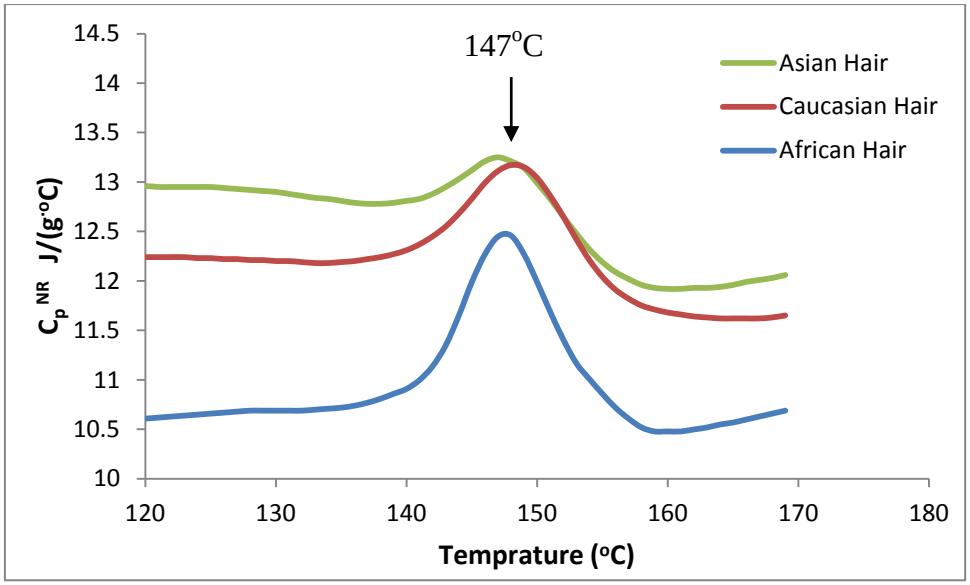

Figure 5.32: Typical non-reversing C_p^{NR} DSC curve for three types of human hair in water at a heating rate of 5°C/min

In the next step, the virgin hair samples were heated with the temperature increasing linearly at a rate of 5°C/min up to the peak temperature of 147°C, and left for 5, 10 and 20mins of isothermal time, individually, before cooling down. This procedure was chosen to examine the hydrolytic influence on hair morphology at their denaturation temperature (147°C).

5.5.2.3 SEM Experimental work

The residues of denaturated hair samples after DSC were collected and dried at room temperature for the further SEM investigation. All the experimental settings are as same as described in Chapter 4. The sample description for SEM images is given in Table 5.15.

Table 5.15: Description of SEM images for various hair samples

Picture No.	Ethnicity	Isothermal Time(mins)
A	Asian	5
B		10
C		20
D	African	5
E		10
F		20
G	Caucasian	5
H		10
I		20

5.5.3 Results and Discussion

SEM images in Figure 5.33 are employed to document the changes of the morphological structures of the three types of hair after being heated at various isothermal times. The cuticle of Asian hair has a stronger tendency towards distortion. Numerous hydrolysed proteins granules appear with longer isothermal heating time (Pictures 5.33 A-C). The images also have electron dense bodies visible in the cuticle (red arrow), these are consistent in size and shape (approximately 1–5 mm) with melanosomes. Since melanin granules are rarely present in the cuticle (Robbins, 2002), it is possibly an artifact of the contamination process (Stout, 2007) or of the large amount of melanin granules in Asian hair, which has a natural black colour.

African hair, which maintains as smooth and intact cuticle surface as the virgin Caucasian hair, shows a very high thermal resistance (Pictures 5.33 D-F), this may be ascribed to its hardness and the curly properties of the hair nature.

Caucasian hair samples demonstrate a similar phenomenon in Pictures 5.33 G-I, as the virgin Caucasian hair in the kinetic analysis in Chapter 5.4.4.3. The hydrolysed protein granules increase with increasing isothermal heating times, which implies that IFs have been progressively destroyed by heating.

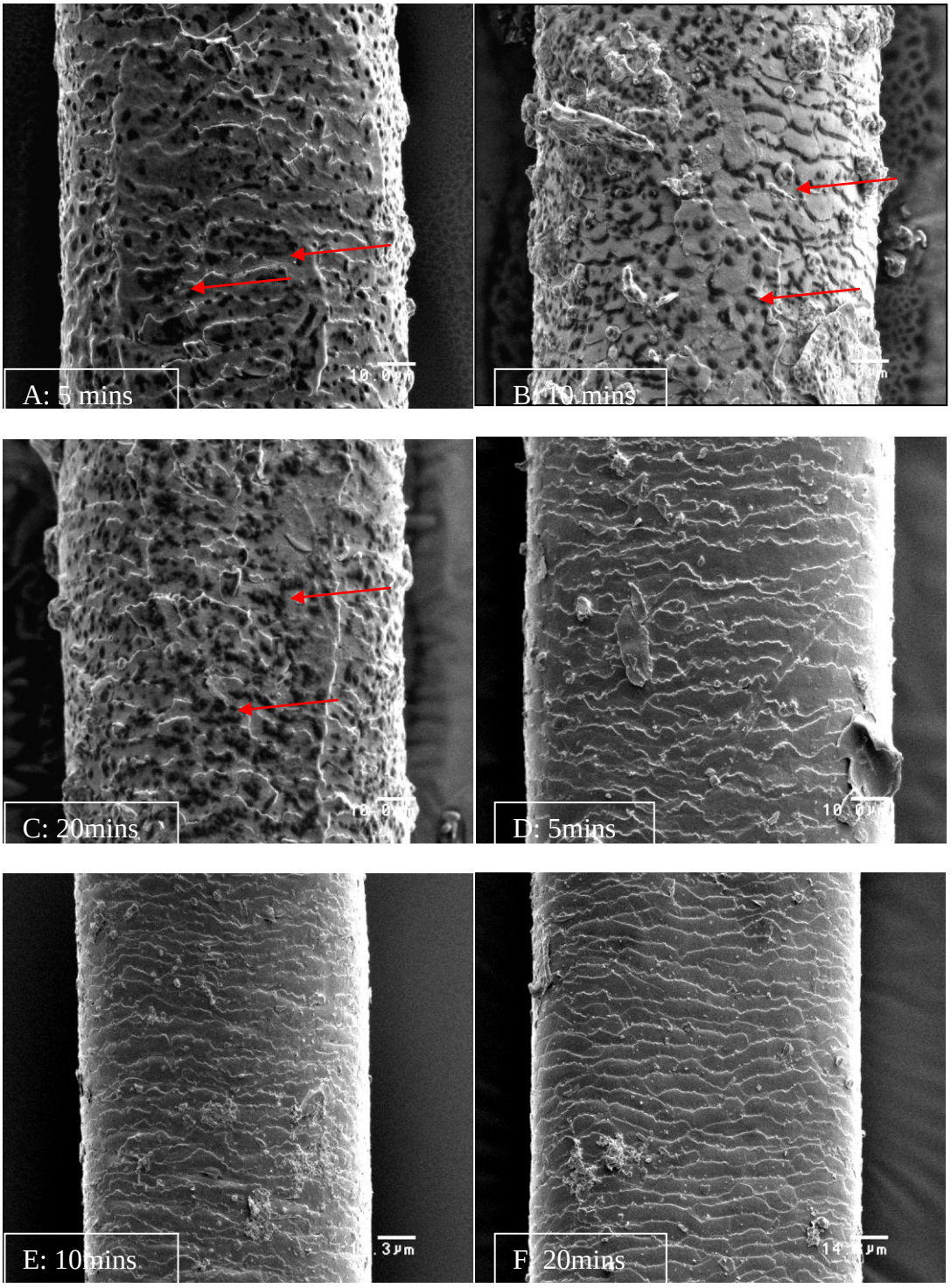
A: 5 mins
B: 10 mins
C: 20mins
D: 5mins
E: 10mins
F: 20mins

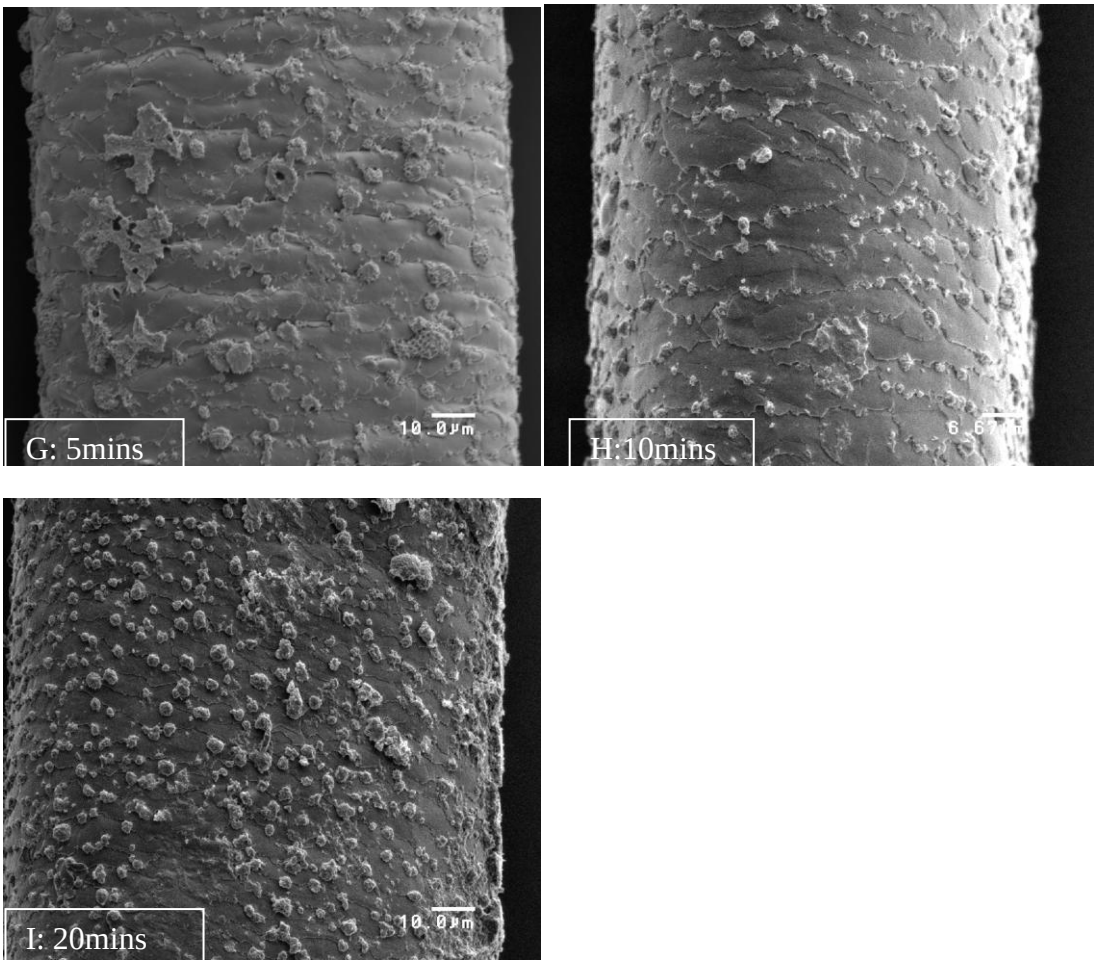

Figure 5.33: SEM images of three types of hair after being heated to their denaturation temperature and left at various isothermal times, before cooling. The image identifications are described in Table 5.14.

5.6 Conclusion

DSC analyses confirm the effect of bleaching on hair damage. Since ΔH_D and T_D reflect the amount and structural integrity of the α-helical material in the IFs, and respectively the cross-link density of the matrix (IFAPs), in which the IFs are embedded (Wortmann, 2002), there is a consistent decrease in both denaturation temperatures T_D and enthalpies ΔH_D over the bleaching time. This shows that the longer the bleaching time, the greater is the structural damage produced in hair. Thus a lower keratin denaturation enthalpy and a lower denaturation temperature are observed. Consequently the commercial persulphate bleach has a stronger oxidation effect on both intermediate filaments and matrix than 9% H_20_2 commercial bleach and 6% H_20_2

bleach. The deconvolution results of the DSC-curves for the three bleaches confirm this observation. Stronger bleach results in similar damage for the crystalline component in both para- and ortho-cortical cells with prolonged bleaching time.

However, a strong linear relationship was observed for 6% H_2O_2, commercial persulphate bleach and part of 9% H_20_2 commercial bleach by plotting ΔH_D^R against T_D^R, suggesting that the three bleaches have a homogenous bleaching effect on IFs and IFAPs. However, 9% H_20_2 commercial bleached hair after 2h bleaching time is considered that the intermediate filament is subjected to progressive destruction after excessive bleaching treatment, thus causing unfavourable results for the 9% H_20_2 commercial bleached hairs.

SEM examined the appearance changes of virgin and bleached hair after keratin denaturation at various heating rates (kinetic analysis). It is concluded that lower heating rates result in more severe structural changes. The commercial persulphate bleached hairs show an overall shrunk cuticle and less protein granules, due to the previously denaturated α-helix in the cortical cells. In addition, the deconvolution results further support that heating rates effect affects the cystine linkages in the para- and ortho-cortex homogenously, regardless of the previous damage. Commercial persulphate bleached hair shows a uniform damage effect for para-, ortho- and meso-cortical components.

5.7 References

ALBERTS, B., BRAY, D., JOHNSON, A., LEWIS, N., RAFF, M., ROBERT, K., WALTER, P., 1998. *Essential Cell Biology: An Introduction to the Molecular Biology of the Cell,* New York, Garland Publishing, Inc.

BISCHOF, J. C., HE, X., 2005. Thermal Stability of Proteins. *Annals of the New York Academy of Sciences,* 1066**,** 12-33.

BISCHOF, J. C., WOLKERS, W. F., TSVETKOVA, N. M., OLIVER, A. E., CROWE, J. H., 2002. Lipid and protein changes due to freezing in Dunning AT-1 cells. *Cryobiology,* 45**,** 22-32.

BORCHARDT, H. J., DANIELS, F., 1957. The Application of Differential Thermal Analysis to the Study of Reaction Kinetics. *Journal of the American Chemical Society,* 79**,** 41-46.

BRYSON, W. G., HARLAND, D.P., CALDWELL, J.P., VERNON, J.A., WALLS, R.J., WOODS, J.L., NAGASE, S., ITOU, T., KOIKE, K., 2009. Cortical cell types and intermediate filament arrangements correlate with fiber curvature in Japanese human hair. *J. Struct. Biol,* 166**,** 46-58.

BUNJES, H., UNRUH, T., 2007. Characterization of lipid nanoparticles by differential scanning calorimetry, X-ray and neutron scattering *Advanced Drug Delivery Reviews,* 59**,** 379-402.

BURNHAM, A. K. 2000. Computational aspects of kinetic analysis. Part D: The ICTAC kinetics project -multi-thermal-history model-fitting methods and their relation to isoconversional methods. *Thermochimica Acta,* 355**,** 165-170.

BURNHAM, A. K., BRAUN, R. L., 1999. Global Kinetic Analysis of Complex Materials. *Energy & Fuels,,* 13**,** 1-22.

CAO, J. 1997a. Origin of the Bimodal "Melting" Endotherm of a-Form Crystallites in Wool Keratin. *Journal OF Applied Polymer Science,* 63**,** 411-415.

CAO, J. 1999. Melting study of the a-form crystallites in human hair keratin by DSC. *Thermochimica Acta,* 335**,** 5-9.

CAO, J., JOKO, K., COOK, J. R., 1997b. DSC studies of the melting behavior of a-form crystallites in wool keratin. *Textile Research Journal,* 67**,** 117-123.

CAO, J., LEROY, F., 2005. Depression of the melting temperature by moisture for α-form crystallites in human hair keratin. *Biopolymers,* 77**,** 38-43.

CHIEW, Y. C., KUEHNER, D., BLANCH, H. W., PRAUSNITZ, J. M., 1995. Molecular Thermodynamics for Salt-Induced Protein Precipitation. *AIChE Journal,* 41**,** 2150-2159.

COOPER, A. 1999. Thermodynamics of protein folding and stability. *In:* ALLEN, G. (ed.) *Protein: A Comprehensive Treatise.* Stamford, CT: JAI Press.

CRAVALHO, E. G., TONER, M., GAYLOR, D. C., LEE, R. C., 1992. Response of cells to supraphysiological temperatures: Experimental measurements and kinetic models. *In:* LEE, R. C., CRAVALHO, E. G., BURKE, J. F., (ed.) *Electrical Trauma:The Pathophysiology, Manifestations and Clinical Management.* Cambridge: Cambridge University Press.

CREIGHTON, T. E. 1990. Protein folding. *Biochem J,* 270**,** 1-16.

CRIGHTON, J. S. The characterisation of destabilised and stablised wools. Proceeding of the 8th International Wool Textile Research Conference, 1990 Christchurch, New Zealand.

CRIGHTON, J. S., HOLE, E. R.,. A study of wool in aqueous media by high pressure differential analysis. 7th International Wool Textile Research Conferenace, 1985 Tokyo, Japan. 283-292.

DEKIO, S., JIDOI, J., 1988. Hair low-sulfur protein composition does not differ electrophoretically among different races. *J Dermatol.* , 15**,** 393-6.

DEKIO, S., JIDOI, J., 1990. Amounts of fibrous proteins and matrix substances in hairs of different races. *J Dermatol.,* 17**,** 62-4.

DOBB, M. G. 1970. Electron-diffraction Studies of Keratin Cells. *Journal of the Textile Institute,* 61**,** 170.

DUSWALT, A. A. 1974. The practice of obtaining kinetic data by differential scanning calorimetry *Thermochimica Acta,* 8**,** 57-68.

E2041 Estimating Kinetic Parameters by Differential Scanning Calorimetry Using the Borchardt and Daniels Method. West Conshohocken, PA: ASTM International.

E2070 Kinetic Parameters by Differential Scanning Calorimetry Using Isothermal Methods. West Conshohocken, PA ASTM International,.

EYRING, H. 1974. Temperature. *In:* JOHNSON, H. F., EYRING, H., STOVER, B. J., (ed.) *The Theory of Rate Processes in Biology and Medicine.* New York: John Wiley & Sons.

FERNANDEZ D'ARLAS, B., RUEDA, L., STEFANI, P. M., DE LA CABA, K., MONDRAGON, I., ECEIZA, A., 2007. Kinetic and thermodynamic studies of the formation of a polyurethane based on 1,6-hexamethylene diisocyanate and poly(carbonate-*co*-ester)diol. *Thermochimica Acta,* 459**,** 94-103.

FEUGHELMAN, M. 1959. A Two-Phase Structure for Keratin Fibers. *Textile Reseach Journal,* 29**,** 223.

FEUGHELMAN, M. 1989. A note on the water impenetrable component of alpha-keratin fiber. *Textile Res. J.,* 59**,** 739-742.

FEUGHELMAN, M. 1997. *Mechanical Proeprties and Structure of Alpha-Keratin Fibres: Wool, human hair and related fibres*, University of New South Wales Press.

FLYNN, J. H., WALL, L. A., 1966a. General Treatment of the Thermogravimetry of Polymers *Journal of Research of the National Bureau of Standards - A Physics and Chemistry,* 70A**,** 487-523.

FLYNN, J. H., WALL, L. A., 1966b. A Quick, Direct Method for the Determination of Activation Energy from Thermogravimetric Data. *Polymer Letters,* 4**,** 323-328.

FRANBOURG, A., LEROY, F., LEVEQUE, J. L., DOUCET, J., 1996. Synchroton light: A powerful tool for the analysis of humanh air damage. *10th Int. Hair-Science Symp.* Rostock: German Wool Res. Inst.

FREIRE, E., BILTONEN, R. L., 1978. Statistical mechanical deconvolution of thermal transitions in macromolecules. I. Theory and application to homogeneous systems. *Biopolymers,* 17**,** 463-479.

GILL, P. S., SAUERBRUNN, S. R., READING, M., 1993. Modulated Differential Scanning Calorimetry. *Journal of Thermal Analysis,* 40**,** 931-939.

GRAY, J. 2001. Hair Care and Hair Care Products. *Clinics in Dermatology* 19**,** 227-236.

GROENEWOUD, W. M. 2001. *Characterisation of Polymers by Thermal Analysis,* Amsterdam, Elsevier Science.

HALY, A. R., SNAITH, J. W., 1967. Differential thermal analysis of wool: the phase-transition endotherm under various conditions. *Textile Research Journal,* 37**,** 898-907.

HALY, A. R., SNAITH, J.W., 1970. The Heat of the Phase Transformation in Wool Keratin Under Various Conditions. *Textile Research Journal,* 40**,** 142.

HORIO, M., KONDO, T., SEKIMOTO, K., FUNATSU, M., 1965. Pyrolysis of Wool in Sealed Tubes. *Proceedings of 3rd International Wool Textile Research Conference* Paris.

HUMPHRIES, W. T., MILLER, D. L., WILDNAUER, R. H., 1972. The Thermomechanical Analysis of Natural and Chemically Modified Human Hair. *Journal of the Society of Cosmetic Chemists,* 23**,** 359-370.

HUNTER, L., HUNTER, E.L 2001. *Appendix 3 Composition of mohair fibres and of amino acids,* Cambridge, England, Woodhead Publishing Ltd.

ISTRATE, D., POPESCU, C., MÖLLER, M., 2009. Non-Isothermal Kinetics of Hard a-Keratin Thermal Denaturation. *Macromolecular Bioscience,* 9**,** 805-812.

JOLY, M. 1965. *A Physico-chemical Approach to the Denaturation of Proteins,* London, Academic Press.

JONES, L. N., RIVETT, D. E., TUCKER, D. J., 2006. *Wool and Related Mammalian Fibers,* Taylor & Francis Group, CRC Press.

KANETAKA, S., TOMIZAWA, K., IYO, H., NAKAMURA, Y., 1993. The effects of UV radiation on human hair concerning physical properties and fine structure of protein. *J Soc Cosmet Chem Jpn,* 27**,** 424-431.

KONDA, A., TSUKADA, M., KURODA, S., 1973. The change of thermal property of wool keratin with drawing. *Journal of Polymer Science: Polymer Letters Edition,* 11**,** 247-251.

KUZUHARA, A. 2006. Aanalysis of structural changes in bleached keratin fibers (black and white human hair) using Raman spectroscopy. *Biopolymers,* 81**,** 506-514.

KUZUHARA, A. 2007. Analysis of structural changes in permanent waved human hair using Raman spectroscopy. *Biopolymers* 85**,** 274-283.

LEROY, F., FRANBOURGA, A., LEVEQUE, J. L., 1992. Thermoanalytical investigations of reduced hair. *8th lnt. Hair-Scienc Symp.* Kiel: German Wool Res. Inst.

LI, C. R., TANG, T. B., 1999. A new method for analysing non-isothermal thermoanalytical data from solid-state reactions. *Thermochimica Acta,* 325**,** 43-46.

LI, C. R., TANG, T. B., 1997. Dynamic Thermall Analysis of Solid-state Reactions *Journal of Thermal Analysis,* 49**,** 1243-1248.

LUMRY, R., EYRING, H., 1954. Conformation Changes of Proteins. *J. Phys. Chem,* 58**,** 110-120.

LYUBAREV, A. E., KURGANOV, B. I., 2000. Analysis of DSC data relating to proteins undergoing irreversible thermal denaturation *Journal of Thermal Analysis and Calorimetry,* 62**,** 49-61.

MACIEJEWSKI, M. 2000. Computational aspects of kinetic analysis. Part B: The ICTAC Kinetics Project Ð the decomposition kinetics of calcium carbonate revisited, or some tips on survival in the kinetic minefield. *Thermochimica Acta,* 355**,** 145-154.

MENKART, J., WOLFRAM, L.J., MAO, I., 1984. Caucasian hair, Negro hair, and wool: similarities and differences. *Journal Society of Cosmetic Chemists,* 17**,** 769-787.

MILCZAREK, P., ZIELINSKI, M., GARCIA, M. L., 1992. The mechanism and stability of thermal transitions in hair keratin. *Colloid Polymer Science,* 270**,** 1106-1115.

MONTEIRO, V. F., MACIEL, A. P., LONGO, E., 2005. Thermal Analysis of Caucasian Human Hair. *Journal of Thermal Analysis and Calorimetry* 79**,** 289-293.

OPFERMANN, J. 2000. Kinetic Analysis Using Multivariate Non-linear Regression. I. Basic concepts. *Journal of Thermal Analysis and Calorimetry,,* 60**,** 641-658.

OZAWA, T. 1970. Kinetic Analysis of Derivative Curves in Thermal Analysis. *Journal of Thermal Analysis and Calorimetry,* 2**,** 301-324.

POPESCU, C., SEGAL, E., 1998. Critical considerations on the methods for evaluating kinetic parameters from nonisothermal experiments. *International Journal of Chemical Kinetics,* 30**,** 313-327.

POPESCU, C., WORTMANN, F. J., 2003. HPDSC evaluation of cosmetically treated human hair. *Roumanian J Chemistry,* 48**,** 981-986.

ROBBINS, C. R. 2002. *Chemical and Physical Behavior of Human Hair,* New York,, Springer-Verlag.

RÜEGG, M., MOOR, URSULA., BLANC, B., 1977.
A calorimetric study of the thermal denaturation of whey proteins in simulated milk ul trafiltrate. *Journal of Dairy Research,* 44**,** 509-520.

SAKABE, H., ITO, H., MIYAMOTO, T., INAGAKI, H., 1987. States of Water Sorbed on Wool as Studied by Differential Scanning Calorimetry. *Textile Research Journal,* 57**,** 66-72.

SANCHEZ-RUIZ, J. M. 1992. Theoretical analysis of Lumry-Eyring models in differential scanning calorimetry. *Biophys J,* 61**,** 921-935.

SCHAWE, J. E. K., HOHNE, G. W. H., 1996. The analysis of temperature modulated DSC measurements by means of the linear response theory. *Thermochimica Acta,* 287**,** 213–223.

SCHICK, C. 2002. Temperature modulated differential scanning calorimetry (TMDSC) - basics and applications to polymers. *In:* CHENG, S. Z. D. (ed.) *Handbook of Thermal Analysis and Calorimetry.*

SCHMIDT, H., WORTMANN, F. J., 1994. High pressure differential scanning calorimetry and wet bundle tensile strength of weathered wool. *Textile Research Journal,* 64**,** 690-695.

SCHWENKER, R. F., DUSENBURY, J. H., 1960. Differential Thermal Analysis of Protein Fibers *Textile Research Journal,* 30**,** 800.

ŠESTAK, J., BERGGREN, G., 1971. Study of the Kinetics of the Mechanism of SolidState Reactions at Increasing Temperatures. *Thermochimica Acta,* 3**,** 1-12.

SPARROW, L. G., DOWLING, L. M, LOKE, V. Y, STRIKE, P. M., 1988. Amino acid sequence of wool keratin IF proteins. *In:* ROGERS, G. E., REIS, P. J, WARDS, K. A, MARSHALL, R. C., (ed.) *The Biology of Wool and Hair*. London: Chapman & Hall.

SPEI, M. 1984. Time-dependent deposition of anionic detergents in a-Keratins. *COLLOID & POLYMER SCIENCE,* 262**,** 596.

SPEI, M. 1990. Thermoanalytical methods and their meaningfulness in keratin research. *Melliand Textilberichte,* 11**,** 902.

SPEI, M., HOLZEM, R., 1989. The α-β transition of fiber keratins. *Melliand Textilber,* 70**,** 371.

SPEI, M., HOLZEN, R., 1987. Thermoanalytical investigations of extended and annealed keratins. *Colloid Polymer Science,* 265**,** 965-970.

SPEI, M., THOMAS, H., 1983. Thermoanalytische Untersuchungen von Wollproteinen in der Disulfidform. *Colloid Polym. Sci.,* 261**,** 968-969.

STOUT, P. R., ROPERO-MILLER, J. D., BAYLOR, M. R., MITCHELL, J. M., 2007. Morphological changes in human head hair subjected to various drug testing decontamination strategies. *Forensic Science International,* 172**,** 164-170.

THIBAUT, S., BERNARD, B. A., 2005a. The biology of hair shape. *Int. J. Dermatol,* 44**,** 2-3.

THIBAUT, S., GAILARD, O., BOUHANNA, P., CANNELL, D. W., BERNARD, B. A., 2005b. Human hair shaped is programmed from the bulb. *British Journal of Dermatology,* 152**,** 632-638.

TONIN, C., ALUIGI, A., BIANCHETTO SONGIA, M., D'ARRIGO, C., MORMINO, M., VINEIS, C., 2004. Thermoanalytical Characterisation of Modified Keratin Fibres. *Journal of Thermal Analysis and Calorimetry,* 77**,** 987-996.

VYAZOVKIN, S., SBIRRAZZUOLI, N., 2006. Isoconversional Kinetic Analysis of Thermally Stimulated Processes in Polymers. *Macromolecular Rapid Communications,* 27**,** 1515-1532.

WATT, I. C. 1980. Sorption of Water Vapor by Keratin *Journal of Macromolecular Science, Part C: Polymer Reviews,* 18**,** 169-245.

WATT, I. C., KENNETT, R. H., JAMES, J. F. P., 1959. The Dry Weight of Wool. *Textile Research Journal,* 29**,** 975-981.

WEI, G. H., BHUSHAN, B., TORGERSON, P. M., 2005. Nanomechanical characterization of human hair using nanoindentation and SEM. *Ultramicroscopy,* 105**,** 248-266.

WHITELEY, K. J., KAPLIN, I. J., 1977. The comparative arrangement of microfibrils in ortho--, meso-, and para-cortical cells of Merino-wool fibers. *J.Text.Inst,* 68**,** 384-386.

WORTMANN, F. J., DE JONG, S., 1985. Analysis of the humidity-time superposition for wool fibers. *Text Res J.* , 55**,** 750-756.

WORTMANN, F. J., DEUTZ, H., 1993. Characterizing keratins using high-pressure differential scanning calorimetry (HPDSC). *Journal of Applied Polymer Science,* 48**,** 137-150.

WORTMANN, F. J., DEUTZ, H., 1998. Thermal analysis of ortho- and para-cortical cells isolated from wool fibres. *Journal OF Applied Polymer Science,* 68**,** 1991-1995.

WORTMANN, F. J., HULLMANN, A., POPESCU, C., 2007. Water management of human hair. *International Journal of Cosmetic Science,* 30**,** 388-389.

WORTMANN, F. J., POPESCU, C., SENDELBACH, G., 2006. Nonisothermal denaturation kinetics of human hair and the effects of oxidation. *Biopolymers,* 83**,** 630-635.

WORTMANN, F. J., SPRINGOB, C., SENDELBACH, G., 2002. Investigations of cosmetically treated human hair by differential scanning calorimetry in water. *J. Cosmet. Sci.,* 53**,** 219-228.

Chapter 6 FTIR Investigations of Human Hair

6.1 Introduction

Almost every compound, whether organic or inorganic, has covalent bonds. Different bonds absorb different frequencies of electromagnetic radiation in the infrared region of the electromagnetic spectrum. Although some of the frequencies absorbed in two different molecules might be the same, no two molecular structures produce the identical infrared spectrum. Therefore, infrared spectroscopy (IR) can result in a qualitative analysis of each material. Furthermore infrared spectroscopy is also an excellent tool for quantitative analysis, using specialised software tools. The size of the peaks in the spectrum provides useful information of the amount of material, e.g., in a mixture (Hsu, 1997).

In infrared spectroscopy, IR radiation is passed through a sample. Some of the infrared radiation is absorbed by the sample and some of it is transmitted. The produced absorption or transmission spectrum represents a characteristic fingerprint of the sample. An infrared spectrum represents a fingerprint of a sample with absorption peaks, which generally presents wavelengths or wavenumber as the x-axis and absorption intensity or percent transmittance as the y-axis. Transmittance (T) is the ratio of radiant power transmitted by the sample (I) to the radiant power incident on the sample (I_0). Absorbance (A) is the logarithm to the base 10 of the reciprocal of the transmittance (T) (see Equation.6.1):

$$A = \ln(1/T) = -\ln T = -\ln I/I_0 \qquad (6.1)$$

The transmittance spectra provide better contrast between intensities of strong and weak bands because transmittance ranges from 0 to 100% whereas absorbance ranges from infinity to zero. It should be noted that the same sample can give different IR spectra, such as one spectrum presented in wavenumber, while another is presented in

wavelength. Depending on this IR bands may become contracted or expanded (Khan, 2012).

The IR region is categorised into three smaller areas: Near IR, Mid IR and Far IR, as shown in Table 6.1.

Table 6.1: Characteristics of the three IR regions

	Near IR	Mid IR	Far IR
Wavenumber	13,000-4,000 cm^{-1}	4,000-200 cm^{-1}	200-10 cm^{-1}
Wavelength	0.78-2.5 μm	2.5-50 μm	50-1000 μm

This FTIR investigation of human hair focus in the mid IR region, between 4000 and 400cm^{-1} (2.5 to 25 μm). The far IR region is used for analysis of organic, inorganic, and organo-metallic compounds, which contain heavy atoms (mass number over 19). It is useful in structural studies such as conformation and lattice dynamics of samples. There is minimal or no sample preparation required for the near IR spectroscopy. It provides high-speed quantitative analysis without consumption or destruction of the sample, and is gaining increased attention in process control applications.

In the mid-infrared (MIR) spectrum, different functional chemical groups lead to unique fundamental vibrations. An important use of the infrared spectrum is to determine structural information about a molecule. Different atoms in the molecules vibrate and rotate at particular wavelengths. The frequencies at which the molecules absorb depend on the masses of the atoms, the force constants of the bonds, and the geometries of the atoms. The absorption bands for different moieties are generally known, so an unknown spectrum can be compared to the known one to identify the material. In general, C-C, C-O, and C-N absorb between 1300-800 cm^{-1}, C=O, C=C, C=N, and N=O absorb between 1900- 1500 cm^{-1}, C≡C and C≡N absorb between 2300-2000 cm^{-1}, and C-H, O-H, and N-H absorb between 3800-2700 cm^{-1} (Silverstein, 1981).

6.1.1 Infrared Spectrometer

The instrument that determines the absorption spectrum for a compound is called an infrared spectrometer or a spectrophotometer. Two types of infrared spectrometers are in common use: dispersive and Fourier transform (FT) instruments. Both of these types of instruments provide spectra of compounds in the common range of wavenumbers of 4000 to 400 cm^{-1}.

6.1.1.1 Dispersive Infrared Spectrometer

"Dispersive" or "scanning monochromator" is an alternative method for taking spectra, which measures radiation intensity over a narrow range of wavelengths at one time. In the dispersive system, infrared light is separated and scanned with the whole range of infrared frequencies so the energy is sequentially presented to the detector. The dispersive method is more common in UV-Vis spectroscopy, but is less practical in the infrared than the FTIR method. A FT infrared spectrometer provides the infrared spectrum much more rapidly than a dispersive instrument.

6.1.1.2 Fourier Transform Infrared Spectrometer

FTIR is the preferred method of infrared spectroscopy, which is used to obtain infrared spectra of absorption, emission, photoconductivity of a solid, liquid or gas.

Fourier transform infrared (FTIR) spectrometers have been widely used in modern infrared spectrometers and have improved the acquisition of infrared spectra. The schematic diagram in Figure 6.1 represents the Michelson interferometer, which is the central unit of a FTIR spectrometer. It has a fixed and a movable mirror. When radiation from a broadband source strikes the beamsplitter, some of the light is transmitted to a movable mirror and some of the light is reflected to a fixed mirror. The moving mirror generates a variable optical path between two beams which gives detector signal about the spectral information. A beam splitter splits the emitted light

from the light source: half of the initial light is reflected towards the fixed mirror and then reflected back towards the beamsplitter, where about 50% passes to the detector. The other half passes the beam splitter on its first encounter, is reflected by the movable mirror back to the beamsplitter, where 50% of it is reflected towards the detector (Barth, 2007). When the two beams recombine they interfere constructively or destructively depending on the optical path difference to produce a pattern called an interferogram (Pavia, 1996, Harris, 1999). The interferogram contains all the frequencies, which form an IR spectrum. A mathematical operation known as a Fourier transform is used to distinguish the individual absorption frequencies from the interferogram to produce a plot of intensity versus frequency, i.e. an IR spectrum (Pavia, 1996, Harris, 1999).

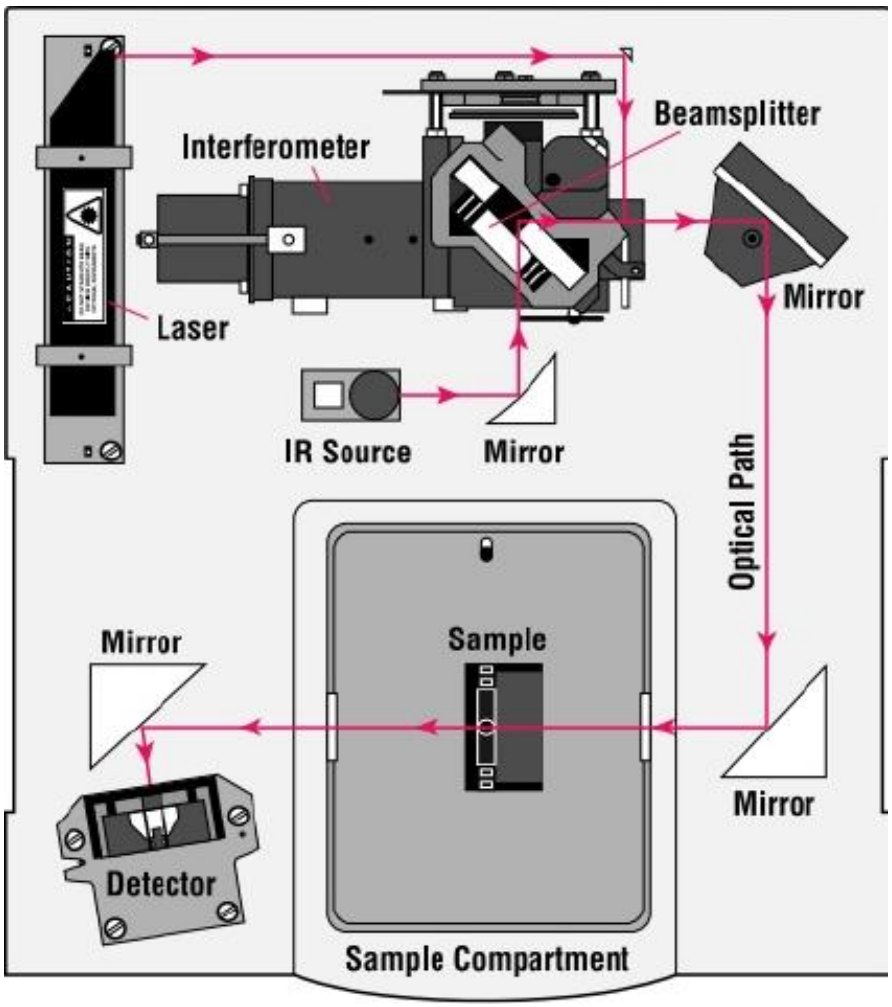

Figure 6.1: Schematic diagram of an FTIR spectrometer, showing its layout (ThermoNicolet, 2001)

6.1.1.2.1 The Advantages of FTIR

FTIR instruments have several significant advantages over older dispersive instruments (Barbara, 2004).

1. Multiplex advantage (Felgett advantage) – Many scans can be completed and combined on an FT-IR in a shorter time, resulting in faster data collection of an FT-IR spectrum and the improvement of the signal-to-noise ratio (SNR).
2. Throughput advantage (Jacquinot advantage) – The total source output can be passed through the sample continuously, resulting in a substantial gain in energy at the detector, hence translating to higher signals and improved SNRs.
3. Co-addition of scans – Increase SNR by signal-averaging, leading to an increase of signal-to-noise proportional to the square root of the time, as follows:

$$SNR \alpha n^{½}$$

4. High scan rate – The mirror has the ability to move over short distances rapidly to acquire spectra on a millisecond timescale.
5. High resolution – By closing down the slits, a narrow band is achieved.
6. Laser Referencing (Connes Advantage) – By using a Helium-Neon laser as a reference, the wavenumber calibration of interferometers is much more accurate and has much better long term stability than the calibration of dispersive instruments.
7. Negligible stray light – The detector responds only to modulated light, so there is no direct equivalent of the stray light found in dispersive spectrometers.
8. Powerful computers – Advances in computers and new algorithms have allowed for fast Fourier-transformation.

The main advantage of Fourier transform spectrometers is their rapid data collection and high light intensity at the detector and in consequence a high signal to noise ratio. Different types of detectors, light sources and other optical components are chosen to optimise different requirements of the infrared spectral spectrum.

These advantages make FT-IR an invaluable tool for quality control and assurance applications. It can detect even the smallest contaminants because of its sensitivity. In

addition, the accuracy of FT-IR detectors, as well as a wide variety of software algorithms, have dramatically improved the applicability of infrared spectroscopy for quantitative analysis, as it is non-destructive in nature.

6.1.2 FTIR Sampling Techniques

Infrared spectroscopy is a versatile analytical technique, which is feasible for liquids, solids, and gases. However, many materials are opaque to IR radiation and must be dissolved or diluted in a transparent matrix in order to obtain spectra, which is the traditional transmission method of infrared spectroscopy (Hsu, 1997). Alternatively, it is possible to obtain reflectance or emission spectra directly from opaque samples, though attenuated total reflectance. A wide range of sampling accessories is employed to take advantage of the capabilities of FTIR instruments.

6.1.2.1 Transmission spectroscopy measurements

Transmission spectroscopy is the most basic infrared method by transmitting the infrared radiation directly through the sample at specific wavelengths, as shown in Figure 6.2. However, sometimes sample preparation is required. When the sample is liquid or solid, its intensity of the spectral appearance depends on the thickness of the sample which is generally between 1 and 20 μm thick (Smith, 1996).

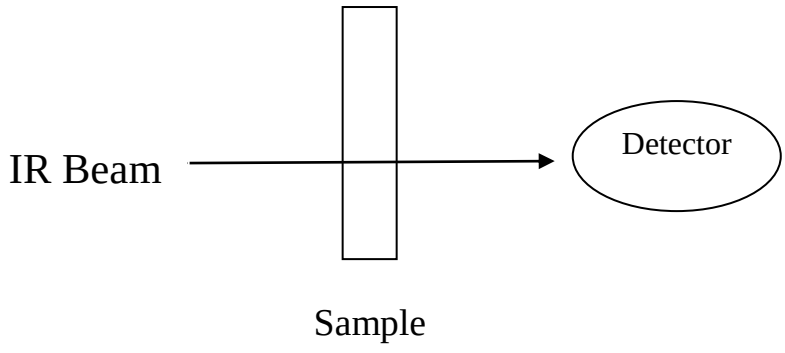

Figure 6.2: An illustration of transmission FTIR sampling, where the infrared beam passes through the sample and then strikes the detector

6.1.2.1.1 Sample Preparation

A. Liquids

In conventional transmission infrared spectroscopy, the IR beam passes directly through the solution. To minimise effects of IR light scattering, samples should be presented in thin films or suspensions.

In the process of sample preparation, a drop of a liquid organic compound is placed between a pair of polished sodium chloride or potassium bromide plates, which is referred as salt plates. A thin liquid film is produced by gently pressing the plates. Since there is no solvent is involved, a background spectrum is considered as a neat spectrum (Pavia, 2001).

Water is an intense absorber. One drawback of aqueous solutions is the strong absorbance of water in the mid-infrared spectral region (near 1645 cm^{-1}) (Venyaminov, 1997), which masks or overlaps the important amide I band of proteins and some side chain bands of interest. Thus protein solutions cannot be used for structure analysis of, e.g., the α- and β- conformation. And organic compounds analysed by this technique must be free of water.

B. Solids

There are three general methods for preparing solid samples in transmission spectroscopy: alkali halide pellet, mulls and films.

I. Alkali Halide Pellet or Discs

This method involves mixing a solid sample (a few mg) with a dry alkali halide powder (100-200 mg). The mixture is usually ground in an agate mortar with a pestle under sufficiently high pressure in an evacuable die. The most commonly used alkali halide is potassium bromide (KBr), which is completely transparent in the mid-infrared region. But KBr is hygroscopic, so that the "water effect" may interfere with the

obtained spectrum. In addition, the preparation of a KBr pellet is very time consuming and sample weight and grinding conditions may cause further problems in the infrared spectrum of a sample (Painter, 1978, 1981). As light scattering shifts the spectral baseline towards the high-frequency region (Painer, 1985), in order to minimize band distortion, the sample should be ground to particles of 2 μm (the low end of the radiation wavelength) or less in size (Hsu, 1997).

II. Mulls

This method is used as alternatives for pellets. It involves grinding the sample (no more than 20 mg) and suspending it (about 50mg) in 1-2 drops of a mulling agent. The mixture is further ground until a smooth paste is obtained, which is then spread between two mid-infrared transparent windows e.g. NaCl, KBr, CaF_2. Ideally, a mulling agent should be infrared transparent between 4000 and 600 cm^{-1}, unfortunately no such agent exists. The most commonly used mulling agent is Nujol (liquid paraffin), but mineral oil obscures the bands that may be present in the analysed compound. Normally, Nujol bands appear at 2924, 1462, and 1377 cm^{-1} (Pavia, 2001).

Similarity as for the alkali halide pellet, sample particles of 2 μm or less in size are very important for obtaining a satisfactory spectrum.

III. Films

Films can be produced by either solvent casting or by melt casting. These methods are particularly useful for examining polymers.

In solvent casting the sample is dissolved in an appropriate solvent, which is chosen not only to dissolves the sample, but also to produce a uniform film. The concentration of solvent depends on the required film thickness. The solution of the sample is poured onto a glass plate (such as a microscope slide) or a metal plate and is spread to a uniform thickness. Once the solvent has evaporated in an oven, the film is free to be

isolated from the plate. Alternatively, it is possible to cast a film directly onto the infrared window.

Solid samples which melt at relatively low temperatures without decomposition can also be prepared by melt casting. A film is achieved by hot-pressing the sample in a hydraulic press between heated metal plates (Barbara, 2004).

6.1.2.1.2 Sample Preparations of Transmission Spectroscopy for Keratin Fibres

Various researchers have attempted various methods for preparing fibrous and elastic materials for infra-red spectral investigations. Beer et al. (1959) cut fibrous proteins into small pieces with a microtome, while Crook and Taylor (1958) mulled the textile material between ground-glass plates with a few drops of paraffin or hexachlorobutadiene. Devaney and Thompson (1958) used diamond powder embedded in steel to grind a powder of epoxy-resin from a film of the epoxy resin and hardener. There is some evidence using the microtome that it affects the conformational structure of the fibre (Caroti, 1956), while the grinding procedure described above reduces the crystallinity of the wool and human hair. This finding is also in agreement with the observations made by other researchers (Beer, 1959). Strasheim et al. (1961) adopted the Wig-L-Bug, which is a wrist-type mortar with a hard-tempered steel vial has been found most suitable for the KBr disk technique.

But one of the main problems with the transmission IR spectroscopy is that the fibres are impossible to arrange in a cross-sectional direction because the fibres are randomly mixed with alkali halide pellet. If the proper sample preparation for the fibre cross-section could be developed, IR spectroscopy could be used to examine specific locations in the fibre's internal structure.

6.1.2.2 Reflectance Techniques

Reflectance technique is an alternative method to analyse the samples, when they are difficult to analyse by the transmittance methods. Reflectance methods can be divided into two categories: internal reflectance measurement, which is using an attenuated

total reflectance cell in contact with the sample, and external reflectance measurement which involves an infrared beam reflected directly from the sample surface.

6.1.2.2.1 Attenuated Total Reflectance Spectroscopy

Attenuated Total Reflectance (ATR) Spectroscopy, also known as Internal Reflection Spectroscopy (IRS), has widely been used for the study of the near-surface of biological materials, and has been used for investigating samples which are too thick for transmission measurements (Harrick, 1979).

Generally, ATR spectra are similar to regular transmission spectra. But ATR sampling does not produce totally absorbing spectral bands because its effective path-length is controlled by the crystal properties, thereby the sample re-preparation time is reduced. Moreover, ATR spectra have both absorption and reflection features, so they cannot be used in quantitative analysis directly (Grdadolnik, 2002).

A. The principle of Attenuated Total Reflectance Spectroscopy

In FTIR-ATR, the sample is placed on a crystal with an index of refraction that is larger than that of the sample, such as diamond, zinc selenide (ZnSe), ZnS, germanium (Ge) and thallium/iodide (KRS-5). Different ATR cells properties are used for samples in liquid or solid form. For a liquid sample, ATR produces a less intense solvent contribution for the overall infrared spectrum, so that solvent spectra can be easily subtracted from the sample spectrum of interest. Solid samples are best analysed by single reflection ATR accessories, and diamond is widely used for most applications because of its robustness and durability.

ATR spectroscopy examines the phenomenon of total internal reflection. A beam of radiation is transmitted into a crystal and directed towards the sample interface at an angle of incidence. When the incidence angle θ_i, at the interface between sample and crystal exceeds the critical angle θ_c, total internal reflection is achieved. Total internal reflection at the surface of the crystal produces an evanescent wave, which has the same frequency as the incoming light. But the amplitude of the electric field decays

exponentially with the distance from the interface. The evanescent wave penetrates the surface of the sample, and some of the light diffuses and is selectively absorbed in the sample. When diffused light reflects back into the crystal, this part of the light carries the information about the infrared spectrum of the sample. Afterwards it reaches the detector to produce an IR spectrum. Because the IR beam is not transmitted through the sample, the produced spectra are unaffected by turbidity. The attenuated radiation is measured and plotted as a function of the wavelength to give the absorption spectral characteristics of the sample.

B. ATR-diamond cell Investigation on Hair Fibres

FTIR spectroscopy using attenuated total reflectance (ATR) is an established technique for non-destructive qualitative and quantitative surface analysis of keratin fibres, namely, for cysteic acid and intermediate oxidation products of cystine. Researchers employed an ATR diamond cell to measure the concentration of cysteic acid in bleached hair. Although the intensity differences between untreated and bleached hair were not discussed, the method of data analysis as described by Signori (1997) is excellent for the determination of the cysteic acid content of both damaged and untreated hair. Martin (1999) further compared ATR using ZnS cells and diamond cells, confirming that the diamond cell ATR has good applicability for hair keratin analysis because of its reproducible results. Although the ATR technique is not suitable for single hair fibre measurements, it will provide information about the surface of the hair sample (up to 4μm into the bulk of the fibre) (Signori, 1997).

ATR is a powerful IR method as it is insensitive to sample thickness, less destructive (only a small point of the fibre is compressed by the pressure tower), and permitting the surface or near-surface analysis of thick or highly absorbing materials, i.e. α-keratin fibres (Bartick, 1994, Signori, 1997). But IR radiation does not penetrate the hair fibre, so a lot of reflectance may occur on the hair fibres surface. Thus ATR can only investigate the cuticle and possibly outer layers of the cortex.

C. Depth of Penetration in ATR

The depth of penetration (D_P) in an ATR experiment is a measure of how far the evanescent wave penetrates into a sample. Equation 6.2 for depth of penetration in an ATR experiment yields:

$$D_P = \lambda / 2\pi\, n_1 \{\sin^2\theta - (n_2/n_1)^2\}^{1/2} \qquad (6.2)$$

Where,

D_P = Depth of Penetration (in cm)

λ = Wavelength of the infrared light in cm^{-1}

n_1 = Refractive index of ATR crystal

θ = Angle of incidence of IR beam with crystal surface

n_2 = refractive index of sample

Generally the depth of penetration in ATR ranges from about 0.1 μm up to about 5 μm depending on the refractive index of the crystal and the sample (Smith, 1996), the frequency and the incident angle of the IR beam (Harrick, 1985). The penetration depth, d_p, is defined as the distance at which the amplitude of the evanescent wave has decreased to (1/e) or 37% of its original value at the surface (Smith, 1996). Figure 6.3 indicates that the strength of the evanescent wave decreases exponentially in intensity from the surface of the crystal.

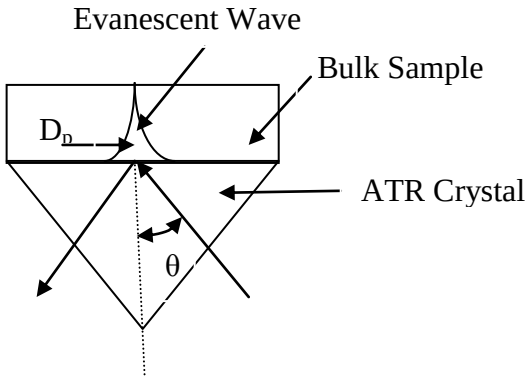

Figure 6.3: Schematic diagram of a single reflection ATR showing the radiation path through an infra-red transmitting crystal of high refractive index. The sampling area of the crystal makes contact with the sample. IR radiation from the spectrometer is deflected firstly via a mirror to the ATR crystal, in which it then undergoes total internal reflection, penetrating superficially into the sample, before exiting the crystal and being re-directed to the detector.

6.1.3 FTIR Technique and Protein Structure

6.1.3.1 Introduction

The FTIR technique measures the absorption peaks of various infrared wavelengths and, thus provides information about the chemical composition of various polymers, including amino acids from proteins. FTIR has been widely used in the research of wool and other hair fibres, which are natural protein fibres.

It has been suggested that at the molecular level, FTIR analysis can provide rapid and specific structural information of proteins and their composition (Panayiotou, 1999). Therefore, a brief introduction to protein structure is given before discussing the molecular structure in the sample. Proteins are linear biological polymers, for which the monomeric units are amino acids. In general, protein may have about twenty different amino acids, which are distinguished by the identity of the "R" group (side chains of different structure). The amino acids are bonded together to form a polymer by linking the amino group between one amino acid with the carboxylic acid group with adjacent amino acid to form an amide bond (Figure 6.4).

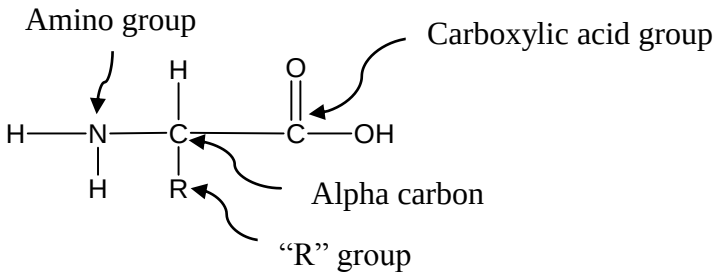

Figure 6.4: The structure of an amino acid: the basic building block for making proteins

In all proteins, the amide bond is the most abundant structure. The atoms take part in this bond lead to a number of vibrational bands that can be observed in the IR spectrum of proteins. Characteristic bands found in the infrared spectra of proteins and polypeptides include the Amide I, Amide II, and III bands, which absorb in the 1600-1700, 1500-1600, and 1200-1350 cm^{-1} regions, respectively. These regions arise from the amide bonds which are used to link the amino acids. The absorption associated

with the Amide I band is predominantly (80%) attributed to the C=O stretching mode of the amide functional group, while the remaining contribution (20%) arises from C-N stretching. The absorption associated with the Amide II band primarily originates from the bending vibrations of the N—H bond and C-N stretching vibrations. The amide III absorption is caused by coupling C-N stretching vibrations with N-H in plane bending vibrations, and the weak contributions from C-C and C=O stretching (Figure 6.5).

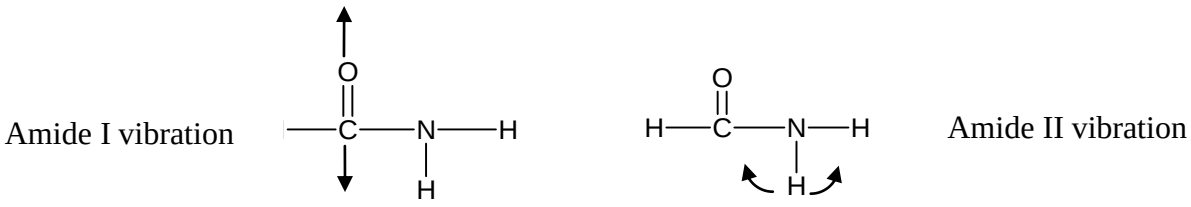

Figure 6.5: The vibrations mainly responsible for the Amide I and Amide II bands in the infrared spectra of proteins and polypeptides. The Amide I band is due to carbonyl stretching vibrations while the Amide II is due to NH bending vibrations.

Other vibration modes also appear in the Mid-IR range, include the amino acid side chains, such as C-H deformations (1471-1460 cm^{-1}), CH_2 and CH_3 deformations (1453-1443 cm^{-1} and 1411-1399 cm^{-1}), and the cystine oxide stretches, such as the asymmetric and symmetric cysteic acid (1171 cm^{-1} and 1040 cm^{-1}), symmetric cystine dioxide (1121 cm^{-1}), and cystine monoxide (1071 cm^{-1}) stretches.

6.1.3.2 FTIR Peak Assignments on Human Hair

6.1.3.2.1 Introduction

In FTIR-ATR spectroscopy, the beam of radiation penetrates the outer surface of the hair, which is the cuticle. The cuticle has a high concentration of cystine, along with other amino acids which are not always found in α-helical polypeptides. Oxidising agents such as alkaline hydrogen peroxide can break the disulfide bond and oxidise the sulphur atoms to sulphonate groups. Other oxidation products involve the addition of one or more oxygen atoms to the disulfide group, so that sulphoxide or sulfone linkages are also formed. These intermediates are not very stable. Once the hair keratin

is subject to hydrolysis, they are converted to cysteic acid. Since sulphonate, sulphoxide, and sulphone groups can be distinguished from one another by their infra-red absorption (Bellamy, 1958), with the application of FTIR spectroscopy the S-O vibrations can be analysed and cystine monoxide and cystine dioxide can be detected. Figure 6.6 summarises the structures of the most important sulphur-containing amino acids in bleached hair.

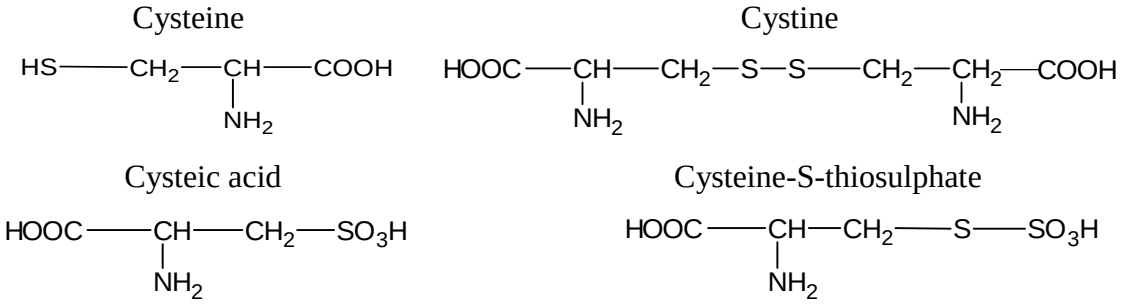

Figure 6.6: The structures of the most important sulphur-containing amino acids in bleached hair

6.1.3.2.2 Literature Review

Methods capable of measuring oxidative hair damage are of great interest to the hair care industry. FTIR spectroscopy had been applied to study the effects of oxidative treatment on human hair fibres for a long time (Robbins, 1967, Strasheim, 1961, Shah, 1968, Alter, 1969). Brenner et al. (1985) investigated untreated and bleached hair fibres by using FTIR spectroscopy with a diamond anvil cell. For the bleached hair fibres, they discovered the presence of a peak at 1044 cm^{-1}, which was attributed to the symmetric stretch of cysteic acid. This peak was considered to discriminate between treated and untreated hair samples. Ohnishi et al. (1993) furthered this study by analysing permanently waved hair fibres. In his investigation, the concentration of cysteic acid and random damage patterns increased along the hair length.

Alter et al (1969) mention that new peaks appear at 1175 and 1040 cm^{-1} for bleached hair (treated with H_2O_2) for various oxidising times. These peaks correspond to sulphonates and cysteic acid, respectively. The assignment of the bands as sulfonate linkages from cysteic acid residues seems well established (Colthup, 1964, Bellamy, 1975). Cysteic acid residues arise from disulfide bond fission of cystine, which is the most abundant amino acid in hair (Robbins, 1994). Cystine dioxide peaks (1220 and

1310 cm^{-1}) and increased sulphonates intensity are also observed at 1175 cm^{-1} from oxidation of cysteine. These peaks show an increase in intensity after successive bleaching treatment, resulting in the overall shape of the bleached hair spectrum is significantly different from the untreated hair spectrum.

Kirschenbaum et al (2000) examined some structural information changes for treated hair samples. Their results showed not only the disulphide bond breakage, but the peptide backbone was also affected by chemical treatments. The damaged hair spectrum indicated an increased intensities of C-H peaks, which was attributed to the structural transformation of α−helices to β−sheets.

Previous FT-IR spectroscopic studies have assigned several absorbance frequencies to particular component amino acids (Carr, 1993, Lewis, 1993, Fredline, 1997, Pielesz, 2000). It was shown that hair samples including the untreated sample show cystine derivatives. IR peaks at 1040, 1075, 1175, and 1229 cm^{-1} correspond to cystine oxidation products, but the other peaks at 1241, 1454, 1550, and 1655 cm^{-1} correspond to the amino acids. Table 6.2 shows the peak assignments of cystine derivatives and amino acids.

Table 6.2: The Peak Assignments for Cystine Derivatives and Amino Acids in the mid-IR Spectrum

Wavenumbers (cm^{-1})	Assignment
1040	Sulphonate, S-O sym, stretch
1075	Cystine monoxide (R-SO-S-R)
1175	Sulphonate, S-O asym, stretch
1229	Cystine dioxide ($R-SO_2-S-R$)
1241	Amide III (N-H stretch)
1454	CH_2
1550	AmideII (C-N stretch)
1655	Amide I (C=O stretch)
2885	CH
2960	CH
3315	NH (Primary amine)
3550	OH (H_2O)

6.1.3.3 FTIR Investigation on Human Hair

Cystine is an important amino acid in hair keratin fibres, as its disulphide bond plays an important role in determining the mechanical and physical properties of the fibre. It has been confirmed that IR spectroscopy can detect the oxidation products of cystine, i.e. cystine monoxide, cystine dioxide, and cysteic acid (Hilterhaus-Bong, 1987), without directly supplying spatially resolved information.

Other FTIR studies on hair include analysing the hydrogen bonds around hair protein to understand the mechanism of improving the durability of hair-setting with acid and ethanol treatment (Itou, 2006) and also studying isolated melanins from fair, red and dark hair (Bilinska, 1991). IR has also been used to study other keratin fibre, such as horse hair (Lyman, 2001), plant cutin (Benítez, 2004) and human skin, nails, and lipids (Gniadecka, 1998).

6.2 Objectives

The IR- spectrum of bleached hair is different from untreated hair. Since cysteic acid is the most abundant amino acid in hair, its oxidation can be studied by FTIR spectroscopy. Reflectance and transmission are two modes of IR spectroscopic measurements. Reflectance mode measurements are easier to obtain; however, variations in the surface properties of the sample may influence calibrations. Transmission mode may be less susceptible to surface properties, but the amount of light penetrating the sample is a problem (Schaare, 2000). The objective of this research was to combine attenuated reflectance and transmission modes of FTIR spectroscopy for detecting oxidation effect of cysteic acid caused by three types of bleaching treatments. An ATR diamond cell accessory and KBr pellets were employed in this investigation.

6.3 Experimental Work

The experimental work for the FTIR investigation includes sample preparations, spectral processing and data analysis.

6.3.1 Sample Preparation

All hair samples were randomly collected, and the virgin hairs are considered as those, which had never been subjected to chemical damage.

6.3.1.1 ATR Sample Preparation

As describe in Section 6.1.2.2.1, FTIR-ATR requires no sample preparation. The hair fibre spectra were collected and recorded on a Thermo Nicolet 5700 FTIR Spectrometer for an angle of incidence of 45° with a Diamond-ATR Smart Orbit Accessory to provide information about the surface of the hair fibres in a spectral range between 4000 - 400 cm^{-1}. The background spectrum was obtained for air (the crystal in contact with no sample) before collecting the sample spectrum. 64 sample scans were added at a resolution of 4 cm^{-1} to produce infrared spectrum for each sample. Since hair is a heterogeneous material, its physical and morphological properties may vary greatly, even thought hair may be collected from the same head. As a result, the area from the tip at 2cm, 5cm, 8cm, 11cm and 14cm (commercial bleaching only) was twisted tightly and measured on the same hair tress to examine the uniformity of bleaching effects. Three tresses of each treatment were measured to yield reproducible oxidation values. All spectrum analyses were carried out using the OMNIC software (Nicolet).

In the spectral sampling process, the solid material is placed on the cleaned diamond crystal surface after the background spectrum is collected, and then sufficient consistent pressure is applied using the pressure tower to record the sample spectrum. Any inadequate contact between sample and pressure tower could cause a narrow

transmission range, noisy spectra and poor reproducibility. Once the sample spectrum had been recorded, the spectrum information is collected using OMNIC 7.2 spectral software program (as .SPA files).

A. Calculation of the penetration depth

Hair diameter is a variable parameter that affects the result of FTIR-ATR. Oxidative attack is likely to be concentrated in the cuticle and outer cortical cells of the human hair. This is because of the impervious nature of the cuticle scales and of cystine being more concentrated in the cuticle than in the cortex. The penetration depth (d_p) of the infrared beam into the hair sample was calculated as:

$$D_P = \lambda / 2\pi\, n_1 \{\sin^2\theta - (n_2/n_1)^2\}^{1/2} \qquad (6.2)$$

The refractive index of hair (η_{hair}) is reported to be 1.555 (Baddiel, 1968). The depth of penetration and the total number of reflections along the crystal can be controlled either by varying the angle of incidence or by selection of crystals. Different crystals have different refractive indices. When the Diamond/ZnSe crystal (n_1=2.4) is used, the FTIR-ATR penetration depth for a human hair fibre with a refractive index of 1.5 at 1000cm^{-1} (cysteic acid band, 1042cm^{-1}), is approximately 2.0μm when the incidence angle is 45°. As described in Chapter 1, each cuticle cell is approximately 0.5μm thick and the overall cuticle layer thickness varies between 5-10 layers (Robbins, 2002). Hence, the average thickness of the cuticle layer for individuals is believed to be around 3μm, which is much thicker than the penetration depth of hair (2μm) at 1000cm^{-1}. Thus the IR beam is not able to penetrate into the cortex, and FTIR-ATR mainly focuses on the cuticle (surface) part of the hair fibres.

6.3.1.2 KBr Pellet preparation

Three batches of hair samples from each treatment were mixed and cut to a length of approximately 2mm snippets, dried at 105^{o}C for one hour to remove the moisture. A bottle of sealed KBr powder was left in a 90^o oven overnight before pellet preparation. After removal from the oven, 200 mg dried KBr was immediately weighed and ground

to a fine powder. About 6-7 mg of hair snippets was added and mixed well with KBr using a mortar and pestle by hand. This mixture was then transferred to a Graseby Specac die that has a barrel diameter of 15 mm. Using a Carver press at a pressure of 10 kbar under vacuum for 2-3min a clear glassy disk was formed of about 4.5 mm thickness (shown in Figure 6.7). The pellet is placed in a transmission holder to record the spectrum.

Figure 6.7: KBr pellets of virgin and bleached hair and a pure KBr crystal

FT-IR spectra of hair samples, which are in a pellet form, were acquired with 5700 FT-IR spectrometer of Thermo Nicolet equipped with KBr optics and deuterated triglycine sulphate (DTGS) detector. The FT-IR data analysis was conducted using the infrared spectra analysis software package OMNIC. All recorded spectra were average over 32 scans in the mid Infrared (IR) region of 4000-400 cm^{-1} by optimising the resolution of the instrument at 4 cm^{-1}. A background spectrum was obtained as a reference through a KBr pellet without fibres. The sample spectrum was obtained for the pellet containing fibre snippets. Each time before obtaining the spectrum of a sample, a fresh background spectrum from a KBr pellet was recorded. All the spectra were recorded four times at different points to obtain reproducible results. The transmittance spectra were then converted to absorbance spectra for further investigation.

6.3.2 Spectral Processing

In order to study the influence of different acquisition techniques (transmission and attenuated total reflectance) for the quantification of oxidative hair damage incurred by bleaching, different mathematical procedures (normalisation, second derivatives) are applied to enhance peak resolution and to reduce the signal-to-noise ratio.

6.3.2.1 Normalisation

All of OMNIC spectral (.SPA) files from ATR and Transmission measurements (KBr) were imported and save as a .CSV file before transferring the data to a Microsoft Excel 2007 spreadsheet. In order to facilitate spectral comparison, normalisations of keratin hair spectra were carried out based on the $\delta(CH_2)$ stretching band (ca. 1452cm^{-1}). The reason for choosing this wavelength as an internal standard is that this molecular bond is associated with the amino acid side chains thus is not affected by cosmetic chemical treatment, which otherwise results in peptide backbone conformational changes, e.g. peroxides or thioglycolic acid or natural weathering processes, such as water or carbon dioxide (Church, 1997, Kuzuhara, 2005). It has been confirmed that the intensity of this band is consistent from sample to sample (Church, 1997).

6.3.2.2 Derivative Spectroscopy

Since Fourier transform infrared spectrum is a mathematical function, its derivative can be calculated (Smith, 1996). The derivative spectroscopy describes the rate of change of a signal recorded as a function of the wavelength or frequency (Bridge, 1987). For a given absorbance curve, the first derivative ($dA/d\lambda$) is the gradient of the original spectrum at each wavelength. The first derivative of a spectrum is called a first order derivatives, the derivative of the first derivative is called a second order derivative and so on. The simplest way to calculate a spectral derivative is the "point difference" method, where the difference in Y values between successive data points is calculated, then plotted versus wavenumber (Smith, 1996). There are other ways of calculating derivatives, depending on the software package used.

In a raw spectrum, the individual vibration peaks are difficult to identity as a consequence of band broadening, thus, derivative spectroscopy is used to resolve overlapping absorption peaks.

It can be seen that in the derivative spectroscopy the odd number derivatives show a shift in the wavenumber of the peak, and the even numbered derivatives show the main

peak at the original wavelength of maximum absorption (Joy, 1991). Therefore it is more practical to use the even numbered derivatives to interpret the spectra. However, due to the spectra become increasingly complicated as the derivative order increases (Joy, 1991), it becomes feasible to utilize the second order derivative to enhance the resolution of spectrum for the further deconvolution or curve fitting analysis, since the second order derivative method can at high resolution acquire the maximum information from each spectrum, while minimising the background noise.

For the derivative analysis of FTIR spectra, the first step is to choose a part of the spectrum containing bands of interest. The raw spectra (after normalisation) between 980 -1140 cm^{-1} was imported into Peakfit peak separation and analysis software (version 1.2), and were converted into second derivatives spectra by using the Gaussian deconvolution derivative method. As the PeakFit software decides the peak position based on the second derivative, and peak fitting is followed for the closest match to the original spectra, the data obtained by PeakFit seem to correspond reliably to each real peak. The second derivative spectra were reduced to minimum signal-to-noise ratio spectra using an automatic smoothing function, and the achieved spectra were then imported to a Microsoft Excel 2007 spreadsheet for further investigation.

Also, the possibility of deconvolution of IR spectra was explored using second derivative and PeakFit deconvolution software. This method improved peak selection and peak fitting, however, the results depend on the values of the deconvolution parameters, and it requires appropriate parameter settings.

6.4 Result and Discussion

6.4.1 FTIR spectrum of Human Hair

The vibrational spectrum of human hair keratin, particularly between 1750-900 cm^{-1}, is very complex. This is due to the protein-polypeptide structure in hair keratin. Three molecular structures that each generates characteristic vibrational absorption bands can be identified within this fingerprint region:

(a) The peptide bond (primary protein structure). Caused by a condensation reaction between the carboxylic acid and amine group of adjacent amino acids. It is the most fundamental element within the keratin protein and yields the Amide I, II, and III IR spectral bands.

(b) The secondary protein structure. Built up around the C-C skeletal stretching backbone of all keratin proteins, it can exhibit one to three sensitive structure conformations, those are the α-helical, β-sheet and random coil or amorphous structures which are directly related to the Amide region.

(c) The amino acid side chains (R groups). The C-H vibrations originating from the ─CH, ─CH_2 and ─CH_3 of the aliphatic and aromatic rings of phenylalanine, tyrosine, tryptophan and significant vibrations of the oxidative intermediates from the amino acid cystine (i.e. S=O, SO_2, SO_3^-, and –S–SO_3^-)

The frequencies and peak assignments for virgin human hair in ATR mode and in transmission are compared in Figures 6.8 and 6.9. They show that two hair spectra exhibit many similarities in their characteristic bands, such as amide I, II, III, however some variations in both the band positions and absorbance intensities and some impurities in the transmission spectrum are observed. The impurities are represented by the noise on the curve in the amide I region in Figure 6.8. They are thought to be associated with water, whose vibration band is near 1650 cm^{-1}. Because of the hydrophilic nature of KBr, moisture in the air is easily absorbed by the KBr during sample preparation. As a result, the 1240 to 1750 cm^{-1} region of the spectrum is excluded for further analysis. However, in order to make the spectrum of FTIR-ATR and transmission mode comparable, a normalization of spectrum has to be applied because of the systematic differences of the spectra.

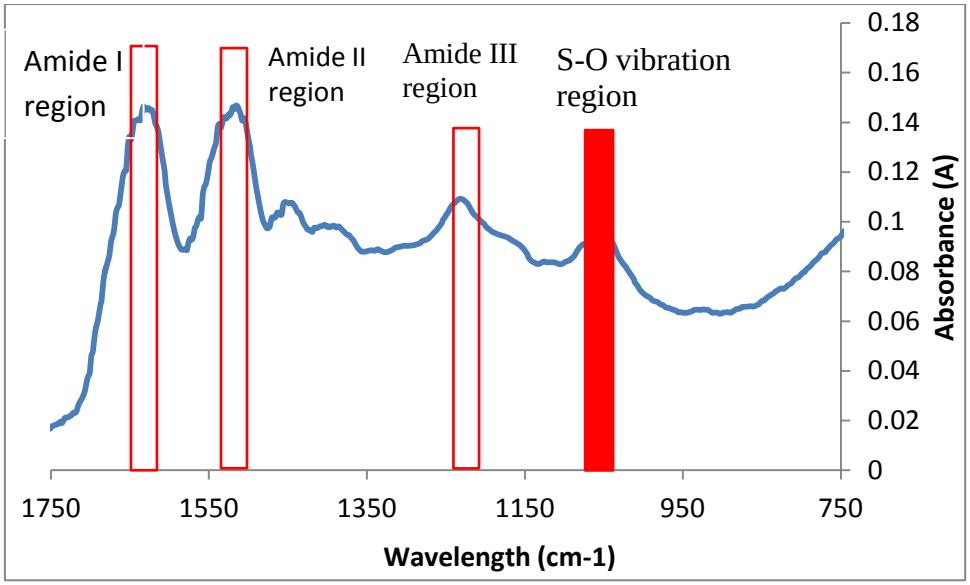

Figure 6.8: The raw FTIR-ATR spectrum of an untreated hair sample. Spectral assignments of some bands are made. The S-O vibration (represented as a solid bar on the graph) is of particular interest in this research.

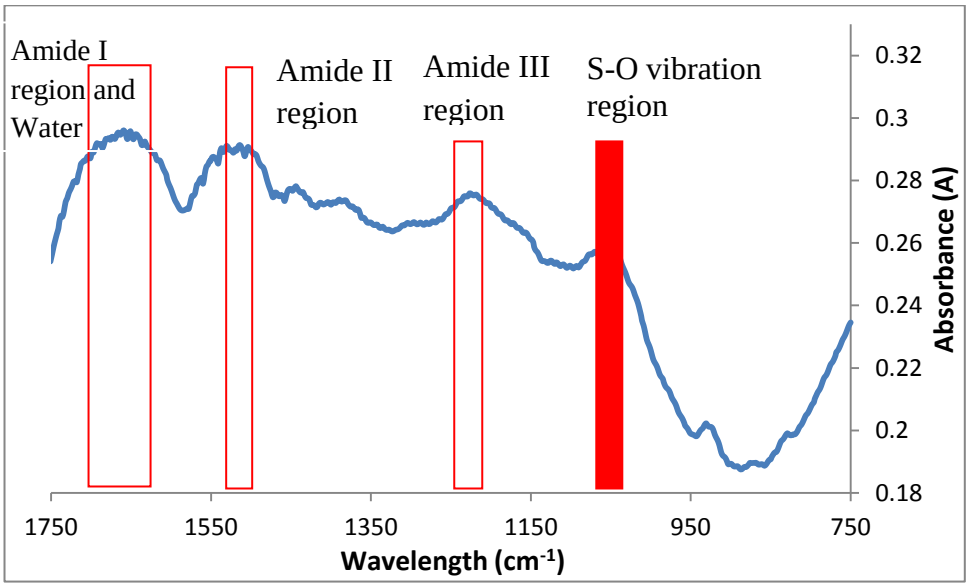

Figure 6.9: The raw FTIR-KBr spectrum of an untreated hair sample. Some bands are assigned. The S-O vibration (represented as a solid bar on the graph) is of particular interest in this research.

6.4.1.1 Assignment of Absorption Bands

As discussed in Section 6.4.1, the raw spectrum of α-keratin between 1750-900 cm^{-1} is extremely complex, as there are many overlapping and broad bands. The application of second derivative spectra resolves the complexity of keratin raw spectrum in Figures 6.10 and 6.11. However some peaks in a second derivative spectrum are too subtle to

be detected. A peak in the second derivative located reasonably near to a known peak wavenumber was considered as being a representative peak of the IR spectrum.

IR absorptions associated with cystine oxidation occur between 1200─1000 cm^{-1}. It is obvious that both resolution-enhanced spectra in Figures 6.10 and 6.11 represent well resolved peaks. Previous band assignments identified the symmetric and asymmetric sulfonate S =O stretching vibrations at 1042 cm^{-1} and 1175 cm^{-1} (Weston, 1955, Strasheim, 1961, Robbins, 1967, Alter, 1969), while we found these vibrations at 1039 cm^{-1} and 1171cm^{-1} in Figure 6.10 and at 1038 cm^{-1} and 1174 cm^{-1} in Figure 6.11.

The band at approximately 1039 cm^{-1} has been assigned to a symmetric S=O stretching vibration of sulfonate or sulfonic acid groups of cysteic acid residues, and therefore its absorbance is a measure of the $-SO_3^-$ content of hair. In addition, another weaker anti-symmetric cysteic acid band is shown at 1173 cm^{-1}, which is actually a shoulder of the Amide III band. Since cystic acid is the most abundant amino acid found in hair, followed by monoxide (1076 cm^{-1}), the absorbance peak heights of cysteic acid **(**1039 cm^{-1}) were measured and compared in order to measure the chemical changes arising from bleaching of hair.

Other oxidative intermediate products also appear as oxidation bands in this region, such as cystine monoxide (S-S=O) at 1076 cm^{-1}, cystine dioxide ($S=O_2$) at 1123 cm^{-1} and cysteine-S-thiosulphate (Brunte Salt) at 1018 cm^{-1}. Previous researchers reported bands near 1190, 1022 cm^{-1} for methyl and ethylthiosulfate ions, which they assigned to the S=O asymmetric and symmetric stretch vibrations of the thiosulfate ions, respectively (Simon, 1961).

In addition, the differences between ATR and transmission spectra in spectral appearance and intensity of peaks depend on their sampling properties. Since transmission analyses the internal region of hair, while FTIR-ATR samples the near-surface chemistry only. Thus, with the application of these two methods, a comprehensive result for oxidation of cysteine from the internal regions to the surface of hair and for the three types of bleaching treatments is achieved.

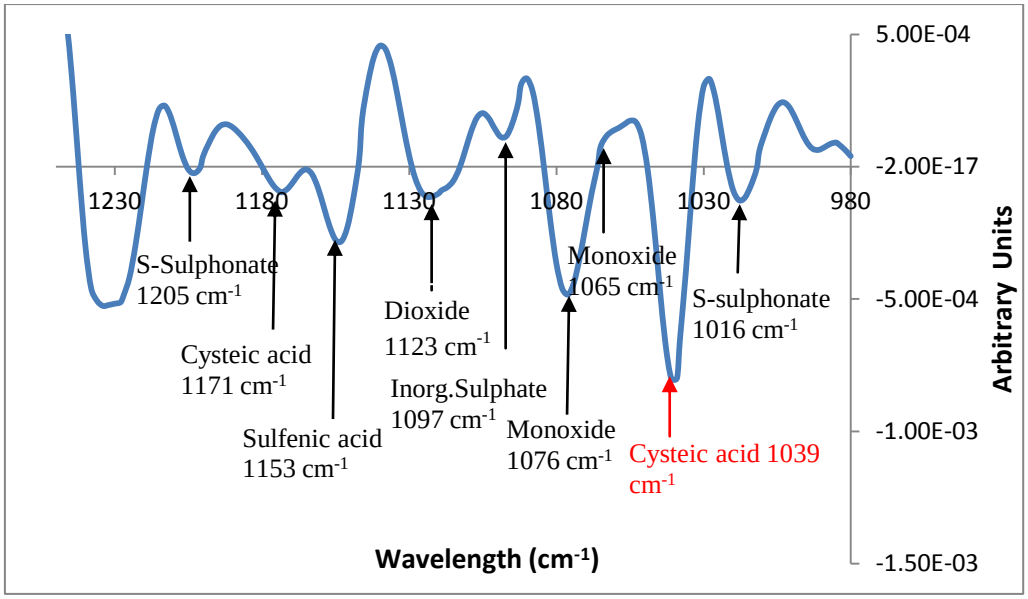

Figure 6.10: Second derivative analysis of untreated hair (Batch I, 8cm) in the ATR mode in the region 1240 - 980 cm^{-1}, which resolves the overlapping cysteic acid, cysteine-S-sulphonate and cysteine monoxide peaks. Note the inversion of the peak maxima with respect to the normal spectra (original data in absorption mode).

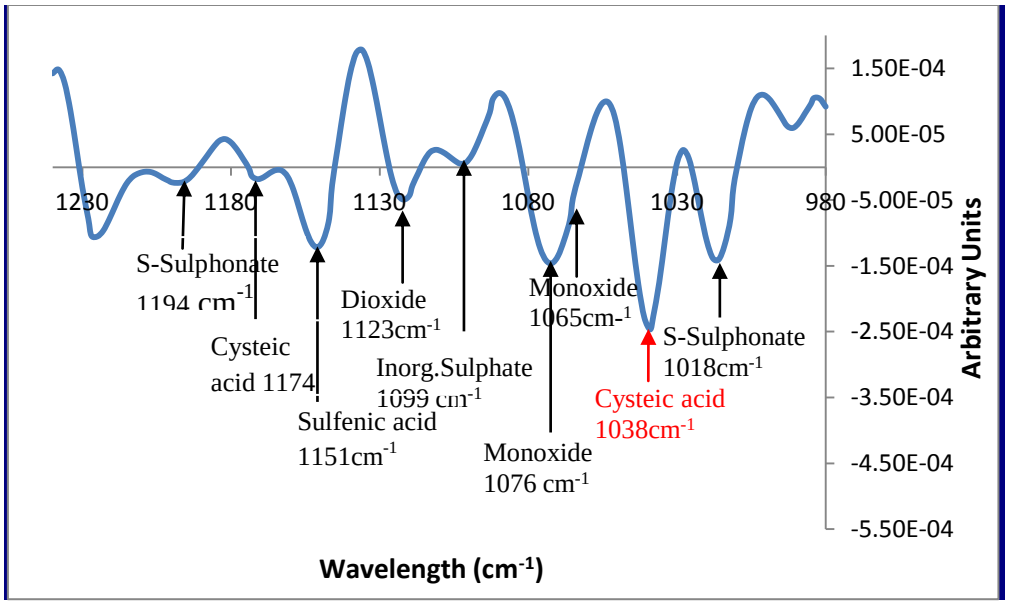

Figure 6.11: Second derivative analysis of untreated hair (Batch I) in the transmission mode in the region 1240 - 980 cm^{-1}, which resolves the overlapping cysteic acid, cysteine-S-sulphonate and cysteine monoxide peaks. Note the inversion of the peak maxima with respect to the normal spectra (original data in absorption mode).

6.4.2 Comparison of FTIR Spectra of Untreated and Bleached Human Hair

The cuticle cells, which protect the inner layers of hair, have a larger content of cystine than the cortex (Robinson, 1976, Robbins, 2002), thus oxidative attack to the hair fibre is likely to occur firstly in the cuticle and there mainly to the exocuticle, which is very rich in cystine. For this reason, FTIR-ATR was firstly employed to investigate the oxidation damage of the surface or near-surface regions of human hair.

6.4.2.1 ATR Technique

It has been discussed that in order to allow comparison of changes in cysteic acid peak intensity after oxidation, all raw spectra have to be normalized against the peak intensity of the C-H stretch band at 1452 cm^{-1}. The maximum oxidation duration (4h) was taken as an example to illustrate the impact of oxidation on the cysteic acid yielded by various bleaching conditions.

Figure 6.12 shows the relative peak heights of ATR–FTIR spectra that were standardized against the peak heights at 1452 cm^{-1}. The differences in FTIR–spectra between untreated and bleached hairs for different agents are shown in the range of 1300 - 900 cm^{-1}, where the cystine oxidation bands are located. The intense symmetric cysteic acid band is located at 1040 cm^{-1}. A similar phenomenon is also observed with the weaker anti-symmetric cysteic acid band at 1172 cm^{-1}. Commercial persulphate bleach (4h) has the strongest effect on both cysteic acid bands, suggesting that the commercial persulphate bleach has an extensive oxidation influence, followed by 9% H_2O_2 commercial bleach, 6% H_2O_2 and then virgin hair.

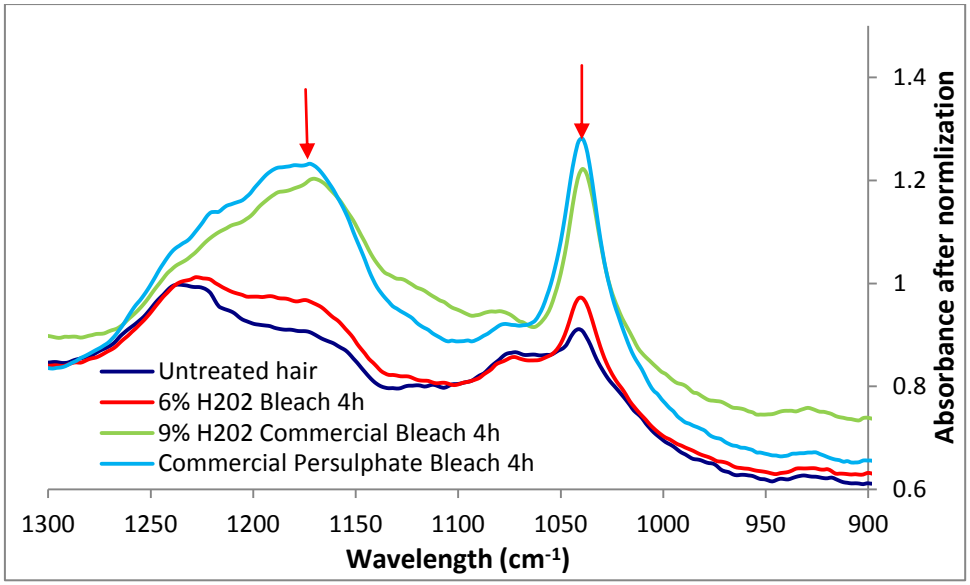

Figure 6.12: FTIR-ATR spectra of untreated and 3 types of 4h treated fibers at 1300 – 900cm^{-1}, after normalization by against the peak intensity of the C-H stretch at 1452 cm^{-1}**.** The cysteic acid peak is clearly visible at 1040cm^{-1} and 1172 cm^{-1} for bleached hair, (marked by the red arrows). Each curve is randomly chosen from one of three tresses' results.

The ATR second derivative spectra of three types of bleached hairs are compared in Figure 6.13 with untreated hair to demonstrate the differences in cysteic acid formation after 4h bleaching treatment. In principle, the second derivative contains three features corresponding to each absorbance peak in the original spectrum, two pointing upward and one pointing down. The valley in the second derivative corresponds to the wavenumber of maximum absorbance of a band in the original spectrum. Since the valley depth of the second derivative spectrum is a negative value, the absolute valley depth is employed in the following discussion for the better understanding. The cysteic acid peak is clearly visible as a valley at 1040cm^{-1} for the bleached fibre, confirming the oxidation of disulphide.

Commercially persulphate bleached hair (4h) exhibits the most intensive valley depth of cysteic acid, due to the aggressive oxidizing agent, persulfate, followed by 9% H_2O_2 commercial bleached (4h) hair, 6% H_2O_2 bleached (4h) hair and virgin hair. The differences between the valley depths are associated with the fission of amino acid chains by different damage extents of oxidation treatments, causing different amount of cystine to be oxidised to cysteic acid.

However, a slight shift in the valley position for cysteic acid after second derivative is observed for the bleached hair. The valley moves from the expected 1042 to 1037cm^{-1}. This is attributed to a change in disulphide conformation as a result of partial disulphide bond rupture (Hogg, 1994).

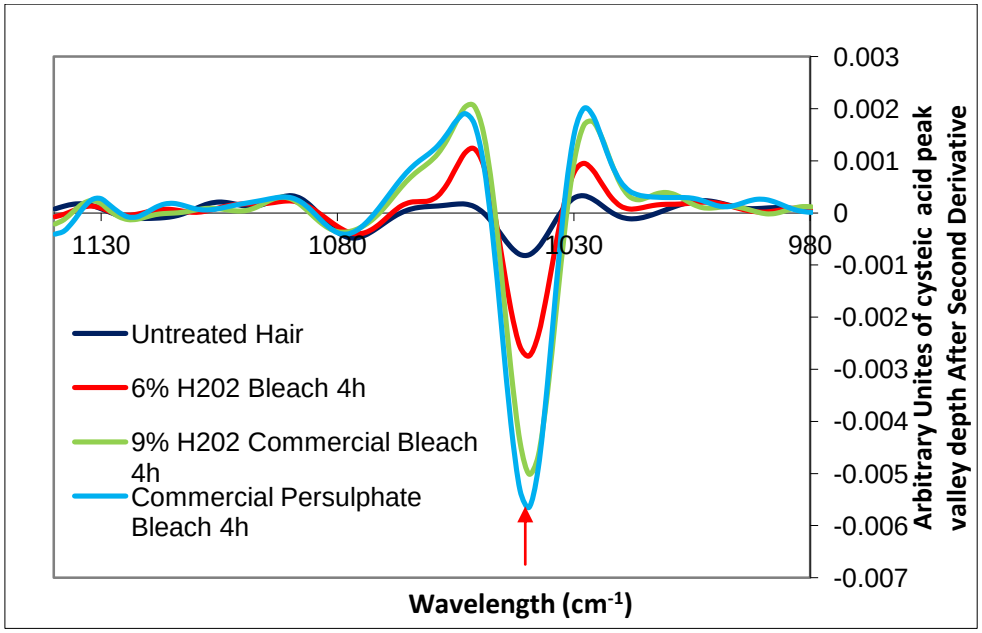

Figure 6.13: FTIR-ATR spectrum 2nd derivative of untreated and 3 types of 4h treated fibers at 1300 – 900cm^{-1}. Cysteic acid becomes clearly visible as a valley at 1040cm^{-1} for the bleached fiber, (marked by the red arrow). Each curve is randomly chosen from one of three tresses' results.

6.4.2.1.1 Oxidation Effects along the Fibre Length

Due to the heterogeneity of hair fibre, different parts of hair are subject to damage differently. In addition, hair also undergoes natural oxidative degradation processes (weathering) due to its exposure to sun and atmospheric oxygen. To explore further the variability of the hair samples after the three types of bleaches, five measurement points from the root end of a tress at 2cm, 5cm, 8cm, 11cm and 14cm (commercial bleaching only) are chosen. The corresponding results for the absolute valley depth for cysteic acid in the second derivative spectra are presented in Tables 6.2 – 6.10.

Tables 6.2 – 6.10 demonstrate the changes in terms of intensity of cysteic acid absolute valley depth (second derivative) through the extensive treatment time for bleached hairs. All the bleached hairs show the progressively increased absolute valley depths

for cysteic acid. It is obvious that with longer bleaching time, higher intensities of cysteic acid are observed. Taking a 5cm measurement from the root end, as an example, the intensity of 6% H_2O_2 bleached hair for cysteic acid had a gradual increase with the bleaching time, from 1.34 at 0.5h to 2.34 at 2h, and to 2.7 at 3h, and to 2.89 at 4h. Furthermore, 9% H_2O_2 commercial and commercial persulphate bleached hair increased from 1.97 and 2.32 at 0.5h, to 5.45 and 4.62 at 2h, and to 5.39 and 5.56 at 3h, and to 5.61 and 5.81 at 4h, respectively.

In addition, the higher peroxide concentration and the stronger oxidizing agent, the higher the intensities of cysteic acid will be. The absolute valley depth for cysteic acid intensity at the tip part (11cm) increases from 1.37 to 2.28, when comparing 6% H_2O_2 bleach with persulphate bleach at 0.5h in Table 6.3. Similarly 4h commercial persulphate bleached hairs yielded a bigger absolute valley depth of cysteic acid 5.66 at the tip part (11cm), while the 6% H_2O_2 bleach has a cysteic acid intensity of 2.64 in Table 6.10. These results are consistent with the findings that the tip of hair is more damaged than the root end (Wolfram, 1971, Robinson, 1976, Tolgyesi, 1983), hence they are more susceptible to oxidative attack.

Table 6.2: Absolute valley depth for cysteic acid of five measurement points of virgin hair for the second derivative

Hair Types	2cm	5cm	8cm	11cm	14cm
Batch I	0.72	0.8	0.76	0.87	
Batch II	0.8	0.73	0.94	1.02	1.05

Table 6.3: Absolute valley depth for cysteic acid of five measurement points of three bleached hairs for the second derivative at the bleaching time of 0.5h

	2cm	5cm	8cm	11cm	14cm
6% H_20_2	1.55	***1.34***	1.22	***1.37***	
9% H_2O_2 Commercial	1.97	1.97	2.1	2.08	
Commercial Persulphate	1.98	2.32	2.46	***2.28***	2.53

Table 6.4: Absolute valley depth for cysteic acid of five measurement points of three bleached hairs for the second derivative at the bleaching time of 1h

	2cm	5cm	8cm	11cm	14cm
6% H_20_2	1.88	1.89	1.69	1.91	
9% H_2O_2 Commercial	2.93	2.99	3.14	3.41	
Commercial Persulphate	3.15	3.46	3.06	3.56	3.67

Table 6.5: Absolute valley depth for cysteic acid of five measurement points of three bleached hairs for the second derivative at the bleaching time of 1.5h

	2cm	5cm	8cm	11cm	14cm
6% H_20_2	2.08	2.02	2.02	2.22	
9% H_2O_2 Commercial	4.35	4.53	4.57	4.77	
Commercial Persulphate	3.52	4.01	3.87	3.99	3.87

Table 6.6: Absolute valley depth for cysteic acid of five measurement points of three bleached hairs for the second derivative at the bleaching time of 2h

	2cm	5cm	8cm	11cm	14cm
6% H_20_2	2.18	***2.34***	2.39	2.43	
9% H_2O_2 Commercial	5.34	5.45	5.39	5	
Commercial Persulphate	4.32	4.62	4.74	4.76	4.76

Table 6.7: Absolute valley depth for cysteic acid of five measurement points of three bleached hairs for the second derivative at the bleaching time of 2.5h

	2cm	5cm	8cm	11cm	14cm
6% H_20_2	2.48	2.4	2.39	2.36	
9% H_2O_2 Commercial	5.23	5.14	5.08	5.16	
Commercial Persulphate	4.72	4.89	4.91	4.95	4.92

Table 6.8: Absolute valley depth for cysteic acid of five measurement points of three bleached hairs for the second derivative at the bleaching time of 3h

	2cm	5cm	8cm	11cm	14cm
6% H_20_2	2.7	***2.7***	2.41	2.44	
9% H_2O_2 Commercial	5.66	5.39	5.21	5.05	
Commercial Persulphate	5.4	5.56	5.29	5.58	5.45

Table 6.9: Absolute valley depth for cysteic acid of five measurement points of three bleached hairs for the second derivative at the bleaching time of 3.5h

	2cm	5cm	8cm	11cm	14cm
6% H_20_2	2.72	2.44	2.6	2.64	
9% H_2O_2 Commercial	6.17	5.57	5.79	5.48	
Commercial Persulphate	5.38	5.67	5.35	5.45	5.86

Table 6.10: Absolute valley depth for cysteic acid of five measurement points of three bleached hairs for the second derivative at the bleaching time of 4h

	2cm	5cm	8cm	11cm	14cm
6% H_20_2	3.02	***2.89***	2.86	***2.64***	
9% H_2O_2 Commercial	5.32	5.61	4.96	5.23	
Commercial Persulphate	5.36	5.81	5.6	***5.66***	5.27

Figures 6.14- 6.16 investigate the oxidation effects on bleached hair sample at the shortest oxidation time (0.5h), for the middle stage of the oxidation times (2h) and for the maximum oxidation time (4h). Since the valley depth of cysteic acid of commercial persulphate bleached hair is always higher than that of the 6% H_2O_2 oxidation treatment, indicates that more cystine is oxidised to cysteic acid. This further confirms that commercially persulphate bleach has a stronger oxidation impact on the keratin than 6% H_2O bleach.

It was also found for the three types of bleached hairs that the differences of valley depth for cysteic acid between the different parts of the hair fibres become smaller with longer bleaching time. This shows that there is a uniform and homogenous bleaching effect on the hair length from tip to root. Extensive oxidation treatment thus reduces the variability of hair properties along length. However, small differences in absorption intensities for each tress of hair still exist. This is likely because the pressure applied to the hair fibres by the pressure tower of the ATR cell is different every time.

Although different points on hair fibres have different amounts of oxidised cystine, the oxidation effect yielded by different oxidizing agents is still our main interest. Therefore, all of the valley depths results were combined to undertake an overall oxidation damage comparison.

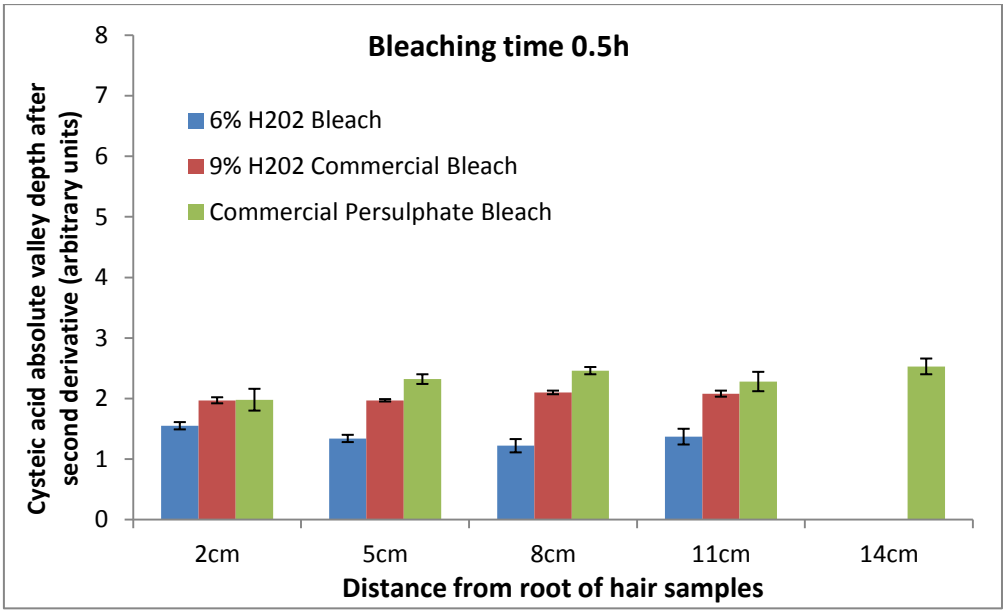

Figure 6.14: Cysteic acid absolute valley depth for bleached hair measured using FTIR-ATR after bleaching time of 0.5h. The graph shows the mean and the standard error for the cysteic acid absolute valley depth at 5 different measurements points for three bleached hairs. The absolute valley depth is expressed in arbitrary units.

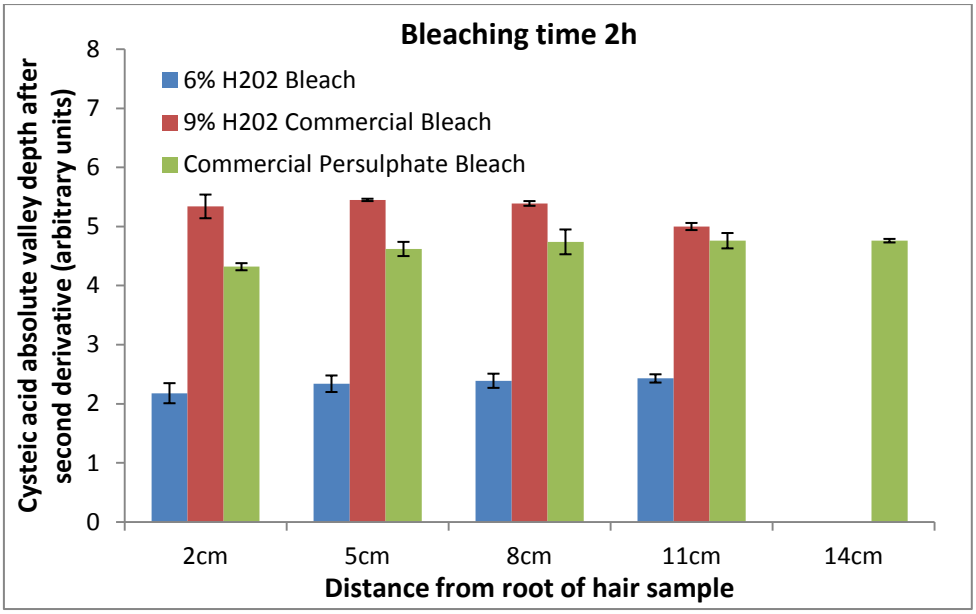

Figure 6.15: Cysteic acid absolute valley depth for bleached hair measured using FTIR-ATR after bleaching time of 2h. The graph shows the mean and the standard error for the cysteic acid absolute valley depth at 5 different measurements points for three bleached hairs. The absolute valley depth is expressed in arbitrary units.

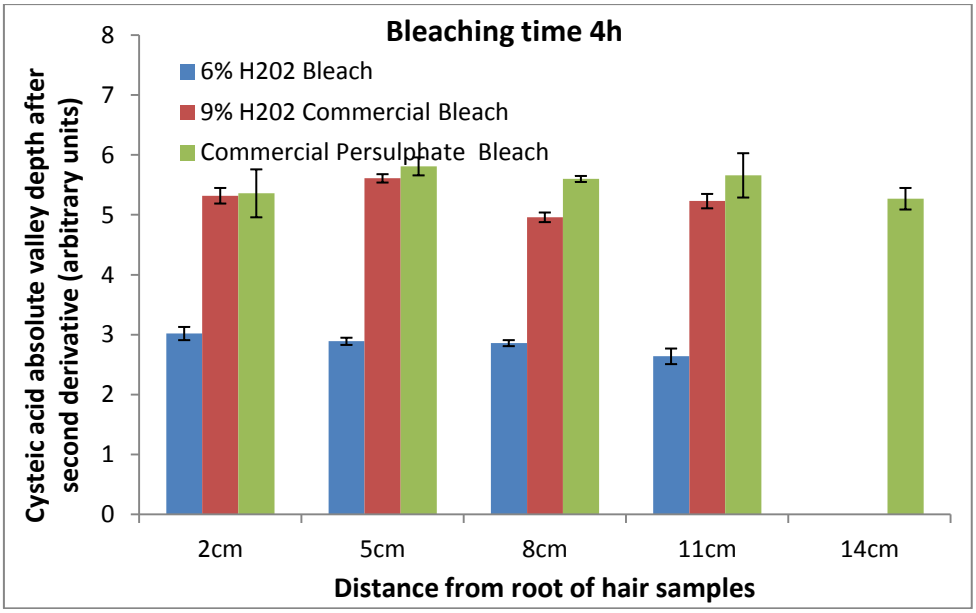

Figure 6.16: Cysteic acid absolute valley depth for bleached hair measured using FTIR-ATR after bleaching time of 4h. The graph shows the mean and the standard error for the cysteic acid absolute valley depth at 5 different measurements points for three bleached hairs. The absolute valley depth is expressed in arbitrary units.

6.4.2.1.2 Effects of the Oxidizing Agents

As has been discussed in Section 6.3.1.2, it is sensible to apply spectral averaging prior to peak height calculation, since hair is a highly heterogeneous material (Signori, 1997). A selected region of a spectrum is normalized against the intensity of CH_2 at 1452cm^{-1}. The absorbance value of the absolute valley depth of cysteic acid is calculated and compared to carry out quantitative analysis (using arbitrary units of measurement) after second derivative analysis. After combining all of the results from each measured point on a hair tress, Figure 6.17 is achieved according to the procedure described above to demonstrate the effects of different oxidizing agents.

In Figure 6.16, commercial persulphate bleach and 9% H_2O_2 commercial bleach have a stronger oxidation effect on cystine than 6% H_2O_2 bleach, which only has a moderate oxidation influence. This observation is in a good agreement with the colour measurements described in Chapter 4. Although all three oxidation treatments demonstrate a consistent, increasing tendency towards equilibrium, 6% H_2O_2 bleach increases steadily for the whole treatment time, whereas values for both 9% H_2O_2 commercial bleach and commercial persulphate bleach increase rapidly at the beginning until they reach an equilibrium level. For 9% H_2O_2 commercial bleach the equilibrium is reached at 2h and for commercial persulphate bleach is reached at 3.5h. These two commercial bleach agents are formulated differently. 9% H_2O_2 commercial bleach is in the form of a creamy solution, whereas commercial persulphate bleach is prepared as a paste. Since the ATR technique is used to examine the surface of the hair samples, the creamy solution facilitates the penetration of further layers of the cuticle or of the cortex compared to the paste state of the commercial persulphate bleach. Thus, 9% H_2O_2 commercial bleach reaches its maximum value for cysteic acid intensity earlier than the commercial persulphate bleach.

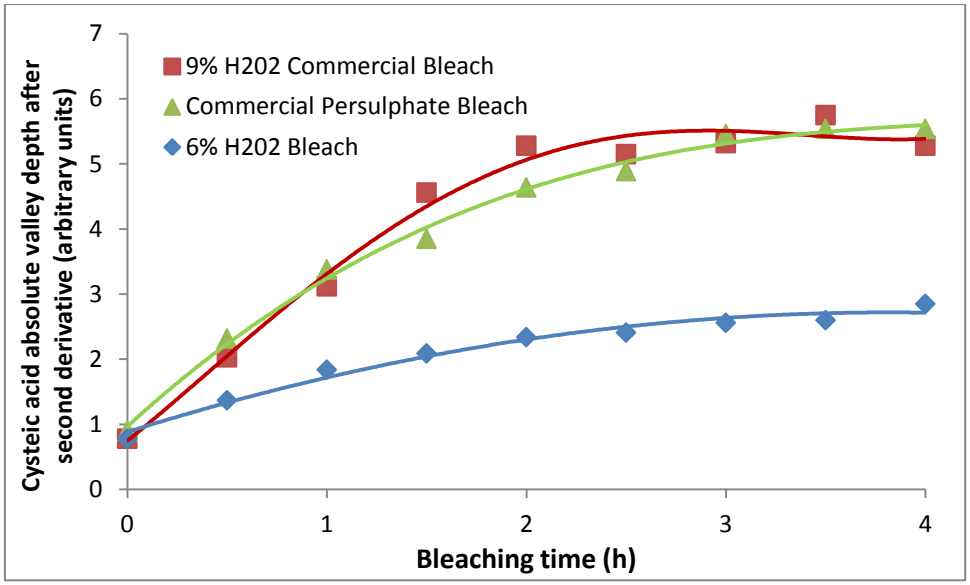

Figure 6.17: Oxidation effects on hairs measured using FTIR-ATR at various oxidizing agents. Valley of cysteic acid after second derivative is shown at 1040 cm^{-1}. The trendline curve has been calculated by a polynomial relationship.

Since two types of virgin hair sources were employed to perform the oxidation treatments, such as hair batch I was used for 6% H_2O_2 bleach and 9% H_2O_2 commercial bleach, and hair batch II was adopted for commercial persulphate bleach, their relative value of absolute valley depth of cysteic acid ($H_{gt}{}^{R} = (H_{gt}/H_{gt}{}^{0})$, where $H_{gt}{}^{0}$ represents the absolute valley depth of cysteic acid of virgin hair, were introduced and were normalized against the internal standard. Figure 6.18 presents the comparison of the relative values of valley depth of cysteic acid for the different oxidizing agents. Here the relative values for 9% H_2O_2 commercial bleach are very dominant, which were expected to take a middle place between commercial persulphate bleach, which is the stronger oxidizing agent (persulphate), and 6% H_2O_2 bleach, which shows the mild damage effect all the time. This observation is related to the "Knot Test" results (Chapter 3) that 9% H_2O_2 commercial bleach induces the severer surface damage, which leaves the cortex exposed at extreme bleaching conditions. However, 6% H_20_2 bleach and commercial persulphate bleach lead to some remaining cuticle or has only one layer of cuticle, which is less damaged than for the 9% H_2O_2 commercial bleach.

The values of the standard error SE, which arise from each treatment are too small to be visible. This indicates that a relatively consistent bleaching effect produced on each hair sample along the fibre length.

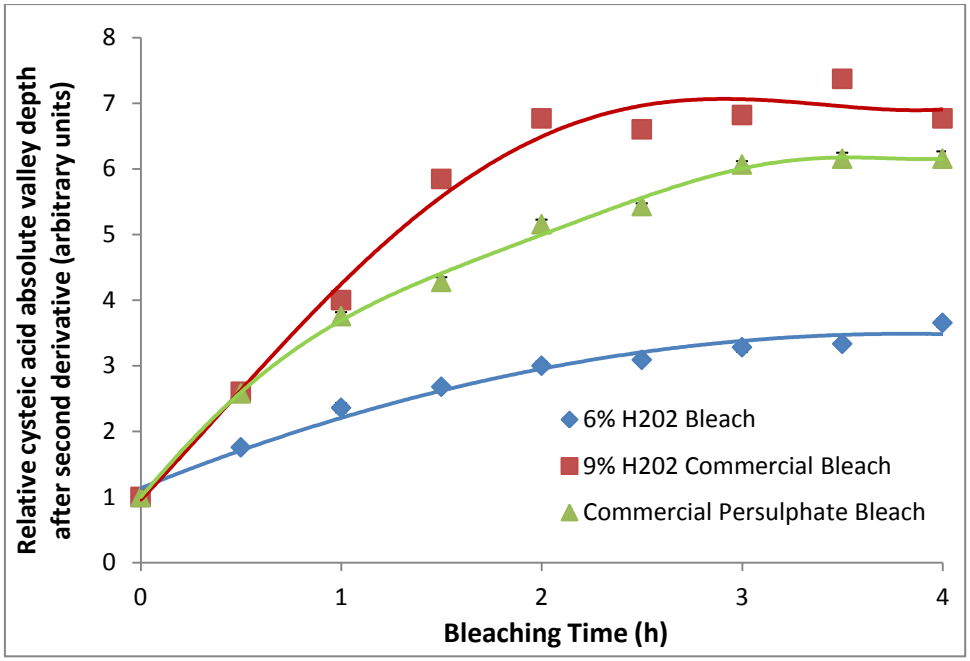

Figure 6.18: Oxidation effects on bleached hair measured using FTIR-ATR at various oxidizing agents. Relative values were employed, as $H_{gt}{}^{R} = (H_{gt}/H_{gt}{}^{0})$, where $H_{gt}{}^{0}$ represents the absolute valley depth of cysteic acid of virgin hair. The trendline curve has been calculated by polynomial relationship.

6. 4. 2.2 KBr Transmission Mode

6.4.2.2.1 Effects of the Oxidizing Agents

The IR transmission technique, as a widely used routine method of FTIR spectroscopy, was also utilised to detect the oxidation conditions of cystine in bleached hair keratin. When the light is transmitted through the keratinous sample, spectral information is provided not only from the surface layer, such as cuticle, but also from the inner part of the fibre, the cortex. Although the reflectance mode of ATR can detect as deeply as the evanescent wave penetrates in the cuticle (~2μm), it is not effective to analyse the internal properties of hair. Consequently, transmission spectroscopy in the form of the KBr pellet sampling technique was employed to investigate the internal chemistry changes caused by oxidation in the cortex.

In Figure 6.19, the normalized FTIR spectra of untreated and treated hairs, which were standardized against the peak heights at 1452 cm^{-1} clearly display the prominent peak

of cysteic acid at 1040 cm^{-1}, and secondly at 1172 cm^{-1} with the prolonged treatment time (3h). The reason for choosing 3h treatment time as the terminal bleaching time is because the 9% H_20_2 commercial bleached hairs and commercial persulphate bleached hairs were rinsed with water overnight (see Chapter 2). From the results of Chapter 5, it is clear that the cross-linked matrix, which contributes most of the cystine in the cortex, is highly affected by prolonged rinsing with water. We thus exclude the 3.5h and 4h oxidation period for this internal property analysis.

The second cysteic acid peak at 1172 cm^{-1} is not obvious as shown in Figure 6.19 for the 6% H_20_2 treated and untreated hair samples. This indicates that these two types of hair samples are subject to less oxidation damage than for 9% H_20_2 commercial bleach and commercial persulphate bleach. 9% H_20_2 commercial bleach achieved the strongest absorbance intensity for the cysteic acid peak among the three types of bleached hair samples. This corresponds to the previous ATR results, even though the commercial persulphate bleach contains the intensive oxidizer, persulphate. The reason for this abnormal result is explained by the DSC result in Chapter 5, in that the matrix for 9% H_20_2 commercial bleach is heavily damaged after the intensive oxidation time (≥2h), thus resulting in the abundance of cysteic acid.

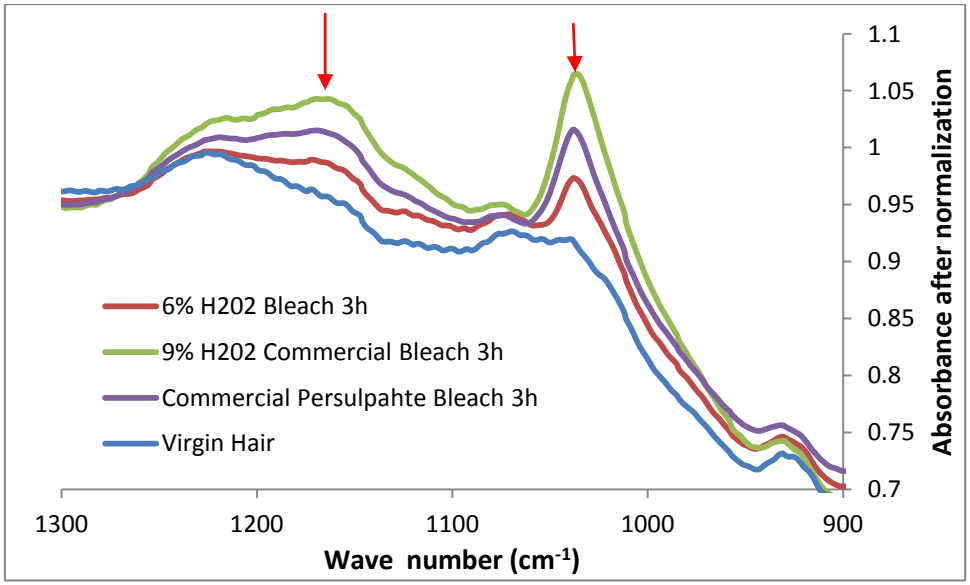

Figure 6.19: FTIR-KBr spectrum of untreated and 3 types of 4h treated fibers at 1300 – 900cm^{-1} after normalization**.** Cysteic acid peak becomes clearly visible at 1040cm^{-1} and 1171 cm^{-1} for the bleached fiber, (marked by the red arrows). Each curve is randomly chosen from one of three tresses' results.

After second derivative transformation, the obtained absorbance of valley depths for cysteic acid at 1042 cm^{-1} were calculated and compared to illustrate the transformation of the chemical structure of cystine to cysteic acid, caused by the three types of bleaching treatments.

The second derivative spectra of untreated and three types of bleached hairs for 3h bleaching time are shown in Figure 6.20. It is noticed that the cysteic acid valley appears at 1040cm^{-1}. 9% H_2O commercial bleach (3h) exhibits the most intensive damage impact, followed by commercial persulphate bleach (3h), 6% H_2O bleach (3h) and virgin hair.

In agreement with the observations in Figure 6.13, the peak location after second derivative moves slightly for the peak of cysteic acid from 1042 to 1037cm^{-1}. The reason for this transformation is explained by the Hogg (1994) that partial disulphide bond rupture causes the disulphide conformation.

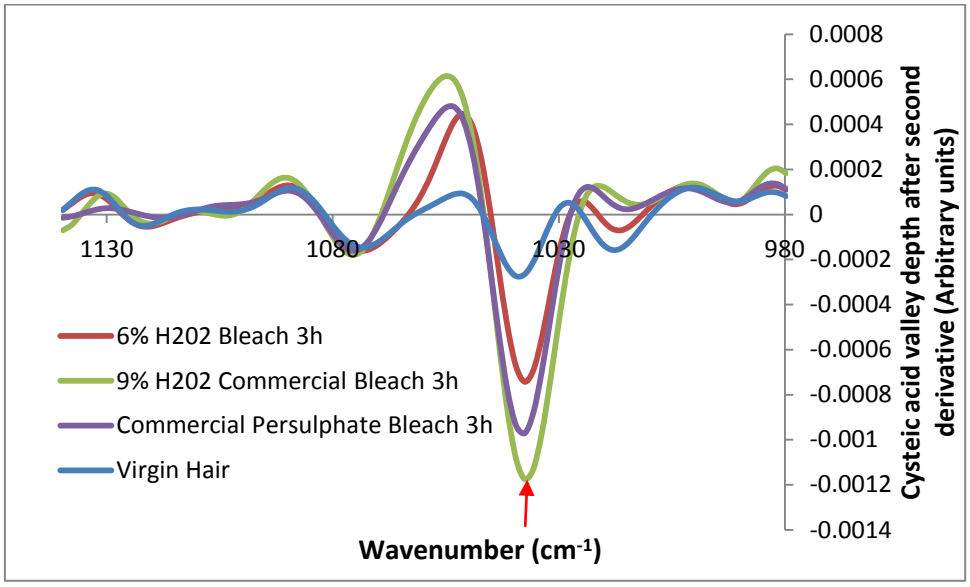

Figure 6.20: FTIR-KBr spectrum of untreated and 3 types of 4h treated fibres at 1300 – 900cm^{-1} after second derivative**.** Cysteic acid becomes clearly visible as a valley at 1040cm^{-1} for the bleached fiber, (marked by the red arrow). Each curve is randomly chosen from one of three tresses' results.

It has been shown that the curves for 6% H_2O_2 and commercial persulphate bleach behave in a similar way in Figure 6.21. They both increase during the first hour and then remain constant. This reveals a homogenous oxidation effect on the matrix in the

cortex over the treatment time, which corresponds to the conclusions in Chapter 5. Thus these results, which both investigate the internal and surface properties of the human hair, will be compared in Chapter 7 for a better explanation.

The curve for 9% H_2O_2 commercial bleach shows an upward tendency towards its saturation, however it seems that its equilium level has not been reached during three hours of oxidation.

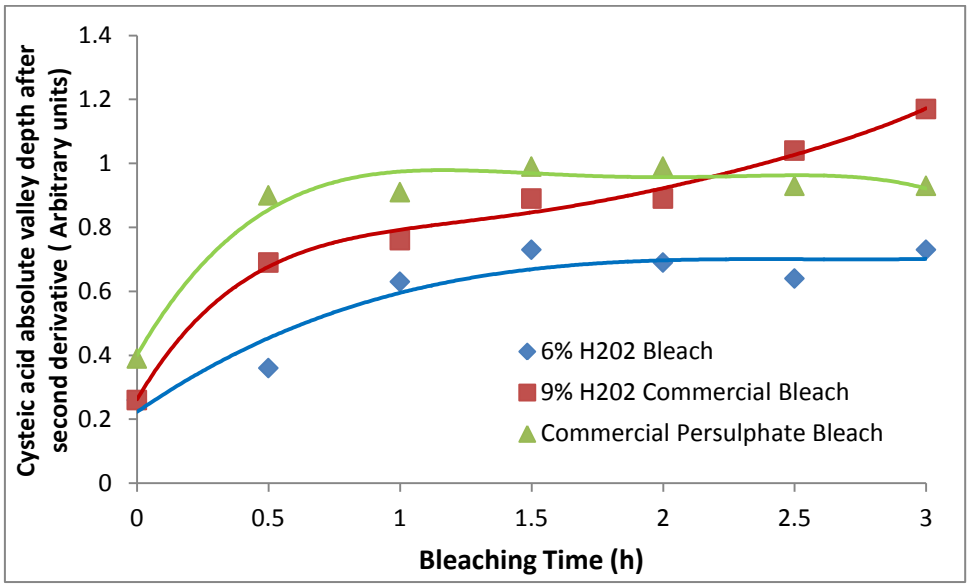

Figure 6.21: Oxidation effects on bleached hair measured using FTIR-KBr for various oxidizing agents. The trendline curve has been calculated by polynomial relationship.

Though two different hair sources were used in the sample preparation, the relative values of peak intensity for cysteic acid of virgin hair batch I and II are shown in Figure 6.22 to yield comparable curves for different oxidizing agents after normalization. It is obvious that 6% H_2O_2 bleach and commercial persulphate bleach have a similar, almost overlapping steady trend line while the 9% H_2O_2 commercial bleach is increasing during the time of the oxidation treatment. This implies that 9% H_2O_2 commercial bleach has a stronger oxidation effect on the matrix during 3h bleaching. The cysteic for both 6% H_2O_2 bleach and commercial persulphate bleach are coinciding, which is unexpected because there is an aggressive oxidiser agent in the commercial persulphate bleach. The “Knot Test” result could provide a good explanation that both 6% H_2O_2 bleach and commercial persulphate bleach has a

moderate surface damage on the cuticle, since cuticle is used to protect the inner layers of hair, there is a similar oxidation effect on the matrix on the cortex by 6% H_2O_2 and commercial persulphate bleach.

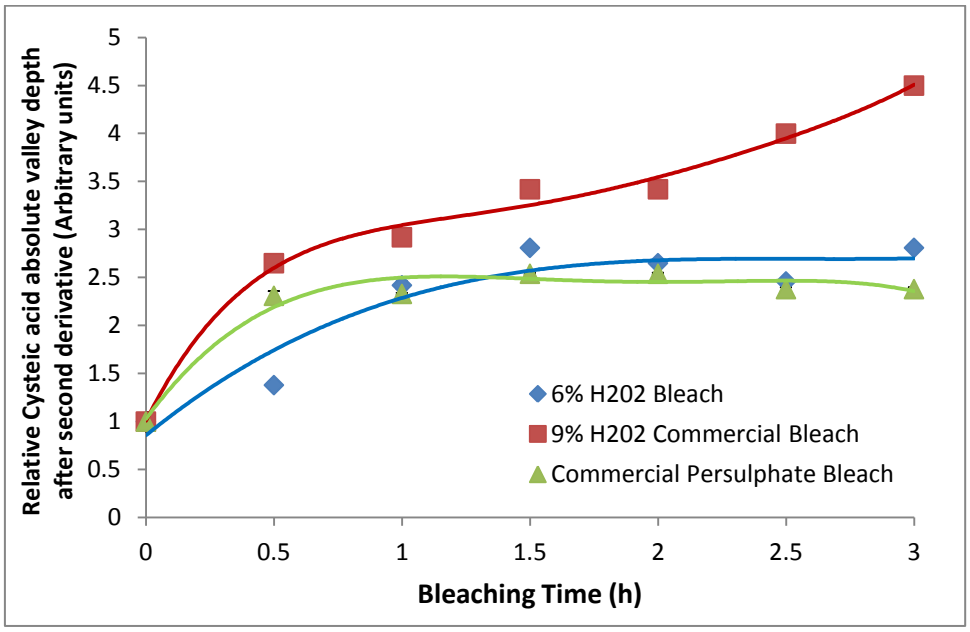

Figure 6.22: Oxidation effects on bleached hair measured using FTIR-KBr at various oxidizing agents. Relative values were employed, as $H_{gt}{}^{R} = (H_{gt}/H_{gt}{}^{0})$, where $H_{gt}{}^{0}$ represents the absolute valley depth of cysteic acid of virgin hair. The trendline curve has been calculated by polynomial relationship.

6.5 Conclusion

Transmission FTIR spectroscopy detects the internal region of the hair, while the FTIR-ATR technique analyses surface properties only. Thus, a comprehensive analysis of cysteic acid was conducted by using these two methods.

9% H_2O_2 commercial bleach demonstrates high absorbance intensity for cysteic acid in both FTIR-ATR and transmission, which was supposed to take the middle place between commercial persulphate bleach and 6% H_2O_2 bleach. The reason for this abnormal result is explained by the SEM and DSC results, which show that the hair surface of 9% H_2O_2 commercial bleach undergoes severer damage, which leaves the cortex exposed and in extreme poor condition. The intermediate filament for 9% H_2O_2 commercial bleach is heavily damaged after intensive oxidation treatment (≥2h). Relatively, both 6% H_2O_2 bleach and commercial persulphate bleach are subject to

very similar oxidation effects on the cortex. It is found in the "Knot Test" that 6% H_2O_2 bleach and commercial persulphate bleach have a moderate surface damage for the cuticle. Since the cuticle is used to protect the inner structures of hair, there is a similar oxidation effect on the matrix in the cortex by 6% H_2O_2 and commercial persulphate bleach.

As shown in Section 6.4.1, Attenuated Total Reflectance (ATR) spectra measured by FTIR are similar to those collected by transmission measurements. Thus the relationship of two FTIR-modes can be compared after normalisation. The results are presented in Figure 6.23.

It is obvious that 6% H_20_2 bleached hair is subject to a milder effect on both surface and internal properties. This is reflected in the ATR and transmission results. A consistent progressive damage effect is observed for 9% H_20_2 commercial bleached hair for both cuticle and cortex layers, indicating that abundant cysteic acid is formed during the whole treatment time. Commercial persulphate bleach, containing the stronger oxidising agent, has an unexpected result, in that it has a less surface damage than 9% H_2O_2 commercial bleached hair in FTIR-ATR test, and a similar oxidation effect on the matrix as 6% H_20_2 bleached hair in FTIR transmission mode investigation.

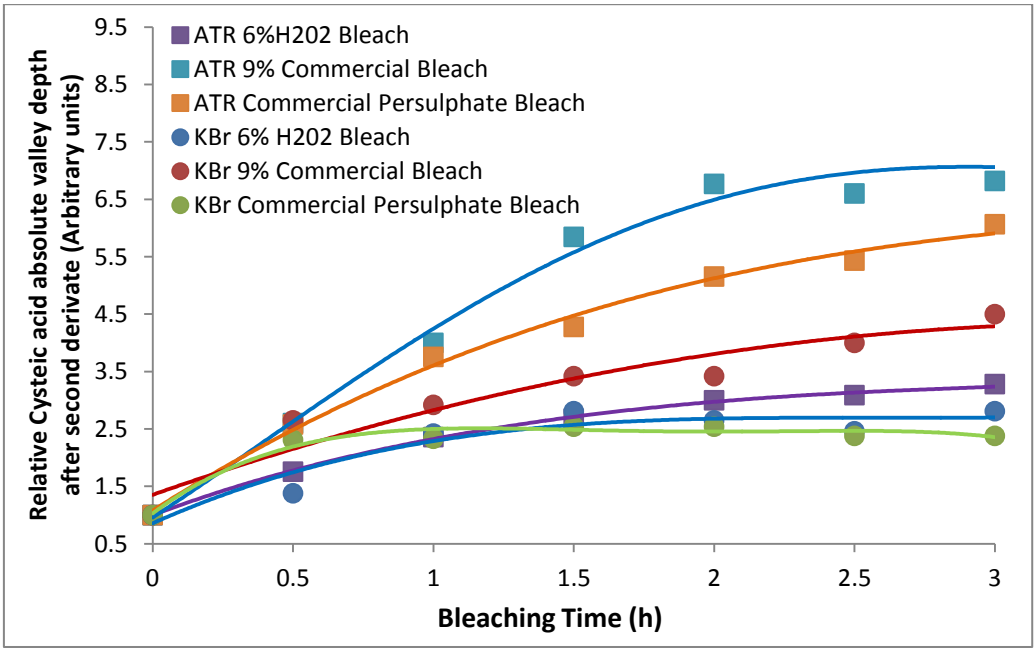

Figure 6.23: Oxidation effects on bleached hair measured using FTIR-ATR and FTIR-transmission mode for various oxidizing agents. Relative values were employed, as $H_{gt}{}^{R} = (H_{gt}/H_{gt}{}^{0})$, where $H_{gt}{}^{0}$ represents the absolute valley depth of cysteic acid of virgin hair. The trendline curve has been calculated by polynomial relationship.

6.6 References

ALTER, H., MICHAEL, BIT -ALKHAS., 1969. Infrared Analysis of Oxidized Keratin. *Textile Research Journal, ,* 39**,** 479-481.

BADDIEL, C. B. 1968. Structure and reactions of human hair keratin: an analysis by infrared spectrsocopy. *Molecular biology,* 38**,** 181-199.

BARBARA, H. S. 2004. *Infrared spectroscopy: fundamentals and applications,* England, John Wiley&Sons.

BARTH, A. 2007. Infrared spectroscopy of proteins. *Biochimica et Biophysica Acta,* 1767**,** 1073-1101.

BARTICK, E. G., TUNGOL, MARY W., REFFNER, JOHN A., 1994. A new approach to forensic analysis with infrared microscopy: Internal reflection spectroscopy. *Analytical Chimica Acta,* 288**,** 35-42.

BEER, M., SUTHERLAND, G. B. B. M., TANNER, K. N., AND WOOD, D. L., 1959. Infrared Spectra and Structure of Proteins. *Proceedings of the Royal Society***,** 147-172.

BELLAMY, L. J. 1958. *The infrared Spectra of Complex Molecules,* New York, Wiley.

BELLAMY, L. J. 1975. *The Infrared Spectra of Complex Molecules,* New York, Wiley.

BENÍTEZ, J., MATAS, AJ., HEREDIA A., 2004. Molecular characterization of the plant biopolyester cutin by AFM and spectroscopic techniques. *J Struct Biol,* 147**,** 179-184.

BILINSKA, B., KOLCZYNSKA-SZAFRANIEC, U., BUSZMAN, E., 1991. The structure of melanin biopolymers from human hair. I. IR spectroscopy studies. *Postepy Fizyki Medycznej,* 26**,** 75-80.

BRENNER, L., SQUIRES, P. L., GARRY, M., AND TUMOSA, C. S., 1985. A Measurement of Human Hair Oxidation by Fourier Transform Infrared Spectroscopy. *Journal of Forensic Sciences,* 13**,** 420-426.

BRIDGE, T. P., FELL, A. F., WARDMAN, R. H., 1987. Perspective in Derivatives Spectroscopy, Part 1: Theoretical Principles. *Journal of the Society of Dyers and Colourists,* 103**,** 17-27.

CAROTI, G., DUSENBURY, JOSEPH H., 1956. Effect of drawing on the infrared dichroism of nylon 66 filaments. *Polymer Science***,** 399-407.

CARR, C. M., LEWIS, D. M. 1993. An FTIR spectroscopic study of the photodegradation and thermal-degradation of wool. *Journal of the Society of Dyers and Colourists,,* 109**,** 21-24.

CHURCH, J. S., CORINO, G. L., WOODHEAD, A. L., 1997. The analysis of Merino wool cuticle and cortical cells by Fourier transform Raman spectroscopy. *Biopolymers,* 42**,** 7-17.

COLTHUP, N. B., DALY, LAWRENCE H., WIBERLEY, STEPHEN E., 1964. *Introduction to Infrared and Raman Spectroscopy,* New York, Academic Press.

CROOK, A., TAYLOR, P. J., 1958. *Chemistry and industry***,** 95.

DEVANEY, R. G., THOMPSON, AVON L., 1958. An Improved Technique for Preparasiong Samples of Organic Solids for Infrared Analysis. *Applied Spectroscopy,* 12**,** 154-155.

FREDLINE, V., KOKOT, S., GILBERT, C., 1997. An FT-IR and Raman spectroscopy study of electrochemically modified woollen fabric. *Mikrochimica Acta***,** 183-184.

GNIADECKA, M., NIELSEN, O. F., CHRISTENSEN, D. H., WULF, H. C., 1998. Structure of water, proteins, and lipids in intact human skin, hair, and nail. *J Invest Dermatol,* 110**,** 393-398.

GRDADOLNIK, J. 2002. ATR-FTIR Spectrscopy: its advantages and limitations. *Acta Chim. Slov,* 49**,** 631-642.

HARRICK, N. J. 1979. *Internal Reflection Spectroscopy,* Ossining, New York, Harrick Scientific Corp.

HARRICK, N. J. 1985. *Internal Reflectance Spectroscopy,* New York, Interscience Publishers.

HARRIS, D. C. 1999. *Quantitative Chemical Analysis* USA, W. H. Freeman & Co Ltd.

HILTERHAUS-BONG, S., ZAHN, H., 1987. Contributions to the chemistry of human hair. I. Analyses of cystine, cysteine and cystine oxides in untreated human hair. *International Journal Cosmetic Science,* 9**,** 101-110.

HOGG, L. J., EDWARDS, H. G. M., FARWELL, D. W., AND PETERS, A.T., 1994. FT-Raman Spectroscopic Studies of Wool. *Society of Dyers Colourists,* 110**,** 196-199.

HSU, C. P. S. 1997. *Infrared Spectroscopy,* New Jersey, Prentice Hall.

ITOU, T., NOJIRI, M., OOTSUKA, Y., NAKAMURA, K., 2006. Study of the interaction between hair protein and organic acid that improves hair-set durability by near-infrared spectroscopy. *J Cosmet Sci,* 57**,** 139-151.

JOY, M., LEWIS, D. M., 1991. The use of Fourier transform infrared spectroscopy in the study of the surface chemistry of hair fibres. *International Journal of Cosmetic Science,* 13**,** 249-261.

KHAN, J. I., KENNEDY, THOMAS J., CHRISTIAN, JR DONNELL R., 2012. *Basic Principles of Forensic Chemistry,* Springer, Humana Press.

KIRSCHENBAUM, L. J., COUTINHO, L., HUFFMAN, S. W., BROWN, C. W., 2000. Assessment of Strctural Changes in Human Hair by Near IR Spectroscopy (Abstract). *Abstract of Papers of the American Chemical Society.*

KUZUHARA, A. 2005. Analysis of structral change in keratin fibers resulting from chemical treatment using Raman spectrscopy. *Biopolymers,* 77**,** 335-344.

LEWIS, D. M., YAN, G., 1993. The effect of various chromium species on wool keratin. *Journal of the Society of Dyers and Colourists,* 109**,** 193-198.

LYMAN, D. J., MURRAY-WIJELATH, JACQUELINE., FEUGHELMAN, MAX., 2001. Effect of temperature on the conformation of extended alpha-keratin. *Applied Spectroscopy,* 55**,** 552-554.

MARTIN, K. 1999. Cosmetic Spectroscopy: A review of infrared and Raman studies of skin and hair. *The Internet Journal of Vibrational Spectroscopy,* 3**,** 1.

OHNISHI, K., SAKANO, T., FUJIWARA, N., 1993. Application of FTIR diamond cell method to discrimination of personal hair. *Journal of Toxicology and Enviromental Health,* 39**,** 247-250.

PAINER, P., STARSINIC, M. AND COLEMAN, M. 1985. *Fourier Transform Infrared Spectroscopy,* Orlando, Academic Press.

PAINTER, P. C., COLEMAN, M.M., JENKINS, R.G., WHANG, P.W. AND WALKER, P.L. 1978. Fourier transform infrared study of mineral matter in coal: a novel method for quantitative mineralogical analysis. *Fuel,* 57**,** 337-344.

PAINTER, P. C., RIMMER, S. M., SNYDER, R. W., DAVIS, A 1981. A Fourier transform infrared study of mineral matter in coal: the application of a least-squares curve-fitting program. *Applied Spectrsocopy,* 35**,** 102-106.

PANAYIOTOU, H., KOKOT, S., 1999. Matching and discrimination of single human-scalp hairs by FT-IR micro-spectroscopy and chemometrics. *Analytica Chimica Acta,* 392**,** 223-235.

PAVIA, D. L., LAMPMAN, GARY M., KRIZ, GEORGE S., 2001. *Introduction to Spectroscopy,* USA, Harcourt College Publishers.

PAVIA, D. L., LAMPMAN, GARY M., KRIZ, GEORGE S., VYVYAN, JAMES A., 1996. *Introduction to spectroscopy,* USA, Saunders College Publishing.

PIELESZ, A., WKOCHOWICZ, A., BINIAS, W., 2000. The evaluation of structural changes in wool fibre keratin treated with azo dyes by Fourier Transform Infrared Spectroscopy. *Spectrochimica Acta Part A-Molecular and Biomolecular Spectroscopy,* 56**,** 1409-1420.

ROBBINS, C. R. 1967. Infrared Analysis of Oxidised Keratins. *Textile Research Journal,* 37**,** 811-813.

ROBBINS, C. R. 1994. *Chemical and Physical Behavior of Human Hair,* Berlin, Springer.

ROBBINS, C. R. 2002. *Chemical and Physical Behavior of Human Hair,* New York,, Springer-Verlag.

ROBINSON, V. N. E. 1976. A Study of Damged Hair *Journal of the Society of Cosmetic Chemists,* 27**,** 155-161.

SCHAARE, P. N., FRASER, D. G., 2000. Comparison of reflectance, interactance and transmission modes of visible-near infrared spectroscopy for measuring internal properties of kiwifruit (Actinidia chinensis). *Postharvest Biology and Technology,* 20**,** 175-184.

SHAH, R. C., GANDHI, R. S., 1968. Infrared Analysis of Oxidized Keratins. *Textile Research Journal* 38**,** 874.

SIGNORI, V., LEWIS, D. M., 1997. FTIR Invesigation of the damage produced on human hair by weathering and bleaching processes: Implementation of different sampling techniques and data processing. *International Journal of Cosmetic Science,* 19**,** 1-14.

SILVERSTEIN, R. M., BASSLER, G. CLAYTON., MORRILL, TERENCE C., 1981. *Spectrometric Identification of Organic Compounds,* New York, Wiley.

SIMON, A., KUNATH, D., 1961. Vibrational spectra and structure of s-alkyl thiosulfates (Bunte salts). *Ber. Deutche Chem. Ges,* 94**,** 1980-1986.

SMITH, B. C. 1996. *Fundamentals of Fourier transform infrared spectroscopy,* USA, CRC Press

STRASHEIM, A., BUIJS, K., 1961. An infrared study of the oxidation of the disulfide bond in wool. *Biochimica Biophysical Acta,* 47**,** 538-541.

THERMONICOLET 2001. Introduction to Fourier Transform Infrared Spectrometry.

TOLGYESI, E. 1983. Weathering of hair *Cosmetics and Toiletries,* 98**,** 29-33.

VENYAMINOV, S. Y., PRENDERGAST, F. G., 1997. Water (H_20 and D_20) molar absorptivity in the 1000-4000 cm-1 range and quantitative infrared spectroscopy of aqueous solutions. *Analytical Biochemistry,* 248**,** 234-245.

WESTON, G. J. 1955. The infrared spectrum of peracetic acid-treated wool. *Biochim. Biophys. Acta,* 47**,** 462-464.

WOLFRAM, L. J., LINDEMANN, M. K. O., 1971. Some observations on the hair cuticle. *Journal of the Society of Cosmetic Chemists,* 22**,** 839-850.

Chapter 7 Summary and Conclusion

Evaluation of hair damage is particularly important in assessing the performance of hair bleaches, which involves an oxidation reaction during the application. A variety of methods was combined to correlate the surface and structural changes in human hair imparted by the oxidation treatments. They are: Scanning Electron Microscopy (SEM), Reflective Spectrophotometry, Differential Scanning Calorimetry (DSC) and Fourier transform infrared spectroscopy (FTIR). Different levels of damage were achieved by changing the time of treatment up to 4 hours for 6% H_20_2 (hydrogen peroxide) as well as commercial bleaches, such as 9% H_20_2 commercial bleach and commercial persulphate bleach (contains 9% H_20_2).

The morphological changes of the cuticle as a consequence of damage processes are investigated by means of SEM. When hair fibres are subject to bleach damage, the cuticle is progressively destroyed, resulting in the cuticle edges being gradually chipped away. Under severe treatment conditions, the layer of cuticular sheets is entirely removed, leaving the underlying cortex exposed. A systematic numerical approach named “Knot Test” as a new methodology is applied using cuticle descriptors to evaluate hair damage. There are two types of damage classifications: mild and heavy damage classifications. The “Knot Test” results show that surface changes increase with peroxide treatment time. The longer treatment time results in the greatest surface damage. Surprisingly, commercial persulphate bleaching treatment produced the least topographical damage with the extended treatments among all the bleaching conditions. 6% H_20_2 bleach has an overall moderate damage effect over the treatment time. 9% H_20_2 commercial bleach shows a distinctive damage result. For the first 1.5h bleached hairs show mild oxidative damage, while severe damage occurs after 2h.

Colour changes of bleached hair with increasing treatment time are evaluated, since the initial response of oxidation to the hair fibre is colour change. In general, bleached hairs have an overall lighter, yellowish and reddish colour change. The lightness change of the treated hair is due to pigment oxidation. Yellowness change is associated

to two steps, namely, solubilisation of black-brown melanin and keratin degradation. It has been verified that a* (redness) of hair plays a minor role in determining the colour change, so that b* (yellowness) and L* (lightness) are the main controlling components in the CIE L*a*b* colour space, which is an objective tool for the evaluation of colour specification. The higher the concentration of peroxide and the longer the treatment time, the larger is the ΔE* (total colour change) value, so the greater is the hair colour difference. 9% H_20_2 commercial bleach and especially the commercial persulphate bleach demonstrate an overall larger increase in colour change than the 6% H_20_2 bleach, which always has a mild oxidation effect. Consequently, commercial persulphate bleached hair is much lighter and more yellow than 9% H_20_2 commercial bleached hair and 6% H_20_2 bleached hair.

Thermal analysis (DSC) investigates the structural changes and degree of degradation of the cortex based on the denaturation enthalpy ΔH_D and denaturation temperature T_D of keratin. These parameters reflect the amount and structural integrity of the α-helical material in the IFs, and the cross-link density of the matrix (IFAPs), respectively. There is a consistent decrease in both T_D and ΔH_D by the three bleaching treatments over the bleaching time, showing that the structural damage becomes greater with the longer treatment time. The deconvolution results for the three bleaches using three Gaussian distributions confirm this observation. The stronger bleach results in a homogenous structural damage on both para- and ortho-cortex with prolonged bleaching time. Commercial persulphate bleach and 9% H_20_2 commercial bleach have a larger progressive damage effect on the *ortho*- and *para*- cortex than 6% H_20_2 bleach.

A strong linear relationship between ΔH_D and T_D was observed for 6% H_2O_2 bleach, commercial persulphate bleach and for parts of the data for 9% H_20_2 commercial bleach, revealing that the three bleaches have a homogenous bleaching effect on IFs and IFAPs. However, deviating results for 9% H_20_2 commercial bleach after 2 hours bleaching time are observed. This is because the intermediate filament is progressively damaged after excessive bleaching treatment (≥2h), so that there is a larger decrease in ΔH_D than in T_D. "Knot test" results show the cuticle surfaces of 9% H_20_2 commercial bleach to be strongly degradated after 2h. As a consequence, 9% H_20_2 commercial bleach (2h) has a severe oxidative damage effect on both cuticle and cortex of hairs.

Kinetic analysis is conducted for virgin and commercial persulphate bleached hairs by combining data for the various heating rates according to ASTM-E698. It is confirmed that the denaturation temperature shifts to higher values with increasing heating rate. The activation energies of 260 kJ/mol for the virgin hair and 295 kJ/mol for the commercial persulphate bleached hair (2h) are determined from the slope of the linear regression between the non-reversing denaturation peak temperature (as $1/T_D$) and heating rate, β (as lnβ) on the basis of the Arrhenius-equation. Since the difference of their activation energies is quite small (35 kJ/mol), there is no obvious damage change in the matrix, thus the predominant structural damage by heating rate only occurs in the IF. The relationship between denaturation enthalpy ΔH_D and heating rate provides a better explanation for this finding. A linear increase in ΔH_D for lower heating rates is observed between 0.15 ~ 1^oC/min, while it is constant for higher heating rates (up to 7^oC/min). This can be ascribed to the hypothesis that a lower heating rate favours a crystal transformation change (α-β transformation), while a higher rate favours a crystalline-amorphous transformation. Virgin mohair is also compared with virgin hair using this approach. The slope of linear regression for the lower heating rates increase from mohair to human hair, however they overlap at the higher heating rates, indicating that both virgin keratin fibres have similar amounts of "native" α-helix.

SEM has been used to examine the morphological changes of the denaturated hair samples after DSC. There is a common characteristic that the cortex is dissolved at lower heating rates. The commercial persulphate bleached hairs show an overall shrunk cuticle surface and fewer and smaller hydrolysed protein granules, due to the previously damaged α-helix in the cortical cell.

Although commercial persulphate bleached hair (2h) has an overall lower denaturation temperature for each cortical cell type for all heating rates, the distance between the para- and ortho- cortex is the same as for virgin hair. This shows that the heating rate affects the cystine linkages of para- and ortho- cortex homogenously, regardless of the previous damage. However, a homogenous damage on the three cortical components can only occur for the previously damaged fibres.

Reflectance and transmission are two modes of FTIR spectroscopic measurements. Since the cuticle surfaces and the matrix of 9% H_20_2 commercial bleach are subjected

to the severe damage after prolonged oxidation treatment (2h), as confirmed by SEM and DSC, 9% H_20_2 commercial bleach shows the highest absorbance intensity for cysteic acid peak in both FTIR-ATR and transmission. Both 6% H_2O_2 and commercial persulphate bleach show a similar oxidation effect in the FTIR transmission investigations. This findings are interpreted such that the 6% H_2O_2 and commercial persulphate bleach have a moderate surface damage on the cuticle, which protects the cortex of hair, thus a similar oxidation effect on the cortex is achieved. Although commercial persulphate bleach contains the stronger oxidising agent, it has a less severe surface damage than 9% H_20_2 commercial bleached hair as shown by the FTIR-ATR measurements, and the similar oxidation effect on the matrix for 6% H_20_2 bleached hair as shown by the FTIR transmission investigation.

7.1 Comparison of FTIR-KBr and DSC Results

Since both FTIR-KBr and DSC are detecting internal properties of the cortex, the comparison of relative cysteic acid absolute valley depth $H_{gt}{}^{R}$, $H_{gt}{}^{R} = (H_{gt}/H_{gt}{}^{0})$ in the FTIR transmission mode, against the values of relative denaturation temperature T_D, $T_D{}^{R} = (T_D/T_D{}^{0})$ in DSC measurement is given in Figure 7.1. One phenomenon, which draws attention is that the data generated by 6% H_20_2 bleach and 9% H_20_2 commercial bleach follow a regular decreasing pattern, while the results for commercial persulphate bleach behave differently, which is unexpected.

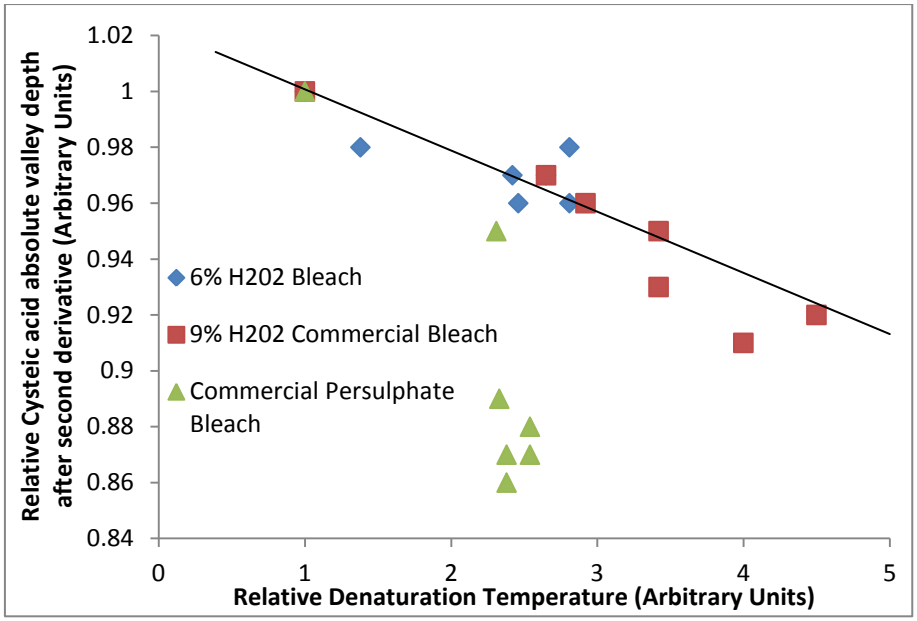

Figure 7.1: Comparison of the relative cysteic acid absolute valley depth H_{gt}^{R}, $H_{gt}^{R} = (H_{gt}/H_{gt}^{0})$ from FTIR-KBr, with relative denaturation temperature T_D, $T_D^{R} = (T_D/T_D^{0})$ from DSC measurements.

Overall, 6% H_2O_2 has a moderate damage effect on both surface and structural change. Commercial persulphate bleach causes much less surface damage than 9% commercial peroxide bleach. Although structural changes increase with peroxide treatment time, FTIR transmission mode found that 9% commercial peroxide treatment has stronger damage effects on the cortex than the commercial persulphate bleach. This is corroborated by DSC investigations, which show that the IF for 9% commercial bleach is heavily damaged after the intensive oxidation treatment time (≥2h).

7.2 Future Work

This information provides more insight into how hair changes on the molecular level, and in turn may lead to better treatment formulations or procedures with minimal damage to the hair. In order to assess hair damage more systemically, it has been suggested to combine the approach with other analysis, such as amino acid analysis, dynamic mechanical analysis (DMA), gloss test, tensile test, nano-indentation and others, which seem to be effective in identifying hair damage.

Chapter 8 Appendix

Table 8.1: The reflectance data for 6% H_20_2 bleached hair samples in the visible spectrum

Wavelength (nm)	0h	0.5h	1h	1.5h	2h	2.5h	3h	3.5h	4h
400	3.28	3.34	4.2	4.4	4.47	4.85	4.64	5.03	5.59
410	3.07	3.39	3.9	4.1	4.28	4.66	4.68	5.29	5.62
420	3.14	3.52	4	4.28	4.48	4.92	5	5.72	6.1
430	3.21	3.68	4.25	4.61	4.83	5.36	5.45	6.23	6.66
440	3.31	3.88	4.5	4.96	5.23	5.82	5.94	6.82	7.31
450	3.4	4.08	4.79	5.34	5.67	6.31	6.48	7.43	7.99
460	3.51	4.3	5.11	5.78	6.18	6.85	7.05	8.1	8.73
470	3.61	4.54	5.46	6.23	6.71	7.43	7.67	8.78	9.49
480	3.75	4.85	5.9	6.79	7.35	8.12	8.4	9.59	10.38
490	3.87	5.16	6.33	7.35	8.01	8.82	9.17	10.42	11.29
500	4.03	5.52	6.83	7.98	8.74	9.59	9.98	11.31	12.28
510	4.21	5.9	7.37	8.65	9.52	10.41	10.86	12.24	13.32
520	4.39	6.31	7.94	9.35	10.33	11.27	11.75	13.19	14.39
530	4.58	6.76	8.55	10.11	11.19	12.18	12.68	14.18	15.49
540	4.79	7.21	9.19	10.88	12.08	13.11	13.65	15.19	16.62
550	5.03	7.72	9.88	11.71	13.01	14.09	14.67	16.25	17.81
560	5.28	8.24	10.6	12.56	13.98	15.09	15.71	17.33	19
570	5.55	8.79	11.36	13.46	15	16.14	16.79	18.43	20.23
580	5.83	9.37	12.16	14.38	16.04	17.22	17.89	19.55	21.46
590	6.14	9.98	13	15.35	17.12	18.32	19.04	20.7	22.71
600	6.48	10.62	13.89	16.36	18.24	19.46	20.21	21.89	24.01
610	6.83	11.3	14.8	17.39	19.4	20.62	21.42	23.11	25.3
620	7.2	11.97	15.74	18.44	20.55	21.78	22.62	24.3	26.57
630	7.59	12.69	16.72	19.52	21.76	22.99	23.87	25.54	27.87
640	8.02	13.46	17.75	20.64	22.99	24.21	25.15	26.82	29.19
650	8.47	14.23	18.8	21.77	24.24	25.45	26.44	28.1	30.51
660	8.94	15.05	19.9	22.96	25.54	26.73	27.78	29.43	31.83
670	9.42	15.86	20.97	24.1	26.79	27.96	29.07	30.71	33.09
680	9.95	16.72	22.11	25.28	28.09	29.24	30.42	32.05	34.38
690	10.46	17.53	23.22	26.43	29.33	30.45	31.71	33.27	35.55
700	11.06	18.47	24.45	27.71	30.72	31.81	33.14	34.7	36.88

Table 8.2: The reflectance data for 9% H_20_2 commercial bleached hair samples in the visible spectrum

Wavelength (nm)	0h	0.5h	1h	1.5h	2h	2.5h	3h	3.5h	4h
400	3.28	3.93	4.71	5.62	7.39	8.71	8.25	11.59	12.26
410	3.07	3.94	4.86	5.86	7.5	9.06	8.54	12.31	13.09
420	3.14	4.14	5.18	6.34	8.2	9.92	9.37	13.62	14.44
430	3.21	4.4	5.6	6.92	9.01	10.89	10.29	14.97	15.82
440	3.31	4.69	6.1	7.57	9.88	11.86	11.25	16.21	17.08
450	3.4	5.05	6.64	8.27	10.76	12.85	12.22	17.41	18.29
460	3.51	5.45	7.24	9.04	11.69	13.88	13.24	18.63	19.51
470	3.61	5.88	7.88	9.85	12.65	14.91	14.28	19.82	20.69
480	3.75	6.36	8.6	10.75	13.72	16.07	15.42	21.12	21.98
490	3.87	6.87	9.35	11.68	14.79	17.2	16.55	22.37	23.2
500	4.03	7.47	10.18	12.69	15.91	18.38	17.72	23.63	24.45
510	4.21	8.08	11.04	13.72	17.05	19.57	18.9	24.88	25.7
520	4.39	8.73	11.92	14.78	18.19	20.76	20.06	26.11	26.9
530	4.58	9.42	12.85	15.88	19.36	21.96	21.25	27.33	28.1
540	4.79	10.16	13.82	17.01	20.52	23.16	22.43	28.53	29.26
550	5.03	10.94	14.83	18.18	21.73	24.39	23.64	29.74	30.45
560	5.28	11.74	15.86	19.36	22.93	25.61	24.84	30.94	31.6
570	5.55	12.59	16.91	20.57	24.16	26.85	26.05	32.14	32.77
580	5.83	13.47	17.99	21.8	25.4	28.1	27.28	33.35	33.93
590	6.14	14.37	19.09	23.05	26.66	29.35	28.52	34.57	35.09
600	6.48	15.32	20.23	24.33	27.94	30.64	29.78	35.79	36.27
610	6.83	16.32	21.41	25.64	29.22	31.9	31.03	37	37.43
620	7.2	17.32	22.58	26.94	30.51	33.16	32.27	38.19	38.57
630	7.59	18.36	23.78	28.26	31.81	34.44	33.53	39.41	39.74
640	8.02	19.44	25.01	29.61	33.16	35.73	34.83	40.64	40.92
650	8.47	20.54	26.24	30.96	34.53	37.03	36.14	41.89	42.12
660	8.94	21.69	27.52	32.35	35.93	38.37	37.47	43.2	43.36
670	9.42	22.82	28.76	33.69	37.26	39.61	38.73	44.38	44.51
680	9.95	23.96	30.01	35.03	38.64	40.9	40.03	45.6	45.7
690	10.46	25.1	31.23	36.33	39.94	42.09	41.25	46.73	46.81
700	11.06	26.36	32.57	37.77	41.36	43.45	42.62	48	48.07

Table 8.3: The reflectance data for commercial persulphate bleached hair samples in the visible spectrum

Wavelength (nm)	0h	0.5h	1h	1.5h	2h	2.5h	3h	3.5h	4h
400	3.44	5.48	6.29	7.58	9.15	10.54	12.85	14.52	16.37
410	3.34	5.52	6.55	8	9.94	11.48	14.25	16.37	18.52
420	3.41	5.98	7.22	8.94	11.32	13.12	16.33	18.94	21.4
430	3.49	6.53	8.04	10.05	12.86	14.93	18.46	21.57	24.2
440	3.58	7.16	8.92	11.24	14.45	16.76	20.55	24.07	26.78
450	3.69	7.83	9.88	12.48	16.09	18.59	22.59	26.47	29.17
460	3.79	8.57	10.88	13.78	17.78	20.47	24.62	28.8	31.48
470	3.93	9.36	11.95	15.12	19.45	22.31	26.57	31	33.64
480	4.1	10.25	13.13	16.57	21.25	24.28	28.63	33.27	35.86
490	4.26	11.17	14.35	18.05	23.04	26.21	30.62	35.41	37.97
500	4.47	12.17	15.66	19.59	24.87	28.17	32.6	37.49	40.03
510	4.67	13.22	17	21.16	26.69	30.1	34.55	39.46	41.99
520	4.88	14.31	18.34	22.73	28.47	31.98	36.4	41.28	43.81
530	5.12	15.46	19.75	24.34	30.28	33.86	38.25	43.03	45.58
540	5.38	16.64	21.19	25.94	32.06	35.7	40.04	44.67	47.24
550	5.67	17.89	22.68	27.6	33.86	37.55	41.83	46.29	48.88
560	5.98	19.16	24.19	29.27	35.65	39.36	43.56	47.82	50.42
570	6.3	20.48	25.72	30.95	37.43	41.16	45.26	49.28	51.89
580	6.66	21.83	27.29	32.64	39.2	42.92	46.91	50.67	53.28
590	7.05	23.22	28.88	34.35	40.97	44.67	48.54	52.01	54.62
600	7.47	24.66	30.51	36.09	42.74	46.41	50.16	53.33	55.93
610	7.9	26.11	32.13	37.81	44.48	48.1	51.7	54.58	57.16
620	8.36	27.54	33.74	39.47	46.11	49.69	53.14	55.75	58.28
630	8.86	29.01	35.37	41.16	47.75	51.28	54.57	56.93	59.42
640	9.39	30.51	37.02	42.86	49.38	52.87	55.98	58.16	60.56
650	9.94	32.03	38.66	44.55	50.98	54.42	57.36	59.43	61.7
660	10.55	33.58	40.33	46.26	52.56	55.99	58.74	60.75	62.87
670	11.14	35.05	41.91	47.84	53.99	57.38	59.93	61.87	63.85
680	11.8	36.57	43.51	49.45	55.44	58.77	61.16	62.96	64.82
690	12.46	37.99	45.06	50.92	56.74	60.02	62.27	63.91	65.7
700	13.2	39.59	46.72	52.57	58.22	61.42	63.54	64.97	66.69

Table 8.4: Denaturation Temperatures and non-reversing C_p of virgin hair at various heating rates for a typical DSC-curve

T_D \ β (C_p^{NR})	0.5	1.5	2	2.5	3	4	5	7
80	0	0	0	0	0	0	0	0
81	13.12	0	4.17	2.685	4.07	0	0	0
82	13.52	0.9045	3.706	1.664	4.065	12.34	8.771	0
83	13.47	0.5624	3.289	1.792	3.909	13.96	9.602	5.011
84	13.5	0.3366	3.535	1.967	3.748	15.11	10.47	5.224
85	13.46	-0.3933	3.662	1.832	3.485	16.13	11.32	5.286
86	13.43	-0.1043	3.575	1.738	3.768	16.94	11.91	5.332
87	13.37	0.3505	3.526	1.701	3.824	17.46	12.35	5.387
88	13.36	0.698	3.487	1.662	3.77	17.42	12.51	5.407
89	13.35	0.6786	3.438	1.622	3.701	16.96	12.4	5.378
90	13.28	0.5829	3.39	1.586	3.678	16.63	12.24	5.326
91	13.28	0.5733	3.377	1.563	3.678	16.55	12.15	5.299
92	13.32	0.5642	3.362	1.55	3.664	16.63	12.13	5.322
93	13.31	0.5655	3.338	1.537	3.646	16.72	12.18	5.351
94	13.33	0.5634	3.315	1.525	3.625	16.79	12.22	5.336
95	13.31	0.5714	3.297	1.518	3.605	16.83	12.26	5.292
96	13.27	0.5736	3.282	1.518	3.584	16.86	12.29	5.249
97	13.27	0.5802	3.268	1.511	3.575	16.89	12.29	5.216
98	13.25	0.5787	3.253	1.496	3.568	16.92	12.29	5.175
99	13.28	0.5847	3.234	1.485	3.563	16.95	12.29	5.134
100	13.32	0.5928	3.211	1.478	3.559	16.97	12.29	5.115
101	13.3	0.5986	3.189	1.475	3.554	16.98	12.3	5.107
102	13.29	0.5955	3.167	1.468	3.549	16.99	12.31	5.095
103	13.25	0.59	3.142	1.459	3.542	16.99	12.31	5.063
104	13.26	0.5851	3.117	1.452	3.537	16.99	12.31	5.012
105	13.26	0.5779	3.092	1.45	3.533	16.98	12.31	4.968
106	13.27	0.5754	3.075	1.447	3.528	16.97	12.3	4.95
107	13.27	0.571	3.066	1.442	3.526	16.97	12.3	4.936
108	13.28	0.5737	3.061	1.435	3.521	16.96	12.29	4.914
109	13.26	0.5761	3.047	1.433	3.512	16.95	12.29	4.866
110	13.27	0.5744	3.012	1.429	3.508	16.95	12.29	4.796
111	13.29	0.5824	2.983	1.428	3.505	16.95	12.28	4.724

112	13.3	0.582	2.975	1.425	3.504	16.94	12.27	4.653
113	13.35	0.5879	2.96	1.428	3.498	16.94	12.27	4.567
114	13.44	0.5893	2.937	1.432	3.492	16.94	12.26	4.475
115	13.38	0.5882	2.916	1.429	3.491	16.93	12.26	4.393
116	13.41	0.5799	2.896	1.432	3.493	16.93	12.25	4.337
117	13.47	0.5765	2.867	1.439	3.497	16.94	12.25	4.32
118	13.48	0.577	2.833	1.449	3.498	16.94	12.24	4.309
119	13.51	0.5759	2.815	1.457	3.496	16.95	12.24	4.281
120	13.5	0.5699	2.8	1.456	3.497	16.95	12.24	4.254
121	13.55	0.5634	2.775	1.457	3.498	16.94	12.24	4.23
122	13.58	0.5667	2.747	1.462	3.504	16.94	12.24	4.212
123	13.6	0.5585	2.718	1.462	3.505	16.94	12.24	4.214
124	13.67	0.559	2.683	1.452	3.505	16.94	12.23	4.228
125	13.75	0.5548	2.656	1.449	3.504	16.94	12.23	4.237
126	13.86	0.5635	2.639	1.454	3.504	16.93	12.22	4.236
127	13.93	0.5774	2.623	1.457	3.502	16.93	12.22	4.235
128	14.05	0.5955	2.608	1.462	3.501	16.93	12.21	4.237
129	14.22	0.6205	2.589	1.472	3.503	16.93	12.21	4.242
130	14.49	0.6567	2.582	1.494	3.513	16.92	12.2	4.249
131	14.77	0.7017	2.584	1.527	3.527	16.91	12.2	4.257
132	15.25	0.7837	2.601	1.566	3.552	16.91	12.19	4.265
133	15.69	0.8881	2.631	1.617	3.583	16.91	12.18	4.276
134	15.73	1.042	2.677	1.686	3.623	16.93	12.18	4.292
135	15.27	1.269	2.753	1.771	3.671	16.94	12.19	4.311
136	14.79	1.581	2.866	1.899	3.734	16.96	12.2	4.332
137	14.24	1.895	3.048	2.081	3.823	16.99	12.22	4.354
138	13.92	2.078	3.33	2.353	3.951	17.04	12.24	4.377
139	13.88	2.02	3.695	2.734	4.125	17.11	12.27	4.412
140	13.96	1.786	3.938	3.113	4.351	17.2	12.31	4.461
141	14.03	1.423	3.847	3.266	4.598	17.34	12.37	4.53
142	14.08	0.9998	3.521	3.087	4.786	17.53	12.45	4.618
143	14.28	0.5622	3.142	2.738	4.839	17.77	12.55	4.734
144	14.52	0.2006	2.701	2.387	4.74	17.98	12.68	4.876
145	14.7	-0.0167	2.212	2.051	4.555	18.12	12.83	5.031
146	15.03	-0.1299	1.828	1.714	4.311	18.12	12.99	5.171
147	15.45	-0.1754	1.651	1.412	4.024	18	13.11	5.275

148	15.68	-0.2051	1.587	1.218	3.72	17.83	13.17	5.329
149	15.69	-0.2483	1.548	1.154	3.477	17.63	13.15	5.319
150	15.82	-0.299	1.515	1.148	3.351	17.45	13.04	5.236
151	15.89	-0.3467	1.472	1.154	3.318	17.31	12.86	5.093
152	16.02	-0.3888	1.437	1.153	3.316	17.19	12.65	4.911
153	16.16	-0.4267	1.405	1.142	3.318	17.08	12.42	4.708
154	16.28	-0.4682	1.356	1.122	3.316	16.98	12.21	4.506
155	16.39	-0.4975	1.303	1.106	3.316	16.88	12.04	4.323
156	16.48	-0.5093	1.268	1.097	3.32	16.81	11.91	4.174
157	16.64	-0.4856	1.245	1.086	3.317	16.76	11.82	4.069
158	16.78	-0.4182	1.202	1.075	3.312	16.73	11.75	4.013
159	16.94	-0.2669	1.185	1.053	3.305	16.71	11.71	3.987
160	17.08	-0.0043	1.186	1.031	3.295	16.69	11.68	3.975
161	17.2	0.3595	1.214	1.015	3.282	16.68	11.66	3.969
162	17.32	0.8183	1.29	1.009	3.267	16.68	11.64	3.97
163	17.47	1.308	1.435	1.027	3.25	16.68	11.63	3.973
164	17.59	1.754	1.652	1.09	3.229	16.69	11.62	3.977
165	17.75	2.086	1.98	1.208	3.198	16.71	11.62	
166	17.93	2.293	2.422	1.393	3.167	16.74	11.62	
167	17.87	2.405	2.954	1.644	3.158	16.71	11.62	
168	18.09	2.48	3.472	1.968	3.112	16.67	11.63	
169	18.15	2.558	3.876	2.386	3.084	16.66	11.65	
170	18.29	2.619	4.129	2.831	3.089	16.69		
171	18.57	2.705	4.291	3.242	3.17	16.76		
172	18.62	2.799	4.413	3.546	3.296			
173	18.83	2.902	4.531	3.754	3.463			
174	18.89	2.983	4.641	3.904				
175	19.04		4.769					
176	19.2							
177	19.39							
178	19.72							
179								
180								

Table 8.5: Denaturation Temperature and non-reversing C_p of Commercial Persulphate Bleached hair (2h) at various heating rates for a typical DSC-curve

T_D β / C_p^{NR}	0.5	1	1.5	2	3	4	5	7
80	0	0	0	0	0	0	0	0
81	11.28	11.16	10.17	10.18	8.342	0	0	0
82	10.88	10.33	10.41	11.03	9.784	10.89	9.818	0
83	10.89	10.58	10.8	11.73	11.32	11.57	9.643	8.457
84	10.91	10.62	10.25	10.9	12.15	11.97	9.94	8.88
85	10.93	10.6	10.39	10.91	11.86	12.22	9.807	9.104
86	10.93	10.66	10.42	11.04	11.45	12.31	10.28	9.319
87	10.89	10.66	10.45	11.05	11.43	12.71	10.62	9.523
88	10.94	10.68	10.43	11.07	11.55	12.71	10.41	9.655
89	10.94	10.67	10.44	11.09	11.64	12.37	10.31	9.721
90	10.91	10.65	10.44	11.07	11.69	12.15	10.23	9.795
91	10.94	10.65	10.43	11.05	11.72	11.99	10.1	9.908
92	10.89	10.65	10.43	11.05	11.73	12.06	10.1	10.01
93	10.92	10.64	10.43	11.05	11.75	12.12	10.11	10.02
94	10.92	10.63	10.43	11.04	11.74	12.16	10.11	9.969
95	10.93	10.64	10.44	11.03	11.73	12.19	10.12	9.913
96	10.93	10.63	10.45	11.03	11.72	12.2	10.14	9.874
97	10.94	10.63	10.44	11.03	11.72	12.2	10.13	9.841
98	10.98	10.63	10.43	11.01	11.72	12.21	10.13	9.816
99	10.99	10.64	10.44	11	11.71	12.22	10.14	9.818
100	11	10.63	10.43	11	11.7	12.22	10.15	9.835
101	11	10.63	10.42	11	11.68	12.2	10.16	9.843
102	10.98	10.62	10.42	10.99	11.67	12.2	10.17	9.849
103	10.99	10.63	10.45	10.98	11.66	12.19	10.18	9.854
104	11.03	10.64	10.47	10.98	11.65	12.19	10.19	9.86
105	11.12	10.63	10.45	10.98	11.64	12.17	10.21	9.869
106	11.06	10.64	10.44	10.98	11.63	12.16	10.22	9.876
107	11.09	10.65	10.43	10.98	11.62	12.15	10.23	9.884

108	11.12	10.68	10.42	10.98	11.61	12.14	10.25	9.895
109	11.18	10.69	10.42	10.98	11.61	12.13	10.26	9.903
110	11.19	10.72	10.42	10.98	11.6	12.12	10.28	9.912
111	11.26	10.76	10.42	10.97	11.61	12.11	10.3	9.919
112	11.33	10.77	10.44	10.99	11.61	12.11	10.31	9.931
113	11.41	10.82	10.45	11	11.61	12.1	10.33	9.946
114	11.51	10.87	10.49	11.01	11.61	12.1	10.35	9.959
115	11.57	10.92	10.52	11.04	11.61	12.11	10.38	9.971
116	11.66	10.98	10.57	11.07	11.61	12.13	10.42	9.984
117	11.73	11.07	10.64	11.12	11.62	12.15	10.46	9.999
118	11.73	11.18	10.72	11.16	11.64	12.17	10.5	10.02
119	11.66	11.27	10.81	11.23	11.67	12.2	10.55	10.05
120	11.55	11.32	10.9	11.31	11.7	12.25	10.6	10.08
121	11.33	11.32	10.98	11.39	11.75	12.32	10.66	10.12
122	11.24	11.25	11.03	11.48	11.8	12.41	10.72	10.15
123	11	11.08	11.02	11.53	11.85	12.51	10.79	10.2
124	10.97	10.83	10.88	11.54	11.9	12.59	10.87	10.25
125	10.94	10.58	10.66	11.49	11.94	12.66	10.96	10.3
126	10.94	10.41	10.42	11.37	11.96	12.68	11.03	10.34
127	10.98	10.32	10.22	11.18	11.93	12.66	11.08	10.38
128	10.96	10.27	10.08	10.96	11.85	12.59	11.09	10.41
129	10.99	10.27	10.03	10.78	11.71	12.46	11.05	10.43
130	11.08	10.26	10.02	10.68	11.53	12.28	10.95	10.43
131	11.03	10.27	10.01	10.64	11.32	12.09	10.83	10.41
132	11.15	10.33	10.01	10.62	11.13	11.9	10.71	10.36
133	11.22	10.33	10.02	10.61	10.99	11.76	10.59	10.29
134	11.28	10.34	10.02	10.6	10.9	11.66	10.5	10.2
135	11.31	10.36	10.01	10.6	10.85	11.6	10.44	10.11
136	11.37	10.38	10.02	10.6	10.82	11.55	10.41	10.01
137	11.38	10.39	10.03	10.6	10.8	11.52	10.39	9.918
138	11.5	10.41	10.04	10.61	10.78	11.49	10.38	9.838

139	11.62	10.4	10.04	10.62	10.76	11.47	10.4	9.769
140	11.65	10.42	10.06	10.64	10.75	11.46	10.42	9.713
141	11.81	10.45	10.08	10.65	10.73	11.44	10.43	9.671
142	12.11	10.45	10.08	10.66	10.72	11.43	10.46	9.644
143	12.56	10.46	10.09	10.68	10.71	11.42	10.48	9.633
144	13.25	10.46	10.1	10.7	10.7	11.41	10.52	9.63
145	13.54	10.51	10.1	10.72	10.68	11.39	10.55	9.629
146	13.72	10.5	10.11	10.75	10.66	11.37	10.59	9.633
147	13.91	10.51	10.1	10.77	10.64	11.35	10.63	9.638
148	14.09	10.51	10.1	10.77	10.61	11.33	10.67	9.645
149	14.19	10.55	10.08	10.78	10.59	11.32	10.71	9.655
150	14.35	10.66	10.08	10.8	10.56	11.32	10.74	9.665
151	14.56	10.84	10.07	10.8	10.54	11.32	10.78	9.677
152	14.67	11.1	10.06	10.79	10.52	11.32	10.82	9.688
153	14.85	11.47	10.05	10.79	10.49	11.32	10.85	9.699
154	15.02	11.84	10.05	10.79	10.46	11.32	10.89	9.71
155	15.08	12.12	10.06	10.78	10.44	11.31	10.92	9.722
156	15.31	12.27	10.12	10.77	10.41	11.31	10.96	9.733
157	15.45	12.39	10.22	10.76	10.38	11.3	10.99	9.747
158	15.62	12.5	10.37	10.76	10.34	11.3	11.03	9.761
159	15.69	12.55	10.59	10.77	10.31	11.29	11.07	9.775
160	15.87	12.64	10.95	10.79	10.27	11.28	11.1	9.789
161	16.09	12.71	11.45	10.84	10.22	11.28	11.13	9.802
162	16.27	12.75	11.9	10.92	10.17	11.28	11.16	9.816
163	16.5	12.84	12.16	11.04	10.14	11.28	11.19	9.831
164	16.64	12.93	12.3	11.2	10.11	11.28	11.22	9.846
165	16.85	13.01	12.43	11.41	10.09	11.29	11.26	
166	17.02	13.11	12.54	11.69	10.07	11.3	11.28	
167	17.23	13.18	12.66	12.01	10.08	11.31	11.31	
168	17.45	13.29	12.79	12.33	10.12	11.33	11.33	
169	17.67	13.38	12.9	12.6	10.2	11.37	11.36	

170	17.89	13.46	13.02	12.79	10.31	11.42		
171	18.05	13.52	13.13	12.91	10.46	11.5		
172	18.34	13.63	13.27	12.99	10.65			
173	18.5	13.73	13.39	13.05	10.84			
174	18.7	13.85	13.52	13.12				
175	19.03	13.99	13.67	13.18				
176	19.24	14.1	13.81					
177	19.45	14.22						
178	19.74							
179								
180								